NUI Galway
OÉ Gaillimh

RNA metabolism proteins identified as ATM and 53BP1 partners function in the DDR

Janna Luessing

Genome Stability Laboratory,
Centre for Chromosome Biology,
Department of Biochemistry, School of Natural Sciences,
National University of Ireland Galway

A thesis submitted to the National University Ireland, Galway for the degree of Doctor of Philosophy

Supervisor: Prof. Noel F. Lowndes

February 2017

Table of Contents

List of Figures

List of Tables

Abbreviations

9-1-1: Rad9-Rad1-Hus1
53BP1: p53 binding protein 1
1N: haploid
2N: diploid
4N: tetraploid
aa: amino acids
alt-EJ: alternative end-joining
APC: Anaphase promoting complex
A-T: Ataxia Telangiectasia
ATM: Ataxia Telangiectasia Mutated
ATR: Ataxia Telangiectasia and RAD3 related
ATRIP: ATR interacting protein
BER: Base excision repair
BIR: break-induced replication
BLM: Bloom syndrome protein
BRCA1: Breast Cancer associated gene 1
BRCA2: Breast Cancer associated gene 2
BRCC36/45: BRCA1/BRCA2 containing complex subunit 36/45
BRCT: BRCA1 carboxy-terminal
BRDU: Bromodeoxyuridine
BSA: Bovine Serum Albumin
CBP: CREB binding protein
CBP: Calcium binding protein
CD44: cluster of differentiation 44
CDC: cell division cycle
CDK: Cyclin dependent kinase
***C. elegans*:** *Caenorhabditis elegans*
Chd4: Chromodomain Helicase DNA Binding Protein 4
CHK1/2: Checkpoint Kinase ½
CIP1: cyclin-dependent kinase inhibitor 1
C-NHEJ: classical NHEJ
CO: crossover
CRISPR: Clustered regularly interspaced short palindromic repeats
CRM1: Chromosomal Maintenance 1
crRNA: CRISPR-RNA
CSB: Cockayne Syndrome group B
CSR: class-switch recombination
CtIP: CtBP interacting protein
CTRL: control
CTT domain: C-terminal tail domain
DAPI: 4',6-diamidino-2-phenylindole
DDR: DNA damage response
DDX: DEAD box protein
DEAD: Asp-Glu-Ala-Asp
DExD/H box: Asp-Glu-X-Asp/His box
dHJ: double Holiday junction
D-loop: Displacement loop
DGCR8: DiGeorge Critical Region 8
***D. melanogaster*:** *Drosophila melanogaster*
DMEM: Dulbecco's Modified Eagle Medium
DMMB: 1,9-dimethylmethylene blue
DMSO: Dimethyl sulfoxide
DNA: de-oxyribonucleic acid
DNA2: DNA replication ATP-dependent helicase/nulcease DNA2
DNA-PKcs: DNA-dependent protein kinase catalytic subunit
DNA pol II: DNA polymerase II
dRBD: double-stranded RNA binding domain
DR-GFP: DSB reporter GFP
DSB: DNA double strand break
DT-40: chicken lymphoma cell line
DTT: 1,4-Dithiothreitol

E2F: Transcription factor E2F
eIF4F: Eukaryotic initiation factor 4F
EJC: Exon Junction Complex
EM: Electron microscopy
ERα: Estrogen receptor alpha
ERCC1: Excision-Repair, Complementing Defective, In Chinese Hamster
ETO: etoposide
EXO1: Exonuclease 1
FACS: Fluorescence-activated cell sorting
FANCD2: Fanconi anemia group D2 protein
FAT: FRAP-ATM-TRRAP
FAT-C: FAT C-terminal domain
FITC: Fluorescein isothiocyanate
FCS: Foetal calf serum
FSC: Forward scatter
gH2AX: phophorylated H2AX(ser139)
gRNA: guideRNA
G1/2: Gap1/2 phase
GADD45a: growth arrest and DNA damage inducible protein a
GC: gene conversion
GST: Glutathione S-transferase
Gy: Gray
H2AX: variant histone H2AX
H3K9me3: tri-methylated lysine 9 on H3
HBD: Heme binding domain
HCT116: human colon cancer cells
HCV: Hepatitis C virus
HDAC: Histone deacetylase
HDR: homology directed repair
HEAT: Huntingtin, EF3, PP2A, TOR1
HEK293: Human embryonic kidney cells
HeLa: Henrietta Lacks cell line
HFSC: HA-FLAG-STREP-CBP tag
HIV: human immunodeficiency virus
HNH: His-Asn-His
HR: homologous recombination
hTERT: human telomerase transcriptase
ICRF-193: meso-4,4′-(3,2-Butanediyl)-bis(2,6-piperazinedione)
IF: Immunofluorescence
IKKE: Inducible I Kappa-B Kinase Epsilon
IP: Immunoprecipitation
IR: Ionizing Radiation
IRIF: ionizing radiation induced foci
J: Joules
JEV: Japanese encephalitis virus
kb: kilobases
KD: kinase-dead
kDa: kilo Dalton
KIF18b: Kinesin Family Member 18B
KIP1: cyclin dependent kinase inhibitor p27
m7-GTP: 7-Methylguanosine 5′-triphosphate
Mb: megabases
MCF7: Michigan Cancer Foundation-7
MCM3: Minichromosome Maintenance Complex Component 3
MDC1: mediator of DNA damage checkpoint 1
MDM2: Mouse double minute 2 homolog
MEF: mouse embryonic fibroblast
miRNA: microRNA
MMR: mis-match repair
MNV: Murine norovirus
M-phase: Mitosis
MRN: MRE11-RAD50-NBS1 complex
mRNA: messengerRNA
MRE11: Meiotic Recomination11
N: Normality

NBA1: NAB1 and bud neck associated protein 1
NBS1: Nijmegen Breakage Syndrome 1
NCO: non-crossover
NER: Nucleotide excision repair
NES: nuclear export signal
NFAT5: Nuclear factor of activated T-cells 5
NHEJ: non-homologous end-joining
NLS: nuclear localisation signal
ORC: origin of replication complex
p53: tumor suppressor protein 53
PABP1: poly(A)-binding protein 1
PALB2: Partner and localiser of BRCA2
PAM: Protospacer adjacent motif
PARI: PCNA interacting partner
PARP: poly ADP ribose polymerase
PBS: Phosphate buffered Saline
PCNA: Proliferating cell nuclear antigen
PCR: Polymerase chain reaction
PFA: paraformaldehyde
PI: Propidium iodide
PIKK: Phosphatidylinositol 3-kinase like kinase
PLK1/3: Polo-like kinase 1/3
PNK: Polynucleotide 5'-hydroxyl-kinase
PP1: Ser/Thr protein phosphatase 1
PP2A: Protein Phosphatase 2
PRC: Pre-replication complex
pre-crRNA: precursor CRISPR-RNA
pre-miRNA: precusor miRNA
pri-miRNA: primary miRNA
PTIP: Pax transactivation domain-interacting protein
PTM: post-translational modification
qPCR: quantitative PCR
RAD: Radiosensitive
RAP80: Receptor associated protein 80
RB: Retinoblastoma associated protein
RECQ5: ATP-dependent DNA helicase Q5
RIF1: Rap1 interacting factor 1 homolog
RING: Really Interesting New Gene
RISC: RNA induced silencing complex
RNA: ribonucleic acid
RNA pol II: RNA polymerase II
RNF8: ring finger protein 8
RNF168: ring fingerprotein 168
ROS: reactive oxygen species
RPA: Replication protein A
RPE-1: retinal pigmented epithelial 1
RPMI: Roswell Park Memorial Institute media
rRNA: ribosomal RNA
RS-like domain: Ser-Arg rich domain
RT: Room temperature
S-phase: DNA synthesis phase
SAC: Spindle assembly checkpoint
SD: standard deviation
SDS: Sodium dodecyl sulfate
SDSA: synthesis-dependent strand annealing
SEM: standard error of the mean
Ser: serine
SSA: single strand annealing
SSC: side scatter
ssDNA: single stranded DNA
SILAC: Stable isotope labeling with amino acids in cell culture
siRNA: small interfering RNA
SMC1: structural maintainance of chromosomes protein 1
snRNA: short nucleolar RNA
SQ/TQ: Ser/Thr-Glu
TALEN: Transcription activator-like effector nucleases
TBS: Tris-buffered saline
TCE: total cell extract
TIP60: 60kDa Tat-interactive protein

TIR1: Transport inhibitor response 1
TLS: Translesion synthesis
TOPII: Topoisomerase II
TopBP1: Topoisomerase 2 binding protein 1
tracrRNA: trans-activating crRNA
TRIP12: Thyroid Hormone Receptor Interactor 12
TRRAP: Transformation/Transcription domain associated protein
U-2-OS: U2 osteosarcoma cell line
UBR5: Ubiquitin Protein Ligase E3 Component N-Recognin
UDR: ubinquitination-dependent recruitment
UIM: ubiquitin interacting motif
USP10: ubiquitin carboxy-terminal hydrolase 10
USP28: Ubiquitin Specific Peptidase 28
UTR: untranslated region
UV: ultraviolet radiation
V: Volt
V(d)J recombination: Variable (Diversity) Joining recombination
WB: Western Blot
WCE: whole cell extract
WNV: West Nile virus
WRN: Werner syndrome ATP-dependent helicase
WT: wild type
XPB: xeroderma pigmentosum type B
XPD: xeroderma pigmentosum D
XPF: Xeroderma Pigmentosum Group F-Complementing Protein
XRCC3/4: X-Ray Repair Cross Complementing 3/4
Zwint: ZW10 Interacting Kinetochore Protein

Acknowledgements

First and foremost, I would like to thank Noel for giving me the opportunity to do my PhD here in Galway and to letting me follow my own gut, which, in all fairness, wasn't always right. But thanks so much for keeping me on track, challenging me and not giving up on me.

I also owe a big thanks to Andrew, who has guided me through nine years of hard work, stress, laughter and tears. Who also showed me that there are indeed things outside the nucleus and outside of Galway. I owe ya big time.

Many thanks to the girls, especially Emma, who was always there, when I needed a tissue, a rant or just a break away from the lab. I couldn't ask for a better friend.

Also big thanks to Anne, John and Mike for the great support behind the scenes. I would have been lost without you.

I would like to say a special thanks to my mum, who has stuck with me, supported me and was truly my rock throughout my life and my PhD. And my dad and my little sister Sally, thanks for pushing me and making me wanting to be the best I can be. *Ohne euch hätte ich es nie so weit geschafft. Ich hab euch lieb.*

Finally, thanks to all current and former members of the Lowndes lab and the CCB for support, advice and guidance throughout the years.

Thesis Declaration and Contributions

I declare that I have not obtained any previous qualification from NUI Galway or elsewhere based on any of the work contained in this thesis. I conducted all the experiments and wrote the thesis under supervision of Professor Noel Francis Lowndes. There are a few exceptions where experiments were performed by others but included in this thesis to complete the story. For clarity these are clearly indicated in the figure legends when appropriate and included below.

Chapter 2:
Table 2.1: Experiment performed by J. Eykelenboom and F. Pessina
Table 2.2: Experiment performed by A. van Beneden and J. Prieto

Chapter 3:
Table 3.1: Experiment performed by J. Eykelenboom and F. Pessina

Chapter 4:
Table 4.1: Experiment performed by S. Maretto and J. Eykelenboom
Table 4.2: Experiment performed by A. van Beneden and J. Prieto
Figure 4.1a: Experiment performed by S. Maretto

Abstract

The DNA is continually under treat of being damaged by both endogenous and exogenous sources such as reactive oxygen species produced during normal cell metabolism or ionising radiation. It is vital for the maintenance of genome integrity that cells deal with such damage efficiently and faithfully. The most deleterious lesions of the DNA are double strand breaks and the cell has developed to main repair pathways, homologous recombination and non-homologous end-joining, in order to deal with such damage.

In this study we are investigating the role of three RNA metabolism proteins, DGCR8, DDX3X and DDX17, in the DDR. These proteins were identified in recent proteomic screens as potential interacting proteins of ATM and 53BP1, respectively.

We demonstrate that DDX3X is a novel interacting partner of ATM and is required for efficient DNA repair by homologous recombination. We also investigate the role of DGCR8 in the DNA damage response independent of its partner protein Drosha. We propose that DGCR8 has a potential role in regulating ATM kinase activity. In addition to these two ATM interacting proteins, we have also identified DDX17 as a novel 53BP1 interacting partner involved in DSB repair by both homologous recombination and non-homologous end-joining.

Chapter 1: General Introduction

1.1. The DNA damage response

The DNA of cells is continually subjected to damage. It is vital for the maintenance of genome integrity that this damage of the DNA is faithfully repaired. DNA damage arises from endogenous sources during normal cellular metabolism, producing reactive oxygen species (ROS) or during DNA replication causing mutation through incorporation of mismatched nucleotides. Furthermore, the DNA is subject to a wide range of exogenous damaging agents such as ionizing and ultra-violet radiation or chemical agents such as those administered during chemotherapy or smoking. Studies have shown that the cell deals with around 10^5 lesions on a daily basis (Hoeijmakers, 2009). The lesions include base-damage, intra- or inter-strand crosslinks, single- and double strand breaks (Ciccia & Elledge, 2010).

In order to respond to the vast amount of endogenous as well as exogenous DNA damage, the cell has developed a series of pathways, targeting specific type and cellular context of the DNA lesions. These pathways are collectively termed the DNA damage response (DDR).

Small mismatches and other less deleterious types of DNA damage are usually dealt with using nucleotide excision repair (NER), base-excision repair (BER) and mis-match repair (MMR) (Kamileri, Karakasilioti et al., 2012, Martin, Marples et al., 2010, Wallace, Murphy et al., 2012).

The most severe kind of DNA damage is a double-strand break, which directly threatens genomic stability. DSBs are repaired by two main mechanisms, non-homologous end-joining and homologous recombination (Ciccia & Elledge, 2010). If the extent of damage is too high, the cell can also respond by inducing cellular senescence or apoptosis (Alberg, Ford et al., 2007, Chen & Stubbe, 2005, Cheung-Ong, Giaever et al., 2013, Harper & Elledge, 2007).

1.2. Key proteins in the DNA damage response

The DNA damage response is a signalling cascade that has been characterized in detail in yeast and homologues have been found for all key proteins in higher eukaryotes (Harper & Elledge, 2007). However, the increased complexity of higher eukaryotes has resulted in a correspondingly more intricate and only partially characterized DNA damage response.

1.2.1. ATM

Ataxia telangiectasia mutated (ATM) is a 350 kDa serine/threonine kinase that is a member of the phosphatidylinositol-3-kinase-like kinase family (PIKKs) (Lempiainen & Halazonetis, 2009, Lovejoy & Cortez, 2009)

ATM is one of the key regulators of the cellular response to DNA damage, which is a mainly phosphorylation-driven signalling pathway (Bensimon, Schmidt et al., 2010, Matsuoka, Ballif et al., 2007, Smolka, Albuquerque et al., 2007, Stokes, Rush et al., 2007). ATM is present in its inactive form as a dimer. In response to DSBs, ATM monomerises and relocates rapidly to the site of damage where it phosphorylates a large number of target proteins (Bakkenist & Kastan, 2003).

The ATM protein and its relatives ATR and DNA-PKcs consist of a series of HEAT repeats in its N-terminal region (Perry & Kleckner, 2003). These are important for interactions including with NBS1, a component of the DNA damage sensing complex MRN (Falck, Coates et al., 2005, You, Chahwan et al., 2005). The C-terminal region of ATM consists of a kinase domain flanked by two FAT domains. The conserved FRAP-ATM-TRRAP domain is located on the N-terminal flanking site, while the FAT-carboxy-terminal is located on the C-terminal of the kinase domain (Figure 1.1).

Neither ATM nor ATR have yet been crystalised. However, DNA-PKcs has been crystalised in 2010 and its structure was solved to a resolution of 6.6Å (Sibanda, Chirgadze et al., 2010). It is assumed that both ATM and ATR have a similar structure as DNA-PKcs based evidence from EM data (Llorca, Rivera-Calzada et al., 2003).

The activation of ATM in response to DNA damage relies on two essential post-translational modifications. Upon DNA damage sensing, ATM is auto-phosphoylated on serine 1981 (S1981). This post-translational modification (PTM) is located in the dimerisation region and may prevent its re-dimerisation (Bakkenist & Kastan, 2003, So, Davis et al., 2009). The second important PTM is the acetylation of lysine 3016 (K3016) in the FATC domain by Tip60 although Tip60 activates ATM via acetylation is yet to be elucidated. Tip60 interacts with ATM constitutively, but the damage-associated histone methylation H3K9me3 is required for the activation of Tip60 and thus ATM (Sun, Jiang et al., 2005).

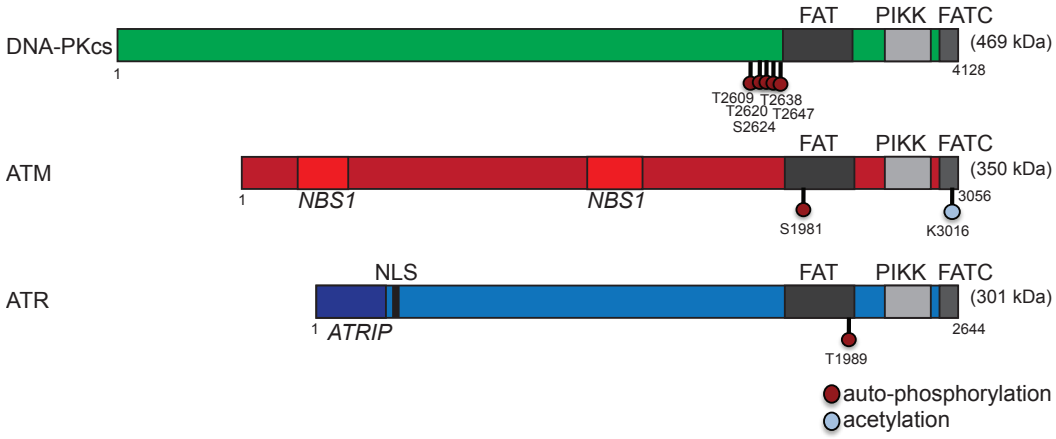

Figure 1.1: Structure of PIKK kinases.

Schematic of the structural domains found in the PIKK kinases DNA-PKcs, ATM and ATR. C-terminal FAT, PIKK and FATC domains are shown as grey boxes. Known interaction sites are shown in italic. Selected PTMs important for activation of the kinases are depicted as lollipops indicating the modified residue.

Other critical targets of ATM are the main ATM effector kinase CHK2 and the mediator proteins 53BP1 and BRCA1, which are essential for error-free homologous recombination (HR) (Anderson, Henderson et al., 2001, Cortez, Wang et al., 1999, Matsuoka, Huang et al., 1998). Furthermore, ATM phosphorylates the ATR activator TopBP1, which promotes TopBP1 binding to ATR. Although ATM is essential for the early activation of the DNA damage response signalling cascade, it is thought that in later stages, there is a switch from ATM to ATR for the repair of the damaged DNA (Yoo, Kumagai et al., 2009).

Mutations in the *ATM* gene cause Ataxia Telangiectasia (A-T), a genetic condition resulting in immune dysfunction, growth retardation, neurodegeneration, incomplete sexual maturity, radiosensitivity and cancer predisposition (Barlow, Hirotsune et al., 1996, Boder, 1975, McKinnon, 2004). A-T is a relatively rare, autosomal recessive genetic disorder and 0.5-1% of the population are carriers. Although carriers do not suffer from A-T, they show a higher frequency of developing cancer (Easton, 1994, Taylor, Metcalfe et al., 1996). Individuals affected by A-T have a very short life expectancy mainly due to neurological deterioration, although 10-15% of all A-T sufferers also develop cancer (Taylor et al., 1996).

AT has been extensively studied in mouse model systems (Barlow et al., 1996). Although mice do not suffer all symptoms presented in humans such as nerve cell loss, ocular telangiectasias or neurological conditions, they do present with the main A-T phenotypes including infertility, growth retardation, immunological defects, radiosensitivity and cancer predispostion (Barlow et al., 1996, Boder, 1975, McKinnon, 2004).

The two most pronounced phenotypes of A-T, radiosensitivity and cancer predisposition, are most likely due the central role of ATM in the DNA damage response, as cell are unable to repair damage properly or arrest the cells in DNA damage checkpoints. It is likely that most of the other

symptoms of A-T are also linked to a defective DDR (Dar, Biton et al., 2006, Gorodetsky, Calkins et al., 2007, Yang & Herrup, 2005).

1.2.2. ATR

ATR (ATM and Rad3-Related) is also a member of the PIKK family and, like ATM, acts as a key regulator of the cellular response to DNA damage. Although they share some common targets for phosphorylation, the functions of ATM and ATR in the DNA damage response are non-redundant. While ATM activation primarily occurs in response to double strand breaks, ATR has a multitude of functions in different DNA repair pathways, and is activated by a variety of DNA lesions including DSBs and breaks that occur naturally during RNA replication (Marechal & Zou, 2013). ATM deficient cells are viable, even though they show increased genome instability and mutation or depletion of ATM renders patients extremely cancer-prone (A-T syndrome). In contrast, ATR is essential and its depletion causes early embryonic lethality in mice (Brown & Baltimore, 2000, Cortez, Guntuku et al., 2001, de Klein, Muijtjens et al., 2000). ATR preferentially binds to ssDNA via the interaction of ATRIP, which it forms a stable and obligate complex with, and the 9-1-1 complex (Ellison & Stillman, 2003).

The main effector kinase of ATR is CHK1. Studies have shown that CHK1 is activated in response to double strand breaks in a time-dependent manner (Shiotani & Zou, 2009, Sorensen, Hansen et al., 2005). Early sensing of DNA damage and repair involves ATM and CHK2, followed by subsequent activation of ATR and CHK1, possible in response to resection upon RPA coating of single-stranded DNA (ssDNA) (Marechal & Zou, 2013).

ATR is activated by auto-phosphorylation on threonine 1989 (T1989) in response to DNA damage, a process that requires kinase activity, ATRIP

and RPA. TOPBP1 binding to ATR-ATRIP potentially leads to conformational change of ATR, which enhances kinase activity and substrate binding (Liu, Shiotani et al., 2011, Mordes & Cortez, 2008, Nam & Cortez, 2011). ATR is a tightly regulated protein and can only achieve its full DNA repair potential when specific substrates are localised to the damage site and when its kinase activity is stimulated through a specific series of phophorylation-mediated protein-protein interactions (Marechal & Zou, 2013).

Many of the proteins that activate and regulate ATR and ATM are also their substrates, such as CHK1 and MDC1 for ATR and ATM, respectively (Lou, Minter-Dykhouse et al., 2006, So et al., 2009, Syljuasen, Sorensen et al., 2005).

Several diseases are associated with mutations in the *ATR* gene. The most prominent and well-studied is the Seckel Syndrome, which was first described in 1960 by Seckel as a genetic disorder presenting with phenotypes including microcephaly, dwarfism, intrauterine growth retardation, mental retardation and UV sensitivity (O'Driscoll, Ruiz-Perez et al., 2003). Although the most frequent Seckel mutation is intronic and not in the protein coding region, it alters the splicing of ATR mRNA, resulting in reduced levels of ATR in the cells (O'Driscoll, Gennery et al., 2004, O'Driscoll et al., 2003). Recent studies have also found further mutations in the *ATR* gene and in the gene of the ATR binding partner *ATRIP*, which have been linked to Seckel Syndrome (Ogi, Walker et al., 2012).

One mutation in the *ATR* gene (c6431A>G) results in a missense mutation of a Glutamine to an Arginine (Q2144R) and predisposes individuals to oropharyngeal cancer (Tanaka, Weinel et al., 2012) and is autosomal-dominant. This was so far found in 24 individuals in the same family over generations. Apart from the susceptibility to orophanryngeal cancer, individuals are also predisposed to mild hair- teeth- and nail abnormalities as well as skin telangiectasia.

1.2.3. 53BP1

p53 binding protein 1 (53BP1), encoded by the *TP53BP1* gene, is a 214 kDa protein with no apparent enzymatic activity. It was first discovered in 1994 as a binding partner of the tumour suppressor protein p53 (Iwabuchi, Bartel et al., 1994). Despite the poorly described function of its interaction with p53, it has been shown to be a central part of the DNA damage response independent of p53 (Ochs, Somyajit et al., 2016, Panier & Boulton, 2014). The 1972 residue protein contains a serine/threonine-glutamine rich N-terminal region with 28 S/T-Q sites, which are extensively phosphorylated by ATM (Adams & Carpenter, 2006). It also contains an oligomerization domain, two tandem Tudor domains followed by an ubiquitin-dependent recruitment domain (UDR) and two BRCA1 carboxy-terminal (BRCT) domains in its C-terminal region (Iwabuchi, Li et al., 1998).

53BP1 acts as a scaffold protein allowing other DDR factors to be recruited to DNA double strand breaks (Huen, Huang et al., 2010, Lee & Paull, 2007, Silverman, Takai et al., 2004). Apart from its role in DSB repair, 53BP1 is also required for V(D)J recombination and Class switch recombination (Difilippantonio, Gapud et al., 2008, Manis, Morales et al., 2004, Reina-San-Martin, Chen et al., 2007, Ward, Reina-San-Martin et al., 2004). It has also been shown that 53BP1 is required for the fusion of de-protected telomeres (Dimitrova, Chen et al., 2008). All these events require distant DNA ends to be joined together, but exact role for 53BP1 in long distance NHEJ remains unclear.

53BP1 is rapidly recruited to double strand breaks via the modification of histones by the E3 ligases RNF8 and RNF168 (Anderson et al., 2001, Rappold, Iwabuchi et al., 2001, Schultz, Chehab et al., 2000). The tandem tudor domain of 53BP1 binds to H4K20me2 and, to a lesser extent H4K20me1. Due to the high abundance of this histone modification, binding by 53BP1 is necessary but not sufficient for focal

recruitment (Zgheib, Pataky et al., 2009). A second histone modification induced by DNA damage though RNF8 and RNF168 is required for 53BP1 binding. Binding of the ubiquitylated lysine 16 (K16ub) on H2A to 53BP1 is mediated by the UDR motif on 53BP1 (Fradet-Turcotte, Canny et al., 2013). How 53BP1 binds to lysine 15 of H2A remains to be elucidated, but only the combination of these two histone marks combined enable focal formation of 53BP1 at DSBs (Mattiroli, Vissers et al., 2012, Stewart, Panier et al., 2009, Zgheib et al., 2009).

A major interaction partner of 53BP1 at DSBs is RIF1, which is recruited in a 53BP1 dependent manner (Silverman et al., 2004). The 53BP1-RIF1 interaction prevents end-resection at DSBs and thus drives the repair towards NHEJ (Chapman, Barral et al., 2013, Di Virgilio, Callen et al., 2013, Escribano-Diaz, Orthwein et al., 2013, Zimmermann, Lottersberger et al., 2013). In G1 cells, this is the predominant repair mechanism and, although 53BP1-RIF is accumulating at all DSBs independent of cell cycle stage, it is replaced by the E3-ligase BRCA1 and CtIP during S and G2, which pushes the cell towards HR. The switching of 53BP1-RIF1 to BRCA-CtIP is dependent on CDK phosphorylation of CtIP at serine 327 (S327) and threonine 487 (T487) (Escribano-Diaz et al., 2013, Feng, Fong et al., 2013).

1.2.4. BRCA1

BRCA1 is a well-known tumour suppressor that plays a crucial role in the DNA damage response. BRCA1 is directly involved in homologous recombination and also in checkpoint activation, transcriptional and translational regulation of DDR factors, chromatin remodelling and apoptosis.

The *BRCA1* gene was the first identified breast cancer susceptibility gene in 1990 (Hall, Lee et al., 1990). It is comprised of 24 exons and is

transcribed into a 220 kDa protein that has two main domains (Miki, Swensen et al., 1994). The N-terminal RING domain has E3 ligase activity and the C-terminal BRCT domain is involved in phospho-protein binding. Both domains are crucial for BRCA1 function in the DDR (Manke, Lowery et al., 2003, Panier & Durocher, 2009, Rodriguez, Yu et al., 2003, Yu, Chini et al., 2003).

Upon DNA damage, BRCA1 forms foci at DSBs (Scully, Chen et al., 1997) mainly in S and G2 phase. Recruitment of BRCA1 to DSBs requires the ubiquitylation of H2A and H2B by RNF8 and RNF 168, which is recognized by the ubiquitin interacting motif (UIM) of RAP80, which in turn recruits the BRCA1/ Abraxas/NBA1/ BRCC36/BRCC45 complex to the DSBs (Feng, Huang et al., 2009, Kim, Chen et al., 2007, Kim, Huang et al., 2007, Liu, Wu et al., 2007, Shao, Patterson-Fortin et al., 2009, Sobhian, Shao et al., 2007, Wang, Hurov et al., 2009, Wang, Matsuoka et al., 2007, Wu, Huen et al., 2009, Zhao, Sonoda et al., 2007). BRCA1 interacts with PALB2 and BRCA2 at the sites of damage, where it facilitates RAD51 loading onto ssDNA (Sy, Huen et al., 2009, Xia, Sheng et al., 2006, Zhang, Fan et al., 2009, Zhang, Ma et al., 2009).

BRCA1 is also required for the activation of the G1, S and G2/M checkpoints. In response to DNA damage in G1 cells, BRCA1 functions as a scaffold protein for the phosphorylation of p53 by ATM, which then induces the G1 checkpoint (Fabbro, Savage et al., 2004). However, BRCA1 is only required for the G1 checkpoint activation in response to IR and is not required for activation in response UV induced DNA damage. BRCA1 also plays a crucial role in the activation of the S phase checkpoint, where it is phosphorylated at S1387 in response to IR and regulates the kinase activity of CHK1 by a yet unknown mechanism (Yarden, Pardo-Reoyo et al., 2002). BRCA1 is phosphorylated by ATM at S1423 in response to damage in G2 cells and this is essential for G2/M checkpoint activation (Xu, Kim et al., 2001).

1.3. The cell cycle

All biological organisms, from unicellular bacteria to multi-cellular plants and humans undergo cell growth and division in order to proliferate. First described in the middle of the 19th century, the process of cell growth, content duplication and division is known as the cell cycle (Alberts, 2008). The cell cycle is the essential mechanism by which all eukaryotic cells proliferate. It is divided into four major stages; two Gap phases, G1 and G2, in which the cells grow, one phase of genome duplication, known as the S phase, and M-phase, in which the cells divide. An additional stage, in which the cells leave the active cell cycle is known as G0 (Funabiki, Hagan et al., 1993, Martin & Stein, 1976).

1.3.1. Cell cycle control

A cell must ensure that its genetic material is precisely and accurately copied to obtain two identical daughter cells in order to proliferate. Accumulation of defects in the cell cycle can have devastating effect, with the most detrimental being uncontrolled cell growth of tumours. Cells have developed a tightly controlled system of biochemical switches that prevents the three main cell cycle defects: genomic instability, chromosomal instability and unscheduled cell proliferation (Alberts, 2008).

Cyclin-dependent kinases (CDKs) are the key determinants of this regulation. The human genome harbours 13 CDK loci and 25 cyclin loci (Malumbres & Barbacid, 2005). Cyclins activate the CDKs. However, only a subset of CDKs and cyclins are directly involved in the cell cycle. There are three interphase CDKs (CDK2, CDK4 and CDK6) and one mitotic CDK (CDK1) as well as ten additional cyclins in four different classes (cyclins D,E,A,B) (Malumbres & Barbacid, 2001). It has been shown that the only essential kinase is the mitotic kinase CDK1, which is able to

force progression through the cell cycle even in the absence of the other CDKs (Santamaria, Barriere et al., 2007, Satyanarayana, Berthet et al., 2008).

All CDKs contribute to accurate development and prevention of developmental defects. Only two classes of cyclins are essential for cell cycle progression, cyclin A and cyclin B, both of which are involved in mitosis. This suggests that cyclins have overlapping functions between different classes (Brandeis, Rosewell et al., 1998, Geng, Whoriskey et al., 1999, Murphy, Stinnakre et al., 1997).

Cyclin D and E also play important CDK-independent roles, although they are not essential. Cyclin D is activates G1 kinases, whereas cyclin E is involved in DNA replication control (Geng, Lee et al., 2007, Kozar, Ciemerych et al., 2004, Malumbres, Sotillo et al., 2004).

CDK-cyclin complexes ensure the irreversible transition through the different cell cycle stages. This is dependent on the level of the respective cyclins in the cell (Figure 1.2). In early G1-phase, Cyclin D levels gradually build up until sufficient amounts are present to activate CDK4/6, which in turn phophorylates the retinoblastoma protein (RB) to deactivate it. Hyperphosphorylation of RB prevents its interaction with E2F, and the release of E2F renders it active to drive transcriptional activation of cyclin E and A. Rb remains hyperphosphorylated throughout interphase before being de-phosphorylated by PP1 during the transition from mitosis to G1-phase (Morgan, 1997, Sherr, 2000).

Cyclin E then binds to CDK2, which regulates transition from G1 to S phase. Cell division cycle 25A (CDC25A) de-phosphorylates CDK2 to activate it (Figure 1.2). The CDK2/cyclin E complex in turn hyperphosphorylates the RB protein and phosphorylates p27 (Kip1), an inhibitor of CDK2 (Boutros, Dozier et al., 2006). This drives a positive feedback loop ensuring degradation of CDK2 in late S-phase, when p27 is sufficiently increased. CDK2/cyclinE upregulates histone biosynthesis

permitting the G1/S transition. Furthermore, it facilitates CDC45 loading to the pre-replication comlex (PRC) at origins of replication to promote origin firing (Bartek & Lukas, 2001).

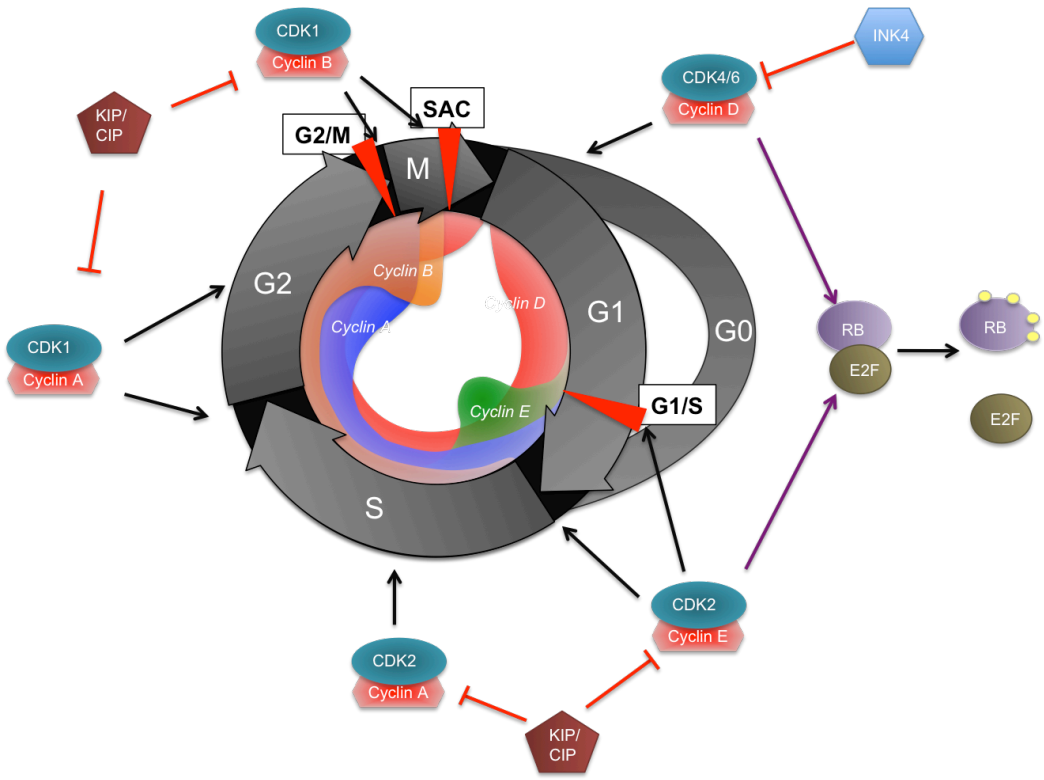

Figure 1.2: Schematic of the cell cycle control by CDKs and cyclins

This schematic shows the four stages of the cell cycle, G1, S, G2 and M, as well as its regulation through different cyclin/CDK complexes and checkpoints. It also shpws the exit from the cell cycle into G0. The inner circle shows the expression level of the four main classes of cyclins throughout the cell cycle. Cyclin D levels (red) increase in G1, remain constant during interphase, before being reduced in mitosis. Cyclin E (green) rapigly increases in late G1 before being degraded in S phase. Cyclin A (blue) transcription, like cyclin E transcription, is activated in G1 phase via E2F, and peaks in laste G2 phase.. E2F was released from Rb through Rb phosphoylation by CDK4/6/cyclin D. Cyclin B levels (orange) increase at the start of S phase before peaking in mitosis. There are three main cell cycle checkpoints (red arrows), G1/S, G2/M and the spindle assembly checkpoint (SAC).

Levels of cyclin E decrease upon entering S phase, while cyclin A increases as shown in Figure 1.2. Cyclin E is gradually replaced by cyclin A to form a complex with CDK2. This further promotes DNA synthesis. Due to the increase of p27, CDK2 in gradually degraded and cyclin A, which remains at high levels during S and G2 phase, forms a complex with the mitotic kinase CDK1. The CDK1/cyclin A complex persists until early mitosis where it influences early mitotic events (Bartek & Lukas, 2001, Morgan, 1997).

Cyclin B transcription is initiated in early S phase but levels rise rapidly in G2 phase (Dynlacht, Flores et al., 1994, Saville & Watson, 1998). CDK1 enters a second complex with cyclin B, which is essential for the transition from G2 phase into mitosis (Ferrari, 2006, Morgan, 1997). The CDK1/cyclin B complex is cytoplasmic in its inactive form in G2. On binding of cyclin B to CDK1, T14 and Y15 become accessible to the kinases Wee1 and Myt1, respectively, and this inactivates the CDK1/cyclin B complex (Russell & Nurse, 1987). The CDK1/cyclin B complex remains in the cytoplasm awaiting rapid relocalisation into the nucleus just prior to mitosis (Hagting, Karlsson et al., 1998, Toyoshima, Moriguchi et al., 1998, Yang, Bardes et al., 1998). This relocalisation requires the activation of CDK1 by dephosporylation of T14 and Y15 via phosphatases of the CDC25 family as well as the phosphorylation of T161 by CDK7/cyclin H (Tassan, Schultz et al., 1994).

CDK1 plays a critical role in mitosis by facilitating chromosome condensation through the phosphorylation of condensin and promoting the breakdown of the nuclear envelope through phophorylation of lamin (Kimura, Hirano et al., 1998, Peter, Heitlinger et al., 1991). In a positive feedback loop CDK1 regulates both its own and cyclin B degradation by the activation of the anaphase promoting complex (APC). CDK1 levels then decrease permitting the segregation of the sister chromatids, de-condensation of the chromosomes, reformation of the nuclear envelop and re-entry into G1 (Queralt & Uhlmann, 2008).

1.3.2. Cell cycle checkpoints and signalling pathways

"Cell cycle checkpoints" are evolutionary conserved mechanisms by which the cell actively stalls cell cycle progression until previous events such as DNA replication, mitosis or DNA repair are completed (Hartwell & Weinert, 1989). These interruptions of the cell cycle can be transient and reversible, or lead to sustained cell cycle arrests in G1 or G2 (Kastan & Bartek, 2004). Cell can only withdraw from the active cell cycle in response to external signals or growth factor deprivation in early- to mid G1 phase (Massague, 2004). As soon as they cross the RB-E2F controlled restriction point in G1 phase, they are committed to the cell cycle including DNA replication and chromosome segregation (Bartek, Bartkova et al., 1997, Sherr & McCormick, 2002).

Activation of the cell cycle checkpoints is initiated by the two apical PIKK kinases ATM and ATR, which phosphorylate the two transducer kinases CHK2 and CHK1, respectively, as well as mediator, or adaptor proteins (Figure 1.3) (Bartek & Lukas, 2003, Shiloh, 2003). ATM activates the three main checkpoint mediators, MDC1, 53BP1 and BRCA1, while the main mediator activated by ATR is claspin (Chini & Chen, 2004, Mochan, Venere et al., 2004, Stucki & Jackson, 2004). ATM activates the checkpoint in response to DSBs and is not required for normal cell cycle progression, whereas ATR is essential for transition into the next cell cycle.

The initial checkpoint response occurs rapidly through phosphorylation and other PTMs of mediator or transducer proteins, re-localisations, dynamic interaction, conformational changes and stability of already existing proteins. Later stages of the checkpoint response require transcriptional activation of protein targets via p53 and BRCA1 (Kastan & Lim, 2000, Sherr & McCormick, 2002, Wahl & Carr, 2001, Xu et al., 2001).

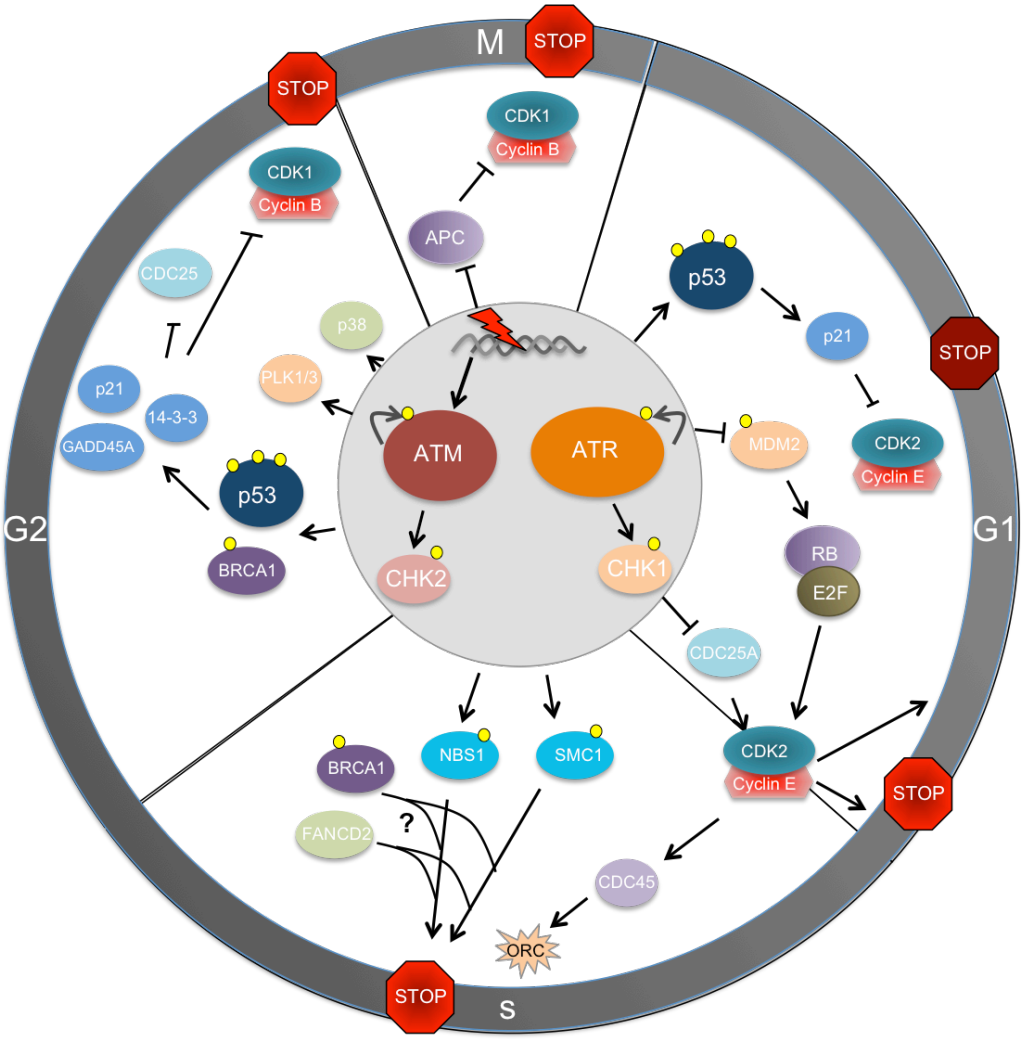

Figure 1.3: The cell cycle checkpoints

This schematic shows the regulation of cell cycle checkpoints via the PIKK kinases ATM and ATR and their respective effector kinases CHK2 and CHK1. Upon DNA damage in G1, p53 is phosphorylated and activates the p21 pathway preventing activation of CDK2, thus arresting the cells in G1. Furthermore, RB is prevented from dissociation from E2F, resulting in a faster, but less prolonged G1 checkpoint arrest. In early S, CDC45 is prevented from initiating new origin firing, prolonging S phase. Furthermore, ATM phosphorylates NBS1 and SMC1, arresting the cells in S phase. In G2, ATM and ATR inhibit CDK1 activation via p53 activated p21 as well as direct inhibition of upstream factors like PLK and activation of p38-mediated subcellular sequestration of CDK1. In mitosis, the spindle assembly checkpoint is prevented from deactivation, which inhibits the APC and subsequent progression through mitosis.

1.3.2.1. G1 and G1/S checkpoints

The two main targets in the G1 checkpoint response are the tumour suppressor proteins p53 and RB. The G1 checkpoint in mammalian cells is predominantly activated by the ATM(ATR)/CHK2(CHK1)-p53/MDM2-p21 pathway in response to DNA damage. Cells can be held in the G1 checkpoint for a prolonged amount of time or even enter permanent G1 arrest known as the G0 phase (Bartek & Lukas, 2003, Kastan & Lim, 2000, Wahl & Carr, 2001). The main checkpoint PIKK kinase in early to mid G1 is ATM, as expression levels of ATR and CHK1 tend to be relatively low and only increase as the cell progresses closer to G1/S transition. Upon DNA damage in G1 phase, ATM/ATR directly phosphorylates the tumour suppressor protein p53, especially on serine 15, while the tranducer kinases CHK2/CHK1 phosphorylate p53 on T18 and T20 (Bartek & Lukas, 2003, Craig, Scott et al., 2003, Kastan & Lim, 2000, Shiloh, 2003, Wahl & Carr, 2001). The phosphorylation of p53 together with the deactivation of the E3-ubiquitin ligase MDM2, which targets p53 for proteasomal degradation, ensures stabilisation of p53. MDM2 is deactivated via phosphorylation by ATM/ATR as well as CHK2/CHK1. p53 in turn activates the transcription of p21CIP1/WAF1, which is an inhibitor of the cyclinE/CDK2 kinase required for transition from G1 into S phase, resulting in G1 arrest. This keeps the RB/E2F complex active, leading to sustained arrest in G1 (Bartek et al., 1997, Massague, 2004, Sherr & McCormick, 2002).

ATR and CHK1 levels, together with key cell cycle regulators Cyclin A and E as well as CDC25A are increased in late G1 via E2F (Figure 1.1). CDC25A is constitutively phosphorylated by ATR/CHK1 at lower levels, which targets it for degradation. ATR/CHK1 activity increases and thus more CDC25A is degraded upon DNA damage, leading to cyclinE/CDK2 complex inhibition and subsequent G1 arrest (Bartek, Lukas et al., 2004, Bartek & Lukas, 2003). This process is much faster than the activation of the G1 checkpoint via p53 as it does not require transcriptional activation. However, while p53-dependent G1 arrest can be sustained for a

substantial amount of time, activation of the checkpoint via down-regulation of CDC25A usually only lasts for a few hours (Kastan & Bartek, 2004).

1.3.2.2. S phase checkpoint

In addition to the previously described down-regulation of CDC25A, which prevents cells from entering S phase, down-regulation of CDC25A also prevents the firing of not yet activated origins of replication in S phase in response to genotoxic stress. The resulting inhibition of CDK2 prevents loading of CDC45 onto chromatin. Since this is required for the recruitment of DNA polymerase a to the pre-replication complex, the firing of origins of replication (ORC) is disabled and progression through S phase is slowed down (Bartek et al., 2004, Bartek & Lukas, 2003).

A second ATM mediated pathway in S phase involves phosphorylation of NBS1 on S343 and SMC1 on S957 and S966 in response to IR or UV. This poorly understood pathway also involves the E3 ubiquitin ligase BRCA1 and FANCD2 (Bartek & Lukas, 2003, Falck, Petrini et al., 2002, Kastan & Lim, 2000, Kim, Xu et al., 2002, Kitagawa, Bakkenist et al., 2004, Nakanishi, Taniguchi et al., 2002, Taniguchi, Garcia-Higuera et al., 2002, Yazdi, Wang et al., 2002).

1.3.2.3. G2/M checkpoint

A third major cell cycle checkpoint during the cell cycle is the G2 or G2/M checkpoint, which stops cells from entering mitosis. The G2/M checkpoint is activated to repair any remaining DNA damage sustained during replication as well as any unrepaired damage sustained during G2. This is crucial as DNA repair during mitosis is very limited (Nyberg, Michelson et al., 2002, Xu, Kim et al., 2002).

ATM/ATR and CHK2/CHK inhibit the essential kinase CDK1. Furthermore, CDK1 is also inhibited by p38-mediated subcellular sequestration and regulation of the CDC25 phosphatases, which usually activate CDK1 (Bulavin, Higashimoto et al., 2001, Mailand, Podtelejnikov et al., 2002, Nyberg et al., 2002). ATM/ATR also target upstream regulators of CDK1 and CDC25 like PLK1 and PLK3 (Nyberg et al., 2002). Evidence suggests that both 53BP1 and BRCA1 are required for maintaining the G2/M checkpoint as in S phase. BRCA1 and p53 act as transcriptional activators of the CDK inhibitors p21, GADD45a and 14-3-3 sigma proteins (Nyberg et al., 2002, Taylor & Stark, 2001). However, cells can sustain the G2/M checkpoint even in the absence of p53, suggesting a p53-independent mechanism is sufficient to maintain the checkpoint.

1.3.2.4. Spindle assembly checkpoint

The spindle assembly checkpoint (SAC) ensures the all kinetochores are attached to microtubules before chromosome segregation. The activated checkpoint delays the metaphase to anaphase transition until all sister chromatids are aligned on the metaphase plate in bi-orientation. However, the mechanism by which unattached kinetochores are detected is not yet fully understood.

The SAC inhibits the APC, which is the key regulator of mitotic progression. The APC is an E3-ligase complex that targets mitotic cyclins and other proteins for degradation by the proteosome (Nakayama & Nakayama, 2006, Peters, 2006). This is essential for the de-activation of CDK1, which is required for mitotic exit. The main cofactors of the APC complex are CDC20 and CHD1. CDC20 mediates ubiquitylation of cyclin B and securin for degradation (Peters, 2006). CHD1 is required for sustained APC function and targets cyclin A, cyclin B, aurora kinases A and B, PLK1 and CDC20, whereby it provides a positive feedback loop (Wolthuis, Clay-Farrace et al., 2008). Prolonged activation of CDK1 by inhibition of the APC complex during the SAC prevents mis-segregation of chromosomes during anaphase. Upon deactivation of the SAC, cells

are able to exit mitosis and restart the cell cycle in G1 (Potapova, Daum et al., 2006).

1.4. DNA damage sensing and initiation of repair

In response to DNA damage, the chromatin around the breaks is altered by PTMs. One of these chromatin marks is tri-methylation of lysine 9 on histone 3 (H3K9me3), which enhances binding and phosphorylation of the histone acetyltransferase TIP60 (Ayrapetov, Gursoy-Yuzugullu et al., 2014). TIP60 acetylates ATM on K3016, leading to the dissociation of the ATM dimer and allowing ATM to auto-phosphorylate (Sun et al., 2005, Sun, Jiang et al., 2009, Sun, Xu et al., 2007).

ATM recognizes and phosphorylates NBS1 as a monomer. NBS1 is one of the proteins of the MRN complex, which in turn recognizes and binds to the broken ends of the DNA at the sites of damage (Gatei, Young et al., 2000). This is followed by ATM dependent phosphorylation of the histone variant H2AX and the amplification of the initial damage signal resulting in the recruitment of other key players of the DDR such as BRCA1, MDC1 and 53BP1 (Shiloh, 2003). One of the earliest events in sensing double strand breaks is the phosphorylation of H2AX on serine 139 by the PIKK kinase ATM and to a certain extent also DNA-PKcs, a process that occurs within minutes of damage induction (Meier, Fiegler et al., 2007, Savic, Yin et al., 2009). The kinases are thought to be partially redundant, although ATM appears to be the main kinase involved in the phosphorylation (Falck et al., 2005, Savic et al., 2009). Histone H2AX is a variant of H2A and contributes approximately 10%-15% of the total H2A in higher organisms (Fernandez-Capetillo, Lee et al., 2004, Rogakou, Boon et al., 1999).

The initial phosphorylation of H2AX leads to a wide spread phosphorylation of H2AX around the site of the DSB and this can spread for an estimated 1-2 megabases (Mb) (Rogakou et al., 1999). The extention of H2AX phosphorylation is driven by ATM only. However, the accumulation and retention of γH2AX proximal to the DSB is not only dependant on ATM, but also on MDC1 and PP2A (Savic et al., 2009).

The phosphorylation of H2AX is a dynamic process, with the serine residue being phosphorylated and dephosphorylated during the recognition and repair process. MDC1 specifically binds to the phosphorylated serine 139 (S139) of H2AX via its C-terminal BRCT-domain, while its N-terminal FHA domain is involved in the intra-S checkpoint. The MDC1-γH2AX interaction is crucial for downstream IRIF formation of DDR factors, but is not required for MDC1 checkpoint function (Stucki, Clapperton et al., 2005). Therefore, MDC1 is not required for initial γH2AX phosphorylation but is essential for the accumulation and retention of DDR factors at DSBs.

1.4.1. Early events in DNA damage signalling

MDC1 directly binds autophosphorylated ATM, which helps to sustain retention of ATM at the break and maintains γH2AX phosphorylation. MDC1 does not impact on the level of ATM autophosphorylation, but instead protects γH2AX from dephosphorylation by phosphatases (Stucki et al., 2005).

After the initial phosphorylation of H2AX, the E3-ubiquitin ligase RNF8 targets chromatin-associated proteins for initial ubiquitination. This initial ubiquitination is recognised by a second E3 ligase, RNF168 to initialise a ubiquitination cascade by ubiquitylating H2A (H2AK15ub) (Mattiroli et al., 2012). RNF168 itself has autoamplificatory potential and is tightly regulated by the E3 ligases TRIP12 and UBR5. 53BP1 is then recruited to ubiquitin-modified chromatin and binds directly to H2AK15ub and H4K20me2 (Bohgaki, Bohgaki et al., 2013, Stewart, 2012). 53BP1 recruitment and subsequent recruitment of RIF1 and PTIP via phosphorylation of 53BP1 leads ultimately to the point at which the cell selects a pathway for the repair of the double strand break.

1.5. DSB repair pathways

Two major DSB repair mechanisms have evolved in the cell: Non-homologous end-joining (NHEJ) and homologous recombination (HR). These can further be divided into two sub-pathways, Classical NHEJ (C-NHEJ) and alternative end-joining (alt-EJ) and gene conversion (GC) and single strand annealing (SSA), respectively. How the cell chooses the most appropriate pathway to repair DNA double strand break and maintain genome integrity is crucial to its survival.

1.5.1. DSB repair pathway choice

The main regulator of DNA DSB repair pathway choice is the extent of resection occuring at the broken DNA ends. This is principally regulated by two main protein interactions of BRCA1-CtIP and of 53BP1-RIF1 (Chapman et al., 2013, Escribano-Diaz et al., 2013). Upon activation of the DDR signalling cascade, 53BP1 rapidly relocalises to the DSB and recruits RIF1, which blocks end resection. This activity of RIF1 the cells towards C-NHEJ, which is the only DSB repair pathway not requiring end-resection (Figure 1.4).

End resection is the process of removing nucleotides from one strand of the DNA to generate single stranded DNA overhangs. The three other pathways do require end resection. CtIP and MRE11 nucleases perform an initial “end-clipping” to remove a small amount of DNA (Figure 1.4). This initial resection is some 20bp in mammalian cells and up to 100-300bp in yeast. The initial resection prepares the DNA for the mutational alt-EJ repair (Huertas & Jackson, 2009, Truong, Li et al., 2013).

A range of proteins, including CtIP, DNA2, BLM, EXO1 and WRN are involved in a second, more extensive resection step, which prevents alt-EJ and directs the cells towards HR or SSA (Sturzenegger, Burdova et al., 2014, Symington & Gautier, 2011). Recent studies have shown that

53BP1 is important in controlling the extent of end-resection, preventing cells from hyper-resection of DNA ends leading to SSA (Ochs et al., 2016).

RAD51 and its regulation by various proteins also exerts an important influence on DSB repair pathway choice. The single stranded DNA resulting from end resection is coated with RPA, which initially competes with RAD51 for ssDNA binding prevents recombination. However, RPA also prevents degradation of broken DNA ends and the formation of secondary ssDNA structures and microhomology annealing (alt-EJ) (Figure 1.4), which is crucial for efficient gene conversion (GC) (Bennardo, Cheng et al., 2008, Chen, Lisby et al., 2013, Deng, Gibb et al., 2014, Wang & Haber, 2004). BRCA2 assists loading of RAD51 onto ssDNA, thereby enhancing GC, while anti-recombinases such as PARI and Polv prevent RAD51 nucleofilament formation and so the repair towards the more error-prone repair pathways such as alt-EJ, trans-lesion synthesis (TLS) or SSA (Ceccaldi, Liu et al., 2015, Lee & Lee, 2007, Li, Dong et al., 2008, Moldovan, Dejsuphong et al., 2012, O'Connor, Dejsuphong et al., 2013, Yu & McVey, 2010). RECQ5 anti-recombinase abolishes the inhibitory effect of RAD51 on RAD52 to promote other error-prone pathways such as synthesis-dependent strand annealing (SDSA) or SSA (Islam, Paquet et al., 2012, Paliwal, Kanagaraj et al., 2014, Schwendener, Raynard et al., 2010). The wide range of proteins that contribute to the regulation of DSB repair pathway choice underlines the crucial role and subtle balance of DNA DSB repair pathway choice.

C-NHEJ and HR are generally high-fidelity processes that are sufficient in healthy cells to maintain genome integrity. Mammalian cells have also developed two more mutagenic pathways, which are highly restricted to prevent genome instability. However, as an act of “last resort” these function as a back-up mechanism in cells where C-NHEJ or HR are not possible, since the mutagenic repair of the DNA might still be favoured over non-repair of DNA damage.

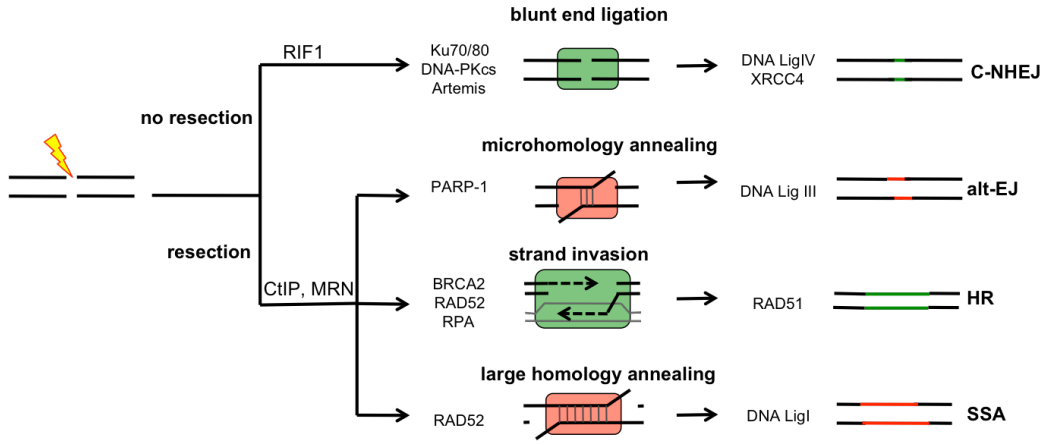

Figure 1.4: DNA DSB repair pathway choice

The cell has four main pathways to repair DSBs depending on the extent of resection. A. C-NHEJ is the major DSB choice and mostly accurate. It requires to resection and ligates the blunt ends together. B. alt-EJ is a mutagenic pathway in which microhomologies anneal leading to insertions and deletions. C. HR is the most accurate DSB repair pathway in which a single strand of the broken DNA invades a sister chromatid using it as a homology template. D. SSA is a mutagenic pathway resulting in large deletion due to extensive resection and large homology annealing mainly in repetitive regions.

1.5.2. Non-homologous end-joining

Classical non-homologous end-joining (C-NHEJ) is the most common and best-characterized double strand break repair pathway. C-NHEJ repair is independent of sequence homology and only requires minimal end processing. It is active throughout interphase, but exhibits highest activity in G1 due to the absence of a homology template for HR. C-NHEJ competes with HR at double strand breaks during S and G2 phase.

Upon DSB induction, the two broken ends are rapidly coated with 53BP1 to form a platform for RIF1 and PTIP upon damage induced phosphorylation by ATM (Callen, Di Virgilio et al., 2013, Chapman et al., 2013, Escribano-Diaz et al., 2013, Wang, Aroumougame et al., 2014, Zong, Callen et al., 2015). These complexes prevent end-resection by blocking CtIP access to the broken ends.

For example, C-NHEJ is initiated by the binding of the Ku70/80 (XRCC6/XRCC5) heterodimer to the broken DNA ends (Lieber, 2010). The large PIKK kinase DNA-PKcs then forms a complex with DNA and Ku70/80. The ring-shaped PIKK kinase is activated via autophosphorylation, which reduces its DNA binding capability allowing the two DNA-PKcs at either sites of the break to form a bridge, lining the two broken ends for subsequent ligation (DeFazio, Stansel et al., 2002, Sibanda et al., 2010, Spagnolo, Rivera-Calzada et al., 2006, Weterings, Verkaik et al., 2003). The broken ends are then processed by the DNA-PKcs interactor nuclease Artemis and the resulting gaps are filled by DNA polymerases DNA pol μ and DNA pol λ (Capp, Boudsocq et al., 2006, Mahajan, Nick McElhinny et al., 2002). Finally, the XRCC4-NHEJ1-DNA ligase 4 complex is recruited to re-ligate the broken ends (Junop, Modesti et al., 2000).

Although C-NHEJ is regarded as an error-prone repair pathway, it is clearly vital for maintaining genome stability, since defective C-NHEJ results in chromosomal translocations, increased accumulation of mutations, radiosensitivity, severe combined immunodeficiency (SCID), lymphomas and neuronal apoptosis (Chiang, Jacobsen et al., 2012, Difilippantonio, Zhu et al., 2000, Ferguson, Sekiguchi et al., 2000, Gao, Ferguson et al., 2000, Huertas, 2010, Robbiani, Bothmer et al., 2008, Zhu, Mills et al., 2002).

Some of these phenotypes may result from the switch to the “back-up” alt-EJ mechanism, when C-NHEJ is defective (Figure 1.5). Alt-EJ is a pathway that requires limited end-resection by CtIP and microhomology annealing (Roth, Porter et al., 1985, Thompson, Doyle et al., 2012). In normal cells, Ku70/80 inhibits alt-EJ and prevents this mutagenic pathway. In cells where C-NHEJ is defective, alt-EJ is used to prevent chromosome breaks. It is also hypothesised that PARP1, which plays a role in alt-EJ, competes with the Ku70/80 complex for binding to the broken DNA ends (Bryant, Schultz et al., 2005, Ceccaldi et al., 2015, Farmer, McCabe et al., 2005).

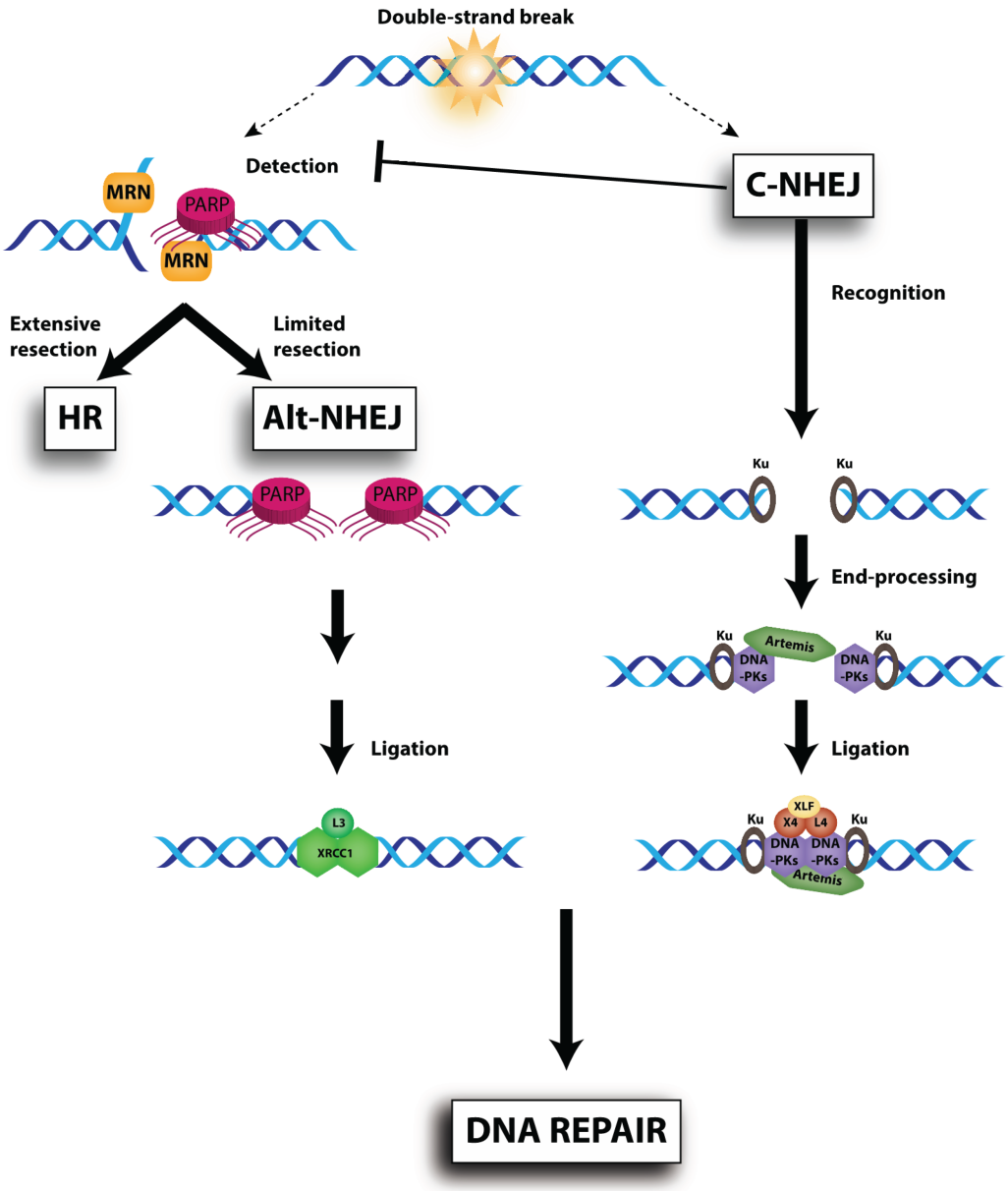

Figure 1.5:Schematic representation of NHEJ

Upon induction of double strand breaks, the cell recognises the DSB and depending on the level of resection, repairs it either via C-NHEJ through the recruitment of Ku70/80, DNA-PKcs and Artemis, followed by religation by XRCC4-DNA ligase 4, or via Alt-EJ through MRN and PARP1 binding followed by microhomology annealling and ligation by XRCC1 and DNA ligase 3. (Figure adapted from (Velic, Couturier et al., 2015).)

The mechanism of alt-EJ is not yet fully understood, since multiple redundant pathways can trigger the pathway. Yeast and mammalian studies have demonstrated the involvement of Mre11, RAD50 and the yeast homolog of CtIP, Sae2, in alt-EJ (McVey & Lee, 2008, Rass,

Grabarz et al., 2009, Xie, Kwok et al., 2009, Zhang & Jasin, 2011). DNA ligases I and III as well as the DNA ligase III cofactor XRCC1 have been implicated in alt-EJ (Boboila, Oksenych et al., 2012, Liang, Deng et al., 2008, Simsek, Brunet et al., 2011).

1.5.3. Homologous recombination

Homologous recombination can be separated into mechanistically distinct pathways, the most prominent being gene conversion (GC) and the most simple being single strand annealing (SSA). All types of HDR require the resection of broken DNA ends, and the presence of a homology template. HR has been extensively studied in yeast and homologs for all main components have been identified in mammalian cells. In yeast, the main HR protein is Rad52, although there is no homolog in *C.elegans* or *D. melanogaster* and it only plays a minor role in HR in mammalian cells, because it has been replaced by the ortholog BRCA2. In mammalian cells the critical component of GC, the error-free pathway of HR, is the recombinase RAD51, which is a DNA-dependent ATPase that forms a filament and promotes strand invasion (Holloman, 2011, Jensen, Carreira et al., 2010, Liu, Doty et al., 2010).

Independent of the HR pathway, the initial steps of repair are shared among GC, SDSA, SSA and break induced replication (BIR). The CtIP-BRCA1 complex replaces the RIF1-53BP1 complex, which effectively blocks resection from the broken DNA ends (Figure 1.6). In yeast the initial resection of some 100 nt is carried out by the Mre11-Rad50-Xrs2 complex in conjunction with the Sar2 protein. After this initial step the Sgs1-Top3-Rmi1-Dna2 complex unwinds the DNA via its helicase activity and removes short oligonucleotides from the 5’ end via its nuclease activity, while the Exo1 endonuclease removes mononucleotides. This process of extensive resection removes approximately 4 kb per hour in yeast (Cejka, Cannavo et al., 2010, Huertas, Cortes-Ledesma et al.,

2008, Mimitou & Symington, 2008, Niu, Chung et al., 2010, Zhu, Chung et al., 2008). Analogous components are present in mammalian cells, where the Sae2 ortholog CtIP and the Sgs1 ortholog BLM play a critical role in resection. While CtIP interacts with BRCA1, the BLM helicase interacts with DNA2 and EXO1, presumably performing the same role as their yeast counterparts (Nimonkar, Genschel et al., 2011, Sartori, Lukas et al., 2007, Sun, Lee et al., 2012). This process is tightly regulated in the absence of a homology template in G1. Many components of the HR machinery are dependent on CDK1 activity and EXO1 is inhibited by the Ku70/80 complex at the broken DNA ends thereby restricting HR in early stages of the cell cycle (Aylon, Liefshitz et al., 2004, Balestrini, Ristic et al., 2013, Barlow, Lisby et al., 2008, Ira, Pellicioli et al., 2004).

The single stranded DNA resulting from resection is rapidly coated by replication protein A (RPA) to prevent DNA degradation and formation of secondary structures. RPA is then displaced by RAD51 via the recombination mediator proteins BRCA2, RAD51B, RAD51C, RAD51D, XRCC2 and XRCC3 (Daley, Gaines et al., 2014, Morrical, 2015). This replacement of RPA by Rad51 takes some 10 minutes in yeast (Sugawara, Wang et al., 2003, Wang & Haber, 2004).

Studies using the Rad51 homolog RecA in *E. coli* have shown that binding of RecA stretches the DNA filament to about 1.5 times longer than the equivalent bases in B-form DNA. The RecA protein binds three nucleotides and stretches between these three nucleotide units to adopt a near B-form like structure, which presumably aids base-pairing with the homology template (Chen, Yang et al., 2008).

The RAD51 nucleofilament then goes on to search for a homology template in a process that can take up to 30-45 minutes in yeast (Hicks, Yamaguchi et al., 2011). Once it encounters homology sequence, the RAD51 nucleofilament invades the template strand in a process that is aided by the Snf2 family protein RAD54 (Hicks et al., 2011, Kiianitsa, Solinger et al., 2006, Sugawara et al., 2003). The 3’ RAD51

nucleofilament then base-pairs with the homology template creating a displacement loop (D-loop), which can be extended by the action of helicases or initiation of 3' DNA synthesis from the invading strand. This extension allows the other broken strand to anneal, forming a double Holliday junction (dHJ) (Figure 1.6). Once synthesis is complete, the dHJ can be resolved or dissolved resulting in either cross-over (CO) or non-crossover (NCO) between the invading and template strands (Wu & Hickson, 2003). Studies have shown that the frequency of both NCO and CO is roughly equal (Mitchel, Lehner et al., 2013).

The second HR pathway is SSA, which is RAD51 independent, and instead relies on RAD52 (Ivanov, Sugawara et al., 1996). SSA occurs after hyper-resection of the broken DNA ends when homology sequences on both sides of the DSB are exposed. This results in annealing of the exposed sequences, deleting the sequence between the repeats. After annealing of the homology sequences in a process requiring RAD52 and RAD59, the overhangs are cleaved off by the endonucleases XPF-ERCC1. The scaffold proteins Slx4 and Saw1 form a complex with the mis-match repair proteins Msh2 and Msh3 together with the XPF-ERCC1 homologs Rad1 and Rad10 to cleave of the ssDNA tails in yeast (Li et al., 2008, Sugawara, Paques et al., 1997, Toh, Sugawara et al., 2010). As SSA is deleting large portions of DNA, it is considered highly mutagenic and is tightly controlled in the cells through the regulation of end resection depending on 53BP1 (Ochs et al., 2016).

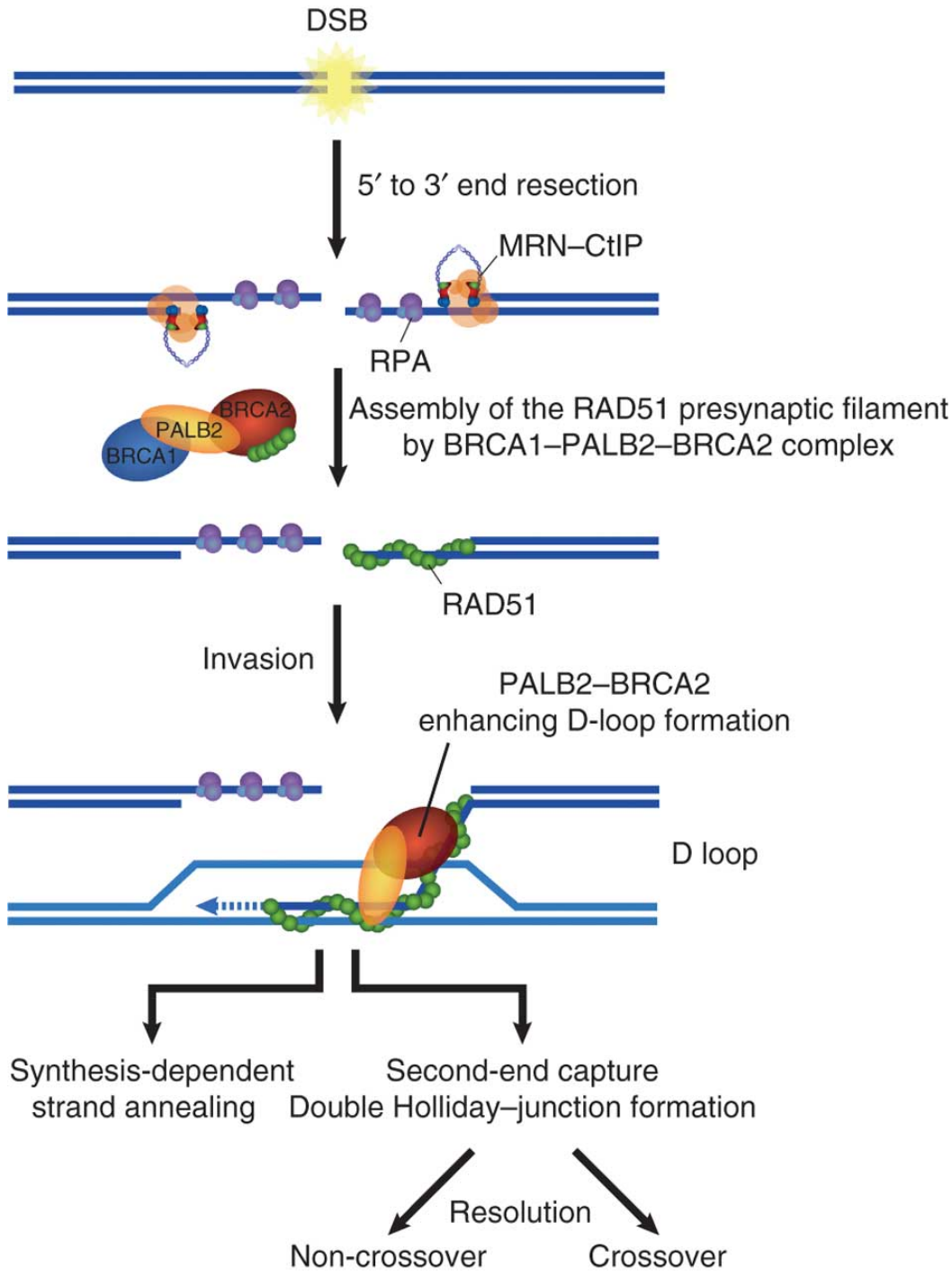

Figure 1.6: Schematic representation of HR

Upon DSB induction, CtIP initiates end resection. The resulting ssDNA is then coated by RPA, which is replaced by RAD51 aided by the BRCA2 complex. The RAD51 nucleofilament then invades the template strand, resulting in D-loop formation, which after DNA replication is complete, is resolved leading to cross-over or non-cross-over products. (Figure adapted from Buisson, Dion-Cote et al., 2010 .)

1.6. Aims and Objectives

In this study, we aim to characterise three RNA metabolism proteins, DGCR8, DDX3X and DDX17, in the DNA damage response. These proteins have been previously identified in a proteomics screen as potential new interacting partners of ATM or 53BP1. Here, we validate the interaction between DGCR8, DDX3X with ATM and DDX17 with 53BP1 in human cells and demonstrate their function in the DNA damage response. We show that DDX3X interacts with ATM and is required for efficient repair of DSBs by homologous recombination. Furthermore, we demonstrate that DGCR8 is a novel ATM interacting partner, with a role in the DNA damage response independent of its miRNA processor partner Drosha. Finally, we show that DDX17, an interacting partner of 53BP1 is partially required for DSB repair by both NHEJ and HR.

1.7. References

Adams MM, Carpenter PB (2006) Tying the loose ends together in DNA double strand break repair with 53BP1. Cell Div 1: 19

Alberg AJ, Ford JG, Samet JM, American College of Chest P (2007) Epidemiology of lung cancer: ACCP evidence-based clinical practice guidelines (2nd edition). Chest 132: 29S-55S

Alberts B, Johnson, A., Lewis, J., Raff, M., Roberts, K., Walter, P. (2008) Molecular Biology of the Cell. Garland Science London, NY,

Anderson L, Henderson C, Adachi Y (2001) Phosphorylation and rapid relocalization of 53BP1 to nuclear foci upon DNA damage. Mol Cell Biol 21: 1719-29

Aylon Y, Liefshitz B, Kupiec M (2004) The CDK regulates repair of double-strand breaks by homologous recombination during the cell cycle. EMBO J 23: 4868-75

Ayrapetov MK, Gursoy-Yuzugullu O, Xu C, Xu Y, Price BD (2014) DNA double-strand breaks promote methylation of histone H3 on lysine 9 and transient formation of repressive chromatin. Proc Natl Acad Sci U S A 111: 9169-74

Bakkenist CJ, Kastan MB (2003) DNA damage activates ATM through intermolecular autophosphorylation and dimer dissociation. Nature 421: 499-506

Balestrini A, Ristic D, Dionne I, Liu XZ, Wyman C, Wellinger RJ, Petrini JH (2013) The Ku heterodimer and the metabolism of single-ended DNA double-strand breaks. Cell Rep 3: 2033-45

Barlow C, Hirotsune S, Paylor R, Liyanage M, Eckhaus M, Collins F, Shiloh Y, Crawley JN, Ried T, Tagle D, Wynshaw-Boris A (1996) Atm-deficient mice: a paradigm of ataxia telangiectasia. Cell 86: 159-71

Barlow JH, Lisby M, Rothstein R (2008) Differential regulation of the cellular response to DNA double-strand breaks in G1. Mol Cell 30: 73-85

Bartek J, Bartkova J, Lukas J (1997) The retinoblastoma protein pathway in cell cycle control and cancer. Exp Cell Res 237: 1-6

Bartek J, Lukas C, Lukas J (2004) Checking on DNA damage in S phase. Nat Rev Mol Cell Biol 5: 792-804

Bartek J, Lukas J (2001) Mammalian G1- and S-phase checkpoints in response to DNA damage. Curr Opin Cell Biol 13: 738-47

Bartek J, Lukas J (2003) Chk1 and Chk2 kinases in checkpoint control and cancer. Cancer Cell 3: 421-9

Bennardo N, Cheng A, Huang N, Stark JM (2008) Alternative-NHEJ is a mechanistically distinct pathway of mammalian chromosome break repair. PLoS Genet 4: e1000110

Bensimon A, Schmidt A, Ziv Y, Elkon R, Wang SY, Chen DJ, Aebersold R, Shiloh Y (2010) ATM-dependent and -independent dynamics of the nuclear phosphoproteome after DNA damage. Sci Signal 3: rs3

Boboila C, Oksenych V, Gostissa M, Wang JH, Zha S, Zhang Y, Chai H, Lee CS, Jankovic M, Saez LM, Nussenzweig MC, McKinnon PJ, Alt FW, Schwer B (2012) Robust chromosomal DNA repair via alternative end-joining in the absence of X-ray repair cross-complementing protein 1 (XRCC1). Proc Natl Acad Sci U S A 109: 2473-8

Boder E (1975) Ataxia-telangiectasia: some historic, clinical and pathologic observations. Birth Defects Orig Artic Ser 11: 255-70

Bohgaki M, Bohgaki T, El Ghamrasni S, Srikumar T, Maire G, Panier S, Fradet-Turcotte A, Stewart GS, Raught B, Hakem A, Hakem R (2013) RNF168 ubiquitylates 53BP1 and controls its response to DNA double-strand breaks. Proc Natl Acad Sci U S A 110: 20982-7

Boutros R, Dozier C, Ducommun B (2006) The when and wheres of CDC25 phosphatases. Curr Opin Cell Biol 18: 185-91

Brandeis M, Rosewell I, Carrington M, Crompton T, Jacobs MA, Kirk J, Gannon J, Hunt T (1998) Cyclin B2-null mice develop normally and are fertile whereas cyclin B1-null mice die in utero. Proc Natl Acad Sci U S A 95: 4344-9

Brown EJ, Baltimore D (2000) ATR disruption leads to chromosomal fragmentation and early embryonic lethality. Genes Dev 14: 397-402

Bryant HE, Schultz N, Thomas HD, Parker KM, Flower D, Lopez E, Kyle S, Meuth M, Curtin NJ, Helleday T (2005) Specific killing of BRCA2-deficient tumours with inhibitors of poly(ADP-ribose) polymerase. Nature 434: 913-7

Buisson R, Dion-Cote AM, Coulombe Y, Launay H, Cai H, Stasiak AZ, Stasiak A, Xia B, Masson JY (2010) Cooperation of breast cancer proteins PALB2 and piccolo BRCA2 in stimulating homologous recombination. Nat Struct Mol Biol 17: 1247-54

Bulavin DV, Higashimoto Y, Popoff IJ, Gaarde WA, Basrur V, Potapova O, Appella E, Fornace AJ, Jr. (2001) Initiation of a G2/M checkpoint after ultraviolet radiation requires p38 kinase. Nature 411: 102-7

Callen E, Di Virgilio M, Kruhlak MJ, Nieto-Soler M, Wong N, Chen HT, Faryabi RB, Polato F, Santos M, Starnes LM, Wesemann DR, Lee JE, Tubbs A, Sleckman BP, Daniel JA, Ge K, Alt FW, Fernandez-Capetillo O, Nussenzweig MC, Nussenzweig A (2013) 53BP1 mediates productive and mutagenic DNA repair through distinct phosphoprotein interactions. Cell 153: 1266-80

Capp JP, Boudsocq F, Bertrand P, Laroche-Clary A, Pourquier P, Lopez BS, Cazaux C, Hoffmann JS, Canitrot Y (2006) The DNA polymerase lambda is required for the repair of non-compatible DNA double strand breaks by NHEJ in mammalian cells. Nucleic Acids Res 34: 2998-3007

Ceccaldi R, Liu JC, Amunugama R, Hajdu I, Primack B, Petalcorin MI, O'Connor KW, Konstantinopoulos PA, Elledge SJ, Boulton SJ, Yusufzai

T, D'Andrea AD (2015) Homologous-recombination-deficient tumours are dependent on Poltheta-mediated repair. Nature 518: 258-62

Cejka P, Cannavo E, Polaczek P, Masuda-Sasa T, Pokharel S, Campbell JL, Kowalczykowski SC (2010) DNA end resection by Dna2-Sgs1-RPA and its stimulation by Top3-Rmi1 and Mre11-Rad50-Xrs2. Nature 467: 112-6

Chapman JR, Barral P, Vannier JB, Borel V, Steger M, Tomas-Loba A, Sartori AA, Adams IR, Batista FD, Boulton SJ (2013) RIF1 is essential for 53BP1-dependent nonhomologous end joining and suppression of DNA double-strand break resection. Mol Cell 49: 858-71

Chen H, Lisby M, Symington LS (2013) RPA coordinates DNA end resection and prevents formation of DNA hairpins. Mol Cell 50: 589-600

Chen J, Stubbe J (2005) Bleomycins: towards better therapeutics. Nat Rev Cancer 5: 102-12

Chen Z, Yang H, Pavletich NP (2008) Mechanism of homologous recombination from the RecA-ssDNA/dsDNA structures. Nature 453: 489-4

Cheung-Ong K, Giaever G, Nislow C (2013) DNA-damaging agents in cancer chemotherapy: serendipity and chemical biology. Chem Biol 20: 648-59

Chiang C, Jacobsen JC, Ernst C, Hanscom C, Heilbut A, Blumenthal I, Mills RE, Kirby A, Lindgren AM, Rudiger SR, McLaughlan CJ, Bawden CS, Reid SJ, Faull RL, Snell RG, Hall IM, Shen Y, Ohsumi TK, Borowsky ML, Daly MJ et al. (2012) Complex reorganization and predominant non-homologous repair following chromosomal breakage in karyotypically balanced germline rearrangements and transgenic integration. Nat Genet 44: 390-7, S1

Chini CC, Chen J (2004) Claspin, a regulator of Chk1 in DNA replication stress pathway. DNA Repair (Amst) 3: 1033-7

Ciccia A, Elledge SJ (2010) The DNA damage response: making it safe to play with knives. Mol Cell 40: 179-204

Cortez D, Guntuku S, Qin J, Elledge SJ (2001) ATR and ATRIP: partners in checkpoint signaling. Science 294: 1713-6

Cortez D, Wang Y, Qin J, Elledge SJ (1999) Requirement of ATM-dependent phosphorylation of brca1 in the DNA damage response to double-strand breaks. Science 286: 1162-6

Craig A, Scott M, Burch L, Smith G, Ball K, Hupp T (2003) Allosteric effects mediate CHK2 phosphorylation of the p53 transactivation domain. EMBO Rep 4: 787-92

Daley JM, Gaines WA, Kwon Y, Sung P (2014) Regulation of DNA pairing in homologous recombination. Cold Spring Harb Perspect Biol 6: a017954

Dar I, Biton S, Shiloh Y, Barzilai A (2006) Analysis of the ataxia telangiectasia mutated-mediated DNA damage response in murine cerebellar neurons. J Neurosci 26: 7767-74

de Klein A, Muijtjens M, van Os R, Verhoeven Y, Smit B, Carr AM, Lehmann AR, Hoeijmakers JH (2000) Targeted disruption of the cell-cycle checkpoint gene ATR leads to early embryonic lethality in mice. Curr Biol 10: 479-82

DeFazio LG, Stansel RM, Griffith JD, Chu G (2002) Synapsis of DNA ends by DNA-dependent protein kinase. EMBO J 21: 3192-200

Deng SK, Gibb B, de Almeida MJ, Greene EC, Symington LS (2014) RPA antagonizes microhomology-mediated repair of DNA double-strand breaks. Nat Struct Mol Biol 21: 405-12

Di Virgilio M, Callen E, Yamane A, Zhang W, Jankovic M, Gitlin AD, Feldhahn N, Resch W, Oliveira TY, Chait BT, Nussenzweig A, Casellas R, Robbiani DF, Nussenzweig MC (2013) Rif1 prevents resection of DNA breaks and promotes immunoglobulin class switching. Science 339: 711-5

Difilippantonio MJ, Zhu J, Chen HT, Meffre E, Nussenzweig MC, Max EE, Ried T, Nussenzweig A (2000) DNA repair protein Ku80 suppresses chromosomal aberrations and malignant transformation. Nature 404: 510-4

Difilippantonio S, Gapud E, Wong N, Huang CY, Mahowald G, Chen HT, Kruhlak MJ, Callen E, Livak F, Nussenzweig MC, Sleckman BP, Nussenzweig A (2008) 53BP1 facilitates long-range DNA end-joining during V(D)J recombination. Nature 456: 529-33

Dimitrova N, Chen YC, Spector DL, de Lange T (2008) 53BP1 promotes non-homologous end joining of telomeres by increasing chromatin mobility. Nature 456: 524-8

Dynlacht BD, Flores O, Lees JA, Harlow E (1994) Differential regulation of E2F transactivation by cyclin/cdk2 complexes. Genes Dev 8: 1772-86

Easton DF (1994) Cancer risks in A-T heterozygotes. Int J Radiat Biol 66: S177-82

Ellison V, Stillman B (2003) Biochemical characterization of DNA damage checkpoint complexes: clamp loader and clamp complexes with specificity for 5' recessed DNA. PLoS Biol 1: E33

Escribano-Diaz C, Orthwein A, Fradet-Turcotte A, Xing M, Young JT, Tkac J, Cook MA, Rosebrock AP, Munro M, Canny MD, Xu D, Durocher D (2013) A cell cycle-dependent regulatory circuit composed of 53BP1-RIF1 and BRCA1-CtIP controls DNA repair pathway choice. Mol Cell 49: 872-83

Fabbro M, Savage K, Hobson K, Deans AJ, Powell SN, McArthur GA, Khanna KK (2004) BRCA1-BARD1 complexes are required for p53Ser-15 phosphorylation and a G1/S arrest following ionizing radiation-induced DNA damage. J Biol Chem 279: 31251-8

Falck J, Coates J, Jackson SP (2005) Conserved modes of recruitment of ATM, ATR and DNA-PKcs to sites of DNA damage. Nature 434: 605-11

Falck J, Petrini JH, Williams BR, Lukas J, Bartek J (2002) The DNA damage-dependent intra-S phase checkpoint is regulated by parallel pathways. Nat Genet 30: 290-4

Farmer H, McCabe N, Lord CJ, Tutt AN, Johnson DA, Richardson TB, Santarosa M, Dillon KJ, Hickson I, Knights C, Martin NM, Jackson SP, Smith GC, Ashworth A (2005) Targeting the DNA repair defect in BRCA mutant cells as a therapeutic strategy. Nature 434: 917-21

Feng L, Fong KW, Wang J, Wang W, Chen J (2013) RIF1 counteracts BRCA1-mediated end resection during DNA repair. J Biol Chem 288: 11135-43

Feng L, Huang J, Chen J (2009) MERIT40 facilitates BRCA1 localization and DNA damage repair. Genes Dev 23: 719-28

Ferguson DO, Sekiguchi JM, Chang S, Frank KM, Gao Y, DePinho RA, Alt FW (2000) The nonhomologous end-joining pathway of DNA repair is required for genomic stability and the suppression of translocations. Proc Natl Acad Sci U S A 97: 6630-3

Fernandez-Capetillo O, Lee A, Nussenzweig M, Nussenzweig A (2004) H2AX: the histone guardian of the genome. DNA Repair (Amst) 3: 959-67

Ferrari S (2006) Protein kinases controlling the onset of mitosis. Cell Mol Life Sci 63: 781-95

Fradet-Turcotte A, Canny MD, Escribano-Diaz C, Orthwein A, Leung CC, Huang H, Landry MC, Kitevski-LeBlanc J, Noordermeer SM, Sicheri F, Durocher D (2013) 53BP1 is a reader of the DNA-damage-induced H2A Lys 15 ubiquitin mark. Nature 499: 50-4

Funabiki H, Hagan I, Uzawa S, Yanagida M (1993) Cell cycle-dependent specific positioning and clustering of centromeres and telomeres in fission yeast. J Cell Biol 121: 961-76

Gao Y, Ferguson DO, Xie W, Manis JP, Sekiguchi J, Frank KM, Chaudhuri J, Horner J, DePinho RA, Alt FW (2000) Interplay of p53 and DNA-repair protein XRCC4 in tumorigenesis, genomic stability and development. Nature 404: 897-900

Gatei M, Young D, Cerosaletti KM, Desai-Mehta A, Spring K, Kozlov S, Lavin MF, Gatti RA, Concannon P, Khanna K (2000) ATM-dependent phosphorylation of nibrin in response to radiation exposure. Nat Genet 25: 115-9

Geng Y, Lee YM, Welcker M, Swanger J, Zagozdzon A, Winer JD, Roberts JM, Kaldis P, Clurman BE, Sicinski P (2007) Kinase-independent function of cyclin E. Mol Cell 25: 127-39

Geng Y, Whoriskey W, Park MY, Bronson RT, Medema RH, Li T, Weinberg RA, Sicinski P (1999) Rescue of cyclin D1 deficiency by knockin cyclin E. Cell 97: 767-77

Gorodetsky E, Calkins S, Ahn J, Brooks PJ (2007) ATM, the Mre11/Rad50/Nbs1 complex, and topoisomerase I are concentrated in the nucleus of Purkinje neurons in the juvenile human brain. DNA Repair (Amst) 6: 1698-707

Hagting A, Karlsson C, Clute P, Jackman M, Pines J (1998) MPF localization is controlled by nuclear export. EMBO J 17: 4127-38

Hall JM, Lee MK, Newman B, Morrow JE, Anderson LA, Huey B, King MC (1990) Linkage of early-onset familial breast cancer to chromosome 17q21. Science 250: 1684-9

Harper JW, Elledge SJ (2007) The DNA damage response: ten years after. Mol Cell 28: 739-45

Hartwell LH, Weinert TA (1989) Checkpoints: controls that ensure the order of cell cycle events. Science 246: 629-34

Hicks WM, Yamaguchi M, Haber JE (2011) Real-time analysis of double-strand DNA break repair by homologous recombination. Proc Natl Acad Sci U S A 108: 3108-15

Hoeijmakers JH (2009) DNA damage, aging, and cancer. N Engl J Med 361: 1475-85

Holloman WK (2011) Unraveling the mechanism of BRCA2 in homologous recombination. Nat Struct Mol Biol 18: 748-54

Huen MS, Huang J, Leung JW, Sy SM, Leung KM, Ching YP, Tsao SW, Chen J (2010) Regulation of chromatin architecture by the PWWP domain-containing DNA damage-responsive factor EXPAND1/MUM1. Mol Cell 37: 854-64

Huertas P (2010) DNA resection in eukaryotes: deciding how to fix the break. Nat Struct Mol Biol 17: 11-6

Huertas P, Cortes-Ledesma F, Sartori AA, Aguilera A, Jackson SP (2008) CDK targets Sae2 to control DNA-end resection and homologous recombination. Nature 455: 689-92

Huertas P, Jackson SP (2009) Human CtIP mediates cell cycle control of DNA end resection and double strand break repair. J Biol Chem 284: 9558-65

Ira G, Pellicioli A, Balijja A, Wang X, Fiorani S, Carotenuto W, Liberi G, Bressan D, Wan L, Hollingsworth NM, Haber JE, Foiani M (2004) DNA end resection, homologous recombination and DNA damage checkpoint activation require CDK1. Nature 431: 1011-7

Islam MN, Paquet N, Fox D, 3rd, Dray E, Zheng XF, Klein H, Sung P, Wang W (2012) A variant of the breast cancer type 2 susceptibility protein (BRC) repeat is essential for the RECQL5 helicase to interact with RAD51 recombinase for genome stabilization. J Biol Chem 287: 23808-18

Ivanov EL, Sugawara N, Fishman-Lobell J, Haber JE (1996) Genetic requirements for the single-strand annealing pathway of double-strand break repair in Saccharomyces cerevisiae. Genetics 142: 693-704

Iwabuchi K, Bartel PL, Li B, Marraccino R, Fields S (1994) Two cellular proteins that bind to wild-type but not mutant p53. Proc Natl Acad Sci U S A 91: 6098-102

Iwabuchi K, Li B, Massa HF, Trask BJ, Date T, Fields S (1998) Stimulation of p53-mediated transcriptional activation by the p53-binding proteins, 53BP1 and 53BP2. J Biol Chem 273: 26061-8

Jensen RB, Carreira A, Kowalczykowski SC (2010) Purified human BRCA2 stimulates RAD51-mediated recombination. Nature 467: 678-83

Junop MS, Modesti M, Guarne A, Ghirlando R, Gellert M, Yang W (2000) Crystal structure of the Xrcc4 DNA repair protein and implications for end joining. EMBO J 19: 5962-70

Kamileri I, Karakasilioti I, Sideri A, Kosteas T, Tatarakis A, Talianidis I, Garinis GA (2012) Defective transcription initiation causes postnatal growth failure in a mouse model of nucleotide excision repair (NER) progeria. Proc Natl Acad Sci U S A 109: 2995-3000

Kastan MB, Bartek J (2004) Cell-cycle checkpoints and cancer. Nature 432: 316-23

Kastan MB, Lim DS (2000) The many substrates and functions of ATM. Nat Rev Mol Cell Biol 1: 179-86

Kiianitsa K, Solinger JA, Heyer WD (2006) Terminal association of Rad54 protein with the Rad51-dsDNA filament. Proc Natl Acad Sci U S A 103: 9767-72

Kim H, Chen J, Yu X (2007) Ubiquitin-binding protein RAP80 mediates BRCA1-dependent DNA damage response. Science 316: 1202-5

Kim H, Huang J, Chen J (2007) CCDC98 is a BRCA1-BRCT domain-binding protein involved in the DNA damage response. Nat Struct Mol Biol 14: 710-5

Kim ST, Xu B, Kastan MB (2002) Involvement of the cohesin protein, Smc1, in Atm-dependent and independent responses to DNA damage. Genes Dev 16: 560-70

Kimura K, Hirano M, Kobayashi R, Hirano T (1998) Phosphorylation and activation of 13S condensin by Cdc2 in vitro. Science 282: 487-90

Kitagawa R, Bakkenist CJ, McKinnon PJ, Kastan MB (2004) Phosphorylation of SMC1 is a critical downstream event in the ATM-NBS1-BRCA1 pathway. Genes Dev 18: 1423-38

Kozar K, Ciemerych MA, Rebel VI, Shigematsu H, Zagozdzon A, Sicinska E, Geng Y, Yu Q, Bhattacharya S, Bronson RT, Akashi K, Sicinski P (2004) Mouse development and cell proliferation in the absence of D-cyclins. Cell 118: 477-91

Lee JH, Paull TT (2007) Activation and regulation of ATM kinase activity in response to DNA double-strand breaks. Oncogene 26: 7741-8

Lee K, Lee SE (2007) Saccharomyces cerevisiae Sae2- and Tel1-dependent single-strand DNA formation at DNA break promotes microhomology-mediated end joining. Genetics 176: 2003-14

Lempiainen H, Halazonetis TD (2009) Emerging common themes in regulation of PIKKs and PI3Ks. EMBO J 28: 3067-73

Li F, Dong J, Pan X, Oum JH, Boeke JD, Lee SE (2008) Microarray-based genetic screen defines SAW1, a gene required for Rad1/Rad10-dependent processing of recombination intermediates. Mol Cell 30: 325-35

Liang L, Deng L, Nguyen SC, Zhao X, Maulion CD, Shao C, Tischfield JA (2008) Human DNA ligases I and III, but not ligase IV, are required for microhomology-mediated end joining of DNA double-strand breaks. Nucleic Acids Res 36: 3297-310

Lieber MR (2010) The mechanism of double-strand DNA break repair by the nonhomologous DNA end-joining pathway. Annu Rev Biochem 79: 181-211

Liu J, Doty T, Gibson B, Heyer WD (2010) Human BRCA2 protein promotes RAD51 filament formation on RPA-covered single-stranded DNA. Nat Struct Mol Biol 17: 1260-2

Liu S, Shiotani B, Lahiri M, Marechal A, Tse A, Leung CC, Glover JN, Yang XH, Zou L (2011) ATR autophosphorylation as a molecular switch for checkpoint activation. Mol Cell 43: 192-202

Liu Z, Wu J, Yu X (2007) CCDC98 targets BRCA1 to DNA damage sites. Nat Struct Mol Biol 14: 716-20

Llorca O, Rivera-Calzada A, Grantham J, Willison KR (2003) Electron microscopy and 3D reconstructions reveal that human ATM kinase uses an arm-like domain to clamp around double-stranded DNA. Oncogene 22: 3867-74

Lou Z, Minter-Dykhouse K, Franco S, Gostissa M, Rivera MA, Celeste A, Manis JP, van Deursen J, Nussenzweig A, Paull TT, Alt FW, Chen J (2006) MDC1 maintains genomic stability by participating in the amplification of ATM-dependent DNA damage signals. Mol Cell 21: 187-200

Lovejoy CA, Cortez D (2009) Common mechanisms of PIKK regulation. DNA Repair (Amst) 8: 1004-8

Mahajan KN, Nick McElhinny SA, Mitchell BS, Ramsden DA (2002) Association of DNA polymerase mu (pol mu) with Ku and ligase IV: role for pol mu in end-joining double-strand break repair. Mol Cell Biol 22: 5194-202

Mailand N, Podtelejnikov AV, Groth A, Mann M, Bartek J, Lukas J (2002) Regulation of G(2)/M events by Cdc25A through phosphorylation-dependent modulation of its stability. EMBO J 21: 5911-20

Malumbres M, Barbacid M (2001) To cycle or not to cycle: a critical decision in cancer. Nat Rev Cancer 1: 222-31

Malumbres M, Barbacid M (2005) Mammalian cyclin-dependent kinases. Trends Biochem Sci 30: 630-41

Malumbres M, Sotillo R, Santamaria D, Galan J, Cerezo A, Ortega S, Dubus P, Barbacid M (2004) Mammalian cells cycle without the D-type cyclin-dependent kinases Cdk4 and Cdk6. Cell 118: 493-504

Manis JP, Morales JC, Xia Z, Kutok JL, Alt FW, Carpenter PB (2004) 53BP1 links DNA damage-response pathways to immunoglobulin heavy chain class-switch recombination. Nat Immunol 5: 481-7

Manke IA, Lowery DM, Nguyen A, Yaffe MB (2003) BRCT repeats as phosphopeptide-binding modules involved in protein targeting. Science 302: 636-9

Marechal A, Zou L (2013) DNA damage sensing by the ATM and ATR kinases. Cold Spring Harb Perspect Biol 5

Martin LM, Marples B, Coffey M, Lawler M, Lynch TH, Hollywood D, Marignol L (2010) DNA mismatch repair and the DNA damage response to ionizing radiation: making sense of apparently conflicting data. Cancer Treat Rev 36: 518-27

Martin RG, Stein S (1976) Resting state in normal and simian virus 40 transformed Chinese hamster lung cells. Proc Natl Acad Sci U S A 73: 1655-9

Massague J (2004) G1 cell-cycle control and cancer. Nature 432: 298-306

Matsuoka S, Ballif BA, Smogorzewska A, McDonald ER, 3rd, Hurov KE, Luo J, Bakalarski CE, Zhao Z, Solimini N, Lerenthal Y, Shiloh Y, Gygi SP, Elledge SJ (2007) ATM and ATR substrate analysis reveals extensive protein networks responsive to DNA damage. Science 316: 1160-6

Matsuoka S, Huang M, Elledge SJ (1998) Linkage of ATM to cell cycle regulation by the Chk2 protein kinase. Science 282: 1893-7

Mattiroli F, Vissers JH, van Dijk WJ, Ikpa P, Citterio E, Vermeulen W, Marteijn JA, Sixma TK (2012) RNF168 ubiquitinates K13-15 on H2A/H2AX to drive DNA damage signaling. Cell 150: 1182-95

McKinnon PJ (2004) ATM and ataxia telangiectasia. EMBO Rep 5: 772-6

McVey M, Lee SE (2008) MMEJ repair of double-strand breaks (director's cut): deleted sequences and alternative endings. Trends Genet 24: 529-38

Meier A, Fiegler H, Munoz P, Ellis P, Rigler D, Langford C, Blasco MA, Carter N, Jackson SP (2007) Spreading of mammalian DNA-damage response factors studied by ChIP-chip at damaged telomeres. EMBO J 26: 2707-18

Miki Y, Swensen J, Shattuck-Eidens D, Futreal PA, Harshman K, Tavtigian S, Liu Q, Cochran C, Bennett LM, Ding W, et al. (1994) A strong candidate for the breast and ovarian cancer susceptibility gene BRCA1. Science 266: 66-71

Mimitou EP, Symington LS (2008) Sae2, Exo1 and Sgs1 collaborate in DNA double-strand break processing. Nature 455: 770-4

Mitchel K, Lehner K, Jinks-Robertson S (2013) Heteroduplex DNA position defines the roles of the Sgs1, Srs2, and Mph1 helicases in promoting distinct recombination outcomes. PLoS Genet 9: e1003340

Mochan TA, Venere M, DiTullio RA, Jr., Halazonetis TD (2004) 53BP1, an activator of ATM in response to DNA damage. DNA Repair (Amst) 3: 945-52

Moldovan GL, Dejsuphong D, Petalcorin MI, Hofmann K, Takeda S, Boulton SJ, D'Andrea AD (2012) Inhibition of homologous recombination by the PCNA-interacting protein PARI. Mol Cell 45: 75-86

Mordes DA, Cortez D (2008) Activation of ATR and related PIKKs. Cell Cycle 7: 2809-12

Morgan DO (1997) Cyclin-dependent kinases: engines, clocks, and microprocessors. Annu Rev Cell Dev Biol 13: 261-91

Morrical SW (2015) DNA-pairing and annealing processes in homologous recombination and homology-directed repair. Cold Spring Harb Perspect Biol 7: a016444

Murphy M, Stinnakre MG, Senamaud-Beaufort C, Winston NJ, Sweeney C, Kubelka M, Carrington M, Brechot C, Sobczak-Thepot J (1997) Delayed early embryonic lethality following disruption of the murine cyclin A2 gene. Nat Genet 15: 83-6

Nakanishi K, Taniguchi T, Ranganathan V, New HV, Moreau LA, Stotsky M, Mathew CG, Kastan MB, Weaver DT, D'Andrea AD (2002) Interaction of FANCD2 and NBS1 in the DNA damage response. Nat Cell Biol 4: 913-20

Nakayama KI, Nakayama K (2006) Ubiquitin ligases: cell-cycle control and cancer. Nat Rev Cancer 6: 369-81

Nam EA, Cortez D (2011) ATR signalling: more than meeting at the fork. Biochem J 436: 527-36

Nimonkar AV, Genschel J, Kinoshita E, Polaczek P, Campbell JL, Wyman C, Modrich P, Kowalczykowski SC (2011) BLM-DNA2-RPA-MRN and EXO1-BLM-RPA-MRN constitute two DNA end resection machineries for human DNA break repair. Genes Dev 25: 350-62

Niu H, Chung WH, Zhu Z, Kwon Y, Zhao W, Chi P, Prakash R, Seong C, Liu D, Lu L, Ira G, Sung P (2010) Mechanism of the ATP-dependent DNA end-resection machinery from Saccharomyces cerevisiae. Nature 467: 108-11

Nyberg KA, Michelson RJ, Putnam CW, Weinert TA (2002) Toward maintaining the genome: DNA damage and replication checkpoints. Annu Rev Genet 36: 617-56

O'Connor KW, Dejsuphong D, Park E, Nicolae CM, Kimmelman AC, D'Andrea AD, Moldovan GL (2013) PARI overexpression promotes genomic instability and pancreatic tumorigenesis. Cancer Res 73: 2529-39

O'Driscoll M, Gennery AR, Seidel J, Concannon P, Jeggo PA (2004) An overview of three new disorders associated with genetic instability: LIG4 syndrome, RS-SCID and ATR-Seckel syndrome. DNA Repair (Amst) 3: 1227-35

O'Driscoll M, Ruiz-Perez VL, Woods CG, Jeggo PA, Goodship JA (2003) A splicing mutation affecting expression of ataxia-telangiectasia and Rad3-related protein (ATR) results in Seckel syndrome. Nat Genet 33: 497-501

Ochs F, Somyajit K, Altmeyer M, Rask MB, Lukas J, Lukas C (2016) 53BP1 fosters fidelity of homology-directed DNA repair. Nat Struct Mol Biol 23: 714-21

Ogi T, Walker S, Stiff T, Hobson E, Limsirichaikul S, Carpenter G, Prescott K, Suri M, Byrd PJ, Matsuse M, Mitsutake N, Nakazawa Y, Vasudevan P, Barrow M, Stewart GS, Taylor AM, O'Driscoll M, Jeggo PA (2012) Identification of the first ATRIP-deficient patient and novel mutations in ATR define a clinical spectrum for ATR-ATRIP Seckel Syndrome. PLoS Genet 8: e1002945

Paliwal S, Kanagaraj R, Sturzenegger A, Burdova K, Janscak P (2014) Human RECQ5 helicase promotes repair of DNA double-strand breaks by synthesis-dependent strand annealing. Nucleic Acids Res 42: 2380-90

Panier S, Boulton SJ (2014) Double-strand break repair: 53BP1 comes into focus. Nat Rev Mol Cell Biol 15: 7-18

Panier S, Durocher D (2009) Regulatory ubiquitylation in response to DNA double-strand breaks. DNA Repair (Amst) 8: 436-43

Perry J, Kleckner N (2003) The ATRs, ATMs, and TORs are giant HEAT repeat proteins. Cell 112: 151-5

Peter M, Heitlinger E, Haner M, Aebi U, Nigg EA (1991) Disassembly of in vitro formed lamin head-to-tail polymers by CDC2 kinase. EMBO J 10: 1535-44

Peters JM (2006) The anaphase promoting complex/cyclosome: a machine designed to destroy. Nat Rev Mol Cell Biol 7: 644-56

Potapova TA, Daum JR, Pittman BD, Hudson JR, Jones TN, Satinover DL, Stukenberg PT, Gorbsky GJ (2006) The reversibility of mitotic exit in vertebrate cells. Nature 440: 954-8

Queralt E, Uhlmann F (2008) Cdk-counteracting phosphatases unlock mitotic exit. Curr Opin Cell Biol 20: 661-8

Rappold I, Iwabuchi K, Date T, Chen J (2001) Tumor suppressor p53 binding protein 1 (53BP1) is involved in DNA damage-signaling pathways. J Cell Biol 153: 613-20

Rass E, Grabarz A, Plo I, Gautier J, Bertrand P, Lopez BS (2009) Role of Mre11 in chromosomal nonhomologous end joining in mammalian cells. Nat Struct Mol Biol 16: 819-24

Reina-San-Martin B, Chen J, Nussenzweig A, Nussenzweig MC (2007) Enhanced intra-switch region recombination during immunoglobulin class switch recombination in 53BP1-/- B cells. Eur J Immunol 37: 235-9

Robbiani DF, Bothmer A, Callen E, Reina-San-Martin B, Dorsett Y, Difilippantonio S, Bolland DJ, Chen HT, Corcoran AE, Nussenzweig A, Nussenzweig MC (2008) AID is required for the chromosomal breaks in c-myc that lead to c-myc/IgH translocations. Cell 135: 1028-38

Rodriguez M, Yu X, Chen J, Songyang Z (2003) Phosphopeptide binding specificities of BRCA1 COOH-terminal (BRCT) domains. J Biol Chem 278: 52914-8

Rogakou EP, Boon C, Redon C, Bonner WM (1999) Megabase chromatin domains involved in DNA double-strand breaks in vivo. J Cell Biol 146: 905-16

Roth DB, Porter TN, Wilson JH (1985) Mechanisms of nonhomologous recombination in mammalian cells. Mol Cell Biol 5: 2599-607

Russell P, Nurse P (1987) Negative regulation of mitosis by wee1+, a gene encoding a protein kinase homolog. Cell 49: 559-67

Santamaria D, Barriere C, Cerqueira A, Hunt S, Tardy C, Newton K, Caceres JF, Dubus P, Malumbres M, Barbacid M (2007) Cdk1 is sufficient to drive the mammalian cell cycle. Nature 448: 811-5

Sartori AA, Lukas C, Coates J, Mistrik M, Fu S, Bartek J, Baer R, Lukas J, Jackson SP (2007) Human CtIP promotes DNA end resection. Nature 450: 509-14

Satyanarayana A, Berthet C, Lopez-Molina J, Coppola V, Tessarollo L, Kaldis P (2008) Genetic substitution of Cdk1 by Cdk2 leads to embryonic lethality and loss of meiotic function of Cdk2. Development 135: 3389-400

Savic V, Yin B, Maas NL, Bredemeyer AL, Carpenter AC, Helmink BA, Yang-Iott KS, Sleckman BP, Bassing CH (2009) Formation of dynamic gamma-H2AX domains along broken DNA strands is distinctly regulated by ATM and MDC1 and dependent upon H2AX densities in chromatin. Mol Cell 34: 298-310

Saville MK, Watson RJ (1998) The cell-cycle regulated transcription factor B-Myb is phosphorylated by cyclin A/Cdk2 at sites that enhance its transactivation properties. Oncogene 17: 2679-89

Schultz LB, Chehab NH, Malikzay A, Halazonetis TD (2000) p53 binding protein 1 (53BP1) is an early participant in the cellular response to DNA double-strand breaks. J Cell Biol 151: 1381-90

Schwendener S, Raynard S, Paliwal S, Cheng A, Kanagaraj R, Shevelev I, Stark JM, Sung P, Janscak P (2010) Physical interaction of RECQ5 helicase with RAD51 facilitates its anti-recombinase activity. J Biol Chem 285: 15739-45

Scully R, Chen J, Ochs RL, Keegan K, Hoekstra M, Feunteun J, Livingston DM (1997) Dynamic changes of BRCA1 subnuclear location and phosphorylation state are initiated by DNA damage. Cell 90: 425-35

Shao G, Patterson-Fortin J, Messick TE, Feng D, Shanbhag N, Wang Y, Greenberg RA (2009) MERIT40 controls BRCA1-Rap80 complex integrity and recruitment to DNA double-strand breaks. Genes Dev 23: 740-54

Sherr CJ (2000) The Pezcoller lecture: cancer cell cycles revisited. Cancer Res 60: 3689-95

Sherr CJ, McCormick F (2002) The RB and p53 pathways in cancer. Cancer Cell 2: 103-12

Shiloh Y (2003) ATM and related protein kinases: safeguarding genome integrity. Nat Rev Cancer 3: 155-68

Shiotani B, Zou L (2009) Single-stranded DNA orchestrates an ATM-to-ATR switch at DNA breaks. Mol Cell 33: 547-58

Sibanda BL, Chirgadze DY, Blundell TL (2010) Crystal structure of DNA-PKcs reveals a large open-ring cradle comprised of HEAT repeats. Nature 463: 118-21

Silverman J, Takai H, Buonomo SB, Eisenhaber F, de Lange T (2004) Human Rif1, ortholog of a yeast telomeric protein, is regulated by ATM and 53BP1 and functions in the S-phase checkpoint. Genes Dev 18: 2108-19

Simsek D, Brunet E, Wong SY, Katyal S, Gao Y, McKinnon PJ, Lou J, Zhang L, Li J, Rebar EJ, Gregory PD, Holmes MC, Jasin M (2011) DNA ligase III promotes alternative nonhomologous end-joining during chromosomal translocation formation. PLoS Genet 7: e1002080

Smolka MB, Albuquerque CP, Chen SH, Zhou H (2007) Proteome-wide identification of in vivo targets of DNA damage checkpoint kinases. Proc Natl Acad Sci U S A 104: 10364-9

So S, Davis AJ, Chen DJ (2009) Autophosphorylation at serine 1981 stabilizes ATM at DNA damage sites. J Cell Biol 187: 977-90

Sobhian B, Shao G, Lilli DR, Culhane AC, Moreau LA, Xia B, Livingston DM, Greenberg RA (2007) RAP80 targets BRCA1 to specific ubiquitin structures at DNA damage sites. Science 316: 1198-202

Sorensen CS, Hansen LT, Dziegielewski J, Syljuasen RG, Lundin C, Bartek J, Helleday T (2005) The cell-cycle checkpoint kinase Chk1 is required for mammalian homologous recombination repair. Nat Cell Biol 7: 195-201

Spagnolo L, Rivera-Calzada A, Pearl LH, Llorca O (2006) Three-dimensional structure of the human DNA-PKcs/Ku70/Ku80 complex assembled on DNA and its implications for DNA DSB repair. Mol Cell 22: 511-9

Stewart GS (2012) The demise of a TUDOR under stress opens a chromatin link to 53BP1. EMBO J 31: 1847-9

Stewart GS, Panier S, Townsend K, Al-Hakim AK, Kolas NK, Miller ES, Nakada S, Ylanko J, Olivarius S, Mendez M, Oldreive C, Wildenhain J, Tagliaferro A, Pelletier L, Taubenheim N, Durandy A, Byrd PJ, Stankovic T, Taylor AM, Durocher D (2009) The RIDDLE syndrome protein

mediates a ubiquitin-dependent signaling cascade at sites of DNA damage. Cell 136: 420-34

Stokes MP, Rush J, Macneill J, Ren JM, Sprott K, Nardone J, Yang V, Beausoleil SA, Gygi SP, Livingstone M, Zhang H, Polakiewicz RD, Comb MJ (2007) Profiling of UV-induced ATM/ATR signaling pathways. Proc Natl Acad Sci U S A 104: 19855-60

Stucki M, Clapperton JA, Mohammad D, Yaffe MB, Smerdon SJ, Jackson SP (2005) MDC1 directly binds phosphorylated histone H2AX to regulate cellular responses to DNA double-strand breaks. Cell 123: 1213-26

Stucki M, Jackson SP (2004) MDC1/NFBD1: a key regulator of the DNA damage response in higher eukaryotes. DNA Repair (Amst) 3: 953-7

Sturzenegger A, Burdova K, Kanagaraj R, Levikova M, Pinto C, Cejka P, Janscak P (2014) DNA2 cooperates with the WRN and BLM RecQ helicases to mediate long-range DNA end resection in human cells. J Biol Chem 289: 27314-26

Sugawara N, Paques F, Colaiacovo M, Haber JE (1997) Role of Saccharomyces cerevisiae Msh2 and Msh3 repair proteins in double-strand break-induced recombination. Proc Natl Acad Sci U S A 94: 9214-9

Sugawara N, Wang X, Haber JE (2003) In vivo roles of Rad52, Rad54, and Rad55 proteins in Rad51-mediated recombination. Mol Cell 12: 209-19

Sun J, Lee KJ, Davis AJ, Chen DJ (2012) Human Ku70/80 protein blocks exonuclease 1-mediated DNA resection in the presence of human Mre11 or Mre11/Rad50 protein complex. J Biol Chem 287: 4936-45

Sun Y, Jiang X, Chen S, Fernandes N, Price BD (2005) A role for the Tip60 histone acetyltransferase in the acetylation and activation of ATM. Proc Natl Acad Sci U S A 102: 13182-7

Sun Y, Jiang X, Xu Y, Ayrapetov MK, Moreau LA, Whetstine JR, Price BD (2009) Histone H3 methylation links DNA damage detection to activation of the tumour suppressor Tip60. Nat Cell Biol 11: 1376-82

Sun Y, Xu Y, Roy K, Price BD (2007) DNA damage-induced acetylation of lysine 3016 of ATM activates ATM kinase activity. Mol Cell Biol 27: 8502-9

Sy SM, Huen MS, Chen J (2009) PALB2 is an integral component of the BRCA complex required for homologous recombination repair. Proc Natl Acad Sci U S A 106: 7155-60

Syljuasen RG, Sorensen CS, Hansen LT, Fugger K, Lundin C, Johansson F, Helleday T, Sehested M, Lukas J, Bartek J (2005) Inhibition of human Chk1 causes increased initiation of DNA replication, phosphorylation of ATR targets, and DNA breakage. Mol Cell Biol 25: 3553-62

Symington LS, Gautier J (2011) Double-strand break end resection and repair pathway choice. Annu Rev Genet 45: 247-71

Tanaka A, Weinel S, Nagy N, O'Driscoll M, Lai-Cheong JE, Kulp-Shorten CL, Knable A, Carpenter G, Fisher SA, Hiragun M, Yanase Y, Hide M, Callen J, McGrath JA (2012) Germline mutation in ATR in autosomal-dominant oropharyngeal cancer syndrome. Am J Hum Genet 90: 511-7

Taniguchi T, Garcia-Higuera I, Xu B, Andreassen PR, Gregory RC, Kim ST, Lane WS, Kastan MB, D'Andrea AD (2002) Convergence of the fanconi anemia and ataxia telangiectasia signaling pathways. Cell 109: 459-72

Tassan JP, Schultz SJ, Bartek J, Nigg EA (1994) Cell cycle analysis of the activity, subcellular localization, and subunit composition of human CAK (CDK-activating kinase). J Cell Biol 127: 467-78

Taylor AM, Metcalfe JA, Thick J, Mak YF (1996) Leukemia and lymphoma in ataxia telangiectasia. Blood 87: 423-38

Taylor WR, Stark GR (2001) Regulation of the G2/M transition by p53. Oncogene 20: 1803-15

Thompson ER, Doyle MA, Ryland GL, Rowley SM, Choong DY, Tothill RW, Thorne H, kConFab, Barnes DR, Li J, Ellul J, Philip GK, Antill YC, James PA, Trainer AH, Mitchell G, Campbell IG (2012) Exome sequencing identifies rare deleterious mutations in DNA repair genes FANCC and BLM as potential breast cancer susceptibility alleles. PLoS Genet 8: e1002894

Toh GW, Sugawara N, Dong J, Toth R, Lee SE, Haber JE, Rouse J (2010) Mec1/Tel1-dependent phosphorylation of Slx4 stimulates Rad1-Rad10-dependent cleavage of non-homologous DNA tails. DNA Repair (Amst) 9: 718-26

Toyoshima F, Moriguchi T, Wada A, Fukuda M, Nishida E (1998) Nuclear export of cyclin B1 and its possible role in the DNA damage-induced G2 checkpoint. EMBO J 17: 2728-35

Truong LN, Li Y, Shi LZ, Hwang PY, He J, Wang H, Razavian N, Berns MW, Wu X (2013) Microhomology-mediated End Joining and Homologous Recombination share the initial end resection step to repair DNA double-strand breaks in mammalian cells. Proc Natl Acad Sci U S A 110: 7720-5

Velic D, Couturier AM, Ferreira MT, Rodrigue A, Poirier GG, Fleury F, Masson JY (2015) DNA Damage Signalling and Repair Inhibitors: The Long-Sought-After Achilles' Heel of Cancer. Biomolecules 5: 3204-59

Wahl GM, Carr AM (2001) The evolution of diverse biological responses to DNA damage: insights from yeast and p53. Nat Cell Biol 3: E277-86

Wallace SS, Murphy DL, Sweasy JB (2012) Base excision repair and cancer. Cancer Lett 327: 73-89

Wang B, Hurov K, Hofmann K, Elledge SJ (2009) NBA1, a new player in the Brca1 A complex, is required for DNA damage resistance and checkpoint control. Genes Dev 23: 729-39

Wang B, Matsuoka S, Ballif BA, Zhang D, Smogorzewska A, Gygi SP, Elledge SJ (2007) Abraxas and RAP80 form a BRCA1 protein complex required for the DNA damage response. Science 316: 1194-8

Wang J, Aroumougame A, Lobrich M, Li Y, Chen D, Chen J, Gong Z (2014) PTIP associates with Artemis to dictate DNA repair pathway choice. Genes Dev 28: 2693-8

Wang X, Haber JE (2004) Role of Saccharomyces single-stranded DNA-binding protein RPA in the strand invasion step of double-strand break repair. PLoS Biol 2: E21

Ward IM, Reina-San-Martin B, Olaru A, Minn K, Tamada K, Lau JS, Cascalho M, Chen L, Nussenzweig A, Livak F, Nussenzweig MC, Chen J (2004) 53BP1 is required for class switch recombination. J Cell Biol 165: 459-64

Weterings E, Verkaik NS, Bruggenwirth HT, Hoeijmakers JH, van Gent DC (2003) The role of DNA dependent protein kinase in synapsis of DNA ends. Nucleic Acids Res 31: 7238-46

Wolthuis R, Clay-Farrace L, van Zon W, Yekezare M, Koop L, Ogink J, Medema R, Pines J (2008) Cdc20 and Cks direct the spindle checkpoint-independent destruction of cyclin A. Mol Cell 30: 290-302

Wu J, Huen MS, Lu LY, Ye L, Dou Y, Ljungman M, Chen J, Yu X (2009) Histone ubiquitination associates with BRCA1-dependent DNA damage response. Mol Cell Biol 29: 849-60

Wu L, Hickson ID (2003) The Bloom's syndrome helicase suppresses crossing over during homologous recombination. Nature 426: 870-4

Xia B, Sheng Q, Nakanishi K, Ohashi A, Wu J, Christ N, Liu X, Jasin M, Couch FJ, Livingston DM (2006) Control of BRCA2 cellular and clinical functions by a nuclear partner, PALB2. Mol Cell 22: 719-29

Xie A, Kwok A, Scully R (2009) Role of mammalian Mre11 in classical and alternative nonhomologous end joining. Nat Struct Mol Biol 16: 814-8

Xu B, Kim S, Kastan MB (2001) Involvement of Brca1 in S-phase and G(2)-phase checkpoints after ionizing irradiation. Mol Cell Biol 21: 3445-50

Xu B, Kim ST, Lim DS, Kastan MB (2002) Two molecularly distinct G(2)/M checkpoints are induced by ionizing irradiation. Mol Cell Biol 22: 1049-59

Yang J, Bardes ES, Moore JD, Brennan J, Powers MA, Kornbluth S (1998) Control of cyclin B1 localization through regulated binding of the nuclear export factor CRM1. Genes Dev 12: 2131-43

Yang Y, Herrup K (2005) Loss of neuronal cell cycle control in ataxia-telangiectasia: a unified disease mechanism. J Neurosci 25: 2522-9

Yarden RI, Pardo-Reoyo S, Sgagias M, Cowan KH, Brody LC (2002) BRCA1 regulates the G2/M checkpoint by activating Chk1 kinase upon DNA damage. Nat Genet 30: 285-9

Yazdi PT, Wang Y, Zhao S, Patel N, Lee EY, Qin J (2002) SMC1 is a downstream effector in the ATM/NBS1 branch of the human S-phase checkpoint. Genes Dev 16: 571-82

Yoo HY, Kumagai A, Shevchenko A, Shevchenko A, Dunphy WG (2009) The Mre11-Rad50-Nbs1 complex mediates activation of TopBP1 by ATM. Mol Biol Cell 20: 2351-60

You Z, Chahwan C, Bailis J, Hunter T, Russell P (2005) ATM activation and its recruitment to damaged DNA require binding to the C terminus of Nbs1. Mol Cell Biol 25: 5363-79

Yu AM, McVey M (2010) Synthesis-dependent microhomology-mediated end joining accounts for multiple types of repair junctions. Nucleic Acids Res 38: 5706-17

Yu X, Chini CC, He M, Mer G, Chen J (2003) The BRCT domain is a phospho-protein binding domain. Science 302: 639-42

Zgheib O, Pataky K, Brugger J, Halazonetis TD (2009) An oligomerized 53BP1 tudor domain suffices for recognition of DNA double-strand breaks. Mol Cell Biol 29: 1050-8

Zhang F, Fan Q, Ren K, Andreassen PR (2009) PALB2 functionally connects the breast cancer susceptibility proteins BRCA1 and BRCA2. Mol Cancer Res 7: 1110-8

Zhang F, Ma J, Wu J, Ye L, Cai H, Xia B, Yu X (2009) PALB2 links BRCA1 and BRCA2 in the DNA-damage response. Curr Biol 19: 524-9

Zhang Y, Jasin M (2011) An essential role for CtIP in chromosomal translocation formation through an alternative end-joining pathway. Nat Struct Mol Biol 18: 80-4

Zhao GY, Sonoda E, Barber LJ, Oka H, Murakawa Y, Yamada K, Ikura T, Wang X, Kobayashi M, Yamamoto K, Boulton SJ, Takeda S (2007) A critical role for the ubiquitin-conjugating enzyme Ubc13 in initiating homologous recombination. Mol Cell 25: 663-75

Zhu C, Mills KD, Ferguson DO, Lee C, Manis J, Fleming J, Gao Y, Morton CC, Alt FW (2002) Unrepaired DNA breaks in p53-deficient cells lead to oncogenic gene amplification subsequent to translocations. Cell 109: 811-21

Zhu Z, Chung WH, Shim EY, Lee SE, Ira G (2008) Sgs1 helicase and two nucleases Dna2 and Exo1 resect DNA double-strand break ends. Cell 134: 981-94

Zimmermann M, Lottersberger F, Buonomo SB, Sfeir A, de Lange T (2013) 53BP1 regulates DSB repair using Rif1 to control 5' end resection. Science 339: 700-4

Zong D, Callen E, Pegoraro G, Lukas C, Lukas J, Nussenzweig A (2015) Ectopic expression of RNF168 and 53BP1 increases mutagenic but not physiological non-homologous end joining. Nucleic Acids Res 43: 4950-61

Chapter 2: DDX3X, identified as a novel partner of ATM, is required for efficient homologous recombination

2.1. Summary

DDX3X is a DEAD-box RNA helicase involved in almost all mRNA metabolism pathways, including transcription, translation and nuclear export. Furthermore, it has been implicated in apoptosis and cell cycle regulation. A recent proteomic screen for interactors of the PIKK kinase ATM has identified DDX3X as a potential interactor of ATM in the chicken DT40 cell line. In this study we confirm the interaction of DDX3X with ATM in human cells and show a novel role for the pleiotropic RNA helicase DDX3X in the DNA damage response. We demonstrate the involvement of DDX3X in homologous recombination by examining its effect on the HR repair factors BRCA1 and RAD51. We show that loss of DDX3X results in reduced BRCA1 and RAD51 damage foci and increased sensitivity to IR and Olaparib. Furthermore, we demonstrate that DDX3X depletion results in a delay in exiting the G1/S and G2/M checkpoints in response to ionising radiation induced DNA damage as well as a persistence of γH2AX IRIF. Together, this data suggests that DDX3X is required for efficient DSB repair by homologous recombination.

2.2. Introduction

The DEAD-box protein 3 (DDX3) belongs to the DEAD-box RNA helicase famliy and was first identified in a systematic search of the non-recombinational region of the Y chromosome in 1997 (Lahn & Page, 1997). DDX3 is encoded by the two closely related genes *DDX3X* and *DDX3Y*. *DDX3Y* is located on the Y-chromosome and presumably linked to male fertility (Lahn & Page, 1997). The *DDX3X* gene is located on the non-recombinational region of the X chromosome and is highly conserved from yeast to human (Tarn & Chang, 2009). DDX3X is ubiquitously expressed, although at different levels depending on the cell type, and escapes X-inactivation (Kim, Lee et al., 2001, Lahn & Page, 1997). The pleiotropic DDX3X is involved in a wide range of cellular processes, including most steps of mRNA processing as well as in cell cycle control and apoptosis.

DDX3X is a nucleo-cytoplasmic shuttling protein and its cellular distribution is cell type and cell cycle dependent (Choi & Lee, 2012). DDX3X was thought to be a mostly cytoplasmic protein due it its high rate of nuclear export. More recent studies have shown that DDX3X is located mainly in the nucleus in primary and non-transformed cells, while in cancerous cell lines it appears to be mainly cytoplasmic (Chao, Chen et al., 2006). This change in localisation pattern of DDX3X in different cell lines could be a consequence of the predominant role of DDX3X in transcription or translation in primary and cancer cell lines, respectively (Chao et al., 2006, Choi & Lee, 2012).
The yeast homolog of DDX3X is Ded1p. This protein is essential and unwinds RNA duplexes and DNA-RNA duplexes without strict polarity, unlike canonical translocating helicases (Yang, Del Campo et al., 2007). The same mechanism has also been proposed for DDX3X and other members of the DEAD-box family in higher organisms although supporting data is lacking (Schroder, 2010).

Like other DEAD-box helicase proteins, DDX3X contains 12 conserved helicase motifs in its helicase core, which consists of two RecA-like domains (Figure 2.1). Both of these domains are necessary for RNA unwinding and ATPase activity of DDX3X. The helicase core is highly conserved among all DEAD-box helicases, while flanking N- and C-terminal domains determine the specificity of each protein. DDX3X contains a leucine-rich nuclear export sequence (NES) in its N-terminal and nuclear export is mediated by at least two proteins, CRM1 and TAP. CRM1 exports proteins with a leucine-rich NES, while TAP exports mRNAs (Lai, Lee et al., 2008, Yedavalli, Neuveut et al., 2004). The C-terminal contains an arginine-serine-rich domain (RS-like domain) common to many splicing factors. Although DDX3X partly localises to the splicosome, studies have shown that it only directly interacts with the spliced form of the mRNA in an exon junction complex (EJC) dependent manner analogous to the RNA export machinery (Tarn & Chang, 2009).

The cytoplasmic fraction of DDX3X is highly phosphorylated in G1/S phase, while showing a lower level of phosphorylation in the G2 phase of the cell cycle in HeLa cells (Choi & Lee, 2012). In addition to well-studied functions in mRNA processing, DDX3X has also been implicated in apoptosis and cell cycle regulation (Botlagunta, Vesuna et al., 2008, Chang, Chi et al., 2006, Chao et al., 2006, Lai et al., 2008, Sun, Zhou et al., 2013) and this may be partly due to its interaction with the tumour suppressor protein p53. A recent study has shown that DDX3X is required for stabilization of p53 after CPT-induced DNA damage and positively regulates CPT-induced apoptosis via the activation of caspase 7. However, DDX3X has the opposite effect on cells expressing mutant p53 (Sun et al., 2013).

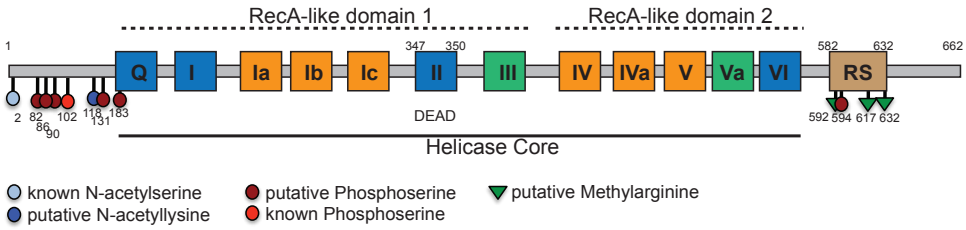

Figure 2.1: Schematic of DDX3X structure.

This schematic shows the structure of DDX3X. The central helicase core is comprised of two RecA-like domains. Blue boxes depict domains involved in ATP binding, orange boxes show domains involved in RNA binding and the linker domains for RNA binding and ATP hydrolysis are shown in green. DDX3X is acetylated on serine 2 (Yague, Alvarez et al., 2000) and phosphoylated on Serine 102 by IKKE (Gu, Fullam et al., 2013). All other depicted PTMs are putative.

Furthermore, DDX3X has been implicated in cell cycle control by its interaction with the transcription factor Sp-1, whereby it helps to regulate p21, cyclin A, cyclin B, cyclin D1, cyclin E1, PABP1 and chk1 expression (Chang et al., 2006, Chao et al., 2006, Lai et al., 2008, Li, Zhang et al., 2014, Wu, Liu et al., 2011). Depletion of DDX3X in mouse blastocysts causes cell cycle arrest, probably due to accumulation of p53 (Li et al., 2014). In contrast, DDX3X is required for the stabilisation of p53 in MCF7 cells (Sun et al., 2013). Depletion of DDX3X in NIH3T3 cells leads to premature entry into S-phase and increased cell proliferation, while depletion in mouse blastocysts results in cell cycle arrest in G1/S as well as G2/M phase. In MCF10A cells, over-expression of DDX3X causes cell transformation and elevated levels of breast cancer (Botlagunta et al., 2008, Chang et al., 2006, Chao et al., 2006). However, the effect of DDX3X depletion on HeLa cells is greatly reduced compared to cell lines with functional p53, suggesting that at least some of the effects of DDX3X depletion are due to its interaction with p53 and subsequent activation of p21 (Chao et al., 2006).

DEAD-box RNA helicases are highly specific enzymes with pleiotropic functions. They use ATP to locally destabilize RNA structures, remodel RNA complexes and serve as immobilized clamps on RNA to recruit larger complexes (Linder & Jankowsky, 2011). Furthermore, DEAD-box helicases are able to bind RNA non-specifically via the sugar-phosphate backbone (Bono, Ebert et al., 2006, Sengoku, Nureki et al., 2006) but are unable to unwind RNA for more than two helical turns (Valiente-Echeverria, Hermoso et al., 2015). DDX3X is not required for general translation, and the role of DDX3X is therefore thought to be supportive of the translation initiation factor eIF4F (Soto-Rifo, Rubilar et al., 2012). DDX3X activity is required for the early steps of translation initiation primarily in mRNAs with large, complex untranslated regions (UTRs) where it binds close to the m7-GTP cap and destabilizes local strands to assist eIF4F (Soto-Rifo et al., 2012).

The ability of DDX3X to unwind highly complex-structured UTRs makes it a prime viral target. Therefore it has been well studied and shown to be essential for viral replication of HIV, HCV, WNV, JEV and MNV viruses (Valiente-Echeverria et al., 2015). Although most research has focused on the role of DDX3X in viral replication and anti-viral immune response, DDX3X has more recently also been implicated in various types of cancer (Su, Lin et al., 2015). Due to its variety of biochemical functions, conflicting results of the role of DDX3X have been published for different types of cancer and even in the same type of cancer. DDX3X is identified as an oncogene or tumour suppressor depending on the cellular context. It is thought to act as an oncogene in breast cancer, while acting as a tumour suppressor in colon cancer where its loss promotes cell migration and invasion via the Snail/E-Cadherin pathway (Su et al., 2015). In hepatocarcinomas DDX3X has been reported to be both an oncogene (Huang, Chao et al., 2004) as well as a tumour suppressor (Chang et al., 2006, Chao et al., 2006).

We have uncovered an additional role for DDX3X by demonstrating that it interacts with the PIKK kinase ATM and contributes to efficient double-

strand break (DSB) repair by regulating the HR factors BRCA1, RAD51 and RAD54.

2.3. Materials and Methods

Cell culture

U2OS (ATCC HTB-96) and HEK293T (ATCC CRL-11268) cells were cultured in Dulbecco's modified Eagles medium (DMEM) (Lonza, F1-BE12-604F) supplemented with 10% FCS (Sigma) and 1% PenStrep (Sigma, P4333). hTERT-RPE1 cells were cultured in DMEM-F12 (Lonza, F1-BE12-719F) supplemented with 10% FCS (Sigma) and 1% PenStep (Sigma, P4333).

siRNA and plasmid transfections

Cells were transfected with Oligofectamine Reagent (LifeTechnologies, 12252011) according to manufacturers instructions. Briefly, $1.2x10^5$ cells were plated on a 35mm cell culture dish. After 24hr cells were transfected with 40pmol of negative control siRNA (Ambion, AM4611) or siDDX3X (Dharmacon, MU-006874-01, L-006874-02). Cells were harvested 48hrs post transfection. Cells were treated with ATM inhibitor (SelleckChem KU-55933, 10μM) 1hr prior to irradiation where indicated.

Immunoblotting

Cells were lysed in 50μl Lysis Buffer (150mM NaCl, 50mM Tris-Hcl, pH7.5, 10% Glycerol, 0.5%NP-40, 1mM $MgCl_2$, 1μl Benzonase (Sigma, E1014), Phosphatase and Protease Inhibitors) for 1h on ice. After pelleting the lysed cells at 14000rpm for 15min at 4°C, whole cell lysates were collected and the concentration was measured using Bradford Reagent (Sigma, B6916). 25μg of TCE was run on a denaturing polyacrylamide gel. Proteins were transferred onto a nitrocellulose membrane for 1h at 100V on ice. Membranes were blocked with TBS-T containing 5% milk for 10min at RT prior to primary antibody incubation overnight. The following primary antibodies were used: Actin (Sigma, A2066), ATM (Bethyl, A300-136A), 53BP1 (Bethyl, A300-272A), BRCA1 (D-9) (Santa Cruz, sc-6954), CSB (Genetex, GTX104589), DDX3X (Bethyl, A300-474A), γH2AX(S139) (Millipore, 05-636), p21 (Abcam,

ab7960), p53 (DO-1) (Santa Cruz, sc126), RAD51 (Calbiochem, PC130), RAD54 (Abcam, 10705), XPB (Genetex, GTX105357), XPD (Genetex, GTX112923), XRCC4 (Abcam, ab145).

Co-Immunoprecipitation

For ATM IPs, 10mg TCE was incubated with 5μl ATM antibody (Bethyl, A300-136A) for 2h on the wheel at 4°C, then incubated with G-beads (GE Healthcare, 17061801) for 1h on the wheel at 4°C. Beads were washed 3 times in Lysis Buffer (150mM NaCl, 50mM Tris-Hcl, pH7.5, 10% Glycerol, 0.5%NP-40, Phosphatase inhibitors (1mM NaF, 1mM β-glycerophosphate, 200μM Na_2VO_4, 1mM EDTA, 5mM $Na_4P_2O_7$), Protease inhibitors (600nM Leupeptin, 1.63μM Pepstatin, 1μM PMSF, 3μM Benzamidine, 2nM Antipain, 1.3nM Chymostatin) and resuspended in 50μl 2x Sample Buffer (Invitrogen, NP0007). 30% of the boiled beads were used for Immunoblotting.

Clonogenic Survival Assays

U2OS were trypsinized 48hrs after siRNA transfection and counted. 500 cells were plated onto a 60mm dish. For IR sensitivity assays, cells were allowed to adhere for 1h prior to irradiation. For Olaparib and ICRF-193 clonogenic survival assays, the medium was supplemented with the appropriate concentration of ICRF-139 (Enzo Life Sciences, GR-332) or Olaparib (SelleckChem, S1060) before addition of cells. Cells were grown at 37°C for 10-14 days until colonies were an average of 1-2mm in diameter. Colonies were stained with DMMB and counted.

Immunofluorescence

Cells were grown on a coverslip and transfected with siRNA. 48h after transfection, cells were irradiated with 3Gy, fixed with 4%PFA (EMS, 15710) for 10min at RT and permeabilised with 0.25% Triton-X for 10min. After blocking in 1%BSA, cells were stained for 1h with 1º antibody at 37°C, washed and incubated 1h with 2º antibody at 37°C. Slides were mounted using VectraShield (Vector Laboratories, H-1200) containing

DAPI. Microscopy imaging was performed on a Deltavision microscope using Softworx software (Applied Precision, Issaquah). 0.5µm Z-stacks were collected, deconvolved and projected. The analysis was carried out using ImageJ software. The following antibodies were used: 53BP1 (Novus Biologicals, NB100-304), BRCA1 (Santa Cruz, sc-6954), γH2AX (Millipore, 05-636), RAD51 (Calbiochem, PC130).

G2/M checkpoint assays

Cells were irradiated with 3Gy, harvested, washed, resuspended in 1ml PBS and fixed in ice-cold Ethanol at a final concentration of 75%. Cells were stained with a mitotic marker (H3pS10, Millipore, 06-570) in PBS containing 1%BSA and 0.5% Triton-X for 2h at RT. Cells were then incubated with FITC conjugated 2º antibody (Bethyl, A120-201F) for 1h in the dark at RT before being resuspended in PBS containing 40µg/ml PI (Sigma, P4170) and 250µg/ml RNaseA (Sigma, R6513). Mitotic cells were then detected using the BD-FACSCantoII and analysed using the BD-FACS DIVA software.

Cell cycle analysis and G1/S checkpoint assay

Cells were transfected with siRNA 48h prior to irradiation and pulse-treated with 25µM BrdU (Sigma, B5002) for 1h, washed with PBS and fresh media was added. Cells were then irradiated (3Gy) with a Cesium-137 source (Mainance, UK), harvested at the indicated times, fixed in 70% ice-cold ethanol, washed with PBS and the DNA was denatured using 2N HCl for 10min before being stained with anti-BrdU antibody (BD, 347580) for 1h and anti-mouse 2º antibody (Jackson ImmunoResearch, 111-096-045) for 1h. Cells were then stained with Propidium iodide solution (40µg/ml of PI (Sigma, P4170) and 250µl/ml of RNAse A (Sigma, R6513) in PBS) for 30min in the dark. The analysis was performed using the FACS CantoII and the BD-FACS Diva Software.

GFP-reporter assay

U2OS were stably transfected with the DR-GFP plasmid (Pierce, Johnson et al., 1999). $2x10^6$ cells were transfected with 5μg I-SceI plasmid (pCBA-ISceI with 3x NLS, gift from C. Morrison), 40nmol siRNA and 1μg cerulean plasmid (Cerulean N1, Addgene, 54742). 24h post transfection, cells were split into a 6-well dish and grown for a further 24h. Then cells were harvested by trypsination at the indicated timepoints and $2x10^4$ cells were analysed using a BD-FACS CantoII flow cytometer. The remaining cells were used for checking the knock-down efficiency.

2.4. Results

2.4.1. DDX3X is a novel interacting protein of ATM

Two independent stable isotope labelling with amino acids in cell culture (SILAC) screens in DT40 cells were carried out using Atm, tagged with a four-residue HFSC affinity tag. Atm was purified from undamaged, IR-treated (10Gy) and, in the second SILAC, UV-treated DT40 cells to identify damage dependent and independent interacting partners of chicken Atm.

In Table 2.1 and Table 2.2 known interacting proteins are shown and their presence validates the results of the SILAC screen. A large proportion of Atm interacting proteins were RNA metabolism proteins, including a number of DEAD-box helicases (Table 2.2) Some DEAD-box helicases have been shown to have a role in the DNA damage response such as DDX1, which co-localises with γH2AX in response to ionising radiation (Li, Monckton et al., 2008).

In this study, we focus on the role of another DEAD-box RNA helicase, DDX3X. In DT40 cells, Ddx3x seems to be more enriched after IR (Table 2.1) with an overall enrichment score of 1.77 and 1.96, respectively, compared to the untagged control cells. However, in the second SILAC, Ddx3x interaction with Atm was also detected in the absence of damage. The variation between the two experiments could be due to the weak interaction of these two proteins leading to a low detection level of Ddx3x. Furthermore, the Ddx3x interaction with Atm seems to be enriched after UV-damage.

In order to confirm this interaction in human cells, we carried out immunoprecipitations (IPs) of endogenous ATM in U2OS cells in the presence or absence of DNA damage (Figure 2.2). DDX3X interacts with ATM independently of DNA damage in human U2OS cells.

Protein	control	IR	Reference
Atm	27.14	26.89	(Bakkenist & Kastan, 2003)
Usp10	2.00	1.92	(Yuan, Luo et al., 2010)
Mcm3	1.73	2.21	(Shi, Dodson et al., 2007)
Ppp2a	1.50	0.00	(Goodarzi & Lees-Miller, 2004)
Chd4	1.86	2.48	(Urquhart, Gatei et al., 2011)
Ddx3x	0	1.77	this study

Table 2.1: Ddx3x interacts with Atm in chicken DT40 cells.

Results of the first SILAC analysis. Cells were grown in heavy, light and medium SILAC media, irradiated with 10Gy as indicated and harvested 1h post IR. Scores represent the relative enrichment of peptides compared to the untagged control samples. (Experiments were carried out by J. Eykelenboom and F. Pessina)

Protein	control	IR	UV	Reference
Atm	100	100	100	(Bakkenist & Kastan, 2003)
Mcm3	1.71	1.85	1.87	(Shi et al., 2007)
Ddx1	1.2	1.11	1.11	(Li et al., 2008)
Ddx3x	1.50	1.81	1.96	this study
Ddx5	1.37	2.22	1.40	uncomfirmed
Ddx6	2.33	2.83	1.99	unconfirmed

Table 2.2: Ddx3x interacts with Atm in DT40 cells.

Results of the second SILAC analysis. Cells were grown in heavy, light and medium SILAC media, irradiated with 10Gy or UV-treated with X J/m^2 as indicated and harvested 1h post IR. Scores represent the relative enrichment of peptides compared to the untagged control (Experiments were carried out by A. van Beneden and J. Prieto).

The detection of damage-independent interaction in the IP but damage-dependent interaction in the two SILAC screen could be due to the sensitivity difference of the assays. IPs are less sensitive than the proteomic screens so the subtle difference detected in the SILACs might not be visualised by IP. Nevertheless, the co-IP of DDX3X with ATM independently confirms the interaction.

DDX3X depletion prevents stabilisation of p53 in response to DNA damage, which consequently affects G1 signalling via the p21 pathway (Sun et al., 2013). We confirmed this result in RPE-1 cells. In response to DNA damage, p53 is stabilised in the siCTRL cells, but not in the cells depleted in DDX3X, which leads to a decreased p21 response (Figure 2.2b). However, DDX3X depletion does not affect the ATM protein level.

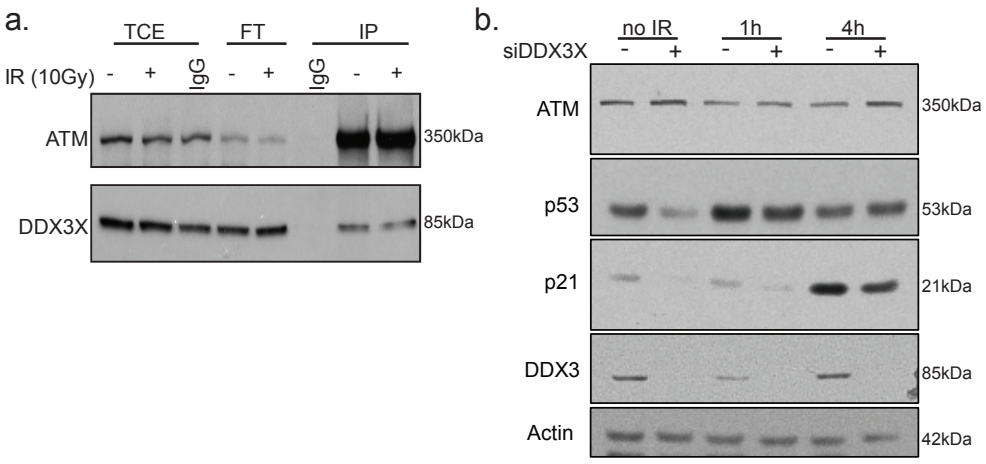

Figure 2.2: DDX3X interacts with ATM independent of DNA damage.

a. Co-immunoprecipitation of ATM and DDX3X. U2OS cells were grown to confluency, irradiated at 10Gy and harvested 30min post IR. Immunoprecipitation was carried out using an anti-ATM antibody and resulting WB was then probed for DDX3X. b. WB of RPE1 cells. RPE1 cells were transfected with control or DDX3X siRNA, irradiated at 3Gy and harvested at the indicated timepoints. The resulting WB was probed with the indicated antibodies.

2.4.2. DDX3 depletion results in IR sensitivity

In order to assess a possible role for DDX3X in the DDR, we used gamma irradiation as a DNA damaging agent to investigate the effect of DDX3X-deficient cells on colony formation. U2OS cells, which contain wild-type p53 and a functioning p21 pathway, grow fewer colonies on average when depleted of DDX3X than mock-transfected cells in the absence of DNA damage (Figure 2.3a). This indicates either increased apoptosis or a defect in cell cycle transition.

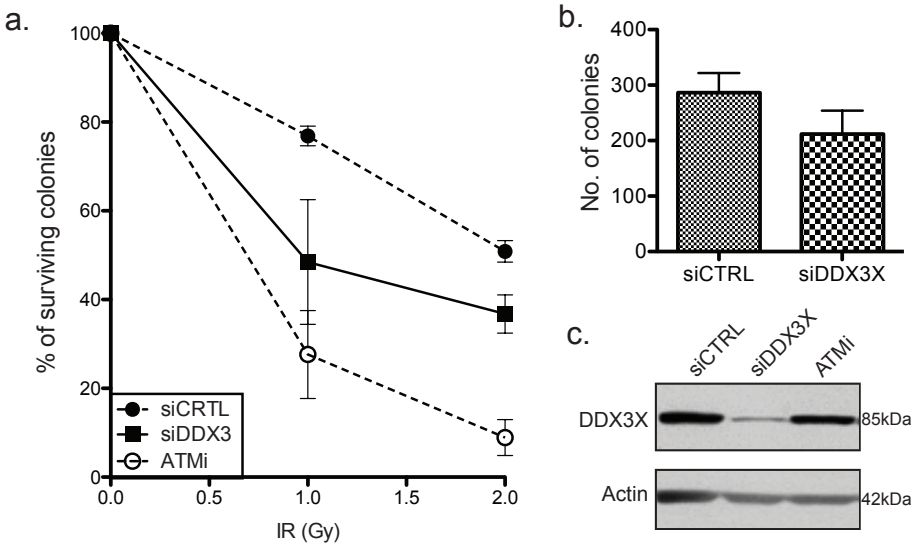

Figure 2.3: DDX3X depletions results in decreased colony formation and increased IR sensitivity.

A. Clonogenic survival assay. Cells were grown for 10-14 days in culture, stained with DMMB and counted. Experiments were carried out in triplicate and error bars represent the SD across three independent experiments. B. Number of colonies counted in undamaged control or DDX3X depleted cells (n=5). 500 cells, transfected with DDX3X or control siRNA, were plated and grown for 12-14 days. Colonies were stained with DMMB and colonies bigger than 1mm in diameter were counted. Error bars represent the SD across all experiments. C. WB of knock-down efficiency.

Moreover, DDX3X-deficient cells showed increased sensitivity to ionizing radiation compared to control cells but less sensitivity than ATM inhibited cells (Figure 2.3b). All counts were normalised to the respective

undamaged control to exclude the growth defect in DDX3X depleted cells. Increased IR sensitivity suggests that depletion of DDX3X negatively impacts on the response of cells to DNA damage when compared to WT (Figure 2.3).

2.4.3. DDX3X is required for efficient checkpoint release

In recent studies DDX3X has been shown to be involved in the transcriptional and translational control of cell cycle regulators, including various cyclins (Li et al., 2014). Additionally, the yeast homolog Ded1 has been shown to interact with Chk1 in a yeast two hybrid screen (Liu, Nefsky et al., 2002). DDX3X was implicated in cell cycle control via transcription regulation of cell cycle factors such as cyclin A (Chao et al., 2006). DDX3X is also required for stabilisation of p53 in mouse cells after camptothecin-induced DNA damage and the regulation of CPT-induced apoptosis, potentially through the activation of caspase 7 in cells with functional p53 (Sun et al., 2013). To study the effect of DDX3X depletion on the cell cycle in response to DNA damage in U2OS and RPE-1 cells, we performed cell cycle analysis and G1/S and G2/M checkpoints assays (Figure 2.4).

Depletion of DDX3X in U2OS cells does not prevent cells from entering into the G2/M checkpoint (Figure 2.4a,b), but instead impedes G2/M checkpoint exit, suggesting loss of DDX3X results in a defect in DNA damage repair or checkpoint recovery. DDX3X cells also have less mitotic cells prior to DNA damage compared to control cells (Figure 2.4b) suggesting a deregulation of the cell cycle. We investigated this further using RPE1 cells treated with a BRDU pulse to separate cell cycle stages (Figure 2.4c,d). . Figure 2.4d shows that populations depleted of DDX3X have a larger percentage of cells in G1, with nearly 10% less cells in S-phase. This is consistent with less mitotic cells in U2OS cells.

In 2006, Chang et al demonstrated that depletion of DDX3X in mouse NIH3T3 cells could lead to premature entry into S-phase and elevated

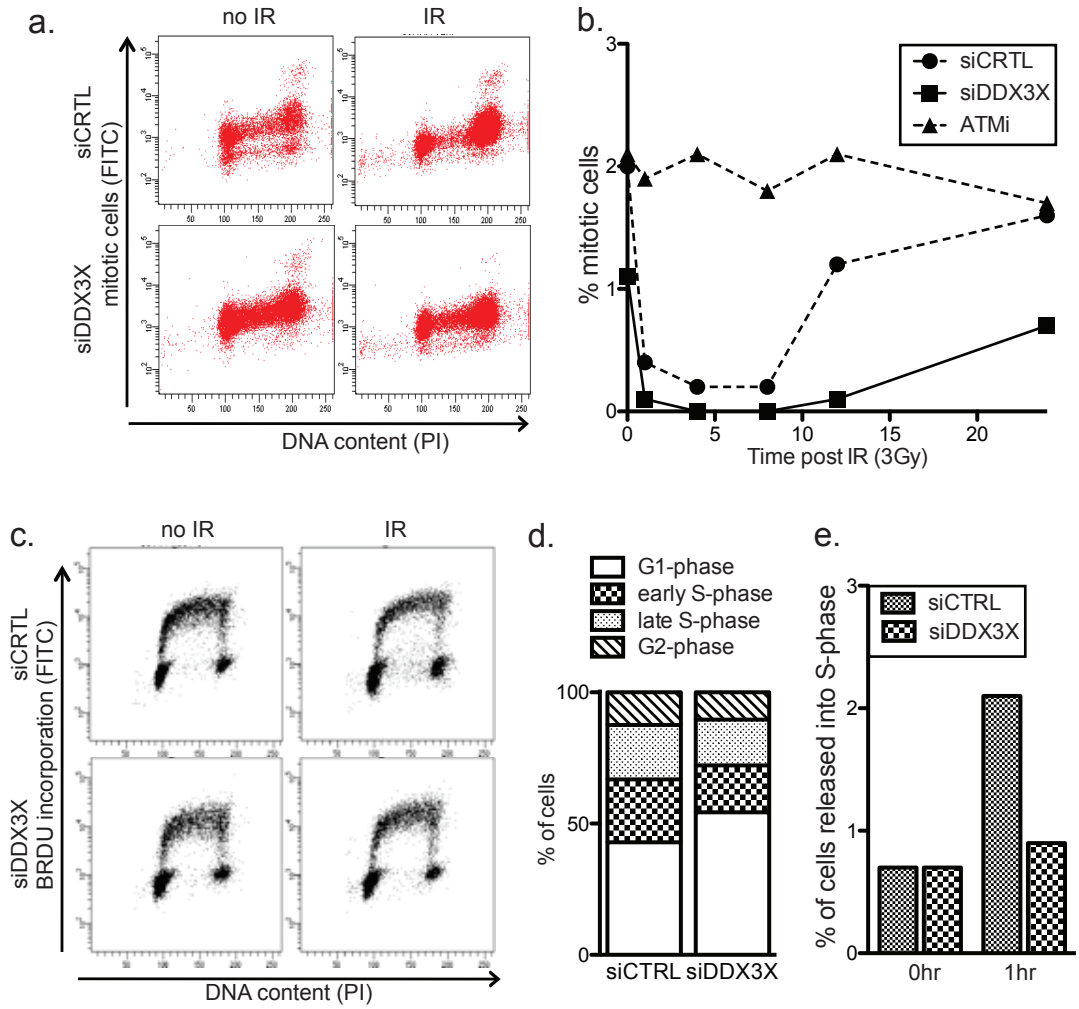

Figure 2.4: DDX3X is required for efficient checkpoint release in U2OS and RPE-1 cells.

A. Dot plot of cells stained with H3pS10 before and 12h post IR (3Gy). B. G2/M checkpoint assay in U2OS cells (n=2). Cells were stained with H3pS10, a mitotic marker, and PI, then analysed using a BD-FACS CantoII. C. Dot plot of RPE-1 cells exposed to a 1h BrdU pulse prior to IR (3Gy). Cells were stained with anti-BrdU antibody and PI to separate cells into G1, early-S, late-S and G2 phases. D. Distribution of undamaged cells in different stages of the cell cycle (n=2). E. Quantification of cells released into S-phase 1hr post irradiation (n=2).

cell proliferation, proposing a role for DDX3X in G1/S transition through the regulation of cyclin D1. We also examined the role of DDX3X in the G1/S checkpoint. After a BrdU pulse, the cells were irradiated and fixed 1h post IR. The percentage of cells newly released into S-phase (BrdU negative S-phase cells) within 1h after damage is decreased upon DDX3X knockdown (Figure 2.4c,e). Loss of DDX3X prevents the transition into S-phase in response to DNA damage suggesting a prolonged arrest in the G1/S checkpoint, which could indicate a defect in DNA repair or checkpoint recovery signalling.

2.4.4. DDX3X is required for DNA damage repair

To investigate whether the delay in checkpoint exit in G1/S and G2/M phases are a result of deficient or delayed DNA repair, we used the phosphorylation of histone H2AX at the sites of damage as a DSB marker to assess the role of DDX3X in DNA repair. Increased numbers of γH2AX IRIF as late as 24h after DNA damage induction indicate a defect in DSB repair in DDX3X depleted cells (Figure 2.5). The main functions of DDX3X vary in from one cell type to another so to exclude cell type specific effects, we have carried out IF of γH2AX foci in two different cell lines, U2OS and RPE-1 cells (Figure 2.5a,d). In response to DNA damage, and equal percentage of cells have more than 10 foci in both control and DDX3X depleted cells, but 24h after damage, 65% of DDX3X deficient cells have persistent γH2AX foci compared to 30% of cells in the control samples, suggesting a defect in DNA repair in the absence of DDX3X (Figure 2.5b).

Depletion of DDX3X also results in a decrease in the total number of γH2AX foci per cell 1h post damage (Figure 2.5f).

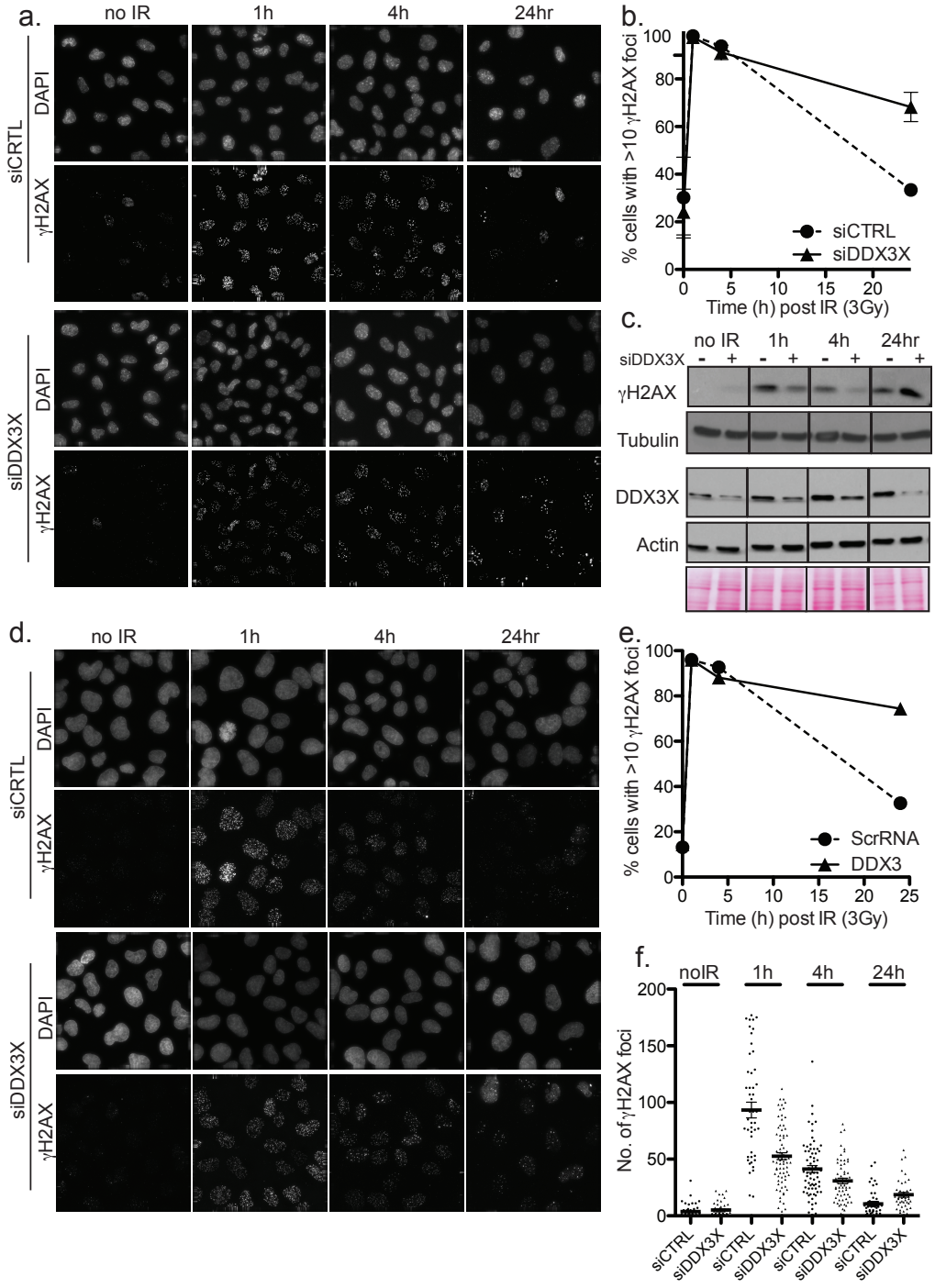

Figure 2.5: Loss of DDX3X results in persistent γH2AX foci

A. IF experiment in RPE-1 cells, showing persistent γH2AX foci in the absence of DDX3X. Cell were irradiated (3Gy) and fixed at indicated timepoints. Cells were then stained with anti-γH2AX(S139) and DAPI. B. Quantification of (a) showing the percentage of cells with more than 10 gH2AX foci. Experiments were carried out in triplicate and error bars represent the SEM across three independent experiments (n=3). (Legend contd on next page)

This indicates a defect in the efficient recruitment of DNA damage factors involved in the maintenance of H2AX phosphorylation or a decrease in H2AX phosphorylation itself.

2.4.5. Depletion of DDX3X has no effect on 53BP1 focal recruitment

We further investigated the role of DDX3X in the DDR cascade by studying 53BP1, a downstream DDR mediator protein of γH2AX, which is recruited to DSBs. DDX3X depletion has no effect on the recruitment of 53BP1 into IRIFs 1h post IR (Figure 2.6a,b). A slight increase in 53BP1 focal number was detected 4h after DNA damage and the 53BP1 foci appear to be more intense (Figure 2.6a).

Furthermore, DDX3X depleted cells exhibit a higher number of 53BP1 nuclear bodies in G1 phase compared to control cells. 53BP1 nuclear bodies appear in G1 cells as a mark for DNA lesions that are generated in G2/M phase and could not be repaired prior to mitosis or DNA lesions at common fragile sites that were generated during late S phase and were carried over to the daughter cell for subsequent repair (Lukas, Savic et al., 2011). The increased amount of 53BP1 nuclear bodies in DDX3X depleted cells further underlines a defect in DNA repair in the absence of DDX3X (Figure 2.6c). This data is consistent with persistence in H2AX phosphorylation and a delay in checkpoint exit.

Figure 2.5 cntd.

C. WB of gH2AX levels in control and DDX3X depleted cell. WB of knock-down efficiency of DDX3X siRNA. D. IF experiment in U2OS cells, showing persistent γH2AX foci in the absence of DDX3X. Cells were irradiated (3Gy) and fixed at indicated timepoints. Cells were then stained with anti-γH2AX(S139) and DAPI. E. Quantification of (d) showing the percentage of cells with more than 10 γH2AX foci per cell (n=2). Experiments were carried out in duplicate. F. Distribution of cells according to the actual number of γH2AX foci per cell. Distribution across one experiment, error bars represent the SEM across the total number of cells in the experiment.

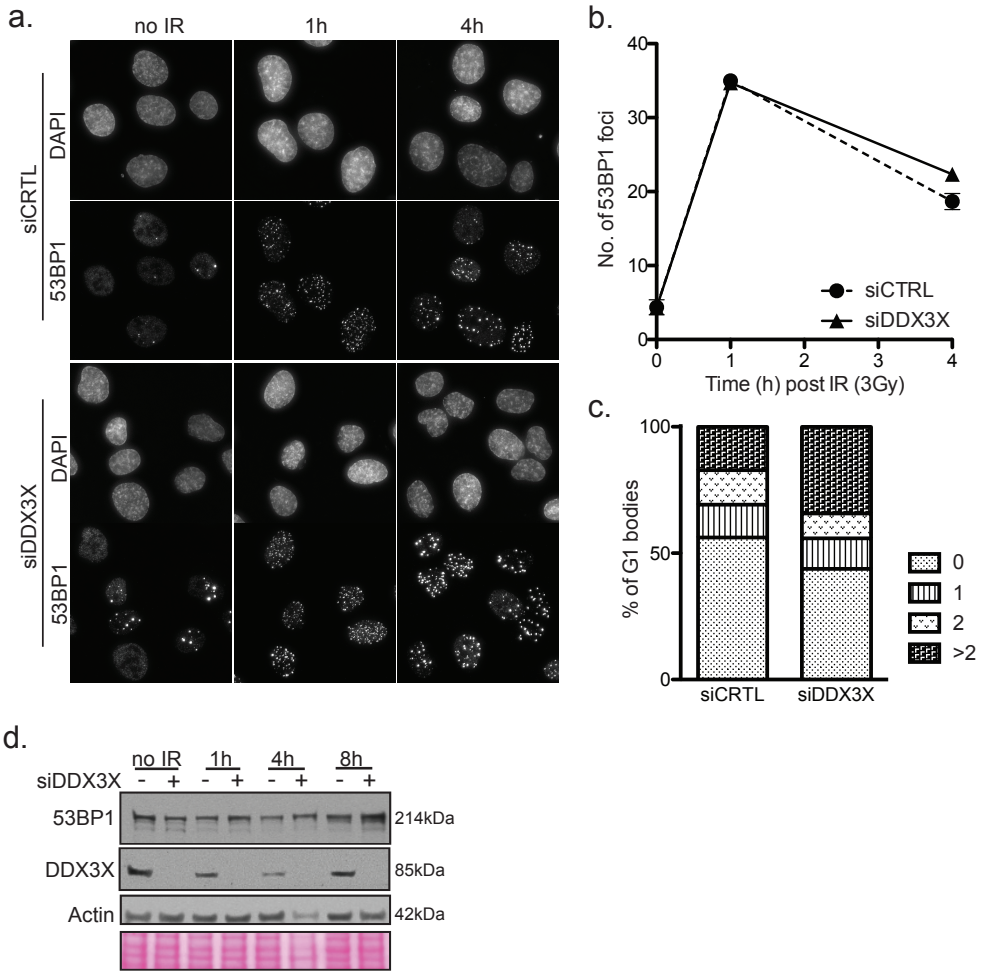

Figure 2.6: DDX3X depletion has no effect on 53BP1 focal number, but shows increased number of 53BP1 nuclear bodies

A. Immunofluorescence of 53BP1 foci in U2OS cells. Cell were transfected with either control or DDX3X siRNA, irradiated at 3Gy and fixed at the indicated timepoints. B. Quantification of (a). Experiments were carried out in triplicate and error bars represent the SEM across three independent experiments (n=3). C. Quantification of 53BP1 nuclear bodies of control and DDX3X depleted U2OS cells. Experiments were carried out in duplicate. Cells were counted as either containing 1, 2 or more than 2 G1 nuclear bodies per cell (n=3). D. WB of total 53BP1 levels in control and DDX3X depleted cells.

2.4.6. Depletion of DDX3X results in decreased BRCA1 and RAD51 IRIF

Next, we assayed the effect of DDX3X depletion on the focal recruitment of the DNA damage factors BRCA1 and RAD51. These proteins are two

of the main proteins involved in HR. BRCA1 forms a complex with CtIP and MRN, which is required for 5'-3' resection of the broken DNA ends (Yun & Hiom, 2009). RAD51 is essential for strand invasion by forming a DNA-RAD51 helix that facilitates binding to the repair template strand (Chen, Yang et al., 2008).

To investigate whether DDX3X plays a role in homology-directed repair, we investigated the effect of DDX3X depletion on the recruitment of BRCA1 and RAD51 into IRIF. DDX3X depletion results in a decrease of BRCA IRIF (Figure 2.7a,b). BRCA1 is also required for nucleotide excision repair (NER) in S-phase and can be visualised at S-phase foci during replication induced DNA damage. DDX3X does not seem to abrogate BRCA1 foci in S-phase cells, as they can be observed in undamaged cells in both DDX3X-depleted as well as control cells (Figure 2.7a). However, no increase in BRCA1 foci can be detected in response to IR, suggesting a defect in the recruitment of BRCA1 to IRIF (Figure 2.7a,b). This could be partially explained by the reduction of the total protein levels of BRCA1 and RAD51 after DDX3X depletion (Figure 2.7c).

The reduction in BRCA1 foci after IR and the reduction in total BRCA1 protein leves in DDX3X depleted cells suggests a defect in homologous-directed repair. To further investigate this, we studied RAD51, a downstream effector protein of BRCA1 in HR. A significant reduction in RAD51 foci in response to IR was observed in DDX3X depleted RPE1 cells (Figure 2.8a,b). This reduction is likely to be a consequence of the overall reduction of RAD51 protein levels (Figure 2.7c) combined with reduction of BRCA1 IRIF, which are required for the recruitment of RAD51 to ssDNA. Moreover, the effect of DDX3X depletion on RAD51 and BRCA1 is not restricted to RPE-1 cells, but can also be seen in U2OS cells (Figure 2.8d,e).

The reduction of BRCA1 and RAD51 IRIF in cells depleted of DDX3X suggests that DDX3X is required for efficient HR at least partially due to the regulation of BRCA1 and RAD51 total protein levels.

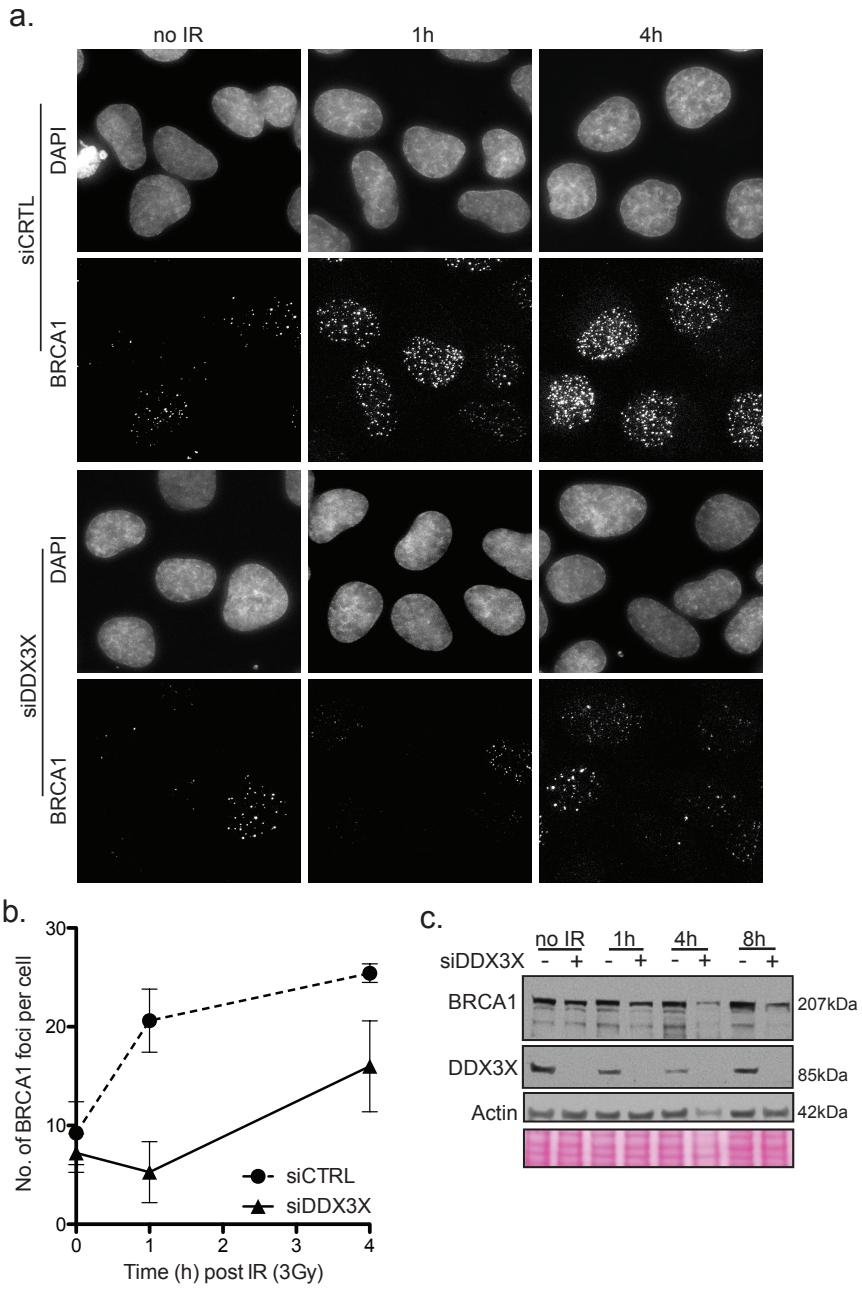

Figure 2.7: DDX3X depletion results in decreased accumulation of BRCA1 at IRIF

DDX3X is required for efficient recruitment of BRCA1 to IRIF, but not S-phase induced DNA damage foci. A. Immunofluorescence of BRCA1 in U2OS cells. Cells were fixed at the indicated times after irradiation (3Gy) and stained with BRCA1 antibody and DAPI. B. Quantification of BRCA1 foci. Experiments were carried out in triplicate and error bars represent the SEM across three independent experiments (n=3). C. Western Blot showing total levels of BRCA1 in control or DDX3X depleted cells.

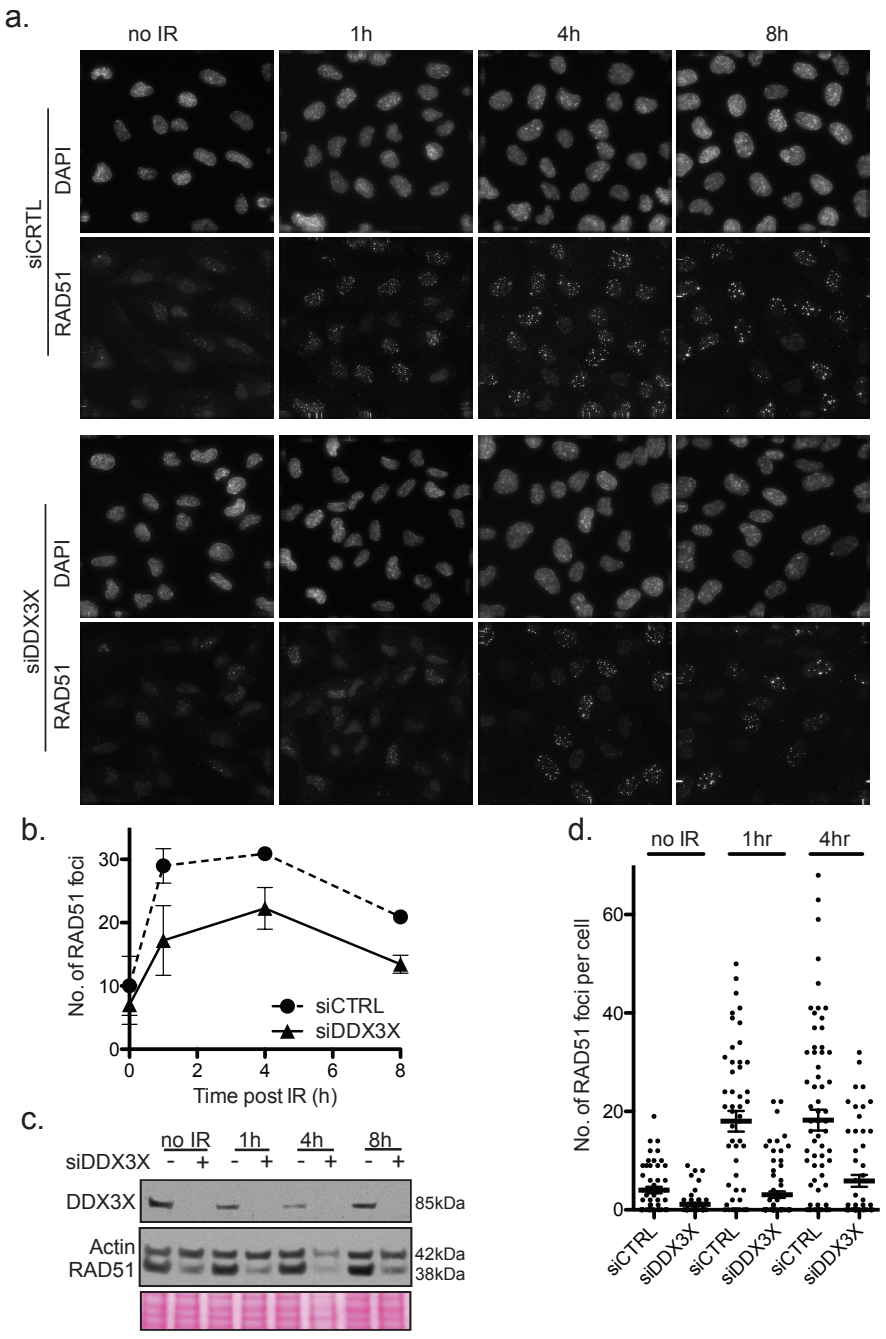

Figure 2.8: Loss of DDX3X results in decreased recruitment of RAD51 to IRIF

A. Immunofluorescence in RPE-1 cells. Cells were fixed at the indicated time after irradiation (3Gy) and then stained with RAD51 antibody and DAPI. B. Quantification of RAD51 foci. Experiments were carried out in triplicate and error bars represent the SEM across three independent experiments (n=3). C. WB of total RAD51 in the presence or absence of DDX3X. D. Distribution of RAD51 foci. Error bars represent the SEM across the total number of cells counted in one experiment.

2.4.7. DDX3X is involved in the expression of HR and some NER factors, but not NHEJ factors

DDX3X is a translational co-factor of eIF4F and assists in the translation of mRNAs with highly structured UTRs (Soto-Rifo et al., 2012). To further investigate whether DDX3X affects the protein levels of key HR, NER and NHEJ factors, we used Western Blotting to determine the expression level in DDX3X deficient cells (Figure 2.9). Depletion of DDX3X results in a decrease of total BRCA1, RAD51 and RAD54 proteins (Figure 2.9a). In addition, loss of DDX3X leads to a reduction of total CSB and XPD protein levels, and XBP levels in response to DNA damage (Figure 2.9b).

Interestingly, cell depleted of DDX3X show an increased level of total XRCC4, the co-factor of DNA ligase IV. DDX3X deficient cells also show increased levels of total 53BP1 1h after IR (Figure 2.9b). One possible explanation is an increased requirement for NHEJ factor in the absence of a functioning HR pathway.

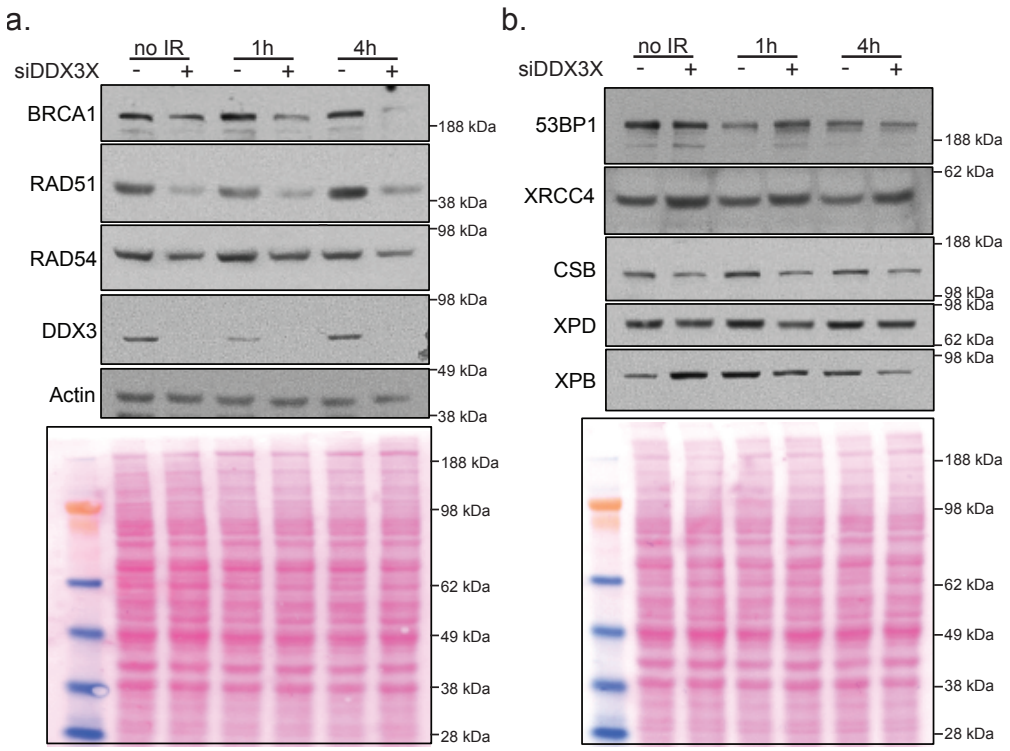

Figure 2.9: DDX3X depletion results in the reduction of protein levels of HR and NER, but not NHEJ factors.

Immunoblotted cell extracts from RPE1 cells transfected with either control or DDX3X siRNA. Cells were irradiated at 3Gy and harvested at the indicated timepoints. A. Western Blot for the HR factors BRCA1, RAD51 and RAD54. The membrane was probed for DDX3X to validate the knock-down efficiency and actin as a loading control. B. Western Blot for the NHEJ factors 53BP1 and XRCC4 as well as the NER factors CSB, XPB and XPC.

2.4.8. DDX3X is required for efficient HR

In order to confirm that DDX3X plays a role in HR, clonogenic survival assays were carried out in U2OS cells using Olaparib and ICRF-193 as damage inducing agents. Olaparib is a PARP inhibitor, which prevents the repair of DNA nicks by PARP1, resulting in DSBs during DNA replication that are primarily repaired by HR (McCabe, Turner et al., 2006). ICRF-193 is an inhibitor of topoisomerase II (TOPII), which prevents re-ligation of DNA ends. The majority of these DNA breaks are repaired by the non-homologous end-joining repair pathway. (Adachi, Suzuki et al., 2003).
Cells depleted of DDX3X were more sensitive to Olaparib although less sensitive than RAD54 knock-down (Figure 2.10a). Furthermore, DDX3X depleted cells treated with ICRF-193 did not show significant survival defects or sensitivity. (Figure 2.10b). This data confirms that DDX3X is required for efficient HR, but does not affect NHEJ.

This led us to investigate whether DDX3X affects gene conversion (GC) directly using the classical DR-GFP reporter assay (Pierce et al., 1999) in our own DR-U2OS cell line. To generate this cell line, we randomly integrated a DR-GFP construct into U2OS cell line (data not shown). DR-U2OS cells depleted in DDX3X show a 20% reduction of efficient DNA repair by HR compared to the control cells (Figure 2.10c). This data suggests that DDX3X plays a role in the efficient HR repair by GC, although it is not essential in this pathway.

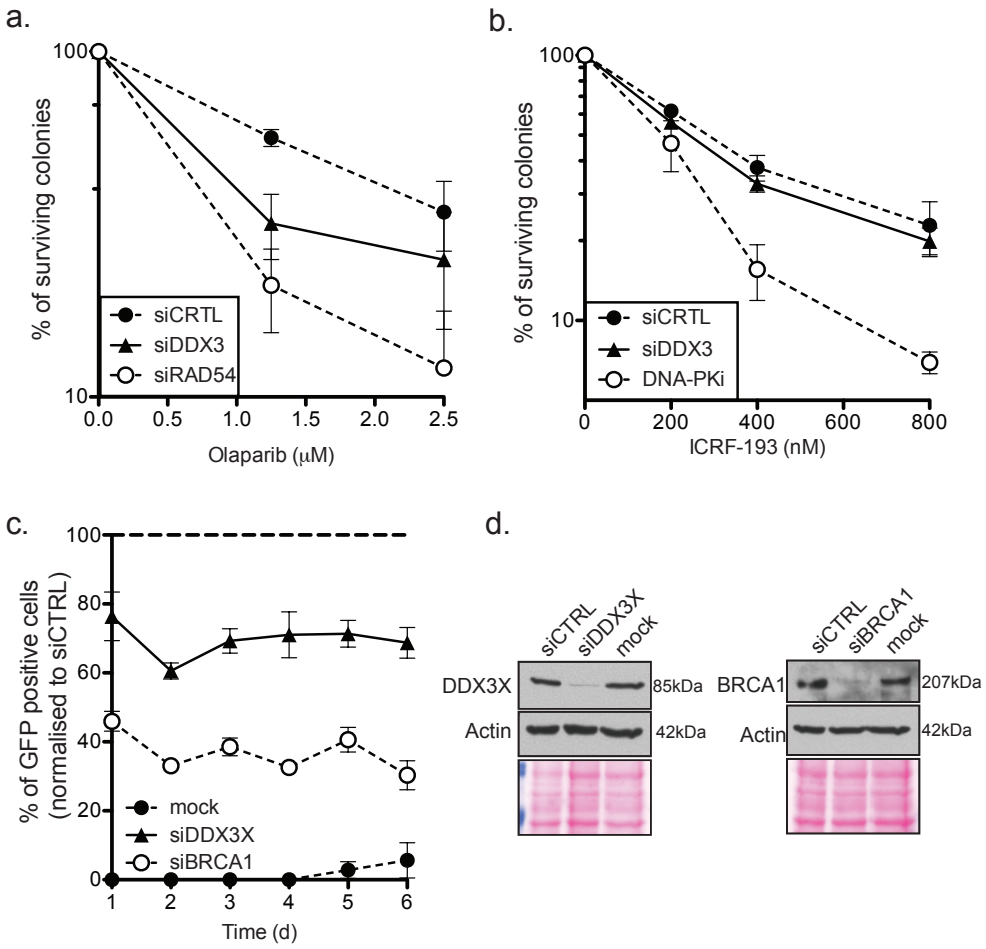

Figure 2.10: DDX3X is required for efficient HR repair.

A. Clonogenic survival assay in U2OS cells. 500 cells were plated in media containing the appropriate concentration of Olaparib, grown for 10-14 days and stained with DMMB. B. Clonogenic survival assay in U2OS cells. 500 cells were plated in media containing the appropriate concentration of ICRF-193, grown for 10-14 days and stained with DMMB. All experiments were carried out in triplicate and error bars represent the SD across three independent experiments (n=3). C. DR-GFP reporter assay. Cells were transfected with siRNA, I-SceI plasmid and cerulean plasmid, split into 6 dishes 24h post transfection and grown for the indicated times. Live cells were harvested and GFP positive cells were analysed using a BD-FACS CantoII flow cytometer. The graph shows the percentage reduction of GFP-positive cells compared to the control cells. Experiments were carried out in triplicate and error bars represent the SEM across three independent experiments (n=3). D. WB of knock-down efficiency for DDX3X and BRCA1 siRNAs, respectively.

2.5. Discussion

In this study, we have investigated the role of DDX3X and implicated it directly in HR. Previous studies have shown that DDX3X is a prime viral target due to its role in the processing of mRNA (Valiente-Echeverria et al., 2015). It is hijacked by several viruses, including HIV and HCV, and is regarded as a potential therapeutic target. However, the pleiotropic nature of DDX3X makes it difficult to target as a drug target as it is essential for a variety of cellular processes and its removal could be fatal for the cell.

Alongside its role as in viral replication and in anti-viral defence, DDX3X has also been implicated in apoptosis and cell cycle regulation in a highly cell type specific manner (Su et al., 2015). There are conflicting results published suggesting DDX3X is an oncogene as well as a tumour suppressor dependent on the cellular context. A number of cancer types such as colon cancer show an up-regulation of DDX3X, whereas in other types of cancer the loss of DDX3X appears to result in cellular transformation (Chao et al., 2006, Huang et al., 2004).

We have focussed on the novel role of DDX3X in the repair of double-stranded DNA by HR. To exclude any cell type variability we used the osteosarcoma cell line U2OS and a karyotypically normal, non-cancerous cell line, hTERT RPE-1 cells. Both cell lines have wild-type p53 and a functioning p21 pathway. This means, we cannot entirely exclude that the effects observed are, at least partially, due to the failure to stabilise p53 in response to DNA damage (Sun et al., 2013).

We identified DDX3X as a novel interacting partner of ATM in chicken and human cells. Although enriched interaction has been detected in response to damage, we observed no IR dependency of DDX3X interaction with ATM in IP experiments. DDX3X harbours four SQ/TQ sites in its protein sequence that could potentially be phosphorylated by

ATM. DDX3X was not identified in proteomic screens of ATM/ATR substrates, and analysis of these potential phosphorylation sites would provide a better understanding of the role of DDX3X in the DDR (Bensimon, Schmidt et al., 2010, Matsuoka, Ballif et al., 2007).

In addition to its interaction with ATM, we have demonstrated that DDX3X is required for efficient DNA repair by HR. The defect in HR in the absence of DDX3X is most likely due to the downregulation of essential HR factors such as BRCA1, RAD51 and RAD54. DDX3X has previously been implicated in the translational regulation of cell cycle regulating proteins involved in the DDR such as PARP, p21, p53, CHK1 and various cyclins (Chao et al., 2006, Lai et al., 2008, Li et al., 2014, Wu et al., 2011). In order to clarify whether DDX3X is involved in the transcriptional or translational control of BRCA1, RAD51 and RAD54, further in depth investigation is required. Transcriptome and proteome analysis of DDX3X deficient cells will reveal whether DDX3X is required as a co-factor of transcription factors selectively of HR and some NER genes, but not NHEJ genes.

In summary, this study we have demonstrated that DDX3X is a new factor involved homologous recombination, possibly via transcriptional or translational regulation of key HR factors.

This is a preliminary study that has only scraped the surface and many more questions have arisen and will need to be answered to obtain a more complete understanding of how this RNA helicase is involved in ensuring efficient DNA repair.

2.6. References

Adachi N, Suzuki H, Iiizumi S, Koyama H (2003) Hypersensitivity of nonhomologous DNA end-joining mutants to VP-16 and ICRF-193: implications for the repair of topoisomerase II-mediated DNA damage. J Biol Chem 278: 35897-902

Bakkenist CJ, Kastan MB (2003) DNA damage activates ATM through intermolecular autophosphorylation and dimer dissociation. Nature 421: 499-506

Bensimon A, Schmidt A, Ziv Y, Elkon R, Wang SY, Chen DJ, Aebersold R, Shiloh Y (2010) ATM-dependent and -independent dynamics of the nuclear phosphoproteome after DNA damage. Sci Signal 3: rs3

Bono F, Ebert J, Lorentzen E, Conti E (2006) The crystal structure of the exon junction complex reveals how it maintains a stable grip on mRNA. Cell 126: 713-25

Botlagunta M, Vesuna F, Mironchik Y, Raman A, Lisok A, Winnard P, Jr., Mukadam S, Van Diest P, Chen JH, Farabaugh P, Patel AH, Raman V (2008) Oncogenic role of DDX3 in breast cancer biogenesis. Oncogene 27: 3912-22

Chang PC, Chi CW, Chau GY, Li FY, Tsai YH, Wu JC, Wu Lee YH (2006) DDX3, a DEAD box RNA helicase, is deregulated in hepatitis virus-associated hepatocellular carcinoma and is involved in cell growth control. Oncogene 25: 1991-2003

Chao CH, Chen CM, Cheng PL, Shih JW, Tsou AP, Lee YH (2006) DDX3, a DEAD box RNA helicase with tumor growth-suppressive property and transcriptional regulation activity of the p21waf1/cip1 promoter, is a candidate tumor suppressor. Cancer Res 66: 6579-88

Chen Z, Yang H, Pavletich NP (2008) Mechanism of homologous recombination from the RecA-ssDNA/dsDNA structures. Nature 453: 489-4

Choi YJ, Lee SG (2012) The DEAD-box RNA helicase DDX3 interacts with DDX5, co-localizes with it in the cytoplasm during the G2/M phase of the cycle, and affects its shuttling during mRNP export. J Cell Biochem 113: 985-96

Goodarzi AA, Lees-Miller SP (2004) Biochemical characterization of the ataxia-telangiectasia mutated (ATM) protein from human cells. DNA Repair (Amst) 3: 753-67

Gu L, Fullam A, Brennan R, Schroder M (2013) Human DEAD box helicase 3 couples IkappaB kinase epsilon to interferon regulatory factor 3 activation. Mol Cell Biol 33: 2004-15

Huang JS, Chao CC, Su TL, Yeh SH, Chen DS, Chen CT, Chen PJ, Jou YS (2004) Diverse cellular transformation capability of overexpressed genes in human hepatocellular carcinoma. Biochem Biophys Res Commun 315: 950-8

Kim YS, Lee SG, Park SH, Song K (2001) Gene structure of the human DDX3 and chromosome mapping of its related sequences. Mol Cells 12: 209-14

Lahn BT, Page DC (1997) Functional coherence of the human Y chromosome. Science 278: 675-80

Lai MC, Lee YH, Tarn WY (2008) The DEAD-box RNA helicase DDX3 associates with export messenger ribonucleoproteins as well as tip-associated protein and participates in translational control. Mol Biol Cell 19: 3847-58

Li L, Monckton EA, Godbout R (2008) A role for DEAD box 1 at DNA double-strand breaks. Mol Cell Biol 28: 6413-25

Li Q, Zhang P, Zhang C, Wang Y, Wan R, Yang Y, Guo X, Huo R, Lin M, Zhou Z, Sha J (2014) DDX3X regulates cell survival and cell cycle during mouse early embryonic development. J Biomed Res 28: 282-91

Linder P, Jankowsky E (2011) From unwinding to clamping - the DEAD box RNA helicase family. Nat Rev Mol Cell Biol 12: 505-16

Liu HY, Nefsky BS, Walworth NC (2002) The Ded1 DEAD box helicase interacts with Chk1 and Cdc2. J Biol Chem 277: 2637-43

Lukas C, Savic V, Bekker-Jensen S, Doil C, Neumann B, Pedersen RS, Grofte M, Chan KL, Hickson ID, Bartek J, Lukas J (2011) 53BP1 nuclear bodies form around DNA lesions generated by mitotic transmission of chromosomes under replication stress. Nat Cell Biol 13: 243-53

Matsuoka S, Ballif BA, Smogorzewska A, McDonald ER, 3rd, Hurov KE, Luo J, Bakalarski CE, Zhao Z, Solimini N, Lerenthal Y, Shiloh Y, Gygi SP, Elledge SJ (2007) ATM and ATR substrate analysis reveals extensive protein networks responsive to DNA damage. Science 316: 1160-6

McCabe N, Turner NC, Lord CJ, Kluzek K, Bialkowska A, Swift S, Giavara S, O'Connor MJ, Tutt AN, Zdzienicka MZ, Smith GC, Ashworth A (2006) Deficiency in the repair of DNA damage by homologous recombination and sensitivity to poly(ADP-ribose) polymerase inhibition. Cancer Res 66: 8109-15

Pierce AJ, Johnson RD, Thompson LH, Jasin M (1999) XRCC3 promotes homology-directed repair of DNA damage in mammalian cells. Genes Dev 13: 2633-8

Schroder M (2010) Human DEAD-box protein 3 has multiple functions in gene regulation and cell cycle control and is a prime target for viral manipulation. Biochem Pharmacol 79: 297-306

Sengoku T, Nureki O, Nakamura A, Kobayashi S, Yokoyama S (2006) Structural basis for RNA unwinding by the DEAD-box protein Drosophila Vasa. Cell 125: 287-300

Shi Y, Dodson GE, Mukhopadhyay PS, Shanware NP, Trinh AT, Tibbetts RS (2007) Identification of carboxyl-terminal MCM3 phosphorylation sites using polyreactive phosphospecific antibodies. J Biol Chem 282: 9236-43

Soto-Rifo R, Rubilar PS, Limousin T, de Breyne S, Decimo D, Ohlmann T (2012) DEAD-box protein DDX3 associates with eIF4F to promote translation of selected mRNAs. EMBO J 31: 3745-56

Su CY, Lin TC, Lin YF, Chen MH, Lee CH, Wang HY, Lee YC, Liu YP, Chen CL, Hsiao M (2015) DDX3 as a strongest prognosis marker and its downregulation promotes metastasis in colorectal cancer. Oncotarget 6: 18602-12

Sun M, Zhou T, Jonasch E, Jope RS (2013) DDX3 regulates DNA damage-induced apoptosis and p53 stabilization. Biochim Biophys Acta 1833: 1489-97

Tarn WY, Chang TH (2009) The current understanding of Ded1p/DDX3 homologs from yeast to human. RNA Biol 6: 17-20

Urquhart AJ, Gatei M, Richard DJ, Khanna KK (2011) ATM mediated phosphorylation of CHD4 contributes to genome maintenance. Genome Integr 2: 1

Valiente-Echeverria F, Hermoso MA, Soto-Rifo R (2015) RNA helicase DDX3: at the crossroad of viral replication and antiviral immunity. Rev Med Virol 25: 286-99

Wu DW, Liu WS, Wang J, Chen CY, Cheng YW, Lee H (2011) Reduced p21(WAF1/CIP1) via alteration of p53-DDX3 pathway is associated with poor relapse-free survival in early-stage human papillomavirus-associated lung cancer. Clin Cancer Res 17: 1895-905

Yague J, Alvarez I, Rognan D, Ramos M, Vazquez J, de Castro JA (2000) An N-acetylated natural ligand of human histocompatibility leukocyte antigen (HLA)-B39. Classical major histocompatibility complex class I proteins bind peptides with a blocked NH(2) terminus in vivo. J Exp Med 191: 2083-92

Yang Q, Del Campo M, Lambowitz AM, Jankowsky E (2007) DEAD-box proteins unwind duplexes by local strand separation. Mol Cell 28: 253-63

Yedavalli VS, Neuveut C, Chi YH, Kleiman L, Jeang KT (2004) Requirement of DDX3 DEAD box RNA helicase for HIV-1 Rev-RRE export function. Cell 119: 381-92

Yuan J, Luo K, Zhang L, Cheville JC, Lou Z (2010) USP10 regulates p53 localization and stability by deubiquitinating p53. Cell 140: 384-96

Yun MH, Hiom K (2009) CtIP-BRCA1 modulates the choice of DNA double-strand-break repair pathway throughout the cell cycle. Nature 459: 460-3

Chapter 3: DGCR8, identified as a novel interacting partner of ATM, is required for fidelity of DNA repair independent of Drosha

3.1. Summary

DGCR8 is required as a co-factor for pre-miRNA processing by the RNAse III enzyme Drosha. In this study we identify DGCR8 as a novel interacting partner of ATM and demonstrate a Drosha independent role for DGCR8 in the DDR. In a proteomic screen, DGCR8 was found to interact with ATM. This interaction was confirmed in human cells. DGCR8 depletion results in increased sensitivity to IR, Olaparib and ICRF-193, but does not show an effect on cell cycle distribution or G2/M checkpoint signalling. In addition, DGCR8 depletion has no effect on γH2AX kinetics, but results in increased activation of ATM and focal recruitment of 53BP1 at early timepoints. Furthermore, DGCR8 is required for efficient HR and depletion of DGCR8 and Drosha simultaneously has a synergistic effect. Together, this data suggests that DGCR8 is required for error-free DNA repair independently of its microprocessor partner Drosha.

3.2. Introduction

DiGeorge Critical Region 8 (DGCR8) is an 86 kDa RNA binding protein with no detectable enzymatic function. The *DGCR8* gene is located on chromosome 22 and is one of the genes most commonly affected in the 22q11.2 deletion syndrome also known as DiGeorge Syndrome. The deletion is a result of mispairing of low copy repeat regions during cell division (Carlson, Sirotkin et al., 1997). It is the most common microdeletion in humans and phenotypes include conotruncal defects of the heart, craniofacial abnormalities and hypocalcemia (Eliez, Blasey et al., 2001, McDonald-McGinn & Sullivan, 2011, van Amelsvoort, Daly et al., 2001).

The DGCR8 protein consists of 773 amino acids and contains two double stranded RNA binding domains (dRBDs), a central heme binding domain (HBD) and a WW motif (Faller, Matsunaga et al., 2007, Gregory, Yan et al., 2004, Sohn, Bae et al., 2007) (Figure 3.1). DGCR8 is present in the nucleus as a dimer connected via a central heme group bound to cysteine 352 (Senturia, Faller et al., 2010) (Figure 3.2b). The cysteine residue is essential for dimerisation of DGCR8 and mutation of this residue C352A or C352H completely abrogates binding (Faller et al., 2007).

The two dRBDs located in the C-terminal form the binding site for the apical UGU motif on pri-miRNA (Nguyen, Jo et al., 2015). Although DGCR8 binding RNA with high affinity *in vitro*, its binding is not very specific and DGCR8 is unable to distinguish between its natural substrates (Roth, Ishimaru et al., 2013) suggesting that it is not the main pre-miRNA recognition protein.

DGCR8 forms a trimeric complex with Drosha consisting of two DGCR8 molecules and one Drosha molecule (Nguyen et al., 2015) (Figure 3.2a). The Drosha/DGCR8 complex is commonly referred to as the

"microprocessor" and is the minimal requirement for the initial processing of miRNAs (Gregory et al., 2004, Landthaler, Yalcin et al., 2004). Both proteins are cross-regulated forming a feedback loop to ensure accurate expression levels. Upon deletion of Drosha, DGCR8 is upregulated 3-4 fold while decreased upon Drosha overexpression (Han, Pedersen et al., 2009).

MiRNAs are small 22 nt non-coding RNA molecules that play an important part in post-translational regulation of genes in higher eukaryotes (Ameres & Zamore, 2013, Ha & Kim, 2014). Pri-miRNAs are transcribed by RNA pol II and processed by the Drosha/DGCR8 complex into pre-miRNA. Drosha is a RNAse III enzyme that cleaves dsRNA at the dsRNA/ssRNA junction at the basal stem of the pri-miRNA (Figure 3.2a). The resulting pre-miRNAs are exported into the cytoplasm, where they are processed by Dicer into miRNA and loaded onto the Argonaute (Kawamata & Tomari, 2010).

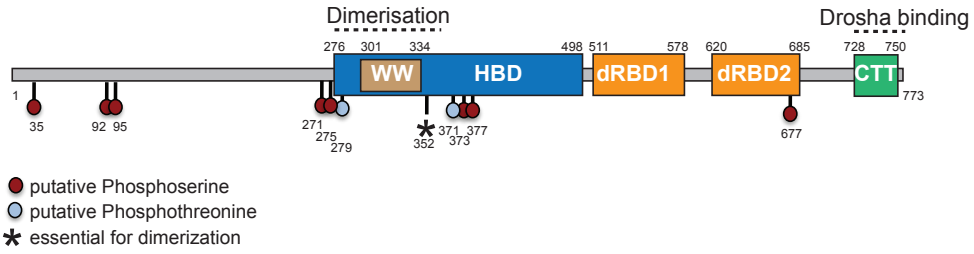

Figure 3.1: Schematic representation of DGCR8

Schematic shows the protein structure of DGCR8. DGCR8 has a central heme binding domain (HBD) (blue) containing a WW motif (beige), followed by two double-stranded RNA binding domains (dRBD1, dRBD2) (orange) and a C-terminal tail (CTT) domain (green) that is essential for Drosha interaction. C352 is essential for dimerisation.

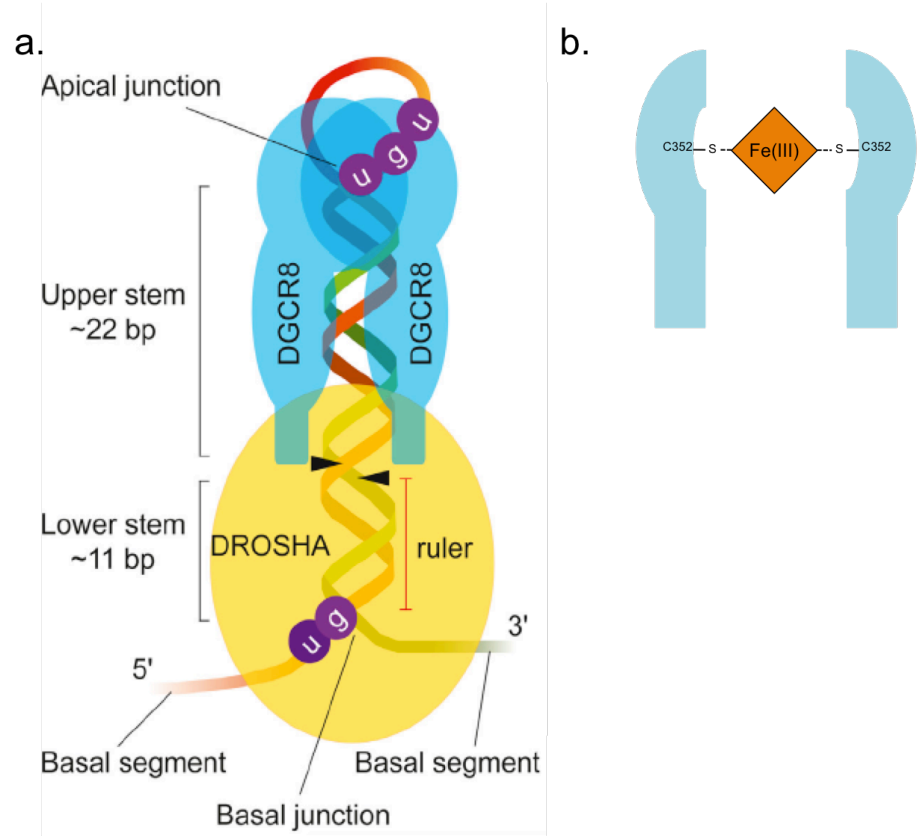

Figure 3.2: DGCR8 dimerisation and Drosha binding

A. Schematic of DGCR8/Drosha binding to pre-miRNA. Two DGCR8 molecules dimerise and bind pre-miRNA via the dRBDs. The CTT region of DGCR8 interacts with Drosha. DGCR8 binds to miRNA on the upper stem recognising the UGU motif on the stem loop, while Drosha binds to the lower stem at the ssRNA/dsRNA junction recognising the UG motif. (Figure adapted from (Nguyen et al., 2015)). B. Schematic of DGCR8 dimerisation via a ferric iron binding to the cysteine 352 of the HBD of DGCR8.

Recent success in producing recombinant Drosha has provided great insight into the mechanism of miRNA processing by Drosha and DGCR8 (Kwon, Nguyen et al., 2016). The Drosha interacting CTT domain of DGCR8 is the minimal requirement for functional pre-miRNA processing by Drosha although at a much reduced efficiency (Nguyen et al., 2015). Full Drosha activity requires the dRBDs of DGCR8, while the dimerization is necessary to prevent unspecific binding (Nguyen et al., 2015)

DGCR8 is a nuclear protein that shows a pan-nuclear staining pattern with denser staining in the nucleoli, which disappear upon transcription inhibition (Shiohama, Sasaki et al., 2007). In addition to its well

characterised interaction with Drosha, DGCR8 is also associated with several RNA helicases including DHX9 and the DEAD box protein helicases DDX5 and DDX17 (Shiohama et al., 2007). However, the function of their interaction remains unclear.

In this study we identify DGCR8 as a novel interacting partner of ATM in both chicken and human cells and demonstrate a potential role for DGCR8 in the DDR independent of its interaction with Drosha.

3.3. Materials and Methods

Cell culture

U2OS (ATCC HTB-96) and HEK293T (ATCC CRL-11268) cells were cultured in Dulbecco's modified Eagles medium (DMEM) (Lonza, F1-BE12-604F) supplemented with 10% FCS (Sigma) and 1% PenStrep (Sigma, P4333). hTERT-RPE1 cells were cultured in DMEM-F12 (Lonza, F1-BE12-719F) supplemented with 10% FCS (Sigma) and 1% PenStep (Sigma, P4333).

siRNA and plasmid transfections

Cells were transfected with Oligofectamine Reagent (LifeTechnologies, 12252011) according to manufacturers instructions. Briefly, $1.2x10^5$ cells were plated on a 35mm cell culture dish. After 24hr cells were transfected with 40pmol of negative control siRNA (Ambion, AM4611), siDGCR8 (Dharmacon, L-0157713-00/ Ambion, s29062) or siDrosha (Dharmacon, L-016996-00). Cells were harvested 48hrs post transfection. Cells were treated with ATM inhibitor (SelleckChem KU-55933, 10μM) 1hr prior to irradiation where indicated.

Immunoblotting

Cells were lysed in 50μl Lysis Buffer (150mM NaCl, 50mM Tris-Hcl, pH7.5, 10% Glycerol, 0.5%NP-40, 1mM $MgCl_2$, 1μl Benzonase (Sigma, E1014), Phosphatase and Protease Inhibitors) for 1h on ice. After pelleting the lysed cells at 14000rpm for 15min at 4°C, whole cell lysates were collected and the concentration was measured using Bradford Reagent (Sigma, B6916). 25μg of TCE was run on a denaturing polyacrylamide gel. Proteins were transferred onto a nitrocellulose membrane for 1h at 100V on ice. Membranes were blocked with TBS-T containing 5% milk for 10min at RT prior to primary antibody incubation overnight. The following primary antibodies were used: Actin (Sigma, A2066), ATM (Bethyl, A300-136A), pATM(S1981) (R&D, AF1655), 53BP1 (Bethyl, A300-272A), BRCA1 (D-9) (Santa Cruz, sc-6954),

pBRCA1(S1423) (Bethyl, A300-008A), γH2AX(S139) (Millipore, 05-636), RAD51 (Calbiochem, PC130), RAD54 (Abcam, 10705), DGCR8 (Bethyl, A203-468A), Drosha (Abcam, ab12286), pChk2(T68) (CST, 2661).

Co-Immunoprecipitation

For ATM IPs, 10mg TCE was incubated with 5μl ATM antibody (Bethyl, A300-136A) for 2h on the wheel at 4°C, then incubated with G-beads (GE Healthcare, 17061801) for 1h on the wheel at 4°C. Beads were washed 3 times in Lysis Buffer (150mM NaCl, 50mM Tris-Hcl, pH7.5, 10% Glycerol, 0.5%NP-40, Phosphatase inhibitors (1mM NaF, 1mM β-glycerophosphate, 200μM Na_2VO_4, 1mM EDTA, 5mM $Na_4P_2O_7$), Protease inhibitors (600nM Leupeptin, 1.63μM Pepstatin, 1μM PMSF, 3μM Benzamidine, 2nM Antipain, 1.3nM Chymostatin) and resuspended in 50μl 2x Sample Buffer (Invitrogen, NP0007). 30% of the boiled beads were used for Immunoblotting.

GST-ATM pull down

Plasmids containing the GST-ATM fragments were a kind gift from KK Khanna (Khanna, Keating et al., 1998). GST-ATM fragments were expressed in *Rosetta E. Coli* cells for 16h at 4C after IPTG induction and purified as decribed in (Khanna et al., 1998). GST-ATM fragment bound beads were then incubated with 1mg TCE from HEK293T cells, washed in Lysis Buffer 150mM NaCl, 50mM Tris-Hcl, pH7.5, 10% Glycerol, 0.5%NP-40, Phosphatase inhibitors (1mM NaF, 1mM β-glycerophosphate, 200μM Na_2VO_4, 1mM EDTA, 5mM $Na_4P_2O_7$), Protease inhibitors (600nM Leupeptin, 1.63μM Pepstatin, 1μM PMSF, 3μM Benzamidine, 2nM Antipain, 1.3nM Chymostatin) and resuspended in 60μl Laemmli Buffer. 50% of the Pull down was used for WB.

Clonogenic Survival Assays

U2OS were trypsinized 48hrs after siRNA transfection and counted. 500 cells were plated onto a 60mm dish. For IR sensitivity assays, cells were allowed to adhere for 1h prior to irradiation. For Olaparib and ICRF-193

clonogenic survival assays, the medium was supplemented with the appropriate concentration of ICRF-139 (Enzo Life Sciences, GR-332) or Olaparib (SelleckChem, S1060) before addition of cells. Cells were grown at 37°C for 10-14 days until colonies were an average of 1-2mm in diameter. Colonies were stained with DMMB and counted.

Immunofluorescence

Cells were grown on a coverslip and transfected with siRNA. 48h after transfection, cells were irradiated with 3Gy, fixed with 4%PFA (EMS, 15710) for 10min at RT and permeabilised with 0.25% Triton-X for 10min. After blocking in 1%BSA, cells were stained for 1h with 1º antibody at 37°C, washed and incubated 1h with 2º antibody at 37°C. Slides were mounted using VectraShield (Vector Laboratories, H-1200) containing DAPI. Microscopy imaging was performed on a Deltavision microscope using Softworx software (Applied Precision, Issaquah). 0.5µm Z-stacks were collected, deconvolved and projected. The analysis was carried out using ImageJ software. The following antibodies were used: 53BP1 (Novus Biologicals, NB100-304), γH2AX (Millipore, 05-636), pATM(S1981) (Millipore, MAB3806).

G2/M checkpoint assays

Cells were irradiated with 3Gy, harvested, washed, resuspended in 1ml PBS and fixed in ice-cold Ethanol at a final concentration of 75%. Cells were stained with a mitotic marker (H3pS10, Millipore, 06-570) in PBS containing 1%BSA and 0.5% Triton-X for 2h at RT. Cells were then incubated with FITC conjugated 2º antibody (Bethyl, A120-201F) for 1h in the dark at RT before being resuspended in PBS containing 40µg/ml PI (Sigma, P4170) and 250µg/ml RNaseA (Sigma, R6513). Mitotic cells were then detected using the BD-FACSCantoII and analysed using the BD-FACS DIVA software.

Cell cycle analysis and G1/S checkpoint assay

Cells were transfected with siRNA 48h prior to irradiation and pulse-treated with 25μM BrdU (Sigma, B5002) for 1h, washed with PBS and fresh media was added. Cells were then irradiated (3Gy) with a Cesium-137 source (Mainance, UK), harvested at the indicated times, fixed in 70% ice-cold ethanol, washed with PBS and the DNA was denatured using 2N HCl for 10min before being stained with anti-BrdU antibody (BD, 347580) for 1h and anti-mouse 2º antibody (Jackson ImmunoResearch, 111-096-045) for 1h. Cells were then stained with Propidium iodide solution (40μg/ml of PI (Sigma, P4170) and 250μl/ml of RNAse A (Sigma, R6513) in PBS) for 30min in the dark. The analysis was performed using the FACS CantoII and the BD-FACS Diva Software.

GFP-reporter assay

U2OS were stably transfected with the DR-GFP plasmid (Pierce, Johnson et al., 1999). $2x10^6$ cells were transfected with 5μg I-SceI plasmid (pCBA-ISceI with 3x NLS, gift from C. Morrison), 40nmol siRNA and 1μg cerulean plasmid (Cerulean N1, Addgene, 54742). 24h post transfection, cells were split into a 6-well dish and grown for a further 24h. Then cells were harvested by trypsination at the indicated timepoints and $2x10^4$ cells were analysed using a BD-FACS CantoII flow cytometer. The remaining cells were used for checking the knock-down efficiency.

3.4. Results

3.4.1. DGCR8 is a novel interacting partner of ATM

We decided to perform a proteomic screen in order to define the ATM "interactome". The main aim of this experiment was to characterise in more detail the mechanisms of action through the analysis of purified ATM complexes from endogenous level of expression. This has been performed in DT40 chicken cells by HFSC-tagging the Atm protein targeting directly in its genomic locus (Pessina & Lowndes, 2014). DT40 cells, derived from avian leucosis virus transformed chicken B-lymphocytes, possess the remarkable property of being highly efficient for Homologous recombination. Atm was purified from undamaged or IR-treated (10Gy) cells. Interestingly, analysing the positive hits of the screen by gene ontology, the main category enriched by ionizing radiation was RNA metabolism proteins. In this study, we focus on the role of the microprocessor subunit DGCR8. In DT-40 cells, Dgcr8 seems to be more enriched after IR with an overall enrichment score of 2.00, compared to the untagged control cells (Table 3.1).

In order to validate the interactions we identified by SILAC we decided to use human cell lines for two main reasons: firstly there are many validated commercial antibodies available against human proteins (that may not cross react with other species) and secondly the DT40 chicken cell line is derived from a tumoral cell line lacking p53 activity. We wanted to be sure that these interactions are also present in human cells and not specific to DT40 cells. Therefore, we immunoprecipitated ATM from the human U2OS cell line, which is p53+ to assure this interaction is not exclusive of p53- cells as DT40 (Figure 3.3a).

Protein	control	IR	Reference
Atm	27.14	26.89	(Bakkenist & Kastan, 2003)
Usp10	2.00	1.92	(Yuan, Luo et al., 2010)
Mcm3	1.73	2.21	(Shi, Dodson et al., 2007)
Ppp2a	1.50	0.00	(Goodarzi & Lees-Miller, 2004)
Chd4	1.86	2.48	(Urquhart, Gatei et al., 2011)
Dgcr8	0	2.00	this study

Table 3.1: Analysis of the SILAC experiment

Results of the SILAC experiment. Cells were grown in heavy, light and medium SILAC media, irradiated with 10Gy as indicated and harvested 1h post IR. Scores represent the relative enrichment of peptides compared to the untagged control samples. (This experiment was performed by F. Pessia and J. Eykelenboom)

We carried out immunoprecipitations before and after IR damage (10 Gy), and in the presence of an ATM inhibitor (KU55933) to explore if the interaction is dependent on the kinase activity (Figure 3.3a). The Western Blot in Figure 3.3a shows that interaction of DGCR8 with ATM seems to be independent of DNA damage, or kinase activity, however, a slight increase can be detected after damage.

We then mapped the interaction of DGCR8 with ATM to the C-terminal of ATM, suggesting DGCR8 binds near the kinase and FAT-C domains of ATM. (Figure 3.3b). It has to be noted that we also detected DGCR8 binding in two additional fragments near the N-terminal. Fragment 1 binding is most likely unspecific binding because of excess recombinant protein required due to the high amount of degradation (Figure 3.3b). More stringent washing would be required to determine specific binding of DGCR8 to the C-terminal of ATM. The strongest interaction could be detected in Fragment 11, which contains part of the PIKK domain as well as the FATC domain. The interaction of DGCR8 with fragment 12 is much weaker and most likely background signal, indicating that DGCR8 could

interact with the C-terminal FATC domain of ATM. Further experiments are required to confirm this result. In addition, we have also generated GST-fusion fragments of DGCR8 to map the interaction of ATM with DGCR8 (data not shown).

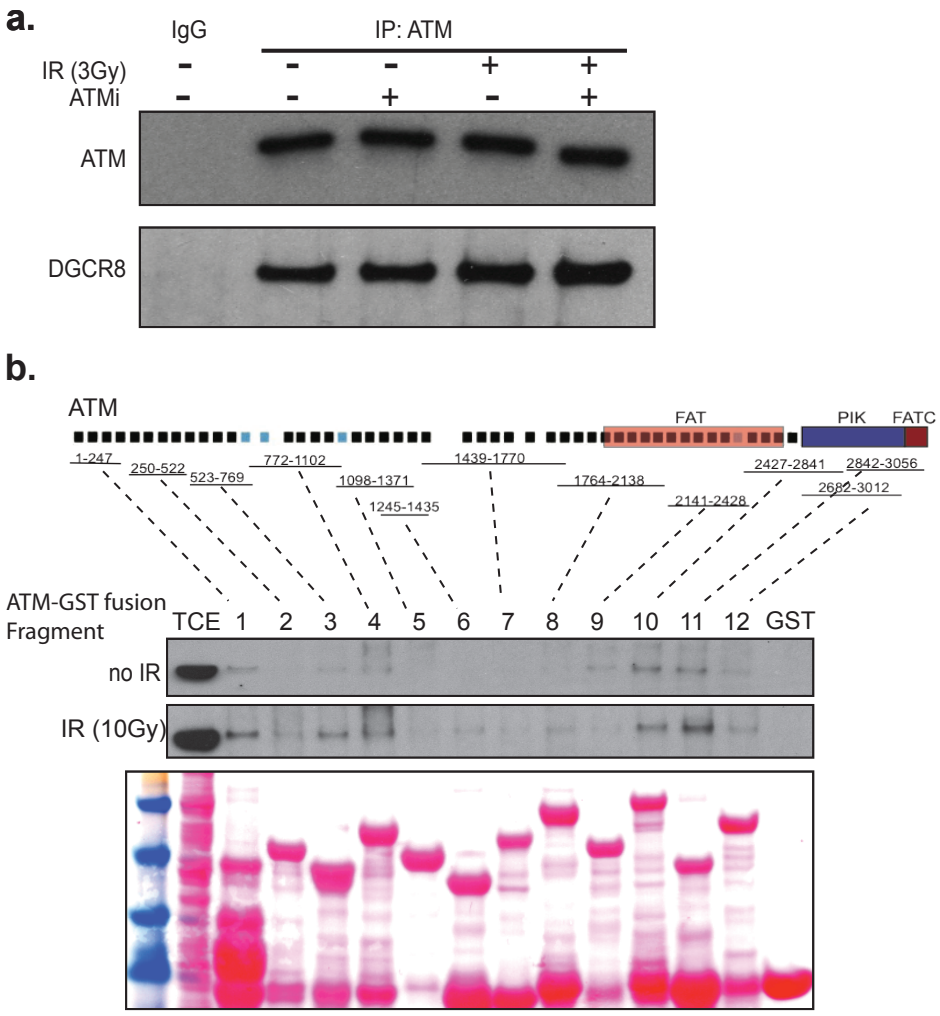

Figure 3.3: DGCR8 interact with ATM in U2OS and HEK293T cells

a. Western blot analysis of an ATM IP probed for DGCR8. ATM was immunoprecipitated in the presence and absence of damage (10Gy) and ATMi. b. Western blot analysis of GST-ATM fragments before and after IR (10Gy). Recombinant GST-ATM fragments were expressed in E.coli and purified using Glutathione beads. The ATM fragment coupled beads were then incubated with TCE from damaged and undamaged HEK293T cells. The resulting Western Blot was then probed for DGCR8.

The DGCR8 protein only has one SQ site (S677) in its protein sequence, no phosphorylation has been detected in substrate screens (Bensimon, Schmidt et al., 2010, Matsuoka, Ballif et al., 2007) and we were also unable to detect any phosphorylation of DGCR8, when immunoprecipitated after damage (Figure 3.4) and probed for an antibody generated against pBRCA1(S1423) that recognises SQ/TQ phosphorylation (Matsuoka et al., 2007). However, we cannot exclude detection of phosphorylation using other SQ/TQ specific antibodies.

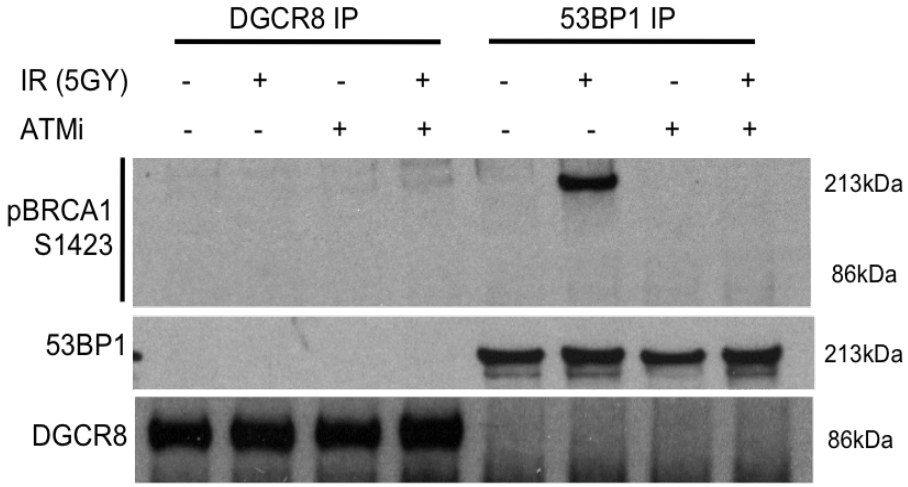

Figure 3.4: DGCR8 is not phosphorylated in response to DNA damage

Immunoprecipitation of DGCR8 and 53BP1. U2OS cells were treated with ATMi 1h prior to irradiation (10Gy) and harvested 1h after damage. DGCR8 and 53BP1 were immunoprecipitated and the resulting western blot was probed for pBRCA1(S1423), which is an antibody commonly used to detect SQ/TQ phosphorylation. 53BP1 was used as a control for ATM phosphorylation.

3.4.2. DGCR8 depletion results in IR sensitivity

DGCR8 is a microprocessor of non-coding microRNA and is in the same pathway with DROSHA and DICER, two proteins recently implicated in the DDR. Depletion by RNA interference of these two proteins leads to severe reduction in pATM and 53BP1 foci upon DNA damage induction using IR in HeLa cells or with I-SceI in NIH2/4 cells, and therefore to a general loss of the response cascade. Interestingly, the presence of γ-H2AX seems not to be affected with these proteins (Francia, Michelini et al., 2012).

In order to study a possible function for DGCR8 in the DDR we carried out clonogenic survival assays (Figure 3.5a). DGCR8 depletion results in sensitivity to ionizing radiation compared to a control sample but less sensitivity when compared to ATM inhibited cells. This indicates that DGCR8 is required for efficient cell proliferation in response to DNA damage.

Loss of DGCR8, like Drosha or Dicer, displays no change in γH2AX kinetics at early timepoints compared to control cells (Figure 3.5b-d). This suggests that DGCR8 is not required for sensing or inititation of DNA repair and is more likely affecting DNA damage downstream of γH2AX.

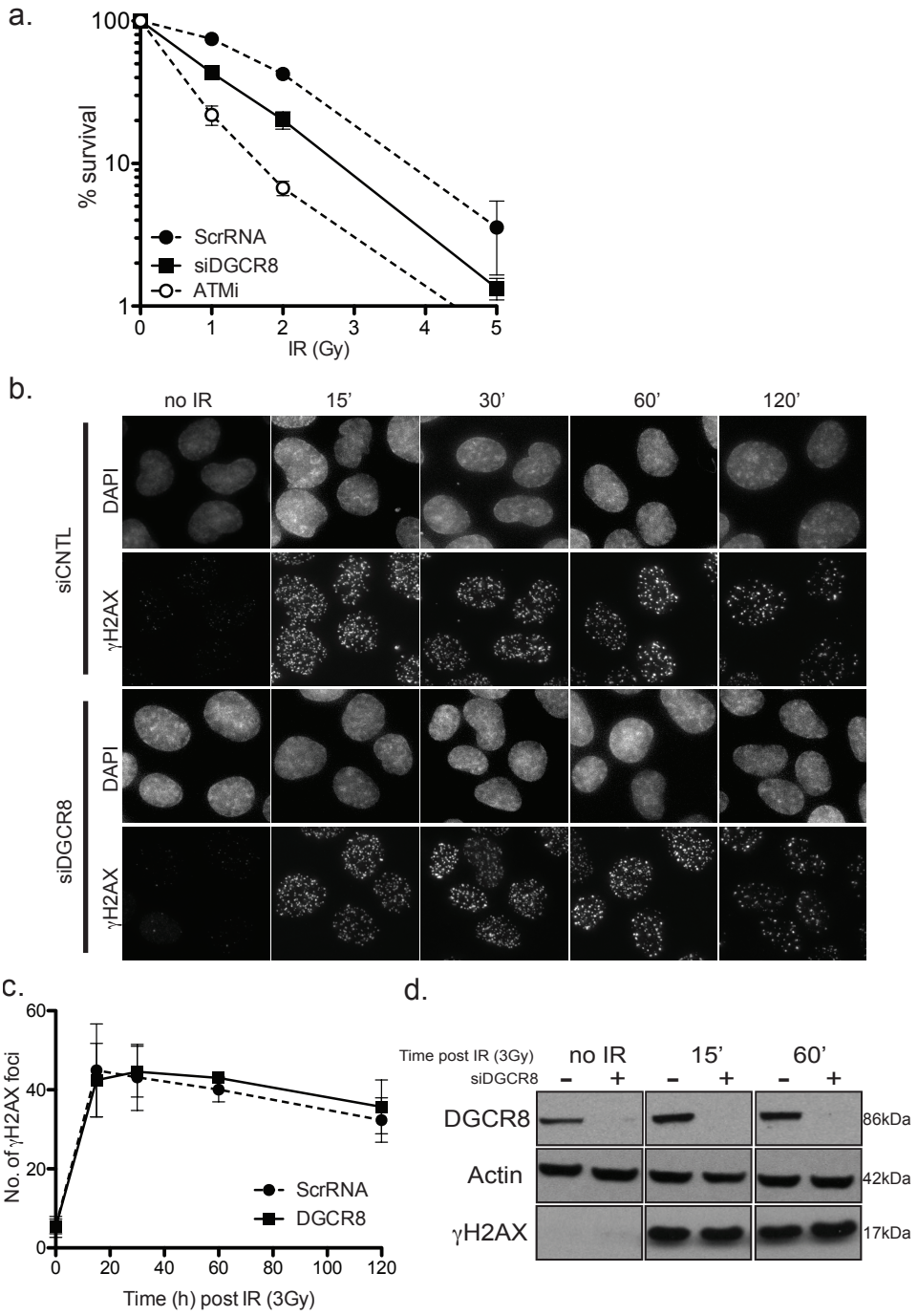

Figure 3.5:DGCR8 depletion results in IR sensitivity but has no effect on H2AX phosphorylation

A. Clonogenic survival assay of control, DGCR8 depleted and ATM inhibited cells at indicated doses of IR. Cells were grown for 10-14 days in culture, stained with DMMB and counted. Experiments were carried out in triplicate and error bars represent the SD across three independent experiments (n=3).

3.4.3. Loss of DGCR8 results in increased IRIF intensity of pATM and 53BP1

In order to investigate the effect of DGCR8 depletion on focal formation of DDR factors downstream of γH2AX phosphorylation, we studied the phopsphorylation of ATM on Serine 1981 at early timepoints after IR. Surprisingly, pATM foci appear to be more numerous and intense in DGCR8 depleted cells compared to control cells, an observation that is especially pronounced at early timepoints and then readjusts to near control levels an hour after DNA damage induction (Figure 3.6b). This phenotype could also be observed at pATM protein levels. DGCR8 deficient cells show an upregulation of ATM S1981 phosphorylation in response to IR compared to the control. This indicates an elevated level of ATM activity in the absence of DGCR8.

To further investigate increased repair kinetics in the absence of DGCR8, we show that 53BP1 focal recruitment is also enhanced at early timepoints after damage in the absence of DGCR8 (Figure 3.7) following similar kinetics than ATM phosphorylation. 53BP1 accumulates faster and more intense in the absence of DGCR8.

Figure 2.5 cntd.

B. Immunofluorescence of U2OS cells stained with yH2AX antibody and DAPI. Cells were transfected with control or DGCR8 siRNA, irradiated (3Gy) and fixed at the indicated timepoints after damage. C. Quantifcation of B. Experiments were carried out in triplicate and error bars indicate the SEM of three independent experiments (n=3). D. WB of control and DGCR8 depleted cells. Cells were transfected with control or DGCR8 siRNA, irradiated at 3Gy and harvested at the indicated times after IR.

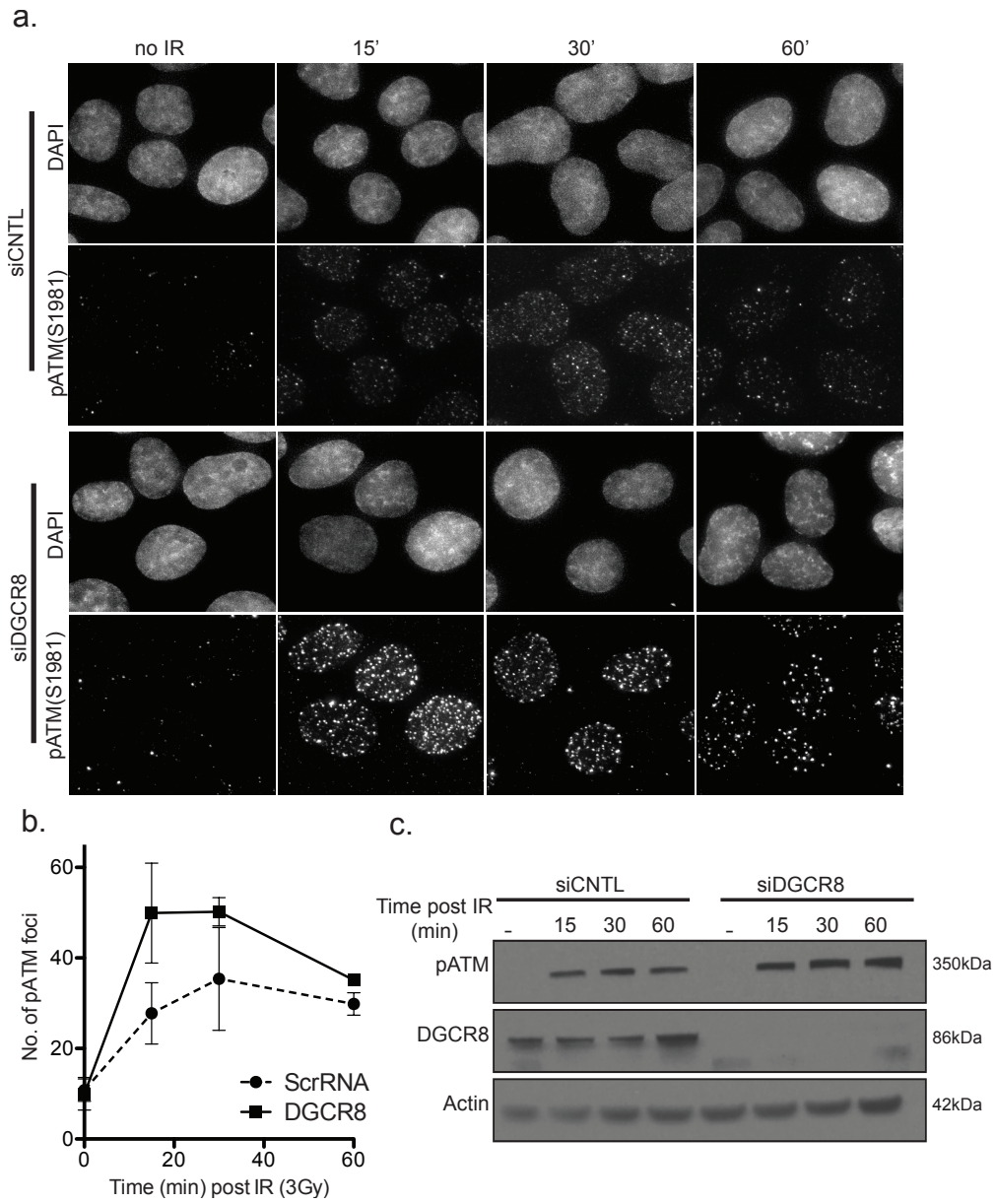

Figure 3.6: DGCR8 depletion increases pATM focal recruitment and intensity at early timepoints after IR

A. Immunofluorescence of pATM(S1981) in U2OS cells. Cells were transfected with control or DGCR8 siRNA, irradiated at 3Gy and fixed at the indicated timepoints after damage. Cell were then stained with pATM(S1981) antibody and DAPI. B. Quantification of the number of ATM foci in control and DGCR8 depleted cells. Experiments were carried out in triplicate and errorbars indicate the SEM across three independent experiments (n=3). C. WB of DGCR8 depleted and control cells. Cells were transfected with control or DGCR8 siRNA, irradiated at 3Gy and lysed at the indicated timepoints after damage.

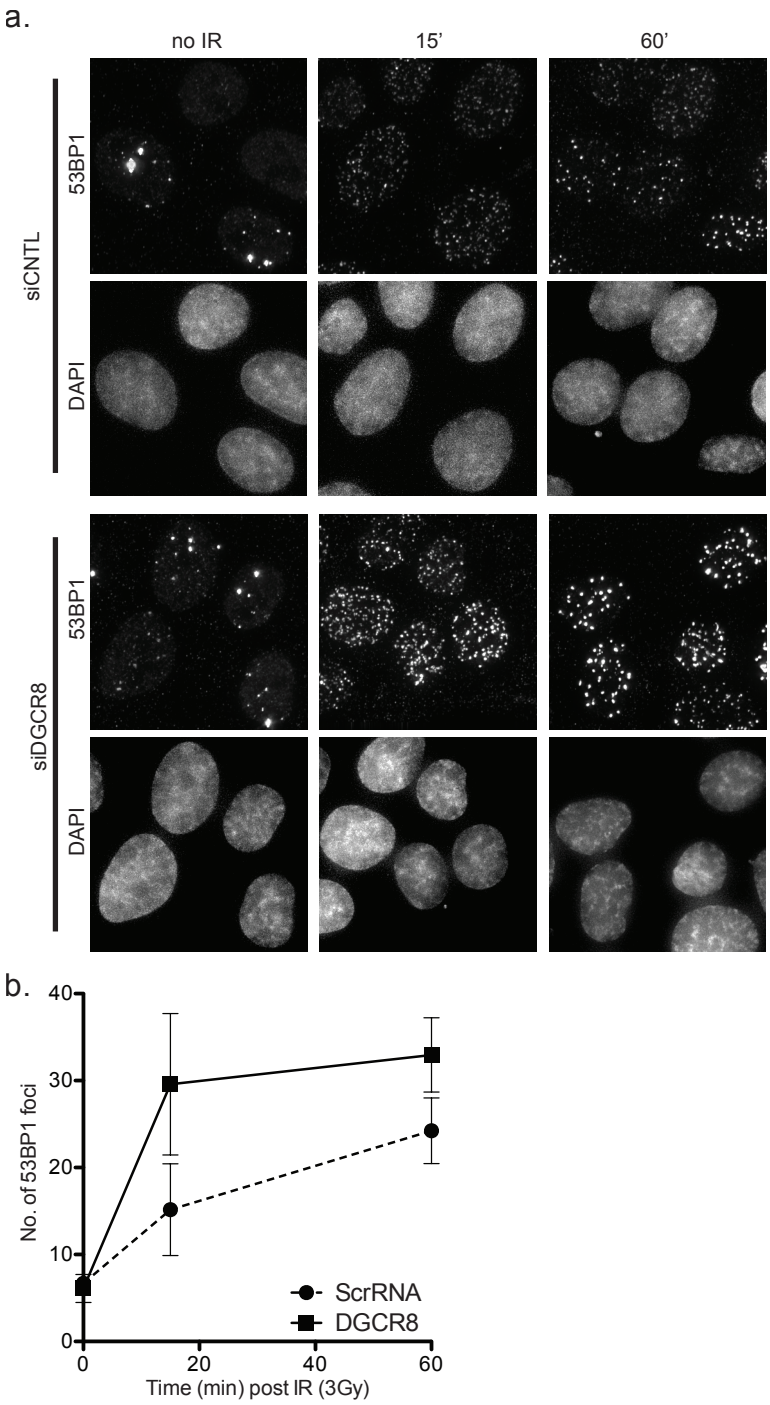

Figure 3.7: Loss of DGCR8 results in increased number and intensity of 53BP1 IRIF

A. Immunofluorescence of 53BP1 in U2OS cells. Cells were transfected with control or DGCR8 siRNA, irradiated at 3Gy and fixed at the indicated timepoints after damage. Cell were then stained with 53BP1 antibody and DAPI. B. Quantification of the number of 53BP1 foci in control and DGCR8 depleted cells. Experiments were carried out in triplicate and error bars indicate the SEM across three independent experiments (n=3).

3.4.4. DGCR8 is not required for efficient checkpoint regulation

Next, we investigated the role of DGCR8 in cell cycle regulation and G2/M checkpoint activation to see whether the increased focal recruitment of DDR factors or increased ATM activity in the absence of DGCR8 has any effect on the cell cycle.

Using Propidium Iodide to stain the DNA, we studied the distribution of cell cycle stages by the DNA content of the cells at different timepoints after damage in DGCR8 depleted and control cells (Figure 3.8a). Loss of DGCR8 appears to have no effect on cell cycle distribution in response to DNA damage

In addition, cells depleted of DGCR8 show no defect in G2/M checkpoint activation or recovery (Figure 3.8b). A similar percentage of mitotic cells are present in the presence and absence of DGCR8 in undamaged cells. In response to IR (3Gy) the control and DGCR8 depleted cells enter the checkpoint with similar kinetics and are fully arrested by 4h post IR. ATM inhibition causes a defective DDR signalling cascade and in turn prevents G2/M checkpoint activation leading to a constant percentage of mitotic cells (Figure 3.8b). After completed repair, the cells are released from the checkpoint 8h after IR. By 12h after damage, the cells have fully recovered. This data suggests that DGCR8 depletion has no effect on the cell cycle or G2/M checkpoint regulation. It has to be noted that pCHK2 levels appear to be increased at later timepoints (4h post IR) (Figure 3.8c). Whether or not this increased is significant will required careful quantification of the western blot.

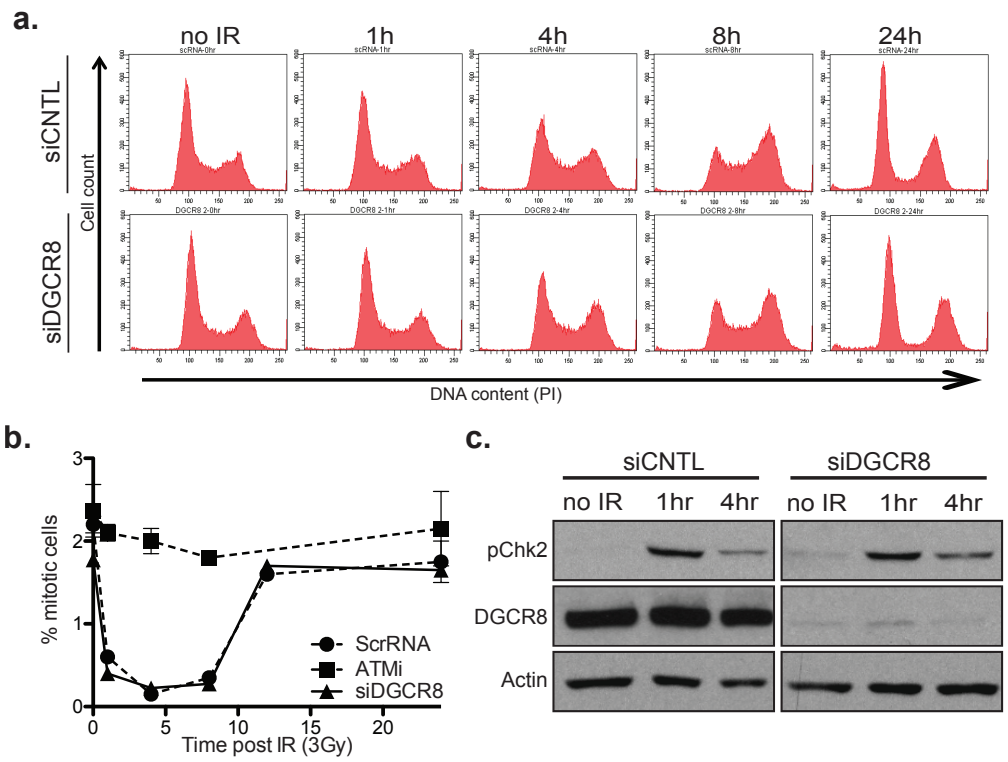

Figure 3.8: DGCR8 has no effect on the cell cycle or CHK2 phosphorylation

A. PI profile of control and DGCR8 depleted cell in response to IR. Cell were treated with control or DGCR8 siRNA, irradiated at 3Gy and fixed in 75% EtOH at the indicated timepoints after damage. The cells were then permeabilized with 0.5% Triton, stained with PI and analysed on the FACS CantoII. B. G2/M checkpoint assay. Cells were treated with control or DGCR8 siRNA, irradiated at 3Gy and fixed in 75% EtOH at the indicated timepoints after damage. Cells were then stained with anti H3pS10 antibody and PI before being analysed with the FACS Canto II. Experiments were carried out in triplicate and error bars show the SD of three independent experiments (n=3). C. WB of pCHK2 in control and DGCR8 depleted cells. Cells were transfected with control or DGCR8 siRNA, irradiated (3Gy) and lysed at the indicated timepoints after damage. The resulting western blot was then probed for DGCR8 to verify knock-down efficiency, actin as a loading control and pCHK2.

3.4.5. DGCR8 is required for efficient repair by HR and NHEJ

To further investigate the effect of DGCR8 in efficient DSB repair and to determine the pathway it is involved in, we have carried out Clonogenic survival assays using ICRF-193 and Olaparib to induce breaks primarily repaired by NHEJ or HR, respectively. Olaparib is a PARP inhibitor that induces DNA nicks that are converted to DSBs primarily repaired by HR. ICRF-193 is a TOPII inhibitor that induces DSBs preferentially repair by NHEJ. DGCR8 depleted cells as well as Drosha depleted cells show increased sensitivity to IRCF-193 when compared to control cells. Double depletion of DGCR8 and Drosha has an epistatic effect suggesting that DGCR8 and Drosha act in the same pathway to repair ICRF-193 induced DSB breaks (Figure 3.9a).

Similarly, DGCR8 depleted cells and Drosha depleted cells are significantly more sensitive to Olaparib when compared to control cells (Figure 3.9b). Suggesting each of these proteins is required for efficient DSB repair of Olaparib induced breaks. Double depletion of DGCR8 and Drosha shows a synergistic effect compared to the individual depletion of DGCR8 or Drosha. This indicated that these proteins act in different pathways to repair DSBs induced by Olaparib.

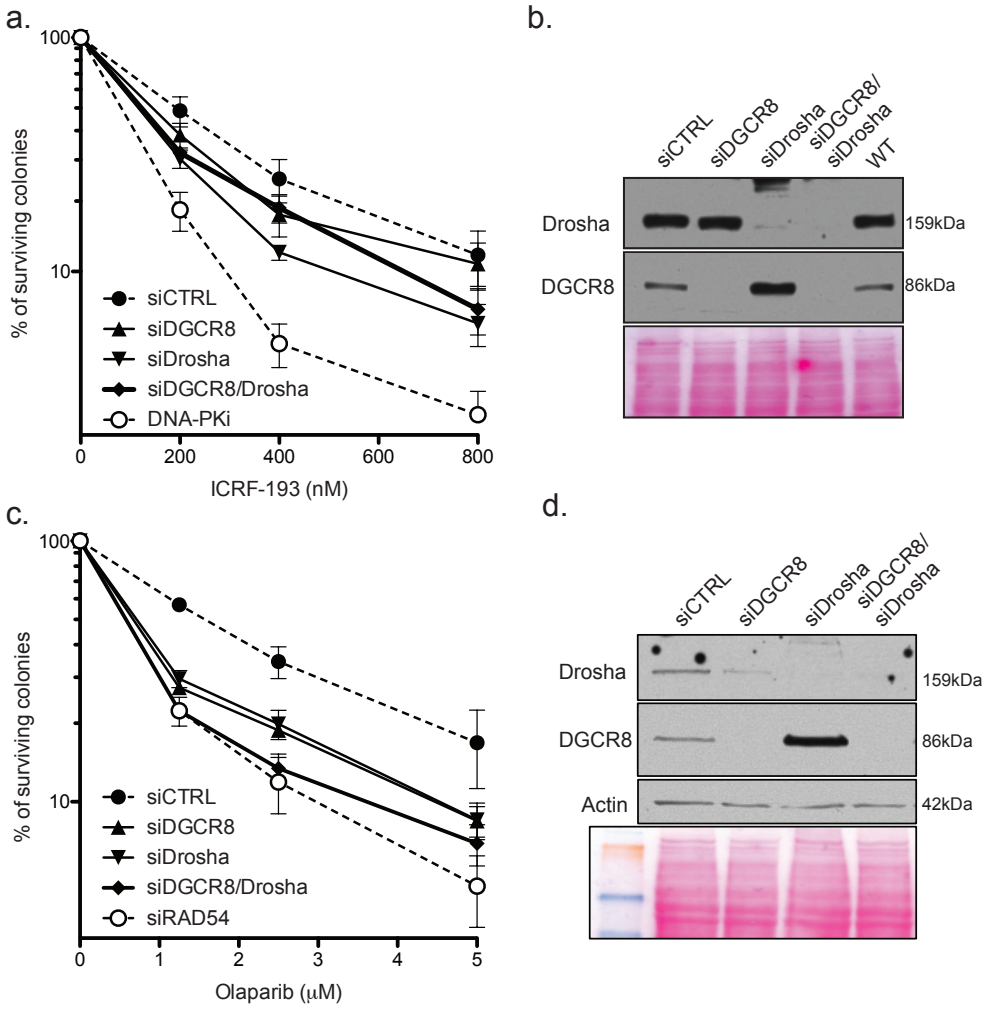

Figure 3.9: DGCR8 depletion results in increases sensitivity to Olaparib and ICRF193 and leads to a defect in HR

A. Clonogenic survival assay in U2OS cells. 500 cells were plated in media containing the appropriate concentration of Olaparib, grown for 10-14 days and stained with DMMB. All experiments were carried out in triplicate and error bars represent the SD across all independent experiments (n=5). B. WB of knockdown efficiency. C. Clonogenic survival assay in U2OS cells. 500 cells were plated in media containing the indicated concentration of ICRF-193, grown for 10-14 days. Colonies were then stained with DMMB and counted. All experiments were carried out in triplicate and error bars represent the SD across all independent experiments (n=5). D. WB of knock-down efficiency.

In order to directly investigate the effect of DGCR8 depletion on HR, we conduced HR assays using the DR-GFP reporter system (Pierce et al., 1999). We used the DR-GFP reporter system over a timecourse of 6 days in order to increase the sensitivity of this assay. Depletion of DGCR8 results in a 10-20% reduction of HR efficiency compared to the control, while Drosha depletion shows a 5-10% reduction. However, double depletion of both DGCR8 and Drosha has a synergistic effect on HR efficiency, suggesting these proteins are functioning in different pathways (Figure 3.9c). This leads to the assumption that DGCR8 plays in the DDR is not only due to its ability to process miRNAs but that it has additional functions independent from Drosha.

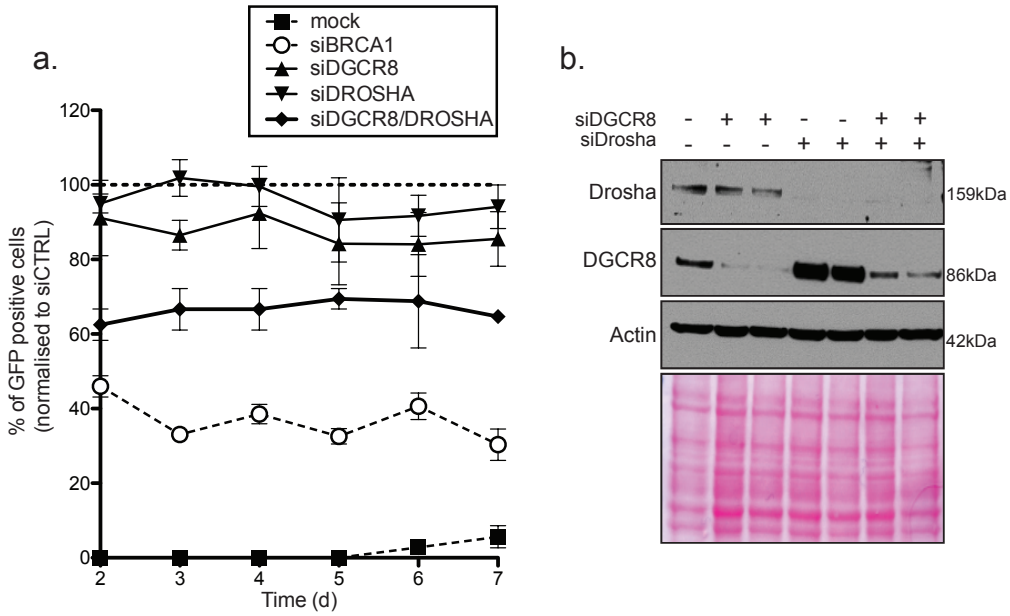

Figure 3.10: DGCR8 and Drosha act in different HR repair pathways

A. DR-GFP reporter assay. Cells were transfected with siRNA, I-SceI plasmid and cerulean plasmid, split into 6 dishes 24h post transfection and grown for the indicated times. Live cells were harvested and GFP positive cells were analysed using a BD-FACS CantoII flow cytometer. The graph shows the percentage reduction of GFP-positive cells compared to the control cells. Error bars represent the SEM across all independent experiments (n=5). B. WB of knock-down efficiency of siRNAs.

DGCR8 is required for functional processing of pri-miRNA together with the RNAseIII Drosha. We confirmed that Drosha depletion results in increased protein levels of DGCR8 (Figure 3.11). Upon Drosha depletion, DGCR8 total protein levels increase three to four fold (Han et al., 2009). The fact that Drosha depleted cells show a decrease in pATM(S1981) (Francia et al., 2012), while loss of DGCR8 results in increased pATM IRIF number and intensity, further underlines a possible role for DGCR8 independent of Drosha in the DNA damage response.

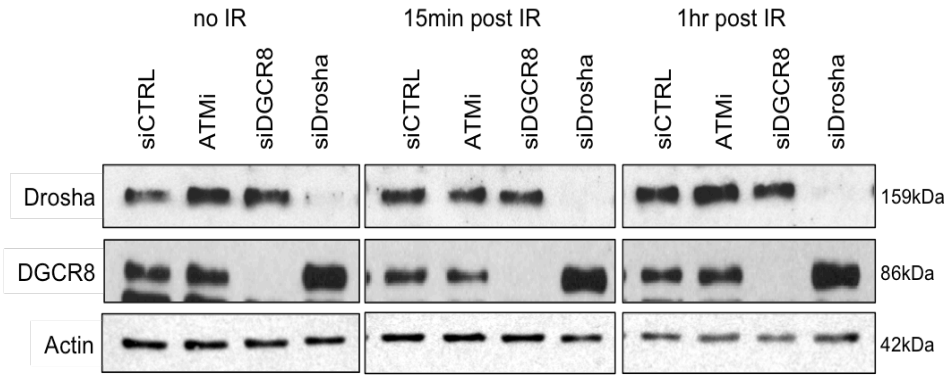

Figure 3.11: DGCR8 protein levels are regulated by Drosha

WB of DGCR8 and Drosha protein levels. U2OS cells were treated with control, DGCR8 or Drosha siRNA, irradiated at 3Gy and lysed at the indicated timepoints. The resulting WB was then probed for DGCR8 and Drosha respectively.

3.5. Discussion

In this study we confirm that DGCR8 is a novel interacting protein of ATM. We have mapped DGCR8 to the C-terminal region of ATM suggesting that DGCR8 is a target or regulator of ATM. This data will need to be verified using more stringent washing conditions to reduce unspecific binding and false positives. In addition, we have generated GST fragments spanning the DGCR8 protein in order to verify the interaction and map it to a region in the DGCR8 protein. DGCR8 binding to the FATC domain of ATM could indicate a regulatory role for DGCR8. The FATC domain of ATM is required for acetylation by TIP60 and activation of ATM (Sun, Jiang et al., 2005). It would be interesting to investigate whether TIP60 also interacts with DGCR8 as both proteins are constitutively bound to ATM. In order to directly address the regulation of ATM kinase activity, we have set up ATM kinase assays using recombinant ATM (WT/KD) (Canman, Lim et al., 1998). Addition of recombinant DGCR8 in the presence of different substrates such as p53, H2AX, CHK2 and 53BP1 will provide a better understanding of whether DGCR8 regulates ATM kinase activity *in vitro* and if this regulation is substrate specific.

DGCR8 phosphorylation could not be detected in IP experiments and was not identified in ATM/ATR substrate screens (Bensimon et al., 2010, Matsuoka et al., 2007) suggesting that it could have a more regulatory role instead of being a target of ATM, which will be clarified in ATM kinase assays.

Loss of DGCR8 results in impaired colony formation in response to IR, Olaparib and ICRF-193. In addition, DGCR8 depletion also results in a partially defective in HR. Therefore, we concluded that DGCR8 negatively impacts on cell survival and proliferation in response to DNA damage. However, all phenotypes were observed in long term experiments requiring the cells to complete several cell cycles. In short term assays

such as cell cycle profiling or G2/M checkpoint assays and activation of the DDR signalling cascade by the phosphorylation of γH2AX, we have not observed any difference between control and DGCR8 depleted cells. DGCR8 is not required for cell cycle regulation, G2/M checkpoint activation or release and phosphorylation of histone H2AX in response to IR.

However, cells depleted of DGCR8 show increased focal recruitment of the DDR factors ATM and 53BP1 to double strand breaks at early timepoints. This data suggests that DNA repair is somewhat deregulated in the absence of DGCR8. Earlier focal recruitment of 53BP1 and ATM and enhanced phosphorylation of ATM indicate an increased ATM kinase acitivity in DGCR8 depleted cells. The data also suggests a role independent of its partner protein Drosha, which is required for efficient focal recruitment of these DDR factors to DSBs (Francia et al., 2012). However, the comparison of data sets with Francia et al., 2012, needs to be carefully interpreted, as the phenotype we observed are exclusively at early timepoints in response to DNA damage, while the defect of pATM and 53BP1 recruitment shown by Francia et al. is at 7h post IR (10Gy). Therefore, we cannot conclude definitely that the role of DGCR8 is separate to Drosha based on this evidence. Preliminary experiment we carried out using Drosha knock-down at early timepoints shows reduction of 53BP1 foci, but these experiments will need to be carefully repeated.

Further evidence for a Drosha independent role of DGCR8 is provided when studying the double depletion of DGCR8 and Drosha in the DR-GFP-reporter system. While single knock down of either DGCR8 or Drosha show a partial defect in efficient gene conversion, the double depletion results in a synergistic effect, indicating the involvement of these two proteins in different pathways.

Due to the fact that Drosha depletion results in upregulated DGCR8 protein levels and defective recruitment of DDR factors to DSBs, it is critical to exclude that the upregulation of DGCR8 is the cause of

defective recruitment of DDR factors in Drosha depleted cells. To eliminate this possibility, the focal recruitment of DDR factor should be assessed in cells with 4-fold overexpressed DGCR8 in the presence of Drosha. This should further narrow down the function of DGCR8 and Drosha in the DDR.

Although showing no apparent effect on the cell cycle, G2/M checkpoint response or repair kinetics, loss of DGCR8 results in survival defects in response to various DNA damaging agents. One possible explanation could be that DGCR8 depletion may lead to increased error-prone DNA repair by either alt-EJ or SSA, which in turn result in increased genome instability. To validate this hypothesis, it would be important to investigate the extent of resection at the double strand break as well as directly assay the rate of C-NHEJ, alt-EJ and SSA. To test this hypothesis, we are planning to investigate these repair pathways using resection assays (Zhou, Caron et al., 2014) in addition to assays specifically interrogating alt-EJ or SSA (Ochs, Somyajit et al., 2016, Yun & Hiom, 2009).

All in all, this study shows that DGCR8 is a novel interacting partner of ATM and it plays a role in the DNA damage response. The exact role and mechanism however remain unclear and further experiments are required to obtain a more detailed understanding the role of the miRNA processor subunit DGCR8 DNA damage and repair.

3.6. References

Ameres SL, Zamore PD (2013) Diversifying microRNA sequence and function. Nat Rev Mol Cell Biol 14: 475-88

Bakkenist CJ, Kastan MB (2003) DNA damage activates ATM through intermolecular autophosphorylation and dimer dissociation. Nature 421: 499-506

Bensimon A, Schmidt A, Ziv Y, Elkon R, Wang SY, Chen DJ, Aebersold R, Shiloh Y (2010) ATM-dependent and -independent dynamics of the nuclear phosphoproteome after DNA damage. Sci Signal 3: rs3

Canman CE, Lim DS, Cimprich KA, Taya Y, Tamai K, Sakaguchi K, Appella E, Kastan MB, Siliciano JD (1998) Activation of the ATM kinase by ionizing radiation and phosphorylation of p53. Science 281: 1677-9

Carlson C, Sirotkin H, Pandita R, Goldberg R, McKie J, Wadey R, Patanjali SR, Weissman SM, Anyane-Yeboa K, Warburton D, Scambler P, Shprintzen R, Kucherlapati R, Morrow BE (1997) Molecular definition of 22q11 deletions in 151 velo-cardio-facial syndrome patients. Am J Hum Genet 61: 620-9

Eliez S, Blasey CM, Schmitt EJ, White CD, Hu D, Reiss AL (2001) Velocardiofacial syndrome: are structural changes in the temporal and mesial temporal regions related to schizophrenia? Am J Psychiatry 158: 447-53

Faller M, Matsunaga M, Yin S, Loo JA, Guo F (2007) Heme is involved in microRNA processing. Nat Struct Mol Biol 14: 23-9

Francia S, Michelini F, Saxena A, Tang D, de Hoon M, Anelli V, Mione M, Carninci P, d'Adda di Fagagna F (2012) Site-specific DICER and DROSHA RNA products control the DNA-damage response. Nature 488: 231-5

Goodarzi AA, Lees-Miller SP (2004) Biochemical characterization of the ataxia-telangiectasia mutated (ATM) protein from human cells. DNA Repair (Amst) 3: 753-67

Gregory RI, Yan KP, Amuthan G, Chendrimada T, Doratotaj B, Cooch N, Shiekhattar R (2004) The Microprocessor complex mediates the genesis of microRNAs. Nature 432: 235-40

Ha M, Kim VN (2014) Regulation of microRNA biogenesis. Nat Rev Mol Cell Biol 15: 509-24

Han J, Pedersen JS, Kwon SC, Belair CD, Kim YK, Yeom KH, Yang WY, Haussler D, Blelloch R, Kim VN (2009) Posttranscriptional crossregulation between Drosha and DGCR8. Cell 136: 75-84

Kawamata T, Tomari Y (2010) Making RISC. Trends Biochem Sci 35: 368-76

Khanna KK, Keating KE, Kozlov S, Scott S, Gatei M, Hobson K, Taya Y, Gabrielli B, Chan D, Lees-Miller SP, Lavin MF (1998) ATM associates with and phosphorylates p53: mapping the region of interaction. Nat Genet 20: 398-400

Kwon SC, Nguyen TA, Choi YG, Jo MH, Hohng S, Kim VN, Woo JS (2016) Structure of Human DROSHA. Cell 164: 81-90

Landthaler M, Yalcin A, Tuschl T (2004) The human DiGeorge syndrome critical region gene 8 and Its D. melanogaster homolog are required for miRNA biogenesis. Curr Biol 14: 2162-7

Matsuoka S, Ballif BA, Smogorzewska A, McDonald ER, 3rd, Hurov KE, Luo J, Bakalarski CE, Zhao Z, Solimini N, Lerenthal Y, Shiloh Y, Gygi SP, Elledge SJ (2007) ATM and ATR substrate analysis reveals extensive protein networks responsive to DNA damage. Science 316: 1160-6

McDonald-McGinn DM, Sullivan KE (2011) Chromosome 22q11.2 deletion syndrome (DiGeorge syndrome/velocardiofacial syndrome). Medicine (Baltimore) 90: 1-18

Nguyen TA, Jo MH, Choi YG, Park J, Kwon SC, Hohng S, Kim VN, Woo JS (2015) Functional Anatomy of the Human Microprocessor. Cell 161: 1374-87

Ochs F, Somyajit K, Altmeyer M, Rask MB, Lukas J, Lukas C (2016) 53BP1 fosters fidelity of homology-directed DNA repair. Nat Struct Mol Biol 23: 714-21

Pessina F, Lowndes NF (2014) The RSF1 histone-remodelling factor facilitates DNA double-strand break repair by recruiting centromeric and Fanconi Anaemia proteins. PLoS Biol 12: e1001856

Pierce AJ, Johnson RD, Thompson LH, Jasin M (1999) XRCC3 promotes homology-directed repair of DNA damage in mammalian cells. Genes Dev 13: 2633-8

Roth BM, Ishimaru D, Hennig M (2013) The core microprocessor component DiGeorge syndrome critical region 8 (DGCR8) is a nonspecific RNA-binding protein. J Biol Chem 288: 26785-99

Senturia R, Faller M, Yin S, Loo JA, Cascio D, Sawaya MR, Hwang D, Clubb RT, Guo F (2010) Structure of the dimerization domain of DiGeorge critical region 8. Protein Sci 19: 1354-65

Shi Y, Dodson GE, Mukhopadhyay PS, Shanware NP, Trinh AT, Tibbetts RS (2007) Identification of carboxyl-terminal MCM3 phosphorylation sites using polyreactive phosphospecific antibodies. J Biol Chem 282: 9236-43

Shiohama A, Sasaki T, Noda S, Minoshima S, Shimizu N (2007) Nucleolar localization of DGCR8 and identification of eleven DGCR8-associated proteins. Exp Cell Res 313: 4196-207

Sohn SY, Bae WJ, Kim JJ, Yeom KH, Kim VN, Cho Y (2007) Crystal structure of human DGCR8 core. Nat Struct Mol Biol 14: 847-53

Sun Y, Jiang X, Chen S, Fernandes N, Price BD (2005) A role for the Tip60 histone acetyltransferase in the acetylation and activation of ATM. Proc Natl Acad Sci U S A 102: 13182-7

Urquhart AJ, Gatei M, Richard DJ, Khanna KK (2011) ATM mediated phosphorylation of CHD4 contributes to genome maintenance. Genome Integr 2: 1

van Amelsvoort T, Daly E, Robertson D, Suckling J, Ng V, Critchley H, Owen MJ, Henry J, Murphy KC, Murphy DG (2001) Structural brain abnormalities associated with deletion at chromosome 22q11: quantitative neuroimaging study of adults with velo-cardio-facial syndrome. Br J Psychiatry 178: 412-9

Yuan J, Luo K, Zhang L, Cheville JC, Lou Z (2010) USP10 regulates p53 localization and stability by deubiquitinating p53. Cell 140: 384-96

Yun MH, Hiom K (2009) CtIP-BRCA1 modulates the choice of DNA double-strand-break repair pathway throughout the cell cycle. Nature 459: 460-3

Zhou Y, Caron P, Legube G, Paull TT (2014) Quantitation of DNA double-strand break resection intermediates in human cells. Nucleic Acids Res 42: e19

Chapter 4: DDX17, identified as a novel partner of 53BP1, is required for efficient DNA repair

4.1. Summary

DDX17 is a member of the DEAD box helicase family and is primarily found as a heterodimer with its paralog DDX5. DDX17 is involved in many aspects of mRNA and miRNA processing such as pre-mRNA splicing and unwinding of pre-miRNA to facilitate access of Drosha. Recent proteomic screens carried out in DT40 have identified DDX17 as a potential interacting partner of 53BP1 and ATM. We have confirmed DDX17 interaction with 53BP1 in human cells and characterised the role of DDx17 in the DDR. DDX17 depletion results in IR sensitivity and delayed G1/s and G2/M checkpoint exit. In addition, we demonstrate that DDX17 regulates cellular levels of BRCA1 and RAD51 leading to a defect in HR. DDX17 is also required for the recruitment of 53BP1 to IRIFs. Furthermore, loss of DDX17 leads to Olaparib and IRCF-193 sensitivity. Together, this data suggests that DDX17 is required for efficient DNA damage repair via both NHEJ and HR repair pathways.

4.2. Introduction

The DDX17 is a DEAD-box RNA helicase closely related to its paralog DDX5, also known as p68. These two DEAD box helicases share 90% amino acid sequence identity in their helicase core (Lamm, Nicol et al., 1996). However, their N- and C-terminal amino acid sequence varies with 60% and 30% amino acid sequence identity, respectively.

The *DDX17* gene is located on the long arm of chromosome 22 and has two main transcripts, 5.3 kb and 9.3 kb. Both transcripts can be spliced into two main splice variants, p72 and p82 and are equally expressed (Mooney, Grande et al., 2010b, Shin & Janknecht, 2007, Shin, Rossow et al., 2007), with near to identical functions and identical helicase properties *in vitro* (Uhlmann-Schiffler, Rossler et al., 2002). Interestingly, p82, the larger splice variant, contains a non-AUG start codon upstream of the AUG of p72 (Uhlmann-Schiffler et al., 2002).

The DEAD box family is the largest RNA helicase family found in humans and due to their remarkable similarity, DDX17 and DDX5 form a highly-related, distinguished sub-group of DEAD box helicases (Fuller-Pace, 2013). DDX17 can form a homodimer as well as a heterodimer with DDX5 (Ogilvie, Wilson et al., 2003). They have redundant roles in some aspects of RNA metabolism, however, due to their different C- and N-termini, both helicases also have distinct, non-overlapping functions (Fuller-Pace, 2013, Jalal, Uhlmann-Schiffler et al., 2007). DDX17 contains multiple RGG RNA binding domains in its N-terminal and has a serine/glycine rich C-terminus (Lamm et al., 1996).

Like other DEAD-box helicases, DDX17 consists of a helical core consisting of 12 conserved motifs, including the Asp-Glu-Ala-Asp (DEAD) box. DEAD-box helicases also have a conserved Q motif and an aromatic amino acid 17 amino acids upstream of the Q motif. Together, they form a recognition site for adenine, which is required for their interaction with

the backbone of RNA and, in some cases, DNA (Cordin, Tanner et al., 2004, Tanner, Cordin et al., 2003) (Figure 4.1). DDX17 is able to bind single stranded as well as double stranded RNA, but shows a higher affinity for the latter (Lee, 2002).

DDX17 is ubiquiously expressed, but its expression level varies greatly between different tissues. It is highly abundant in the kidney, pancreas and skeletal muscle, whereas its expression levels are low in heart, brain placenta, lung and liver, suggesting its level of expression is tightly controlled (Lamm et al., 1996).

Unlike its paralog DDX5, which shuttles between the nucleus and cytoplasm, DDX17 is a mainly nuclear protein, which further indicates some different roles for these two proteins. DDX17 is mainly mono-ubiquitinated, whereas DDX5 tends to be poly-ubiquitinated. This could also be the cause of the difference in half-life of these two proteins, as DDX17 has more than a 3-fold longer half-life compared to DDX5 with 68h and 20h in HEK293T cells, respectively (Mooney et al., 2010b). DDX17 and DDX5 are both sumoylated, on K50 (K129 on p82) and K53, respectively, and are subject to acetylation on lysines in the N-terminal region (Jacobs, Nicol et al., 2007, Mooney, Goel et al., 2010a, Mooney et al., 2010b).

Ddx17 knock-out is lethal in mice at post natal day 2, whereas Ddx5 depletion is embyronic lethal at E11.5. The double deletion leads to earlier embryonic lethality, which is further evidence for separate roles of these two closely related helicases (Fukuda, Yamagata et al., 2007, Fuller-Pace, 2013). Moreover, DDX17-null MEFs exhibit reduced cell growth and increased apoptosis (Fukuda et al., 2007). The levels of DDX17 are significantly reduced during development in Down Syndrome brains, suggesting it plays a role in development and differentiation (Ip, Chung et al., 2000, Kircher, Kim et al., 2002).

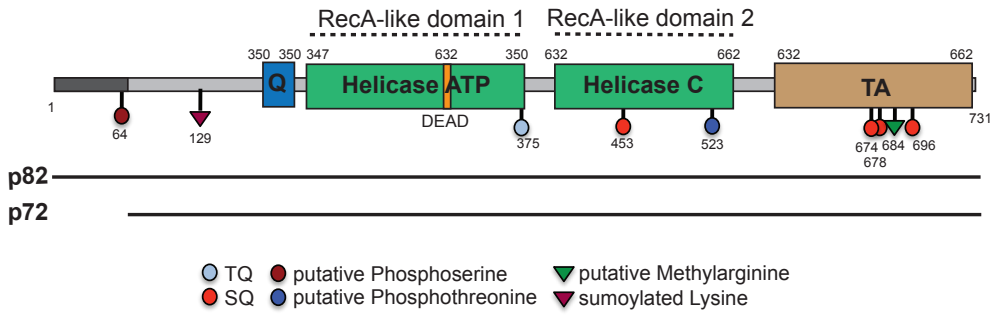

Figure 4.1: Schematic structure of DDX17

This schematic shows the structure of DDX17. The central helicase core is comprised of two RecA-like domains (green). The C-terminal transactivation domain is depicted in brown and the Q motif in blue. DDX17 is sumoylated on lysine 129 and has several putative serine and threonine phosphorylation site (lollipops).

Due to their high sequence similarity and functional overlap, most studies do not distinguish between DDX5 and DDX17, but instead study their combined role. Unfortunately, this makes it difficult to separate their individual functional properties. Both proteins are, like most DEAD-box proteins, pleiotropic with multiple functions, both dependent and independent of their helicase activity.

DDX17 and DDX5 are involved in pre-mRNA splicing (Dardenne, Pierredon et al., 2012, Germann, Gratadou et al., 2012, Lee, 2002, Liu, 2002, Samaan, Tranchevent et al., 2014), alternative splicing of mRNAs (Auboeuf, Honig et al., 2002, Dardenne et al., 2012, Germann et al., 2012, Guil, Gattoni et al., 2003, Honig, Auboeuf et al., 2002), rRNA processing (Fukuda et al., 2007, Jalal et al., 2007) and miRNA processing (Salzman, Shubert-Coleman et al., 2007). All of these functions require their helicases activity, suggesting, in these roles they are, at least partially, redundant.

Both proteins are part of the large Drosha complex and required for the processing of the 5.8S subunit of ribosomal RNA as well as a specific

subset of miRNAs (Fukuda et al., 2007, Gregory, Yan et al., 2004). The two helicases unwind the pre-miRNA locally to facilitate access of Drosha for processing (Fukuda et al., 2007, Suzuki, Yamagata et al., 2009). DDX17 plays a role in pre-mRNA processing through its interaction with U1 snRNA and the 5'splice site (Camats, Guil et al., 2008, Kar, Fushimi et al., 2011, Lee, 2002, Lin, Yang et al., 2005) and also regulates the alternative splicing of the adhesion protein CD44, which is implicated in cancer metastasis (Honig et al., 2002, Jothy, 2003).

In addition to its many functions in RNA processing, DDX17 has also been implicated in transcriptional co-activation as well as transcriptional repression of target genes. DDX17 and DDX5 act as a bridge between transcription factors and co-activators similar to RNA helicase A, for instance between CBP and RNA pol II, with has been shown for several helicases of the DEAD box and DExD/H box family (Anderson, Schlegel et al., 1998, Nakajima, Uchida et al., 1997, Rossow & Janknecht, 2003, Shin & Janknecht, 2007). Moreover, Dardenne et al. has demonstrated a requirement for DDX17 as a transcriptional co-activator of MyoD in myogenesis (Dardenne, Polay Espinoza et al., 2014). DDX5 and DDX17 are both transcriptional co-activators of NFAT5 and required for activation of NFAT5 target genes implicated in tumour cell migration. They also can act as transcriptional activators of ERα (Watanabe, Yanagisawa et al., 2001), but only DDX17 is needed for the estrogen responsive cell growth and estrogen-dependent expression of ERα responsive genes (Wortham, Ahamed et al., 2009).

Both helicases interact with HDAC 1,2 and 3 and their sumoylation enhances interaction with HDAC1 (Jacobs et al., 2007, Mooney et al., 2010b, Wilson, Bates et al., 2004). HDAC1 is associated with transcriptional repression, and unlike DDX5, DDX17 shows both HDAC dependent and independent transcriptional repression (Bates, Nicol et al., 2005).

Unlike DDX5, DDX17 has no effect on p53 transcriptional activity in response to DNA damage (Bates et al., 2005), and is required for transcription of *MDM2* in cells without functional p53 (Bates et al., 2005, Shin & Janknecht, 2007).

DDX17 has been implicated in cell proliferation and survival, and unsurprisingly is deregulated in different types of tumours, e.g. it is over-expressed in colorectal tumours and 72-75% of breast cancers (Fukuda et al., 2007, Jalal et al., 2007, Mooney et al., 2010b, Shin et al., 2007, Wortham et al., 2009). DDX17 has also been associated with various other diseases including Down Syndrome, hepatic fibrosis and obesity (Bolduc, Larose et al., 2004, Huang, Shiffman et al., 2006, Kircher et al., 2002)

A recent screen for homologous recombination proteins has identified DDX17 as a potential HR suppressor. Furthermore, DDX17 localises to DSBs after micro-irradiation (Adamson, Smogorzewska et al., 2012). DDX17 was also identified as a substrate in an ATM/ATR phosphorylation screen (Matsuoka, Ballif et al., 2007). In this screen, two potential phosphorylation sites were identified as S126 and S130.

In this study, we show the interaction of DDX17 with the DDR factor, 53BP1, and suggest a possible role in both DNA repair pathways. Moreover, we show its effect on the recruitment of the HR factors BRCA1 and RAD51 to DNA double strand breaks.

4.3. Materials and Methods

Cell culture

U2OS (ATCC HTB-96) and HEK293T (ATCC CRL-11268) cells were cultured in Dulbecco's modified Eagles medium (DMEM) (Lonza, F1-BE12-604F) supplemented with 10% FCS (Sigma) and 1% PenStrep (Sigma, P4333). hTERT-RPE1 cells were cultured in DMEM-F12 (Lonza, F1-BE12-719F) supplemented with 10% FCS (Sigma) and 1% PenStep (Sigma, P4333).

siRNA and plasmid transfections

Cells were transfected with Oligofectamine Reagent (LifeTechnologies, 12252011) according to manufacturers instructions. Briefly, $1.2x10^5$ cells were plated on a 35mm cell culture dish. After 24hr cells were transfected with 40pmol of negative control siRNA (Ambion, AM4611) or siDDX17 (Dharmacon, MU-013450-01, J-013450-09/12). Cells were harvested 48hrs post transfection. Cells were treated with ATM inhibitor (SelleckChem KU-55933, 10μM) 1hr prior to irradiation where indicated.

Immunoblotting

Cells were lysed in 50μl Lysis Buffer (150mM NaCl, 50mM Tris-Hcl, pH7.5, 10% Glycerol, 0.5%NP-40, 1mM $MgCl_2$, 1μl Benzonase (Sigma, E1014), Phosphatase and Protease Inhibitors) for 1h on ice. After pelleting the lysed cells at 14000rpm for 15min at 4°C, whole cell lysates were collected and the concentration was measured using Bradford Reagent (Sigma, B6916). 25μg of TCE was run on a denaturing polyacrylamide gel. Proteins were transferred onto a nitrocellulose membrane for 1h at 100V on ice. Membranes were blocked with TBS-T containing 5% milk for 10min at RT prior to primary antibody incubation overnight. The following primary antibodies were used: Actin (Sigma, A2066), ATM (Bethyl, A300-136A), 53BP1 (Bethyl, A300-272A), BRCA1 (D-9) (Santa Cruz, sc-6954), γH2AX(S139) (Millipore, 05-636), RAD51

(Calbiochem, PC130), DDX17 (Abcam, 180190), DDX3X (Bethyl, A300-474A)

Co-Immunoprecipitation

For ATM IPs, 10mg TCE was incubated with 5μl ATM antibody (Bethyl, A300-136A) for 2h on the wheel at 4°C, then incubated with G-beads (GE Healthcare, 17061801) for 1h on the wheel at 4°C. Beads were washed 3 times in Lysis Buffer (150mM NaCl, 50mM Tris-Hcl, pH7.5, 10% Glycerol, 0.5%NP-40, Phosphatase inhibitors (1mM NaF, 1mM β-glycerophosphate, 200μM Na_2VO_4, 1mM EDTA, 5mM $Na_4P_2O_7$), Protease inhibitors (600nM Leupeptin, 1.63μM Pepstatin, 1μM PMSF, 3μM Benzamidine, 2nM Antipain, 1.3nM Chymostatin) and resuspended in 50μl 2x Sample Buffer (Invitrogen, NP0007). 30% of the boiled beads were used for Immunoblotting.

Clonogenic Survival Assays

U2OS were trypsinized 48hrs after siRNA transfection and counted. 500 cells were plated onto a 60mm dish. For IR sensitivity assays, cells were allowed to adhere for 1h prior to irradiation. For Olaparib and ICRF-193 clonogenic survival assays, the medium was supplemented with the appropriate concentration of ICRF-139 (Enzo Life Sciences, GR-332) or Olaparib (SelleckChem, S1060) before addition of cells. Cells were grown at 37°C for 10-14 days until colonies were an average of 1-2mm in diameter. Colonies were stained with DMMB and counted.

Immunofluorescence

Cells were grown on a coverslip and transfected with siRNA. 48h after transfection, cells were irradiated with 3Gy, fixed with 4%PFA (EMS, 15710) for 10min at RT and permeabilised with 0.25% Triton-X for 10min. After blocking in 1%BSA, cells were stained for 1h with 1º antibody at 37°C, washed and incubated 1h with 2º antibody at 37°C. Slides were mounted using VectraShield (Vector Laboratories, H-1200) containing DAPI. Microscopy imaging was performed on a Deltavision microscope

using Softworx software (Applied Precision, Issaquah). 0.5μm Z-stacks were collected, deconvolved and projected. The analysis was carried out using ImageJ software. The following antibodies were used: 53BP1 (Novus Biologicals, NB100-304), BRCA1 (Santa Cruz, sc-6954), γH2AX (Millipore, 05-636), RAD51 (Calbiochem, PC130).

G2/M checkpoint assays

Cells were irradiated with 3Gy, harvested, washed, resuspended in 1ml PBS and fixed in ice-cold Ethanol at a final concentration of 75%. Cells were stained with a mitotic marker (H3pS10, Millipore, 06-570) in PBS containing 1%BSA and 0.5% Triton-X for 2h at RT. Cells were then incubated with FITC conjugated 2º antibody (Bethyl, A120-201F) for 1h in the dark at RT before being resuspended in PBS containing 40μg/ml PI (Sigma, P4170) and 250μg/ml RNaseA (Sigma, R6513). Mitotic cells were then detected using the BD-FACSCantoII and analysed using the BD-FACS DIVA software.

Cell cycle analysis and G1/S checkpoint assay

Cells were transfected with siRNA 48h prior to irradiation and pulse-treated with 25μM BrdU (Sigma, B5002) for 1h, washed with PBS and fresh media was added. Cells were then irradiated (3Gy) with a Cesium-137 source (Mainance, UK), harvested at the indicated times, fixed in 70% ice-cold ethanol, washed with PBS and the DNA was denatured using 2N HCl for 10min before being stained with anti-BrdU antibody (BD, 347580) for 1h and anti-mouse 2º antibody (Jackson ImmunoResearch, 111-096-045) for 1h. Cells were then stained with Propidium iodide solution (40μg/ml of PI (Sigma, P4170) and 250μl/ml of RNAse A (Sigma, R6513) in PBS) for 30min in the dark. The analysis was performed using the FACS CantoII and the BD-FACS Diva Software.

GFP-reporter assay

U2OS were stably transfected with the DR-GFP plasmid (Pierce, Johnson et al., 1999). $2x10^6$ cells were transfected with 5μg I-SceI plasmid (pCBA-ISceI with 3x NLS, gift from C. Morrison), 40nmol siRNA and 1μg cerulean plasmid (Cerulean N1, Addgene, 54742). 24h post transfection, cells were split into a 6-well dish and grown for a further 24h. Then cells were harvested by trypsination at the indicated timepoints and $2x10^4$ cells were analysed using a BD-FACS CantoII flow cytometer. The remaining cells were used for checking the knock-down efficiency.

4.4. Results

4.4.1. DDX17 is a novel interacting partner of 53BP1

We have identified new interacting partners of Atm, Atr and 53Bp1 in a proteomic screen in chicken DT40 cells. The SILAC screens were carried out using HFSC-tagged proteins. Atm, Atr and 53Bp1 were purified from undamaged, irradiated (10Gy) and UV-treated cells to identify new interacting partner of these proteins. Interestingly, a large percentage of potential interacting partners were RNA metabolism proteins, including several DEAD-box helicases. Table 4.1 shows the results of the 53BP1 proteomic screen. Several known interacting proteins like p53, PLK1 and USP28 are referenced to validate the screen. Among unknown interacting proteins DDX17 was enriched compared to the control samples, but without its paralog DDX5.

The SILAC screen to identify potential interacting partners of Atm (**Error! Reference source not found.**) suggests interaction of DDX17 with ATM, although not enriched after DNA damage. In this screen, we also identified its paralog DDX5, which is also enriched after IR-induced DNA damage with a relative enrichment of 2.22 compared to undamaged cells with a score of 1.37. UV treatment does not seem to enhance the interaction in neither DDX5 nor DDX17 (**Error! Reference source not found.**).

Next, we validated the interaction of DDX17 in human HEK293T cells. We over-expressed p72 cDNA of DDX17 tagged with V5 in HEK293T cells and then immunoprecipitated 53BP1 (Figure 4.2a). The V5-tagged p72 isoform of DDX17 is co-precipitating with endogenous 53BP1, but we were not able to visualise the endogenous DDX17 due to relatively low abundance or weak antibody. Furthermore, we could not verify the interaction of DDX17 (Figure 4.2b) or DDX5 (not shown) with endogenous ATM.

Protein	Score	Reference
53BP1	34.32	(Zgheib, Pataky et al., 2009)
KIF18b	7.47	L. Frizzell (unpublished)
p53	15.96	(Iwabuchi, Bartel et al., 1994)
USP28	10.27	(Zhang, Zaugg et al., 2006)
PLK1	2.55	(van Vugt, Gardino et al., 2010)
DDX17	1.95	this study

Table 4.1: DDX17 interacts with 53BP1 in DT40 cells

Results of the 53BP1 SILAC analysis. Cells were grown in heavy, light and medium SILAC media, irradiated with 10Gy as indicated and harvested 1h post IR. Scores represent the relative enrichment of peptides compared to the untagged control samples (SILAC experiment was carried out by S. Maretto and J. Eykelenboom).

Protein	control	IR	UV	Reference
ATM	100	100	100	(Bakkenist & Kastan, 2003)
MCM3	1.71	1.85	1.87	(Shi, Dodson et al., 2007)
DDX1	1.2	1.11	1.11	(Li, Monckton et al., 2008)
DDX3X	1.50	1.81	1.96	Chapter 3
DDX17	1.97	1.67	1.39	This study
DDX5	1.37	2.22	1.40	unconfirmed

Table 4.3: Ddx17 interacts with Atm in DT40 cells.

Results of the second SILAC analysis. Cells were grown in heavy, light and medium SILAC media, irradiated with 10Gy or UV-treated with 10 J/m^2 as indicated and harvested 1h post IR. Scores represent the relative enrichment of peptides compared to the untagged control (SILAC experiment was carried out by A. van Beneden and J. Prieto).

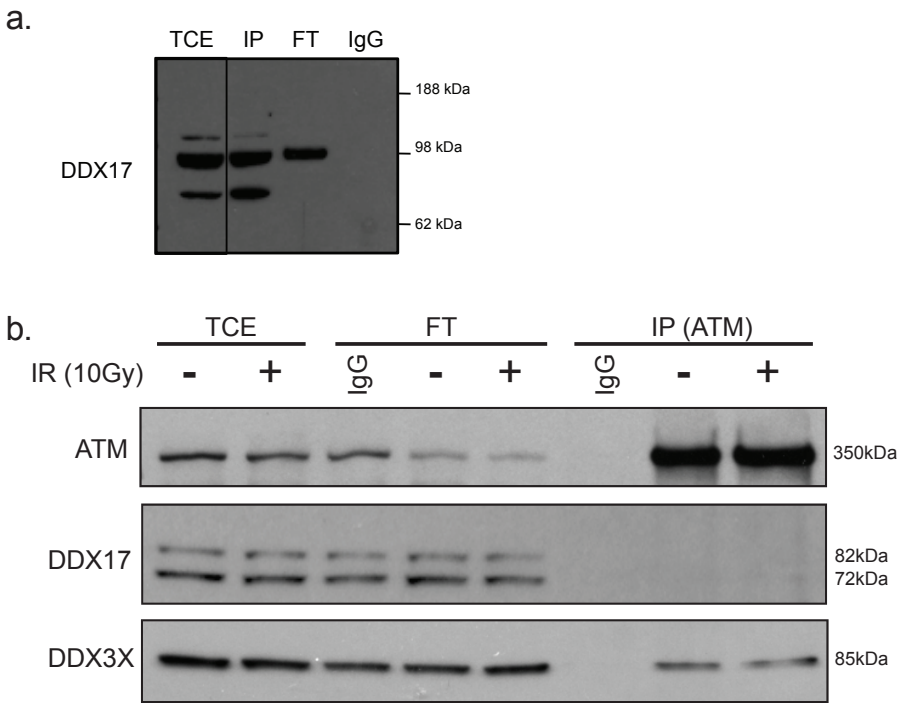

Figure 4.2: DDX17 interacts with 53BP1 but not ATM in HEK293 cells.

DDX17 interact with 53BP1 but not ATM in Immunoprecipitation experiments. A. Immunoprecipitation of 53BP1 in DDX17-V5 overexpressed cells. The resulting western blot was probed for V5 (Experiment was performed by S. Maretto) B. Immunoprecipitation of endogenous ATM in damaged (10Gy) and undamaged cells. Resulting western blot was probed for ATM, DDX3X and DDX17.

The reason for not being able to confirm the SILAC results in human cells could have several reasons. The interaction could be dependent on the time after harvesting as DDX17 localises to DSBs within seconds of break induction with similar kinetics to PARP (Adamson et al., 2012) so interaction could be lost by 1h after damage. Furthermore, the interaction of ATM with DDX17 could be dependent on RNA or DNA. In our IP experiments, we have treated the cells with Benzonase, a nuclease that digests all accessible DNA. Therefore, all interaction that is dependent on RNA could be lost. More experiments with changed conditions will need to be carried out to confirm a possible interaction of DDX17 with ATM.

4.4.2. DDX17 and DDX5 depletion results in IR sensitivity

In order to validate whether DDX17 plays a role in the DDR, we investigated its effect on colony formation in response to IR. Cells depleted in DDX17 show no change in growth rate in undamaged cells, suggesting that DDX17 does not have a role in general cell proliferation (Figure 4.3a). A reason for that could also be the partial redundancy of DDX17 and DDX5. However, colony formation is impaired in cells following IR treatment (Figure 4.3b). DDX17 depletion results in sensitivity to IR compared to the control cells, but this phenotype is less pronounced than in ATM kinase inhibited cells.

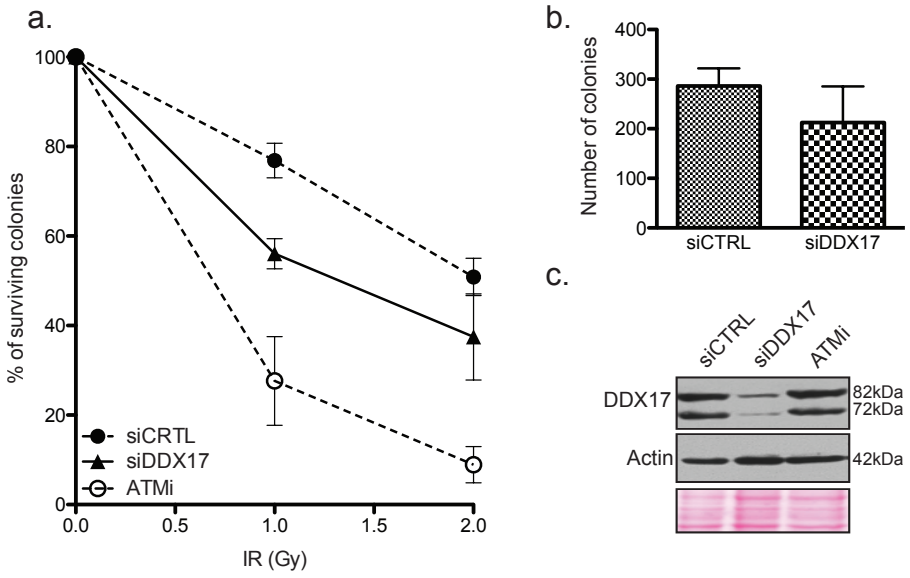

Figure 4.3: DDX17 depletion results in IR sensitivity.

A. Clonogenic survival assay of control, DDX17 depleted and ATM inhibited cells and indicated doses of IR. Cells were grown for 10-14 days in culture, stained with DMMB and counted. Experiments were carried out in triplicate and error bars represent the SD across three independent experiments (n=3). B. Number of colonies counted in undamaged control or DDX17 depleted cells after 10-14 days in culture (n=5). C. WB of knock-down efficiency.

4.4.3. DDX17 is required for efficient checkpoint release

DDX17 and DDX5 have been implicated in cell cycle regulation (Mooney et al., 2010a). We therefore conducted cell cycle analysis and checkpoint assays in RPE-1 and U2OS cells. DDX17 depleted cells are able to enter the checkpoint normally, but exit the checkpoint at a slower rate than the control cells, suggesting a defect in either checkpoint release or DNA repair (Figure 4.4a,b). DDX17 depleted cells have a similar percentage of mitotic cells compared to the control, indicating no apparent defect in the cell cycle. This is supported by analysis of cell cycle distribution (Figure 4.4c). Cells were treated with a BRDU pulse before harvesting, which allows separation of the cells into G1, early S, late S and G2 by flow cytometry (Figure 4.4d). In the absence of DNA damage nearly 50% of DDX17 depleted cells are in G1 compared to 40% in the control. This could indicate an accumulation of non-cycling cells or a defect in G1/S transition in the absence of DDX17. Therefore, we studied the G1/S transition of DDX17 depleted cells in response to DNA damage. The cells were pulse treated with BRDU before irradiation (3Gy) and harvested at the indicated timepoints. The newly released S-phase cells were visualised as BRDU negative cells with a DNA content larger than G1 and smaller than G2 (Figure 4.4d). Cells deficient of DDX17 showed a delay in entering S phase after DNA damage, indicative of a delay in G1/S checkpoint release or a defect in DNA repair of G1 cells compared to control cells (Figure 4.4d,e).

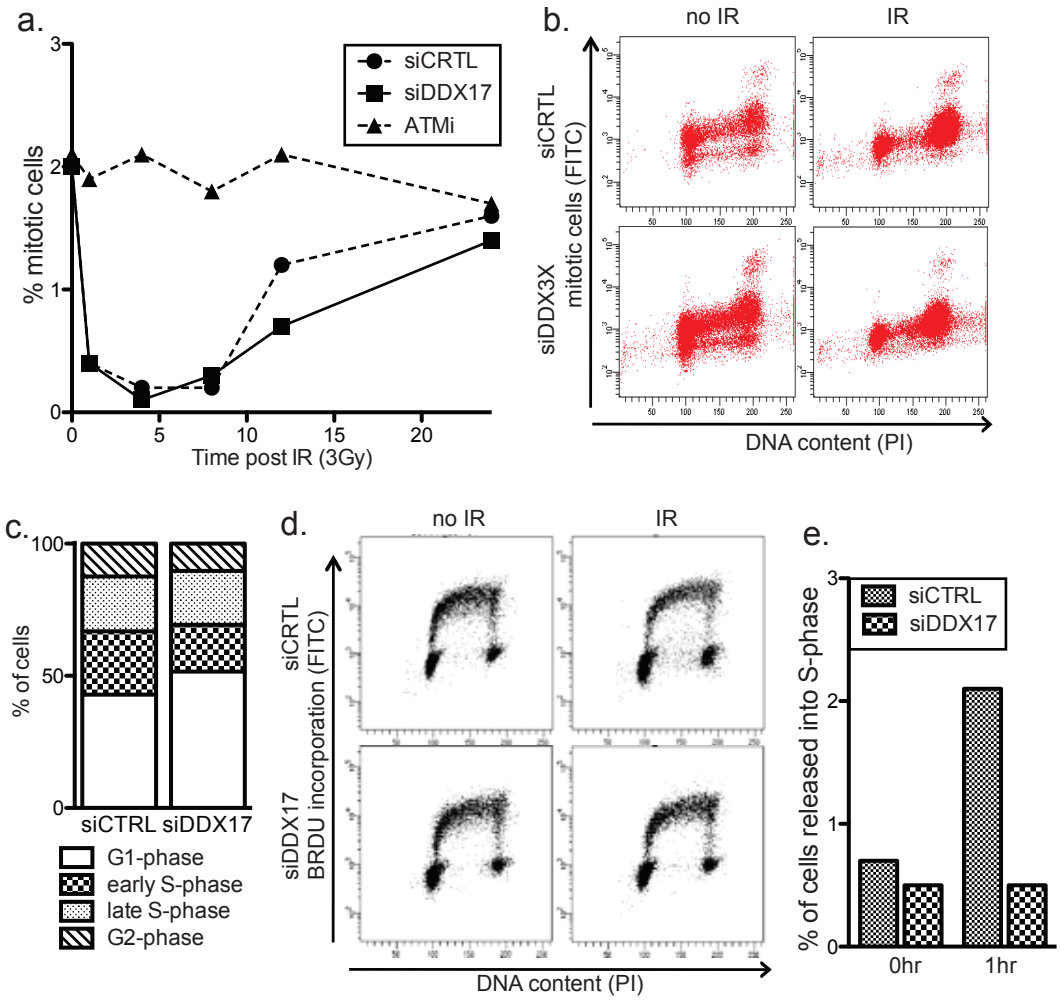

Figure 4.4: DDX17 depletion results in delayed exit from the G1/S and G2/M checkpoints.

A. Dot plot of cells stained with H3pS10 before and 12h post IR (3Gy). B. G2/M checkpoint assay in U2OS cells. Cells were stained with H3pS10 as a marker for mitosis and propidium iodide, then analysed using a BD-FACS CantoII. C. Dot plot of RPE-1 cells exposed to a 1h BRDU pulse prior to IR (3Gy) Cells were stained with anti-BRDU antibody and propidium iodide to separate cells into G1, early-S, late-S and G2 phases. D. Distribution of undamaged cells in different stages of the cell cycle. e. Quantification of cells released into S-phase 1hr post irradiation.

4.4.4. Loss of DDX17 result in decreased DDR factor focal recruitment downstream of γH2AX

IR sensitivity and delayed checkpoint release suggest a defect in DNA repair upon DDX17 depletion, so we investigated the phosphorylation of H2AX in response to DNA damage in the presence or absence of DDX17 as a indicator of DSB presence. DDX17 depleted cells have efficient H2AX phosphorylation in response to DNA damage with repair kinetics similar to the control samples. As shown in Figure 4.5, γH2AX foci are not significantly decreased 1h and 4h post damage in DDX17 depleted compared to control samples. This suggests that DDX17 might act downstream of γH2AX phosphorylation in the DDR cascade.

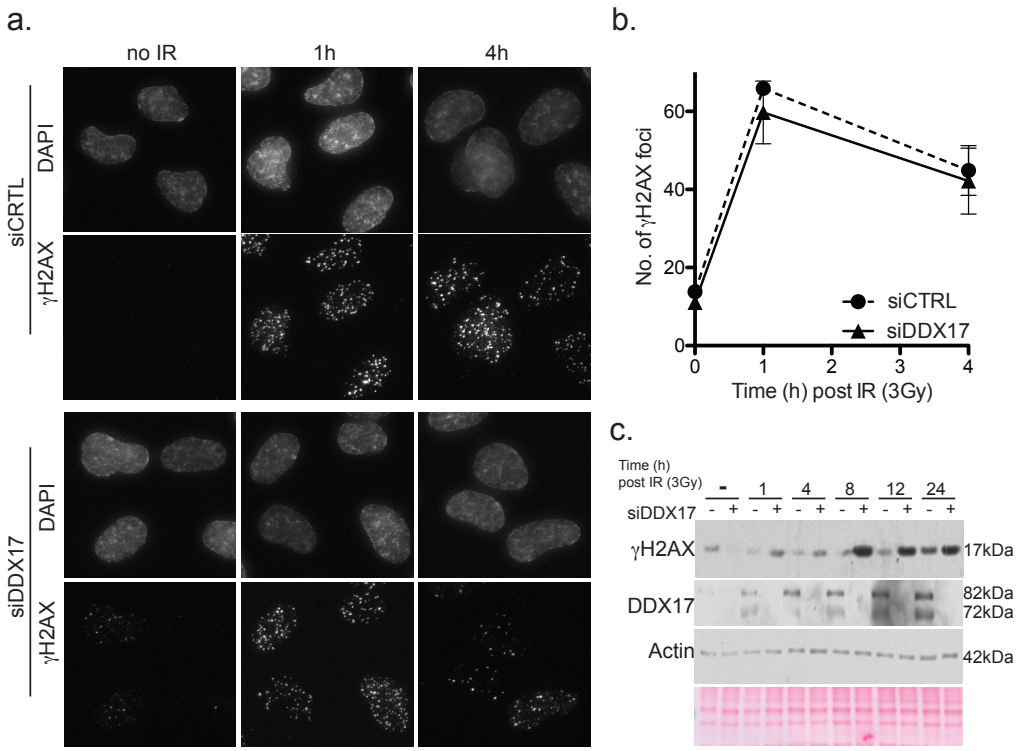

Figure 4.5: DDX17 is not required for H2AX phosphorylation.

A. Immunofluorescence of gH2AX IRIF in RPE cells. Cells were treated with DDX17 or control siRNA and fixed at the indicated timepoints after IR (3Gy). B. Quantification of A. Graph displays the average number of γH2AX foci per cell. Experiments were carried out in triplicate and error bars represent the SEM of three independent experiments (n=3). C. WB of gH2AX kinetics and DDX17 knock-down efficiency.

DDX17 interacts with the DDR mediator protein 53BP1 (Figure 4.2a), so we investigated 53BP1 focal recruitment to DSBs in the absence of DDX17. 53BP1 focal recruitment or retention at DSBs is reduced in DDX17 depleted cells 1h post damage (Figure 4.6a), but 53BP1 foci are up to the same levels as the control 4h post IR although foci appear to be less intense (Figure 4.6a,b). It will be important to analyse the intensity of 53BP1 foci. Total 53BP1 protein levels remain unchanged in DDX17 depleted compared to control cells (Figure 4.6c).

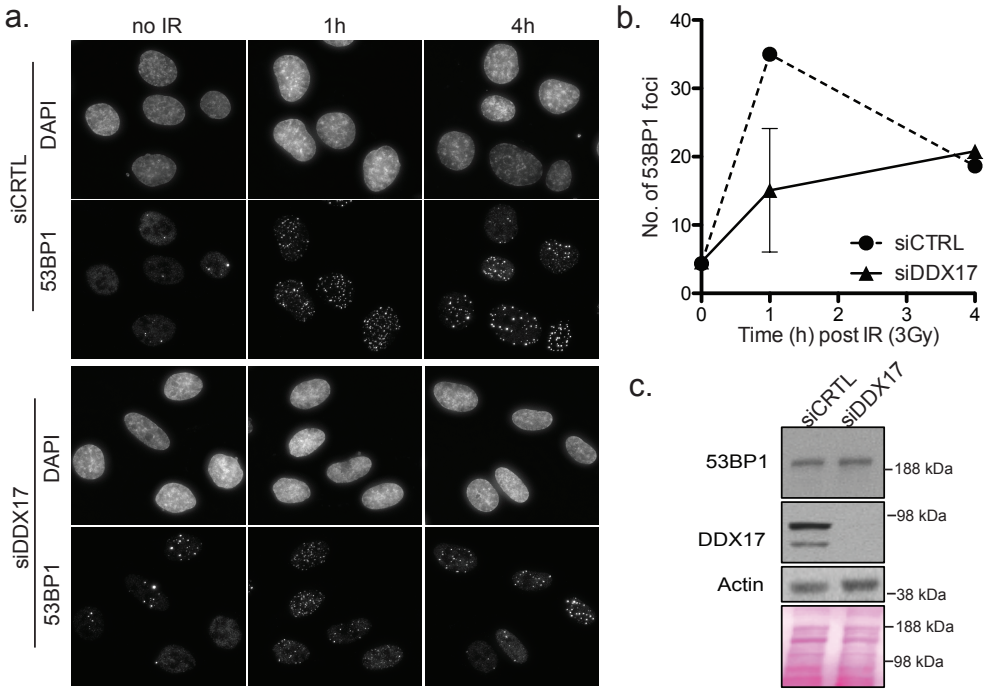

Figure 4.6: Loss of DDX17 results in a defect of 53BP1 recruitment to IRIF

A. Immunofluorescence of 53BP1 IRIF in RPE cells. Cells were treated with DDX17 or control siRNA and fixed at the indicated timepoints after IR (3Gy). B. Quantification of a. Graph displays the average number of 53BP1 foci per cell. Experiments were carried out in triplicate and error bars represent the SEM of three independent experiments. C. Western Blot analysis of 53BP1 protein levels in DDX17 depleted and control cells at indicated times after damage induction (IR, 3Gy).

Similarly, loss of DDX17 also results in a reduction of BRCA IRIF after damage (Figure 4.7a,b). However, BRCA1 foci in S phase are not affected and appear to be at the same level as in the control cells. The reduced levels of BRCA foci correlate with reduced overall BRCA1 protein levels in DDX17 depleted cells (Figure 4.7c). This suggests that DDX17 regulates overall protein level of BRCA1 either on a transcriptional or translational level.

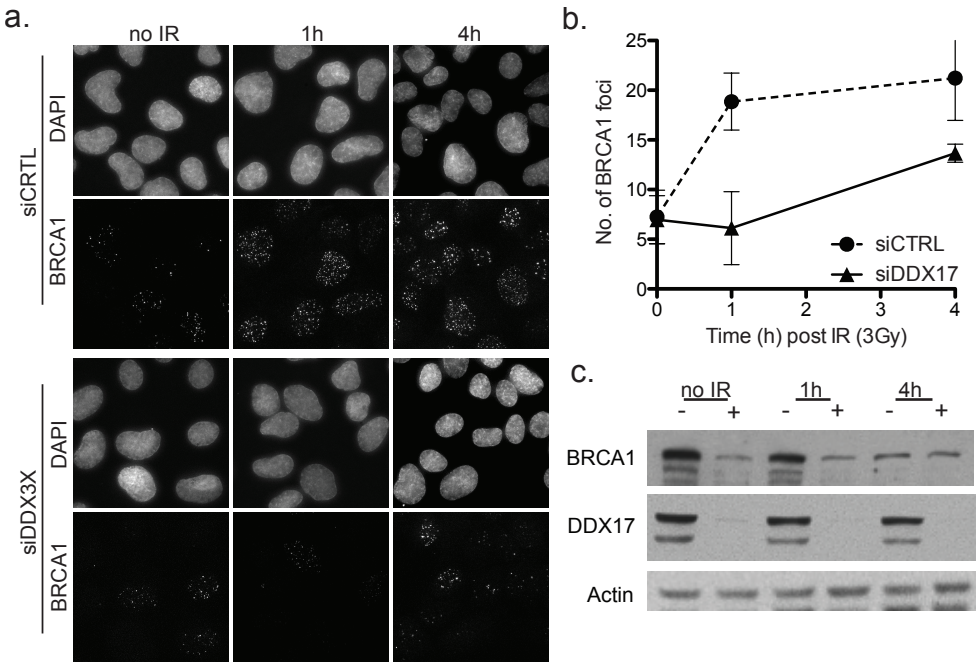

Figure 4.7: DDX17 depletion results in decreased levels of BRCA1

A. Immunofluorescence of BRCA1 IRIF in RPE cells. Cells were treated with DDX17 or control siRNA and fixed at the indicated timepoints after IR (3Gy). B. Quantification of A. Graph displays the average number of BRCA1 foci per cell. Experiments were carried out in triplicate and error bars represent the SEM of three independent experiments. C. Western Blot analysis of BRCA1 protein levels in DDX17 depleted and control cells at indicated times after damage induction (IR, 3Gy).

In addition, loss of DDX17 results in a decreased level of RAD51 foci in response to damage. This may be partially due to reduced total RAD51 protein levels and partially due to the defect in BRCA1 focal recruitment upstream of RAD51 focal formation (Figure 4.8).

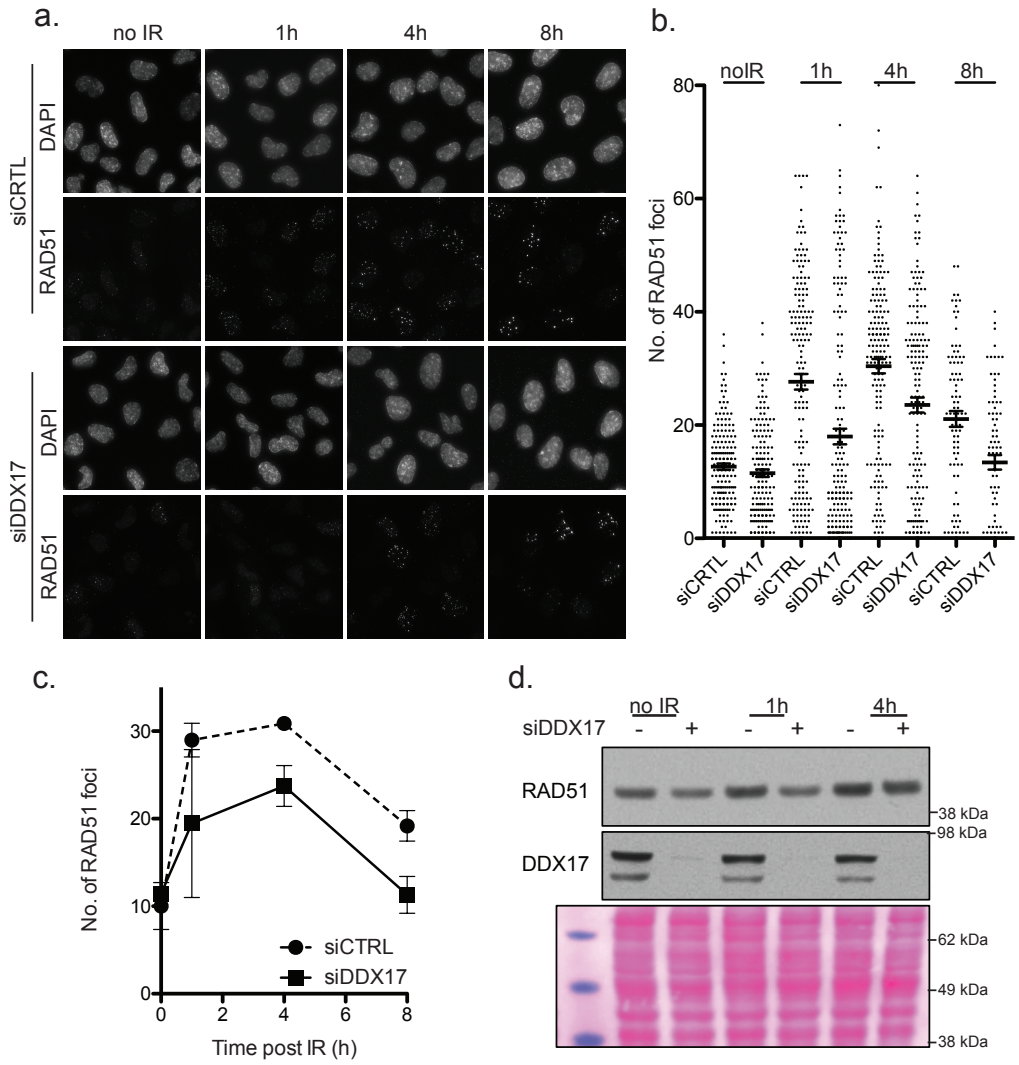

Figure 4.8: Loss of DDX17 results in a decreased RAD51 response

A. IF of RAD51 IRIF in RPE cells. Cells were treated with DDX17 or control siRNA and fixed at the indicated timepoints after IR (3Gy). B. Dot plot showing the distribution of the number of RAD51 foci across three independent experiments. Error bars indicate the SEM. C. Quantification of a. Graph displays the average number of RAD51 foci per cell. Experiments were carried out in triplicate and error bars represent the SEM of three independent experiments. D. WB analysis of BRD51 protein levels in DDX17 depleted and control cells at indicated times after damage induction (IR, 3Gy).

4.4.5. DDX17 are required for efficient HR and NHEJ repair

A defect in foci formation of 53BP1, BRCA1 and RAD51 could indicate that DDX17 deficient cells may be impaired in the two main repair pathways. To obtain indications of impaired NHEJ, we carried out clonogenic survival assays with control and DDX17 depleted cells in response to exposure to the topoisomerase II inhibitor, ICRF-193, which induces breaks primarily repaired by NHEJ. As predicted, cells lacking DDX17 show increased sensitivity to ICRF-193 compared to control cells, but are less sensitive than DNA-PK inhibited cells (Figure 4.9b).

We then carried out clonogenic survival assays using the PARP inhibitor Olaparib, which induced breaks primarily repaired by HR. Cell depleted of DDX17 also show increased sensitivity to Olaparib when compared with the control samples (Figure 4.9a) but less sensitive compared to RAD54 depleted cells.

This data suggests that DDX17 plays a partial role in NHEJ and HR, but is not essential in these repair pathways. This could be due to partial redundancy between DDX17 and DDX5 and further experiments will need to be carried out with double depletion of DDX5 and DDX17.

We then directly assayed the efficiency of HR repair by gene conversion using a DR-GFP reporter system. We have generated a stable DR-U2OS cell line with a randomly integrated GFP-reporter system (Pierce et al., 1999). The cells were then transfected with control, DDX17 and BRCA1 siRNA together with I-SceI to induce a site-specific DSB. Cells were harvested 48h after transfection every day for 6 days and the rate of gene conversion was measured by the percentage of GFP-positive cells. DDX17 is required for efficient gene conversion, showing about 20% reduction in DSB repair efficiency compared to the control samples (Figure 4.9c) while BRCA1 reduced HR efficiency by more than 50%. The reduction of HR efficiency in DDX17 depleted cells could be a result of the decreased BRCA1 protein levels.

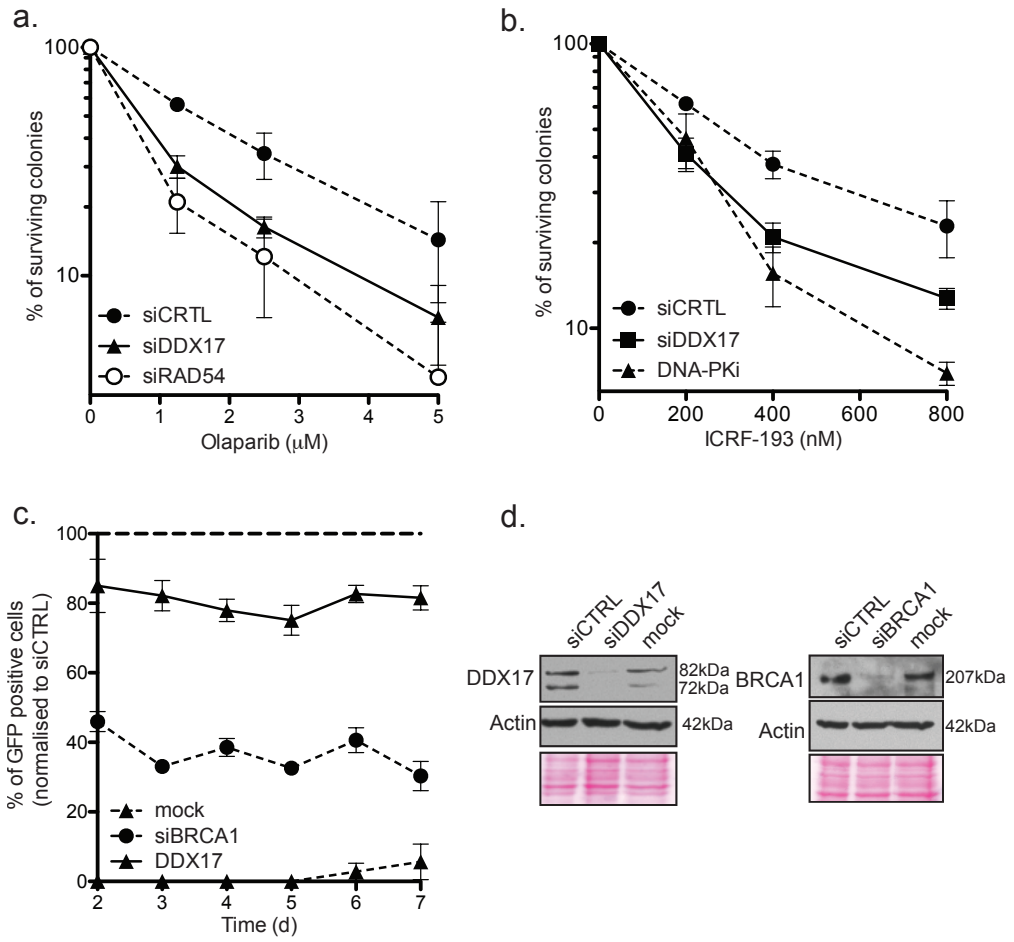

Figure 4.9: DDX17 depletion results in sensitivity to Olaparib and ICRF, but only has a mild effect on HR

A. Clonogenic survival assay in U2OS cells. 500 cells were plated in media containing the appropriate concentration of Olaparib, grown for 10-14 days and stained with DMMB. B. Clonogenic survival assay in U2OS cells. 500 cells were plated in media containing the appropriate concentration of ICRF-193, grown for 10-14 days and stained with DMMB. All experiments were carried out in triplicate and error bars represent the SD across three independent experiments (n=3). C. DR-GFP reporter assay. Cells were transfected with siRNA, I-SceI plasmid and cerulean plasmid, split into 6 dishes 24h post transfection and grown for the indicated times. Live cells were harvested and GFP positive cells were analysed using a BD-FACS CantoII flow cytometer. The graph shows the percentage reduction of GFP-positive cells compared to the control cells. Experiments were carried out in triplicate and error bars represent the SEM across three independent experiments (n=3). D. WB of knock-down efficiency for DDX17 and BRCA1 siRNAs, respectively.

4.5. Discussion

In this study, we have shown that DDX17 is a novel interacting partner of 53BP1 in DT40 and human cells and a potential interacting protein of ATM in DT40 cells. DDX17 interaction with ATM could not be verified in human cells, which could be due to the experimental setup used. The DDX17-ATM interaction could be dependent on RNA or DNA and is lost during benzonase treatment. The proteomic screen in DT40 cells was carried out using micrococcal nuclease, which might not be able to access RNA bound to DDX17. Therefore, it will be important not repeat IP experiments using micrococcal nuclease instead of benzonase.

DDX17 interaction with 53BP1 and a reduction of 53BP1 foci 1h after DNA damage could suggest a role for DDX17 in early DNA repair. DDX17 localises to DSB with similar kinetics to PARP (Adamson et al., 2012) and is involved in miRNA processing (Fukuda et al., 2007, Gregory et al., 2004). Recently, small RNAs similar to miRNAs have been implicated in DNA repair (Francia, Michelini et al., 2012). These diRNAs are processed site specifically at the DSB by Drosha and are required for efficient recruitment of 53BP1 to DSBs. Giving the involvement of DDX17 in miRNA processing, its localisation to DSB and its interaction with 53BP1, DDX17 is a potential candidate for the processing of these miRNAs directly at the site of damage.

Unpublished data (d'Adda di Fagagna) also suggests that transcription of primary miRNA transcripts at DSB is RNA pol II dependent, and DDX17 and DDX5 were proposed to function as a bridge between transcriptional co-factors and RNA pol II similar to RNA helicase A (Anderson et al., 1998, Nakajima et al., 1997, Rossow & Janknecht, 2003). It would be interesting to further investigate the function of DDX17 at the DSB and whether it is involved in processing transcripts generated site specifically in response to DNA damage. To address this, we have mutated the DEAD box motif of DDX17 (E326Q), a mutation that results in defective

ATP hydrolysis (Xiol, Spinelli et al., 2014). Using the ATP-hydrolysis deficient mutant of DDX17, we hope to be able to prevent pre-miRNA degradation and processing and immunoprecipitate a full-length pre-miRNA transcript bound to DDX17^{E326Q} that is induced by DNA damage and site-specifically transcribed.

DDX17 was identified in an ATM/ATR substrate screen (Matsuoka et al., 2007) and has been proposed as a negative regulator of HR in a genome wide HR screen (Adamson et al., 2012). The identification of DDX17 as a negative regulator of HR is based on the DR-GFP reporter system (Pierce et al., 1999) and subsequent microscope analysis of fixed cells. DDX17 being a negative regulator of HR is in conflict with our results showing that DDX17 is required for efficient HR. Discrepancies between the results of the DR-GFP reporter system could be due to differences in the analysis. We used live cells and assessed GFP expression using flow cytometry, which allows us to interrogate a large number of cells. In addition to a reduction of GFP positive cells using the DR-GFP system, DDX17 depleted cells also show increased sensitivity to Olaparib and reduced total BRCA1 and RAD51 protein levels. This data together with the DR-GFP analysis suggests that DDX17 is more likely to be required for efficient HR instead of being a negative regulator. Defects in the DDR in DDX17 depleted cells are only partial and it is very likely that there is a redundancy between DDX17 and DDX5 when the helicase function of these proteins is required, and thus it is hard to separate the distinct function of each protein in the DDR.

The defect in HR is possibly caused by the down regulation of the total protein levels HR factors BRCA1 and RAD51. DDX17 interaction with 53BP1 and localisation of DDX17 to DSB suggests a more direct role in the DDR. Further investigation is required to clarify the function of DDX17 in early events of the DDR and it is necessary to separate its functions from that of its paralog DDX5.

4.6. References

Adamson B, Smogorzewska A, Sigoillot FD, King RW, Elledge SJ (2012) A genome-wide homologous recombination screen identifies the RNA-binding protein RBMX as a component of the DNA-damage response. Nat Cell Biol 14: 318-28

Anderson SF, Schlegel BP, Nakajima T, Wolpin ES, Parvin JD (1998) BRCA1 protein is linked to the RNA polymerase II holoenzyme complex via RNA helicase A. Nat Genet 19: 254-6

Auboeuf D, Honig A, Berget SM, O'Malley BW (2002) Coordinate regulation of transcription and splicing by steroid receptor coregulators. Science 298: 416-9

Bakkenist CJ, Kastan MB (2003) DNA damage activates ATM through intermolecular autophosphorylation and dimer dissociation. Nature 421: 499-506

Bates GJ, Nicol SM, Wilson BJ, Jacobs AM, Bourdon JC, Wardrop J, Gregory DJ, Lane DP, Perkins ND, Fuller-Pace FV (2005) The DEAD box protein p68: a novel transcriptional coactivator of the p53 tumour suppressor. EMBO J 24: 543-53

Bolduc C, Larose M, Yoshioka M, Ye P, Belleau P, Labrie C, Morissette J, Raymond V, Labrie F, St-Amand J (2004) Effects of dihydrotestosterone on adipose tissue measured by serial analysis of gene expression. J Mol Endocrinol 33: 429-44

Camats M, Guil S, Kokolo M, Bach-Elias M (2008) P68 RNA helicase (DDX5) alters activity of cis- and trans-acting factors of the alternative splicing of H-Ras. PLoS One 3: e2926

Cordin O, Tanner NK, Doere M, Linder P, Banroques J (2004) The newly discovered Q motif of DEAD-box RNA helicases regulates RNA-binding and helicase activity. EMBO J 23: 2478-87

Dardenne E, Pierredon S, Driouch K, Gratadou L, Lacroix-Triki M, Espinoza MP, Zonta E, Germann S, Mortada H, Villemin JP, Dutertre M, Lidereau R, Vagner S, Auboeuf D (2012) Splicing switch of an epigenetic regulator by RNA helicases promotes tumor-cell invasiveness. Nat Struct Mol Biol 19: 1139-46

Dardenne E, Polay Espinoza M, Fattet L, Germann S, Lambert MP, Neil H, Zonta E, Mortada H, Gratadou L, Deygas M, Chakrama FZ, Samaan S, Desmet FO, Tranchevent LC, Dutertre M, Rimokh R, Bourgeois CF, Auboeuf D (2014) RNA helicases DDX5 and DDX17 dynamically orchestrate transcription, miRNA, and splicing programs in cell differentiation. Cell Rep 7: 1900-13

Francia S, Michelini F, Saxena A, Tang D, de Hoon M, Anelli V, Mione M, Carninci P, d'Adda di Fagagna F (2012) Site-specific DICER and DROSHA RNA products control the DNA-damage response. Nature 488: 231-5

Fukuda T, Yamagata K, Fujiyama S, Matsumoto T, Koshida I, Yoshimura K, Mihara M, Naitou M, Endoh H, Nakamura T, Akimoto C, Yamamoto Y, Katagiri T, Foulds C, Takezawa S, Kitagawa H, Takeyama K, O'Malley BW, Kato S (2007) DEAD-box RNA helicase subunits of the Drosha complex are required for processing of rRNA and a subset of microRNAs. Nat Cell Biol 9: 604-11

Fuller-Pace FV (2013) The DEAD box proteins DDX5 (p68) and DDX17 (p72): multi-tasking transcriptional regulators. Biochim Biophys Acta 1829: 756-63

Germann S, Gratadou L, Zonta E, Dardenne E, Gaudineau B, Fougere M, Samaan S, Dutertre M, Jauliac S, Auboeuf D (2012) Dual role of the ddx5/ddx17 RNA helicases in the control of the pro-migratory NFAT5 transcription factor. Oncogene 31: 4536-49

Gregory RI, Yan KP, Amuthan G, Chendrimada T, Doratotaj B, Cooch N, Shiekhattar R (2004) The Microprocessor complex mediates the genesis of microRNAs. Nature 432: 235-40

Guil S, Gattoni R, Carrascal M, Abian J, Stevenin J, Bach-Elias M (2003) Roles of hnRNP A1, SR proteins, and p68 helicase in c-H-ras alternative splicing regulation. Mol Cell Biol 23: 2927-41

Honig A, Auboeuf D, Parker MM, O'Malley BW, Berget SM (2002) Regulation of alternative splicing by the ATP-dependent DEAD-box RNA helicase p72. Mol Cell Biol 22: 5698-707

Huang H, Shiffman ML, Cheung RC, Layden TJ, Friedman S, Abar OT, Yee L, Chokkalingam AP, Schrodi SJ, Chan J, Catanese JJ, Leong DU, Ross D, Hu X, Monto A, McAllister LB, Broder S, White T, Sninsky JJ, Wright TL (2006) Identification of two gene variants associated with risk of advanced fibrosis in patients with chronic hepatitis C. Gastroenterology 130: 1679-87

Ip FC, Chung SS, Fu WY, Ip NY (2000) Developmental and tissue-specific expression of DEAD box protein p72. Neuroreport 11: 457-62

Iwabuchi K, Bartel PL, Li B, Marraccino R, Fields S (1994) Two cellular proteins that bind to wild-type but not mutant p53. Proc Natl Acad Sci U S A 91: 6098-102

Jacobs AM, Nicol SM, Hislop RG, Jaffray EG, Hay RT, Fuller-Pace FV (2007) SUMO modification of the DEAD box protein p68 modulates its transcriptional activity and promotes its interaction with HDAC1. Oncogene 26: 5866-76

Jalal C, Uhlmann-Schiffler H, Stahl H (2007) Redundant role of DEAD box proteins p68 (Ddx5) and p72/p82 (Ddx17) in ribosome biogenesis and cell proliferation. Nucleic Acids Res 35: 3590-601

Jothy S (2003) CD44 and its partners in metastasis. Clin Exp Metastasis 20: 195-201

Kar A, Fushimi K, Zhou X, Ray P, Shi C, Chen X, Liu Z, Chen S, Wu JY (2011) RNA helicase p68 (DDX5) regulates tau exon 10 splicing by

modulating a stem-loop structure at the 5' splice site. Mol Cell Biol 31: 1812-21

Kircher SG, Kim SH, Fountoulakis M, Lubec G (2002) Reduced levels of DEAD-box proteins DBP-RB and p72 in fetal Down syndrome brains. Neurochem Res 27: 1141-6

Lamm GM, Nicol SM, Fuller-Pace FV, Lamond AI (1996) p72: a human nuclear DEAD box protein highly related to p68. Nucleic Acids Res 24: 3739-47

Lee CG (2002) RH70, a bidirectional RNA helicase, co-purifies with U1snRNP. J Biol Chem 277: 39679-83

Li L, Monckton EA, Godbout R (2008) A role for DEAD box 1 at DNA double-strand breaks. Mol Cell Biol 28: 6413-25

Lin C, Yang L, Yang JJ, Huang Y, Liu ZR (2005) ATPase/helicase activities of p68 RNA helicase are required for pre-mRNA splicing but not for assembly of the spliceosome. Mol Cell Biol 25: 7484-93

Liu ZR (2002) p68 RNA helicase is an essential human splicing factor that acts at the U1 snRNA-5' splice site duplex. Mol Cell Biol 22: 5443-50

Matsuoka S, Ballif BA, Smogorzewska A, McDonald ER, 3rd, Hurov KE, Luo J, Bakalarski CE, Zhao Z, Solimini N, Lerenthal Y, Shiloh Y, Gygi SP, Elledge SJ (2007) ATM and ATR substrate analysis reveals extensive protein networks responsive to DNA damage. Science 316: 1160-6

Mooney SM, Goel A, D'Assoro AB, Salisbury JL, Janknecht R (2010a) Pleiotropic effects of p300-mediated acetylation on p68 and p72 RNA helicase. J Biol Chem 285: 30443-52

Mooney SM, Grande JP, Salisbury JL, Janknecht R (2010b) Sumoylation of p68 and p72 RNA helicases affects protein stability and transactivation potential. Biochemistry 49: 1-10

Nakajima T, Uchida C, Anderson SF, Lee CG, Hurwitz J, Parvin JD, Montminy M (1997) RNA helicase A mediates association of CBP with RNA polymerase II. Cell 90: 1107-12

Ogilvie VC, Wilson BJ, Nicol SM, Morrice NA, Saunders LR, Barber GN, Fuller-Pace FV (2003) The highly related DEAD box RNA helicases p68 and p72 exist as heterodimers in cells. Nucleic Acids Res 31: 1470-80

Pierce AJ, Johnson RD, Thompson LH, Jasin M (1999) XRCC3 promotes homology-directed repair of DNA damage in mammalian cells. Genes Dev 13: 2633-8

Rossow KL, Janknecht R (2003) Synergism between p68 RNA helicase and the transcriptional coactivators CBP and p300. Oncogene 22: 151-6

Salzman DW, Shubert-Coleman J, Furneaux H (2007) P68 RNA helicase unwinds the human let-7 microRNA precursor duplex and is required for let-7-directed silencing of gene expression. J Biol Chem 282: 32773-9

Samaan S, Tranchevent LC, Dardenne E, Polay Espinoza M, Zonta E, Germann S, Gratadou L, Dutertre M, Auboeuf D (2014) The Ddx5 and

Ddx17 RNA helicases are cornerstones in the complex regulatory array of steroid hormone-signaling pathways. Nucleic Acids Res 42: 2197-207

Shi Y, Dodson GE, Mukhopadhyay PS, Shanware NP, Trinh AT, Tibbetts RS (2007) Identification of carboxyl-terminal MCM3 phosphorylation sites using polyreactive phosphospecific antibodies. J Biol Chem 282: 9236-43

Shin S, Janknecht R (2007) Concerted activation of the Mdm2 promoter by p72 RNA helicase and the coactivators p300 and P/CAF. J Cell Biochem 101: 1252-65

Shin S, Rossow KL, Grande JP, Janknecht R (2007) Involvement of RNA helicases p68 and p72 in colon cancer. Cancer Res 67: 7572-8

Suzuki HI, Yamagata K, Sugimoto K, Iwamoto T, Kato S, Miyazono K (2009) Modulation of microRNA processing by p53. Nature 460: 529-33

Tanner NK, Cordin O, Banroques J, Doere M, Linder P (2003) The Q motif: a newly identified motif in DEAD box helicases may regulate ATP binding and hydrolysis. Mol Cell 11: 127-38

Uhlmann-Schiffler H, Rossler OG, Stahl H (2002) The mRNA of DEAD box protein p72 is alternatively translated into an 82-kDa RNA helicase. J Biol Chem 277: 1066-75

van Vugt MA, Gardino AK, Linding R, Ostheimer GJ, Reinhardt HC, Ong SE, Tan CS, Miao H, Keezer SM, Li J, Pawson T, Lewis TA, Carr SA, Smerdon SJ, Brummelkamp TR, Yaffe MB (2010) A mitotic phosphorylation feedback network connects Cdk1, Plk1, 53BP1, and Chk2 to inactivate the G(2)/M DNA damage checkpoint. PLoS Biol 8: e1000287

Watanabe M, Yanagisawa J, Kitagawa H, Takeyama K, Ogawa S, Arao Y, Suzawa M, Kobayashi Y, Yano T, Yoshikawa H, Masuhiro Y, Kato S (2001) A subfamily of RNA-binding DEAD-box proteins acts as an estrogen receptor alpha coactivator through the N-terminal activation domain (AF-1) with an RNA coactivator, SRA. EMBO J 20: 1341-52

Wilson BJ, Bates GJ, Nicol SM, Gregory DJ, Perkins ND, Fuller-Pace FV (2004) The p68 and p72 DEAD box RNA helicases interact with HDAC1 and repress transcription in a promoter-specific manner. BMC Mol Biol 5: 11

Wortham NC, Ahamed E, Nicol SM, Thomas RS, Periyasamy M, Jiang J, Ochocka AM, Shousha S, Huson L, Bray SE, Coombes RC, Ali S, Fuller-Pace FV (2009) The DEAD-box protein p72 regulates ERalpha-/oestrogen-dependent transcription and cell growth, and is associated with improved survival in ERalpha-positive breast cancer. Oncogene 28: 4053-64

Xiol J, Spinelli P, Laussmann MA, Homolka D, Yang Z, Cora E, Coute Y, Conn S, Kadlec J, Sachidanandam R, Kaksonen M, Cusack S, Ephrussi A, Pillai RS (2014) RNA clamping by Vasa assembles a piRNA amplifier complex on transposon transcripts. Cell 157: 1698-711

Zgheib O, Pataky K, Brugger J, Halazonetis TD (2009) An oligomerized 53BP1 tudor domain suffices for recognition of DNA double-strand breaks. Mol Cell Biol 29: 1050-8

Zhang D, Zaugg K, Mak TW, Elledge SJ (2006) A role for the deubiquitinating enzyme USP28 in control of the DNA-damage response. Cell 126: 529-42

Chapter 5: Conclusion and future directions

5.1. Conclusions and Future Directions

For decades, the DNA damage response was thought to be a purely protein based signalling pathway depending on a variety of post-translational protein modifications such as phosphorylation, methylation, ubiquitylation, actetylation and sumoylation. In recent years however, emerging roles for small and large non-coding RNAs have been described.

98% of our genome does not encode for protein-coding genes and was long thought of as 'junk-DNA' (Alexander, Fang et al., 2010). This 'junk-DNA', however, produces a large variety of non-coding transcripts, which play a vital role in almost all cellular processes, including the cellular response to DNA damage (Esteller, 2011).

In the DDR, ncRNAs can act in two distinct ways to influence the cellular response to DNA damage and repair. One the one hand, ncRNAs can play an indirect role in DNA repair and/or checkpoint activation by their regulation of DDR factor protein levels. The function of miRNAs in post-transcriptional regulation of protein levels is widely studied and well conserved (Bartel, 2009, Fabian, Sonenberg et al., 2010, Huntzinger & Izaurralde, 2011). Several deep-sequencing screens of miRNAs in response to various types of DNA damage have identified a large number of miRNA up or down-regulated in different cell types (Hu & Gatti, 2011, Wan, Mathur et al., 2011).

On the other hand, ncRNAs can play a more direct role in the DDR (Francia, Michelini et al., 2012, Wei, Ba et al., 2012). This becomes evident in multiple ways. The key DDR factors BRCA1, 53BP1 and the Ku-proteins are able to bind ncRNA (Ganesan, Silver et al., 2002, Pryde, Khalili et al., 2005, Yoo & Dynan, 1998). In addition, ATM and BRCA1 are involved in the regulation of several miRNA in response to DNA damage by affecting the processing and biogenesis rather than their transcription

(Zhang, Wan et al., 2011). Furthermore, recent papers suggest that diRNAs, produced at the site of DNA damage, are directly involved in DSB repair by providing a platform for the recruitment of DDR factor to the DSB in plants and mammals (Francia et al., 2012, Wei et al., 2012).

Initially, this project was split into two parts, the first part being the characterisation of three novel ATM interacting proteins in the DNA damage response and the second part was to tie all three together in a broader picture elucidating their role in the generation of small damage-inducible RNAs at the double-strand break.

An obvious candidate for this project was the microprocessor subunit DGCR8, which has been identified in a proteomic SILAC screen carried out in our lab as an interacting protein of the PIK kinase ATM. DGCR8 functions as part of the microprocessor complex together with Drosha in the generation of miRNAs (Kwon, Nguyen et al., 2016, Nguyen, Jo et al., 2015). In 2012, Drosha as well as Dicer were implicated in the DDR by Francia et al. The hypothesis of newly generated diRNAs at the site of DNA damage was further supported by a back-to-back publication in Cell by Wei et al. suggesting a role for diRNAs in DSB repair *Arabidopsis thaliana* (Wei et al., 2012). Regarding the fact that DGCR8 and Drosha form a complex essential for the generation of miRNA, and presumably diRNAs, we hypothesised that DGCR8 would be involved in DNA repair alongside Drosha.

In addition, a DEAD-box helicase, DDX17, was identified as a novel interacting partner of the effector protein 53BP1 in our proteomic screen. DDX17 was shown to localise to laser-striping induced DSB (Adamson, Smogorzewska et al., 2012). Furthermore, DDX17 is known to form part of the large microRNA processing complex with Drosha and is required for the unwinding of pri-miRNA prior to processing by the DGCR8/Drosha complex (Moy & Cherry, 2014, Moy, Cole et al., 2014, Remenyi, Bajan et al., 2016). This background made it an ideal candidate for our study.

We hypothesised that diRNAs, processed at the site of the DSB were processed first by the microprocessor before being exported into the nucleus to be processed further by Dicer in a similar pathway to miRNA processing. The export of these potential diRNAs required a shuttle protein. A well-known DEAD-box protein, DDX3X, was also identified in the SILAC screen as a potential interacting partner of ATM. DDX3X is a DEAD box helicases that closely associates with the nuclear export protein TAP, which is the main nuclear export protein for mRNAs (Lai, Lee et al., 2008). In addition, DDX3X has recently been shown to interact with the microprocessor complex of DGCR8/Drosha to regulate a subset of miRNAs (Zhao, Mao et al., 2016).

DDX3X has been extensively studied as an essential protein in replication of viruses such as HIV (Valiente-Echeverria, Hermoso et al., 2015, Yedavalli, Neuveut et al., 2004) and associates with eIF4F to facilitate translation of mRNA with highly structured UTRs (Lai et al., 2008). In addition to its role in translation, DDX3X was also implicated in cell cycle progression and apoptosis (Chang, Chi et al., 2006, Chao, Chen et al., 2006, Li, Zhang et al., 2014). We propose a novel role for DDX3X in the DNA damage response independent of its function in apoptosis and p53 interaction.

DDX3X interacts with ATM independent of IR in human cells but shows enhanced interaction after damage in the SILAC screen. In order to validate a function of DDX3X, we performed clonogenic survival assay demonstrating increased IR sensitivity in DDX3X depleted cells and also a survival defect independent of DNA damage. This supports previous report that suggest DDX3X is required for cell cycle regulation and apoptosis (Botlagunta, Vesuna et al., 2008, Chang et al., 2006, Chao et al., 2006, Sun, Zhou et al., 2013). In order to further dissect the role of DDX3X in cell cycle regulation in response to DNA damage, we carried out G2/M and G1/S checkpoint assays that suggested a defect in G1/S and G2/M checkpoint exit in DDX3X depleted cells.

Using γH2AX as a marker for DNA damage, we showed that depletion of DDX3X results in a prolonged gH2AX response, suggesting a defect in DNA repair. This evidence is supported by the increased number of 53BP1 nuclear bodies in G1 phase, which indicates the carry-over of unrepaired DNA into the next cell cycle. In addition, DDX3X depletion also resulted in a decreased number of γH2AX foci at early timepoints indicating a defect in DNA damage sensing or signalling.

We then continued to investigate the involvement of DDX3X in the DSB repair pathways NHEJ and HR. Loss of DDX3X does not affect the recruitment of 53BP1 into IRIF, but greatly reduces focal recruitment of the HR factors RAD51 and BRCA1 indicating a defect in HR. This was confirmed in clonogenic survival assays using Olaparib and ICRF-139 as damage inducing agents in addition to using the DR-GFP reporter system to directly assess HR efficiency. DDX3X is known to regulate protein levels of important DDR factors such as p21, p53, several cyclins, PARP and CHK1 (Chang et al., 2006, Chao et al., 2006, Li et al., 2014, Wu, Liu et al., 2011). Here we also show that depletion of DDX3X results in decreased protein levels of the common HR and NER factors BRCA1, RAD51, RAD54, XPB, XPD and CSB.

We concluded that the defect in HR of DDX3X depleted cells is most likely due to a downregulation of the total protein level of these DNA repair factors. However, the exact role of DDX3X in downregulation of these proteins remains to be confirmed. Structural analysis of the UTRs of the HR factors could give an indication of whether DDX3X is involved in the transcription or translation of the respective mRNAs. In addition, Northern Blot analysis or qPCR of the mRNAs of BRCA1, RAD51 and RAD54 could also help to narrow down the role of DDX3X in processing of the mRNAs. Furthermore, bioinformatic analysis of the transcriptome and proteome of DDX3X depleted cells will give a better understanding of the range of mRNAs that are up or down regulated and whether a specific subset of these mRNAs are required for the DNA damage response.

In addition to DDX3X, we have identified DGCR8 as a novel interacting partner of ATM. DGCR8 is a co-factor of the mi-processing RNAIII enzyme Drosha and required for pri-miRNA processing (Nguyen et al., 2015). We have mapped DGCR8 to the C-terminal region of ATM suggesting that DGCR8 is a target or regulator of ATM. DGCR8 phosphorylation could not be visualised in immunoprecipitation experiments and was not identified in ATM/ATR substrate screens (Bensimon, Schmidt et al., 2010, Matsuoka, Ballif et al., 2007) suggesting that it could have a more regulatory role instead of being a substrate of ATM. Furthermore, DGCR8 depletion leads to an increase of pATM and 53BP1 focal recruitment at early timepoints indicating a deregulation of the DDR.

To determine the role of DGCR8 in the DNA damage response, we carried out clonogenic survival assays demonstrating that DGCR8 depletion results in increased sensitivity to IR in addition to sensitivity to Olaparib and ICRF-193. However, loss of DGCR8 has no effect on cell cycle regulation, checkpoint response or formation of γH2AX foci suggesting no defect in DNA repair kinetics.

Together, these results indicate that DGCR8 is not required for DNA repair kinetics but results in long-term genome instability. This could be due to the deregulation of ATM kinase activity leading to DNA repair by error-prone pathways such as alt-EJ or SAA. To test this hypothesis, we are planning to investigate these repair pathways using resection assays in addition to assays specifically interrogating alt-EJ or SSA (Gunn & Stark, 2012, Ochs, Somyajit et al., 2016, Yun & Hiom, 2009).

Furthermore, it will be important to distinguish the role of DGCR8 in DSB repair from its role in microRNA processing. We are in the process of generating DGCR8 mutants with deletions in the dimerization domain and the Drosha binding CTT domain, respectively. This should provide us with greater inside in both the function of DGCR8 in the DDR as well as a Drosha independent function. A role for DGCR8 in the repair of UV-

induced DNA lesions independent of Drosha has recently been published supporting our findings of a Drosha-independent role for DGCR8 in DSB repair (Calses, Dhillon et al., 2017).

Lastly, we identified DDX17 as a novel interacting protein of the DDR mediator protein 53BP1 that is required for efficient 53BP1 recruitment to DSBs. In addition we have also identified DDX17 as a regulator of total BRCA1 and RAD51 protein levels. We demonstrated that DDX17 depletion results in defective HR using the DR-GFP reporter system in addition to clonogenic survival assays with Olaparib and investigated focal recruitment of BRCA1 and RAD51 to IRIF. Together this data suggests that DDX17 is required for efficient HR. However, this hypothesis is in conflict with a recent paper by Adamson et al. suggesting DDX17 as a negative regulator of HR (Adamson et al., 2012).

DDX17 interaction with 53BP1 and localisation of DDX17 to DSB suggests a more direct role in the DDR. It would be interesting to further investigate the function of DDX17 at the DSB and whether it is involved in processing transcripts generated site specifically in response to DNA damage. We have generated ATP-hydrolysis deficient mutants of DDX17 to clamp and precipitate pre-miRNA transcipts that are site specifically induced at DSBs (Francia et al., 2012, Xiol, Spinelli et al., 2014).

After characterisation of these proteins in the DNA damage response, we intended to investigate their role in the DDR with respect to their function in RNA processing. In order to do this, we first needed to establish the tools and essays to visualise the diRNAs and pri-diRNA before we could assess the function of DGCR8, DDX17 and DDX3X in their biogenesis and processing. diRNAs have so far only been detected using reporter systems such as the Cherry-Lac-reporter (Francia et al., 2012, Wei et al., 2012). We decided to take advantage of another, well-establish system in U2OS cells, in which the AsiSI restriction enzyme induced by hydroxytamoxifen, introduces DSBs at known locations in the genome (Iacovoni, Caron et al., 2010). These DSBs are well characterised and

this system would allow us to study the role of our candidate proteins at DSBs repair by either HR or NHEJ (Zhou, Caron et al., 2014). We carried out miRNA-seq using this system in order to detect the diRNAs, however, even with extensive bioinformatic analysis, we were unable to detect small RNAs that were induced site-specifically at AsiSI-induced breaks (Data not shown). In addition, we exchanged data with other labs, who carried out the same or similar experiments using the AsiSI system. Our collegues were also unable to detect any small or long RNA transcripts specifically induced after DNA damage at the site of the break. This led us to believe that the diRNAs detected using the Cherry-Lac System might be an artifact resulting from the repetitive sequences around the DSB. Without being able to detect diRNAs, however, we are unable to assess the role of our candidate proteins in their biogenesis or processing. Furthermore, a recent publication by Miki et al shows that, although diRNAs were detected in a transgene in *A. thaliana* and rice, the group failed to detect diRNAs upon DSB induction in endogenous genes (Miki, Zhu et al., 2017).

Conclusively, this work shows novel roles for three RNA metabolism proteins, DGCR8, DDX17 and DDX3X in the DDR. In order to link these three proteins to the biogenesis or processing of ncRNAs, we will need a robust system to detect these ncRNA, which has not yet been established. Nevertheless, these three RNA metabolism proteins individually are involved in different aspects of DNA repair and it will be interesting to investigate the mechanism by which they act in order the repair the DNA faithfully and thus prevent genomic instability.

5.2. References

Adamson B, Smogorzewska A, Sigoillot FD, King RW, Elledge SJ (2012) A genome-wide homologous recombination screen identifies the RNA-binding protein RBMX as a component of the DNA-damage response. Nat Cell Biol 14: 318-28

Alexander RP, Fang G, Rozowsky J, Snyder M, Gerstein MB (2010) Annotating non-coding regions of the genome. Nat Rev Genet 11: 559-71

Bartel DP (2009) MicroRNAs: target recognition and regulatory functions. Cell 136: 215-33

Bensimon A, Schmidt A, Ziv Y, Elkon R, Wang SY, Chen DJ, Aebersold R, Shiloh Y (2010) ATM-dependent and -independent dynamics of the nuclear phosphoproteome after DNA damage. Sci Signal 3: rs3

Botlagunta M, Vesuna F, Mironchik Y, Raman A, Lisok A, Winnard P, Jr., Mukadam S, Van Diest P, Chen JH, Farabaugh P, Patel AH, Raman V (2008) Oncogenic role of DDX3 in breast cancer biogenesis. Oncogene 27: 3912-22

Calses PC, Dhillon KK, Tucker N, Chi Y, Huang JW, Kawasumi M, Nghiem P, Wang Y, Clurman BE, Jacquemont C, Gafken PR, Sugasawa K, Saijo M, Taniguchi T (2017) DGCR8 Mediates Repair of UV-Induced DNA Damage Independently of RNA Processing. Cell Rep 19: 162-174

Chang PC, Chi CW, Chau GY, Li FY, Tsai YH, Wu JC, Wu Lee YH (2006) DDX3, a DEAD box RNA helicase, is deregulated in hepatitis virus-associated hepatocellular carcinoma and is involved in cell growth control. Oncogene 25: 1991-2003

Chao CH, Chen CM, Cheng PL, Shih JW, Tsou AP, Lee YH (2006) DDX3, a DEAD box RNA helicase with tumor growth-suppressive property and transcriptional regulation activity of the p21waf1/cip1 promoter, is a candidate tumor suppressor. Cancer Res 66: 6579-88

Esteller M (2011) Non-coding RNAs in human disease. Nat Rev Genet 12: 861-74

Fabian MR, Sonenberg N, Filipowicz W (2010) Regulation of mRNA translation and stability by microRNAs. Annu Rev Biochem 79: 351-79

Francia S, Michelini F, Saxena A, Tang D, de Hoon M, Anelli V, Mione M, Carninci P, d'Adda di Fagagna F (2012) Site-specific DICER and DROSHA RNA products control the DNA-damage response. Nature 488: 231-5

Ganesan S, Silver DP, Greenberg RA, Avni D, Drapkin R, Miron A, Mok SC, Randrianarison V, Brodie S, Salstrom J, Rasmussen TP, Klimke A, Marrese C, Marahrens Y, Deng CX, Feunteun J, Livingston DM (2002) BRCA1 supports XIST RNA concentration on the inactive X chromosome. Cell 111: 393-405

Gunn A, Stark JM (2012) I-SceI-based assays to examine distinct repair outcomes of mammalian chromosomal double strand breaks. Methods Mol Biol 920: 379-91

Hu H, Gatti RA (2011) MicroRNAs: new players in the DNA damage response. J Mol Cell Biol 3: 151-8

Huntzinger E, Izaurralde E (2011) Gene silencing by microRNAs: contributions of translational repression and mRNA decay. Nat Rev Genet 12: 99-110

Iacovoni JS, Caron P, Lassadi I, Nicolas E, Massip L, Trouche D, Legube G (2010) High-resolution profiling of gammaH2AX around DNA double strand breaks in the mammalian genome. EMBO J 29: 1446-57

Kwon SC, Nguyen TA, Choi YG, Jo MH, Hohng S, Kim VN, Woo JS (2016) Structure of Human DROSHA. Cell 164: 81-90

Lai MC, Lee YH, Tarn WY (2008) The DEAD-box RNA helicase DDX3 associates with export messenger ribonucleoproteins as well as tip-associated protein and participates in translational control. Mol Biol Cell 19: 3847-58

Li Q, Zhang P, Zhang C, Wang Y, Wan R, Yang Y, Guo X, Huo R, Lin M, Zhou Z, Sha J (2014) DDX3X regulates cell survival and cell cycle during mouse early embryonic development. J Biomed Res 28: 282-91

Matsuoka S, Ballif BA, Smogorzewska A, McDonald ER, 3rd, Hurov KE, Luo J, Bakalarski CE, Zhao Z, Solimini N, Lerenthal Y, Shiloh Y, Gygi SP, Elledge SJ (2007) ATM and ATR substrate analysis reveals extensive protein networks responsive to DNA damage. Science 316: 1160-6

Miki D, Zhu P, Zhang W, Mao Y, Feng Z, Huang H, Zhang H, Li Y, Liu R, Zhang H, Qi Y, Zhu JK (2017) Efficient Generation of diRNAs Requires Components in the Posttranscriptional Gene Silencing Pathway. Sci Rep 7: 301

Moy RH, Cherry S (2014) DDX17: structured RNA recognition drives diverse outputs. Cell Cycle 13: 3467-8

Moy RH, Cole BS, Yasunaga A, Gold B, Shankarling G, Varble A, Molleston JM, tenOever BR, Lynch KW, Cherry S (2014) Stem-loop recognition by DDX17 facilitates miRNA processing and antiviral defense. Cell 158: 764-77

Nguyen TA, Jo MH, Choi YG, Park J, Kwon SC, Hohng S, Kim VN, Woo JS (2015) Functional Anatomy of the Human Microprocessor. Cell 161: 1374-87

Ochs F, Somyajit K, Altmeyer M, Rask MB, Lukas J, Lukas C (2016) 53BP1 fosters fidelity of homology-directed DNA repair. Nat Struct Mol Biol 23: 714-21

Pryde F, Khalili S, Robertson K, Selfridge J, Ritchie AM, Melton DW, Jullien D, Adachi Y (2005) 53BP1 exchanges slowly at the sites of DNA damage and appears to require RNA for its association with chromatin. J Cell Sci 118: 2043-55

Remenyi J, Bajan S, Fuller-Pace FV, Arthur JS, Hutvagner G (2016) The loop structure and the RNA helicase p72/DDX17 influence the processing efficiency of the mice miR-132. Sci Rep 6: 22848

Sun M, Zhou T, Jonasch E, Jope RS (2013) DDX3 regulates DNA damage-induced apoptosis and p53 stabilization. Biochim Biophys Acta 1833: 1489-97

Valiente-Echeverria F, Hermoso MA, Soto-Rifo R (2015) RNA helicase DDX3: at the crossroad of viral replication and antiviral immunity. Rev Med Virol 25: 286-99

Wan G, Mathur R, Hu X, Zhang X, Lu X (2011) miRNA response to DNA damage. Trends Biochem Sci 36: 478-84

Wei W, Ba Z, Gao M, Wu Y, Ma Y, Amiard S, White CI, Rendtlew Danielsen JM, Yang YG, Qi Y (2012) A role for small RNAs in DNA double-strand break repair. Cell 149: 101-12

Wu DW, Liu WS, Wang J, Chen CY, Cheng YW, Lee H (2011) Reduced p21(WAF1/CIP1) via alteration of p53-DDX3 pathway is associated with poor relapse-free survival in early-stage human papillomavirus-associated lung cancer. Clin Cancer Res 17: 1895-905

Xiol J, Spinelli P, Laussmann MA, Homolka D, Yang Z, Cora E, Coute Y, Conn S, Kadlec J, Sachidanandam R, Kaksonen M, Cusack S, Ephrussi A, Pillai RS (2014) RNA clamping by Vasa assembles a piRNA amplifier complex on transposon transcripts. Cell 157: 1698-711

Yedavalli VS, Neuveut C, Chi YH, Kleiman L, Jeang KT (2004) Requirement of DDX3 DEAD box RNA helicase for HIV-1 Rev-RRE export function. Cell 119: 381-92

Yoo S, Dynan WS (1998) Characterization of the RNA binding properties of Ku protein. Biochemistry 37: 1336-43

Yun MH, Hiom K (2009) CtIP-BRCA1 modulates the choice of DNA double-strand-break repair pathway throughout the cell cycle. Nature 459: 460-3

Zhang X, Wan G, Berger FG, He X, Lu X (2011) The ATM kinase induces microRNA biogenesis in the DNA damage response. Mol Cell 41: 371-83

Zhao L, Mao Y, Zhao Y, He Y (2016) DDX3X promotes the biogenesis of a subset of miRNAs and the potential roles they played in cancer development. Sci Rep 6: 32739

Zhou Y, Caron P, Legube G, Paull TT (2014) Quantitation of DNA double-strand break resection intermediates in human cells. Nucleic Acids Res 42: e19

Appendix I: CRISPR genome editing as a tool for generating knock-out and knock-in cell lines

I.1. Introduction

In recent years, the CRISPR-Cas9 gene editing technology has greatly improved gene editing in eukaryotic cells. Using CRISPR technology it is now possible to induce DSBs in virtually any gene, like the related TALEN and Zinc-finger nuclease technologies (Bibikova, Carroll et al., 2001, Boch, Scholze et al., 2009, Christian, Cermak et al., 2010, Miller, Holmes et al., 2007, Miller, Tan et al., 2011, Moscou & Bogdanove, 2009, Urnov, Miller et al., 2005). The generated DSBs can be repaired by NHEJ to introduce point mutations, insertions or deletions, resulting in knock-outs, or HR, which allows insertion of specific alterations of the target genomic region useful for tagging endogenous proteins or inserting specific point mutations to alter protein function.

The clustered regularly interspaced short palindromic repeats (CRISPR)-Cas9 technology is derived from a prokaryotic RNA-guided, adaptive immune system, which can be found in almost all archaea, about 40% of known bacterial genomes and in some bacteriophages (Bondy-Denomy, Pawluk et al., 2013, Seed, Lazinski et al., 2013). This adaptive immune system, similar to eukaryotic RNA interference, has evolved to fight off viral infection and plasmid transfer by sequence-specific detection and silencing of invading nucleic acids (Barrangou, Fremaux et al., 2007, Brouns, Jore et al., 2008, Westra, Swarts et al., 2012).

CRISPR-Cas systems have been divided into three main types based on their locus organization and types of the Cas protein present: Type I, Type II and Type III. These are further classified into eleven distinct subtypes: Type I A-F, Type II A-C and Type III A-B (Chylinski, Makarova et al., 2014, Makarova, Haft et al., 2011). Both Type I and Type III require the Cas6 family of nucleases, while Type II relies on the multifunctional Cas9 endonuclease (Carte, Wang et al., 2008, Deltcheva, Chylinski et al., 2011, Haurwitz, Jinek et al., 2010, Nam, Haitjema et al., 2012). Due to its relative simplicity and low number of involved proteins and nucleic acids,

the Type II CRISPR-Cas system is the most widely used for genome editing (Tycko, Myer et al., 2016).

CRISPR-Cas adaptive immunity consists of three discrete stages: spacer acquisition, Cas expression and DNA/RNA interference (Marraffini & Sontheimer, 2010a, van der Oost, Westra et al., 2014, Wiedenheft, Sternberg et al., 2012). The initial acquisition stage uses a short protospacer sequence from foreign nucleic acids and inserts them into the CRISPR array to be used as a new spacer (Heler, Marraffini et al., 2014). These protospacer sequences are selected by recognition of the protospacer adjacent motif (PAM) sequences of the invading genomes (Mojica, Diez-Villasenor et al., 2009). The selection of the PAM sequence also eliminates the possibility of self-targeting, as these sequences are absent in the CRISPR locus of the host species (Marraffini & Sontheimer, 2010b). In the following stage, the newly integrated sequence is then transcribed into a long precursor CRISPR RNA (pre-crRNA) and further cleaved into single-spacer mature crRNAs (Brouns et al., 2008). The final stage is the assembly of the crRNA and the Cas proteins into a large ribonuclein complex that is able to recognize and target foreign DNA/RNA for degradation (van der Oost et al., 2014).

The type II CRISPR-Cas system mainly uses a single protein of the Cas family, Cas9, for targeting making it an easier to modify system compared to type I or III systems that consist of a targeting cascade of a number of different proteins (Hale, Zhao et al., 2009, Hatoum-Aslan, Maniv et al., 2014, Sinkunas, Gasiunas et al., 2013, Westra, van Erp et al., 2012). The multi-functioning Cas9 protein contains HNH and RuvC-like nuclease domains, which cut the complimentary and non-complementary target strand, respectively (Gasiunas, Barrangou et al., 2012, Jinek, Chylinski et al., 2012). Furthermore, the RNA of the type II system consist of a crRNA in a duplex with a transactivating crRNA (tracrRNA). These two parts of the RNA heteroduplex have been engineered in such a way to produce a single chimeric guideRNA (gRNA) by fusing the 5'end of the tracrRNA to

the 3'end of the crRNA using a linker sequence (Deltcheva et al., 2011, Jinek et al., 2012).

Both, base-pairing of the 20 nt gRNA sequence of the Cas9 complex and the recognition of the PAM sequence in the target nucleic acid are essential for targeting and cleavage, however, studies have shown that perfect sequence complementarity is only required in the first 12 nt adjacent to the PAM sequences, while mismatches in the other 8nt can be tolerated occasionally (Charpentier & Marraffini, 2014, Jinek et al., 2012).

Two arginine residues, R1333 and R1335, of the spCas9 recognise two guanine residues in the target PAM sequence (Anders, Niewoehner et al., 2014, Jinek, Jiang et al., 2014, Nishimasu, Ran et al., 2014, Sternberg, Redding et al., 2014), while point mutations H840A and D10A completely abolish nuclease activity of the HRH and RuvC-like domains, respectively (Anders et al., 2014, Cong, Ran et al., 2013, Nishimasu et al., 2014).

In this study, we use the engineered type II CRISPR-Cas9 system of the bacterium *Streptococcus pyogenes* (spCas9) to knock out three selected genes, *DGCR8*, *DDX3X* and *DDX17*, and to AID tag the DEAD box helicase *DDX5*.

.

I.2. Designing gRNAs for target proteins

The design of the target gRNAs is crucial in order to achieve efficient gene targeting. Table I.1 shows the genomic target sequence used as a template for the design of the gRNAs. All gRNAs display relatively weak to moderate secondary structure, which is important in both cloning into the X330 vector as well as after translation into gRNA in the cell.

We have selected three different gRNA for each of the genes to increase targeting efficiency (Figure I-1). Both *DDX17* and *DGCR8* contain a suitable gRNA target sequence within the first or second exon, *DDX3X* however did not contain a suitable gRNA target sequence until exon 9.

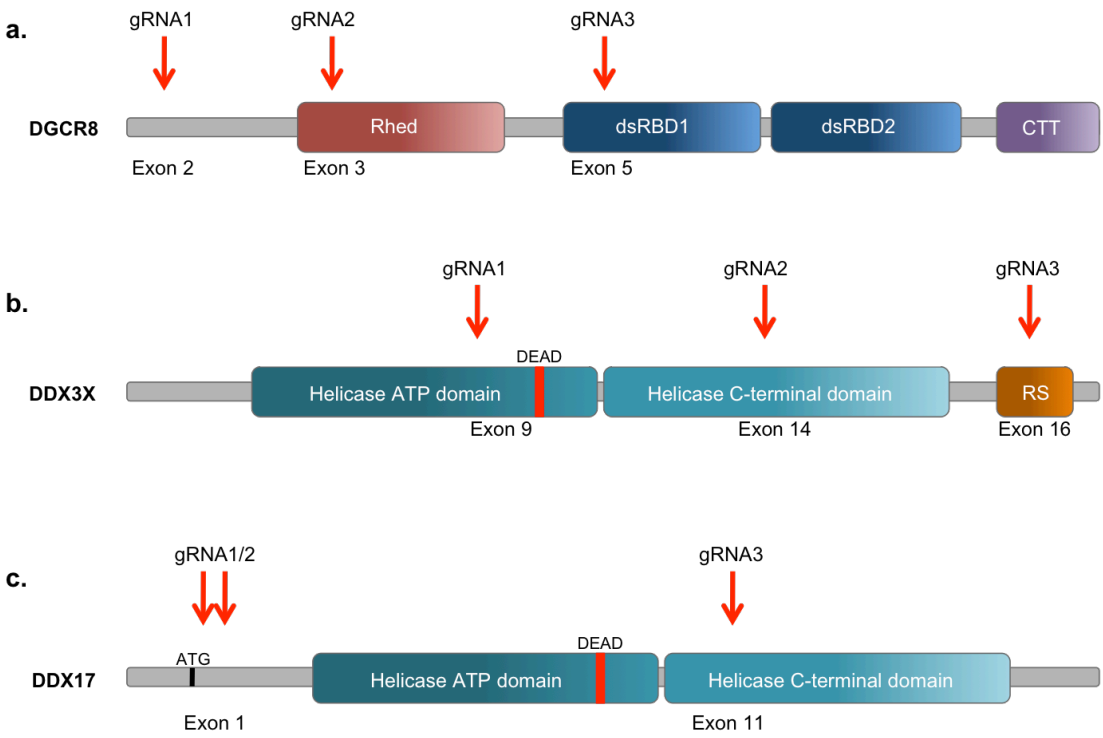

Figure I-1: Distribution of gRNA targets in the selected proteins

A. Schematic of DGCR8 with three selected target gRNA positions (red arrows) in exon 2,3 and 5. B. Schematic of DDX3X with selected target gRNA positions in exon 9,14 and 16.C. Schematic of DDX17 with selected gRNA target positions in exon 1 and 11.

Target gene	gRNA	Strand	genomic Sequence
DDX17	gRNA1	leading	GCCATCGGTCGTCACCAGAC**CGG**
DDX17	gRNA2	leading	GACCGGGATCGTGACCGTGG**AGG**
DDX17	gRNA3	leading	GCTACAGATGTAGCCTCCCG**TGG**
DGCR8	gRNA1	lagging	**CCC**CTGCAAACGTCCAGTGGTGC
DGCR8	gRNA2	leading	GACAGCGACCATCCGTCCGA**TGG**
DGCR8	gRNA3	lagging	**CCT**GACTCTATGGGTGCTGACCC
DDX3X	gRNA1	leading	GTTGGCAGTACAGATCTACG**AGG**
DDX3X	gRNA2	leading	GTACATCGTATTGGTCGTAC**GGG**
DDX3X	gRNA3	leading	GGTGGCCACGGTAGCAGCAG**AGG**
DDX5	gRNA1	lagging	**CCG**CCAACCGCAACCATTGACGC
DDX5	gRNA2	leading	GAGACCGCGGCCGGGACCGA**GGG**

Table I.1: Genomic sequences of gRNAs used in this study.

The genomic sequences of the gRNA used for knock-out (*DDX3X, DDX17, DGCR8*) and knock-in (*DDX5*) gene targeting are shown with the PAM sequences indicated in bold.

I.3. Cloning and transfection of selected gRNAs for knock-out cell lines

After selecting three unigue gRNA target sequences for the gRNA of each gene, *DDX3X*, *DDX17* and *DGCR8*, the PAM sequence was removed and the required overhangs for cloning into the pX330 vector were added to the gRNA sequence (Figure I-2). The oligonucleotides were then annealed prior to PNK treatment, to maximise PNK efficiency. The PNK-treated oligonucleotides were then denatured and re-annealed to deactivate the PNK.

The pX330 vector was digested with the restriction enzyme *Bbs*I and the annealed oligos were inserted. Before sequencing the vectors inserted with the correct guideRNAs, the ligated vectors were digested with *Bbs*I to select only plasmids that were not digested, as insertion of the gRNA causes loss of the *Bbs*I restriction site.

After validation of the vector by sequencing, the gRNA containing vectors were co-transfected with a puromycin resistant selection plasmid at a ratio of 5:1.

In the first round of gene targeting, RPE-1 cells were transfected with one gRNA containg pX330 plasmid per transfection to measure the targeting efficiency of each single gRNA. In the second round of gene targeting, U2OS and HEK293T cells were transfected with gRNA1 and gRNA2 simultaneously to increase knock-out efficiency (Figure I-1).

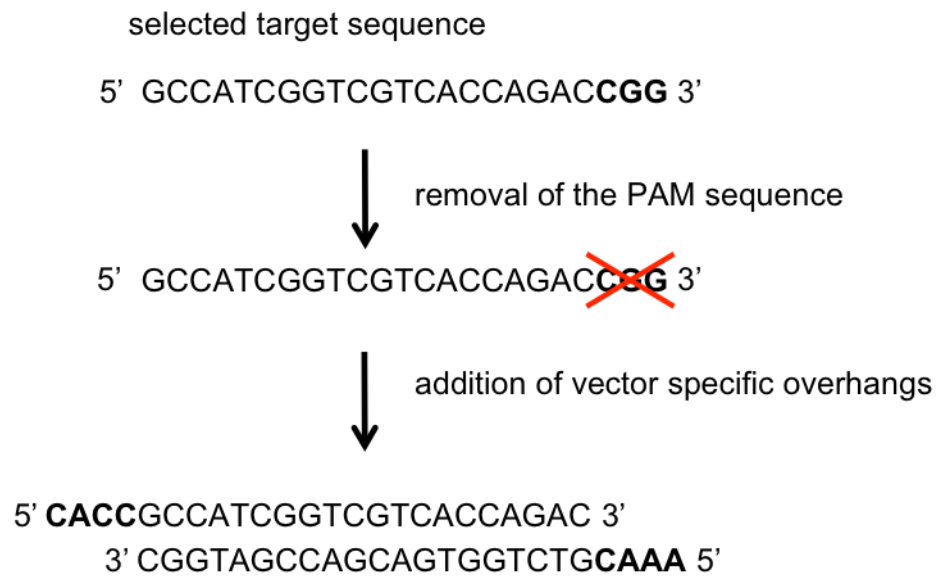

Figure I-2: CRISPR gRNA primer design

Upon selection of gRNA target sequence in the gene of interest, the PAM sequence (bold) was removed and the respective 5’overhangs were added to the template and non-template strand for cloning into the pX330 vector.

Cells were then grown in serial dilutions for ten to fifteen days, depending on the cell line, until single colonies reached about 1-2mm in diameter. The cloned colonies were then transferred into a 24-well plate, grown to confluency and split into a 6-well dish.

I.4. Primary screening of transfected cell lines

Once the clones reached confluency in two wells of a 6-well plate, they were harvested, using a quarter of the cells for primary screening, a quarter for genomic DNA extraction and the rest of the cells were frozen down at -80ºC in FBS containing 10% DMSO.

Primary screening of the selected clones was carried out using Western Blots. The cells were lysed and run on 10% SDS gels. All samples with the protein present were marked as negative, with the protein level significantly reduced or the incorrect protein size in addition to the correct protein size, were marked as heterozygous and all samples with the protein absent were marked as positive. Figure I-3 shows representative images of the primary screen in U2OS and HEK293T cells.

The gRNAs to *DDX17* show the highest efficiency of gene targeting in all the cell lines, while *DGCR8* gRNA targeting efficiency is moderate and *DDX3X* gRNAs failed to knock out the protein (Figure I-4).

Figure I-4a shows the percentage of positive clones that each gRNA produced individually in RPE1 cells. Figure I-4b,c shows the combined targeting efficiency of gRNA1 and gRNA2 in U2OS and HEK293T cells, respectively. Furthermore, in Figure I-4b,c the graph distinguishes between the frequency of knock-out and heterozygous targeting, showing that targeting of both alleles is more likely than targeting of only one allele.

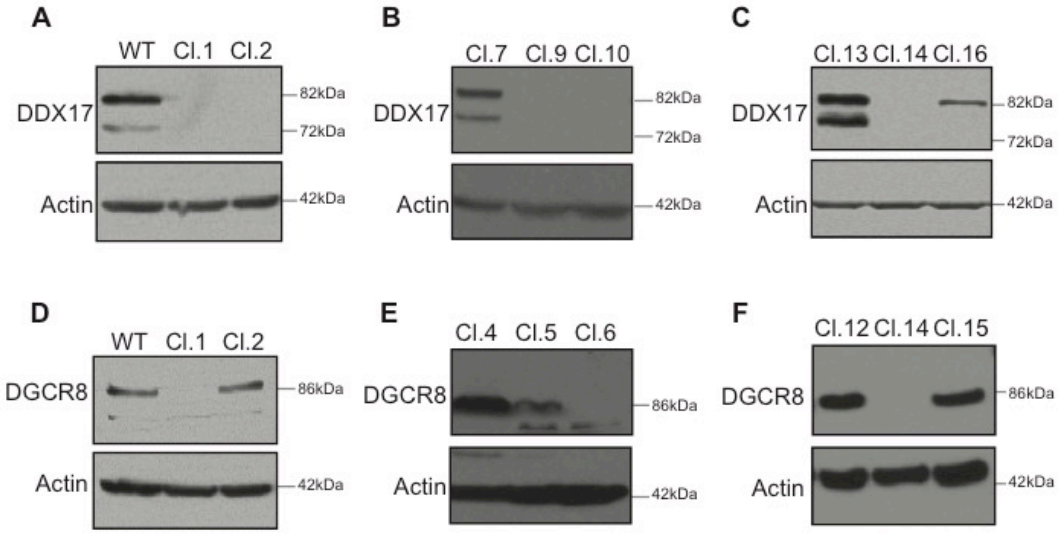

Figure I-3:Western Blot analysis of selected CRISPR clones.

(A) DDX17$^{-/-}$ clones in U2OS cells. (B)(C) DDX17$^{-/-}$ clones in HEK293T cells. (D) DGCR8$^{-/-}$clones in hTERT-RPE1 cells. (E)(F) DGCR8$^{-/-}$ clones in HEK293T cells. All cells were lysed, Benzonase digested and the resulting Western Blot was probed with the indicated antibodies.

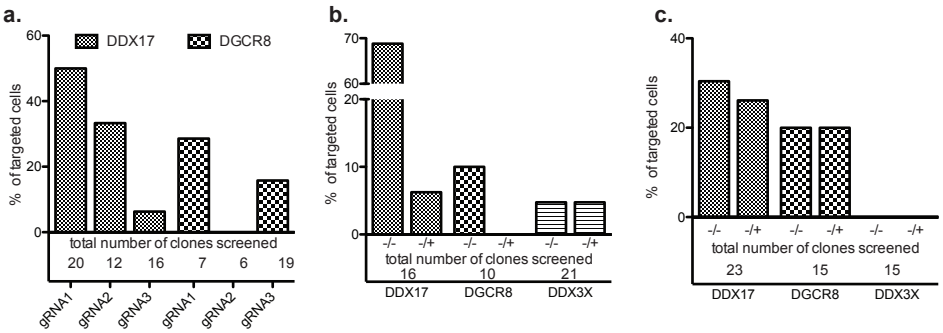

Figure I-4: CRISPR targeting efficiencies in three different cell lines.

A. CRISPR knock out experiment in RPE-1 cell line. Graph shows the percentage of targeting efficiency for each single gRNA construct for *DDX17* and *DGCR8*, *DDX3X* is not shown as all cells died during expansion.B. CRISPR knock-out experiment in U2OS cells. Graph represents the percentage of positive or heterozygous colonies. C. CRISPR knock-out experiment in HEK293T cells. Graph represents the percentage of positive or heterozygous clones.

DDX5 is embryonic lethal at E11.5, so a conditional approach using the Auxin Inducible Degron (AID) system previously established in the lab by J. Eykelenboom was used. Auxin is a plant hormone, that if present in high enough quantities, activates the auxin signalling pathway. Auxin binds to the F-box transport inhibitor response 1 (TIR1), a part of the SCF ubiquitin ligase complex. This leads to polyubiquitination of auxin proteins and thus to their proteosomal degradation (Nishimura, Fukagawa et al., 2009).

The AID tag was cloned into a pLox puro backbone together with two 2.5kb flanging homology arms either side that are sequence specific to the genomic region around the ATG start codon of DDX5 (Figure I-5).

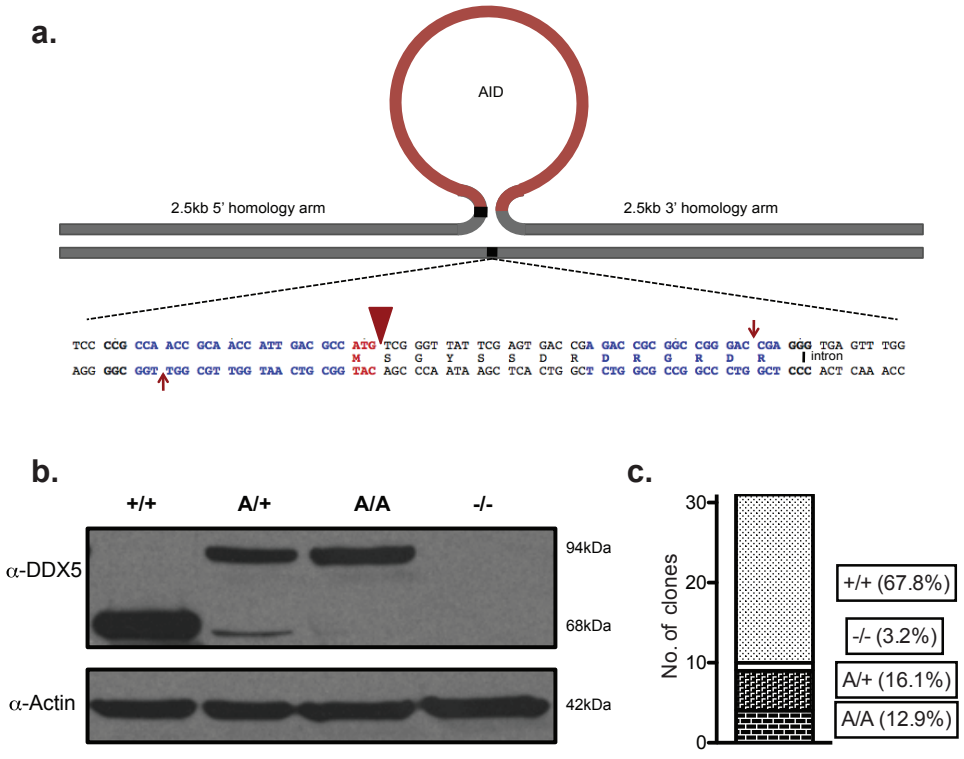

Figure I-5: Generation of endogenous AID-tagged DDX5 in HCT116 cells

A. Schematic of gene editing strategy at the ATG start site of the DDX5 gene. B. Western blot of AID-DDX5 clone screening. +/+ wild type, A/+ heterozygous, A/A homozygous AID-tagged, -/- knock-out. C. Overview of screened clones. Graph shows the distribution of targeting of the screening clones.

A third of all screened clones showed targeting by either having both alleles tagged, only one allele tagged or a missense mutation that resulted in loss of the protein without integration of the template DNA (Figure I-5b,c). In order to obtain a conditional knock-out cell line, we then integrated TIR1 cDNA into the positive clone by random integration, however failed to produce sufficient expression of TIR1 to deplete the tagged protein (data not shown).

I.5. Sequencing for positive clones

Genomic DNA from positive clones that showed a complete loss of either DGCR8 or DDX17 was extracted using a simple TAIL prep. The region of interest around 500bp either side of the cut was amplified and the product(s) were send of for sequencing (Table I.2).

Target gene	guideRNAs	Primer	Sequence
DDX17	gRNA1; gRNA2	forward	CCGCCATTTTGTGCAGTCG
		reverse	GGAAACCAGGCGAGGCG
DDX17	gRNA3	forward	CTACTGACCCCCAACTTTTGG
		reverse	CCTCTGTTTGAATAGTCATGCC
DGCR8	gRNA1	forward	GAAGAAAGGTGCCACTCCGG
		reverse	CACTGACAGGGCTAAGGAGC
DGCR8	gRNA2	forward	CAGTGTGTGCCCCTGGACC
		reverse	CCCTCAGAAGTCCCCTCCC
DGCR8	gRNA3	forward	GCATCAGTCGTGACTTTAGGC
		reverse	GACAGGAGCCTAGGGTGC

Table I.2: List of primers used for PCR amplification and sequencing of Knock-out clones.

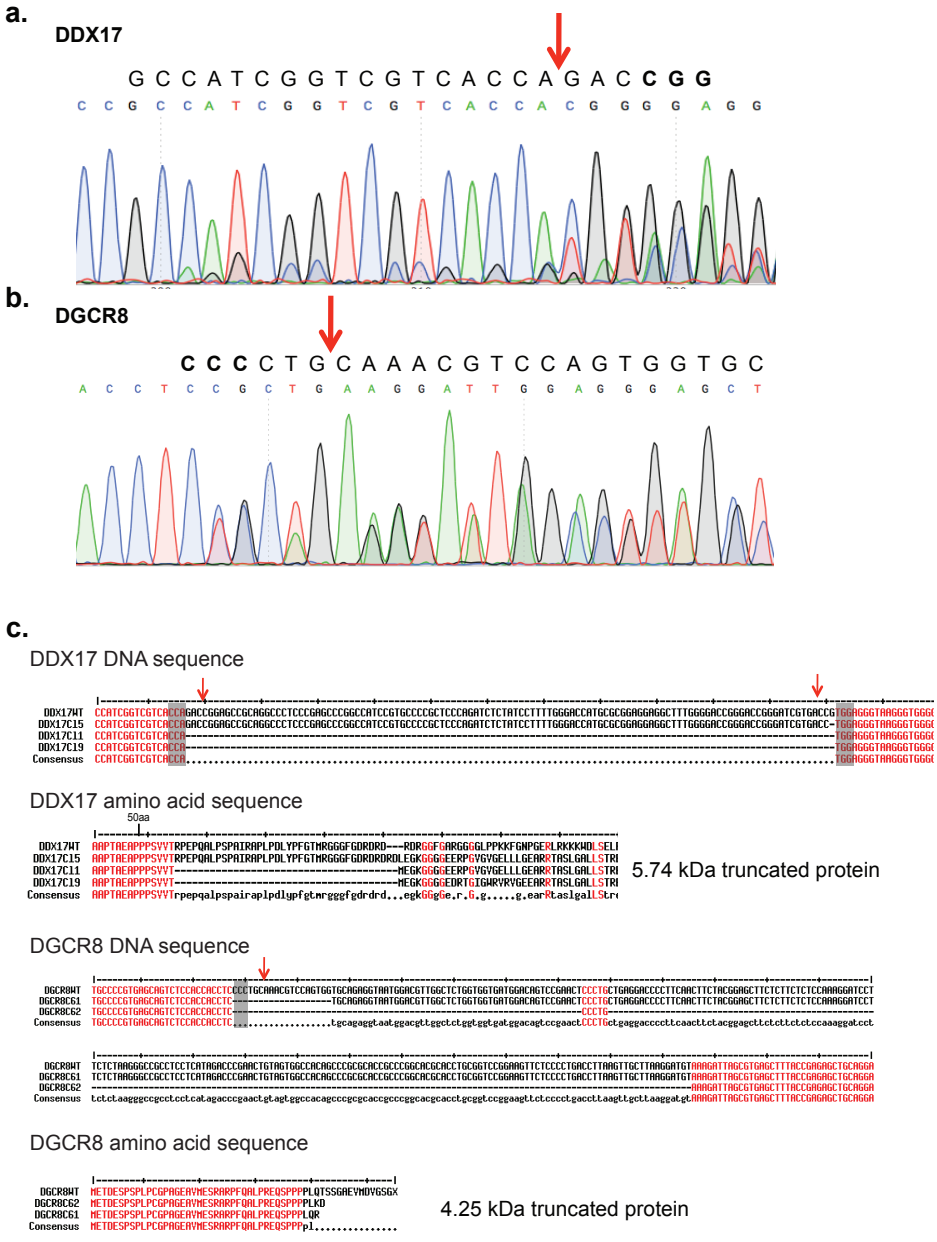

Figure I-6: Sequencing results of knock-out DDX17 and DGCR8 U2OS cell lines

Overview of sequencing results obtained from U2OS cell line. A. Diagram of PCR from DDX17 knock-out cell line showing multiple peaks after the break site (red arrow). B. Diagram of PCR from DGCR8 knock-out cell line showing multiple peaks after the break site (red arrow). C. Sequencing results of individually cloned alleles of candidate DDX17 and DGCR8 knock out cell lines. Red arrows indicate the cut site.

The initial sequencing of the PCR products could lead to different outcomes depending on the repair by NHEJ. Both alleles could be repaired resulting in the same or a different frameshift mutation. In case of the same frameshift mutation, all sequencing peaks would be distinct showing the mutation. In case both alleles obtains a different frameshift mutation, we should see double peaks in the sequencing after the double strand break sites resulting from a different sequence in the two alleles (Figure I-6a,b).

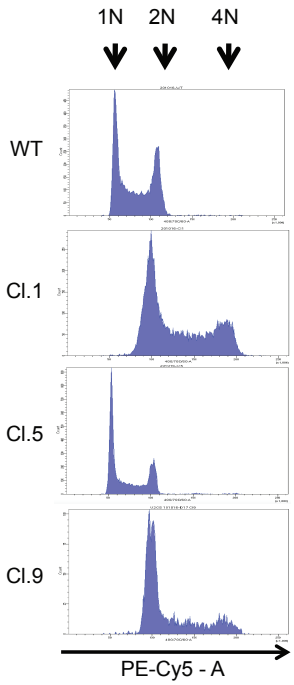

Figure I-7: Polyploidy in DDX17$^{-/-}$ cells

PI profile of candidate DDX17$^{-/-}$ cell lines compared to the parental wild-type cell line. Cell were fixed in 75% Ethanol, permeabilized with 0.5% Triton and stained with PI. In the wild type cell line, the 1N peak indicates cells in G1 and the 2N peak shows cells in G2. Clone 1 and 9 show a shift in the PI profile from 1N/2N to 2N/4N DNA content.

After initial sequencing, the PCR products were cloned into a pGEM-T easy vector and positive colonies were sequenced individually (Figure I-6c). Most positive clones of the *DDX17* knock-out cell line contain a large deletion between the two cut sites of gRNA1 and gRNA2, while one clone showed a deletion of one base pair resulting in a frameshift mutation. All mutations result in a 5.74 kDa truncated protein. Sequencing results from the potential *DGCR8* knock-out cell lines show larger deletions varying in length (Figure I-6c), also resulting in frameshift mutations leading to a 4.25 kDa truncated protein.

Interestingly, when the DNA content of three of the candidate DDX17$^{-/-}$ cell lines was analysed, all individual clones showing the 124 bp deletion between the two guide RNAs, they displayed polyploidy (Figure I-7). While the point deletion mutant shows the same PI profile as the parental wild-type cell line, the other clones would shift their PI profile from 1N/2N to 2N/4N indicating diploidy in G1 and tetraploidy in G2 phase.

I.6. Discussion

CRISPR/Cas9 technology has come a long way in a short space of time. Since the first papers of engineered chimeric gRNAs were published in 2013, a lot of companies have started providing programmes for designing gRNAs or even producing the plasmids or knock-out cell lines available for purchase. In this study, we have shown that the new CRISPR-Cas9 technology is a very powerful easy to use tool for genome editing in a variety of cell lines. We successfully created a knock-out of *DGCR8* and *DDX17* in U2OS, HE293T and RPE-1 cell lines and used a knock-in approach to add an AID tag to the 5'end of the *DDX5* gene. We failed, however, to deplete or mutate the DDX3X gene, which could be due to several possibilities. The design of the gRNAs could be not good enough for efficient targeting or the protein could potentially be essential for the cells to survive. Ded, the yeast homolog of DDX3X, is essential, suggesting that *DDX3X* could also play a vital role in the cell. Therefore, a conditional knock-out approach similar to the AID tagging of DDX5, would be a possibility. Due to the lack of NGG PAM sequences or suitable gRNAs at the 5'end of *DDX3X*, the protein would need to be tagged C-terminally, or a Cas9 with a mutated PAM sequence could be used to insert AID at the 5'end. Furthermore, it would be advantageous to first randomly integrate TIR1 and check the depletion of transiently transfected AID-*DDX3X*, before generating the homologous template and inserting the AID tagged to the endogenous *DDX3X*. This would save time, effort and money in the long run.

Generating stable knock-out cell lines takes from four to six weeks until the sequenced clones can be validated. This is a very fast and easy method of gene editing and can be used with minimal experience. The targeting efficiency in this study using the wild type Cas9 endonuclease ranges from 10% to 70% depending on the guide RNA and cell line used. This is much higher than other gene editing technologies like TALEN or Zinc finger endonuclease. However, the CRISPR-Cas9 system is also prone to off target effects due to the large genome size. Therefore, the

design of the gRNAs is crucial to prevent or minimize off-target effects. In the case of the DDX17$^{-/-}$ U2OS cell line, the change in ploidy could be due to a possible off target effect, rather than a depletion of the DDX17 protein, as a clone with a single point deletion does not result in polyploidy. This suggests than, although chosen carefully, the gRNAs could have off target effects in different parts of the genome deleting proteins responsible for genome integrity.

In summary, CRISPR-Cas9 technology is an easy to use tool for knocking out genes or inserting tags into the genome. However, it is crucial that gRNAs are carefully designed and the resulting knock out cell lines are validated before experimental use, as potential off target effects could lead to misleading phenotypes. It is also important to have different independent clones, ideally containing different frameshift mutations to verify the observed phenotypes.

I.7. References

Anders C, Niewoehner O, Duerst A, Jinek M (2014) Structural basis of PAM-dependent target DNA recognition by the Cas9 endonuclease. Nature 513: 569-73

Barrangou R, Fremaux C, Deveau H, Richards M, Boyaval P, Moineau S, Romero DA, Horvath P (2007) CRISPR provides acquired resistance against viruses in prokaryotes. Science 315: 1709-12

Bibikova M, Carroll D, Segal DJ, Trautman JK, Smith J, Kim YG, Chandrasegaran S (2001) Stimulation of homologous recombination through targeted cleavage by chimeric nucleases. Mol Cell Biol 21: 289-97

Boch J, Scholze H, Schornack S, Landgraf A, Hahn S, Kay S, Lahaye T, Nickstadt A, Bonas U (2009) Breaking the code of DNA binding specificity of TAL-type III effectors. Science 326: 1509-12

Bondy-Denomy J, Pawluk A, Maxwell KL, Davidson AR (2013) Bacteriophage genes that inactivate the CRISPR/Cas bacterial immune system. Nature 493: 429-32

Brouns SJ, Jore MM, Lundgren M, Westra ER, Slijkhuis RJ, Snijders AP, Dickman MJ, Makarova KS, Koonin EV, van der Oost J (2008) Small CRISPR RNAs guide antiviral defense in prokaryotes. Science 321: 960-4

Carte J, Wang R, Li H, Terns RM, Terns MP (2008) Cas6 is an endoribonuclease that generates guide RNAs for invader defense in prokaryotes. Genes Dev 22: 3489-96

Charpentier E, Marraffini LA (2014) Harnessing CRISPR-Cas9 immunity for genetic engineering. Curr Opin Microbiol 19: 114-9

Christian M, Cermak T, Doyle EL, Schmidt C, Zhang F, Hummel A, Bogdanove AJ, Voytas DF (2010) Targeting DNA double-strand breaks with TAL effector nucleases. Genetics 186: 757-61

Chylinski K, Makarova KS, Charpentier E, Koonin EV (2014) Classification and evolution of type II CRISPR-Cas systems. Nucleic Acids Res 42: 6091-105

Cong L, Ran FA, Cox D, Lin S, Barretto R, Habib N, Hsu PD, Wu X, Jiang W, Marraffini LA, Zhang F (2013) Multiplex genome engineering using CRISPR/Cas systems. Science 339: 819-23

Deltcheva E, Chylinski K, Sharma CM, Gonzales K, Chao Y, Pirzada ZA, Eckert MR, Vogel J, Charpentier E (2011) CRISPR RNA maturation by trans-encoded small RNA and host factor RNase III. Nature 471: 602-7

Gasiunas G, Barrangou R, Horvath P, Siksnys V (2012) Cas9-crRNA ribonucleoprotein complex mediates specific DNA cleavage for adaptive immunity in bacteria. Proc Natl Acad Sci U S A 109: E2579-86

Hale CR, Zhao P, Olson S, Duff MO, Graveley BR, Wells L, Terns RM, Terns MP (2009) RNA-guided RNA cleavage by a CRISPR RNA-Cas protein complex. Cell 139: 945-56

Hatoum-Aslan A, Maniv I, Samai P, Marraffini LA (2014) Genetic characterization of antiplasmid immunity through a type III-A CRISPR-Cas system. J Bacteriol 196: 310-7

Haurwitz RE, Jinek M, Wiedenheft B, Zhou K, Doudna JA (2010) Sequence- and structure-specific RNA processing by a CRISPR endonuclease. Science 329: 1355-8

Heler R, Marraffini LA, Bikard D (2014) Adapting to new threats: the generation of memory by CRISPR-Cas immune systems. Mol Microbiol 93: 1-9

Jinek M, Chylinski K, Fonfara I, Hauer M, Doudna JA, Charpentier E (2012) A programmable dual-RNA-guided DNA endonuclease in adaptive bacterial immunity. Science 337: 816-21

Jinek M, Jiang F, Taylor DW, Sternberg SH, Kaya E, Ma E, Anders C, Hauer M, Zhou K, Lin S, Kaplan M, Iavarone AT, Charpentier E, Nogales E, Doudna JA (2014) Structures of Cas9 endonucleases reveal RNA-mediated conformational activation. Science 343: 1247997

Makarova KS, Haft DH, Barrangou R, Brouns SJ, Charpentier E, Horvath P, Moineau S, Mojica FJ, Wolf YI, Yakunin AF, van der Oost J, Koonin EV (2011) Evolution and classification of the CRISPR-Cas systems. Nat Rev Microbiol 9: 467-77

Marraffini LA, Sontheimer EJ (2010a) CRISPR interference: RNA-directed adaptive immunity in bacteria and archaea. Nat Rev Genet 11: 181-90

Marraffini LA, Sontheimer EJ (2010b) Self versus non-self discrimination during CRISPR RNA-directed immunity. Nature 463: 568-71

Miller JC, Holmes MC, Wang J, Guschin DY, Lee YL, Rupniewski I, Beausejour CM, Waite AJ, Wang NS, Kim KA, Gregory PD, Pabo CO, Rebar EJ (2007) An improved zinc-finger nuclease architecture for highly specific genome editing. Nat Biotechnol 25: 778-85

Miller JC, Tan S, Qiao G, Barlow KA, Wang J, Xia DF, Meng X, Paschon DE, Leung E, Hinkley SJ, Dulay GP, Hua KL, Ankoudinova I, Cost GJ, Urnov FD, Zhang HS, Holmes MC, Zhang L, Gregory PD, Rebar EJ (2011) A TALE nuclease architecture for efficient genome editing. Nat Biotechnol 29: 143-8

Mojica FJ, Diez-Villasenor C, Garcia-Martinez J, Almendros C (2009) Short motif sequences determine the targets of the prokaryotic CRISPR defence system. Microbiology 155: 733-40

Moscou MJ, Bogdanove AJ (2009) A simple cipher governs DNA recognition by TAL effectors. Science 326: 1501

Nam KH, Haitjema C, Liu X, Ding F, Wang H, DeLisa MP, Ke A (2012) Cas5d protein processes pre-crRNA and assembles into a cascade-like

interference complex in subtype I-C/Dvulg CRISPR-Cas system. Structure 20: 1574-84

Nishimasu H, Ran FA, Hsu PD, Konermann S, Shehata SI, Dohmae N, Ishitani R, Zhang F, Nureki O (2014) Crystal structure of Cas9 in complex with guide RNA and target DNA. Cell 156: 935-49

Nishimura K, Fukagawa T, Takisawa H, Kakimoto T, Kanemaki M (2009) An auxin-based degron system for the rapid depletion of proteins in nonplant cells. Nat Methods 6: 917-22

Seed KD, Lazinski DW, Calderwood SB, Camilli A (2013) A bacteriophage encodes its own CRISPR/Cas adaptive response to evade host innate immunity. Nature 494: 489-91

Sinkunas T, Gasiunas G, Waghmare SP, Dickman MJ, Barrangou R, Horvath P, Siksnys V (2013) In vitro reconstitution of Cascade-mediated CRISPR immunity in Streptococcus thermophilus. EMBO J 32: 385-94

Sternberg SH, Redding S, Jinek M, Greene EC, Doudna JA (2014) DNA interrogation by the CRISPR RNA-guided endonuclease Cas9. Nature 507: 62-7

Tycko J, Myer VE, Hsu PD (2016) Methods for Optimizing CRISPR-Cas9 Genome Editing Specificity. Mol Cell 63: 355-70

Urnov FD, Miller JC, Lee YL, Beausejour CM, Rock JM, Augustus S, Jamieson AC, Porteus MH, Gregory PD, Holmes MC (2005) Highly efficient endogenous human gene correction using designed zinc-finger nucleases. Nature 435: 646-51

van der Oost J, Westra ER, Jackson RN, Wiedenheft B (2014) Unravelling the structural and mechanistic basis of CRISPR-Cas systems. Nat Rev Microbiol 12: 479-92

Westra ER, Swarts DC, Staals RH, Jore MM, Brouns SJ, van der Oost J (2012) The CRISPRs, they are a-changin': how prokaryotes generate adaptive immunity. Annu Rev Genet 46: 311-39

Westra ER, van Erp PB, Kunne T, Wong SP, Staals RH, Seegers CL, Bollen S, Jore MM, Semenova E, Severinov K, de Vos WM, Dame RT, de Vries R, Brouns SJ, van der Oost J (2012) CRISPR immunity relies on the consecutive binding and degradation of negatively supercoiled invader DNA by Cascade and Cas3. Mol Cell 46: 595-605

Wiedenheft B, Sternberg SH, Doudna JA (2012) RNA-guided genetic silencing systems in bacteria and archaea. Nature 482: 331-8

Appendix II: Funding and poster presentations

II.8. Scholarship Funding

College of Science Scholarship was awarded for the duration of four years by the National University of Ireland, Galway

Thomas Crawford Hayes Scholarship was awarded in 2013

II.9. Poster Presentations

1. Scientific Advisory Board, Centre for Chromosome Biology, Galway, November 2013

Title: The roles of miRNA processing proteins and ncRNA in the DNA damage response

2. SFI midterm review, December 2016

Title: The roles of RNA metabolism proteins and ncRNA in the DNA damage response

3. SFI midterm review, December 2016

Title: A role for the p53 tumour suppressor in regulating the balance between homologous recombination and non-homologous end-joining

The roles of miRNA processing proteins and ncRNA in the DNA damage response

J. Luessing, N. Tsanov, N. F. Lowndes

Genome Stability Laboratory - Centre for Chromosome Biology,
School of Natural Sciences, National University of Ireland, Galway

NUI Galway OÉ Gaillimh

Centre for Chromosome Biology

NDP NATIONAL DEVELOPMENT PLAN

EUROPEAN UNION STRUCTURAL FUNDS

sfi science foundation ireland fondúireacht eolaíochta éireann

1. Abstract

Since their discovery in 1993, microRNAs (miRNAs) have been implicated in various biological processes, mainly as regulators of gene expression. Over the past 4 years, a role in the DNA damage response has been suggested (1-3). In a recent proteomic screen from our lab, a large percentage of RNA metabolism proteins have been identified as interactors with the key DDR proteins ATR, ATM or 53BP1. These proteins include known miRNA processing proteins DGCR8, DDX17 and DDX5. These proteins are part of the miRNA processing machinery, which has been shown to be involved in the maturation of some but not all miRNAs. A recent study has suggested a common pathway in which all of these proteins act to process damage induced small RNAs (diRNAs). In this project, we aim to identify a mechanism by which these proteins, as well as established miRNA processors act at the site of DNA damage. We demonstrate an interaction between RNA metabolism proteins with key players of the DNA damage response in addition to their individual function in DNA repair and diRNA processing. Furthermore, we hypothesize that a long ncRNA is transcribed directly at the site of damage may act like a scaffold for the assembly of the DNA repair machinery.

1. miRNA processing proteins are involved in the DNA damage response

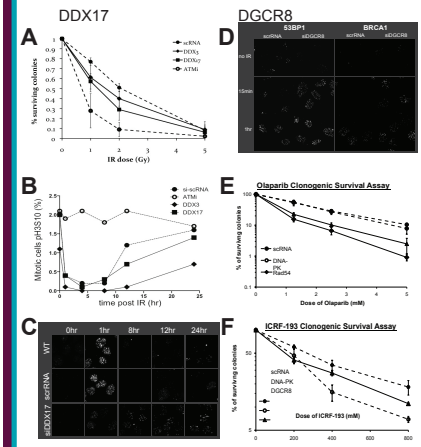

DDX17 is required for cell survival after IR (A). Cell depleted for DDX17 show a delay in checkpoint exit (B) as well as impaired focal recruitment of gH2X (C), indicating a defect in DNA damage repair. DGCR8 regulates focal recruitment of DNA damage repair factor (D) and is required for both efficient homologous recombination (E) and non-homologous end-joining (F).

2. miRNA processing machinery locates to DNA double strand breaks

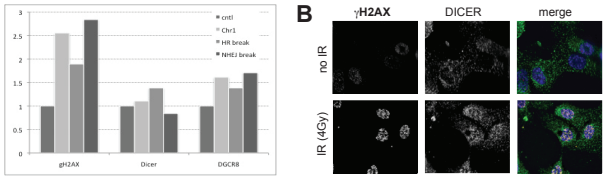

A Chromatin Immunoprecipitation gH2AX, DICER and DGCR8 indicates localization of these proteins at the site of a number of double strand breaks. **B** Immunofluorescence of U2OS cells showing nuclear relocalisation of DICER after IR.

3. Generation and validation of samples for smallRNAseq

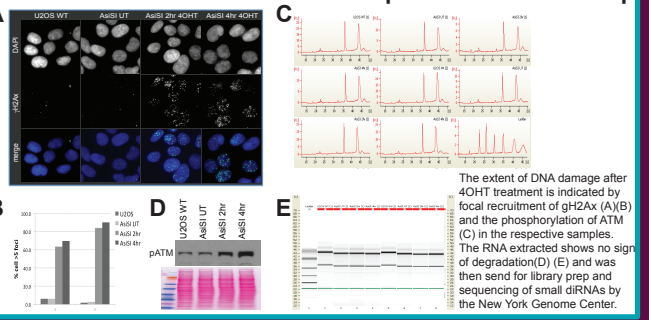

The extent of DNA damage after 4OHT treatment is indicated by focal recruitment of gH2Ax (A)(B) and the phosphorylation of ATM (C) in the respective samples. The RNA extracted shows no sign of degradation(D) (E) and was then send for library prep and sequencing of small diRNAs by the New York Genome Center.

4. detection of primary ncRNA transcript at DNA double strand breaks

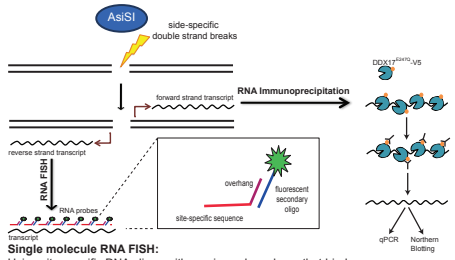

Single molecule RNA FISH:
Using site-specific DNA oligos with a universal overhang that binds to a universal fluorescently labelled secondary oligo allows detection of single RNA molecules *in vitro*.
(with Edouard Bertrand, CNRS, Montpellier, France.)

RNA immunoprecipitation:
The DEAD-box RNA helicase DDX17 is involved in primary RNA processing a mutation at glutamate 247 to glutamine results in the loss of ATP hydrolytic activity thus preventing the release the RNA by DDX17, which would be expected to prevent further processing of the primaryRNA transcript. Using a V5-tag, the protein is then immunoprecipitated with the bound RNA. The RNA is then analysed by both RT-PCR followed by qPCR as well as Northern blotting to estimate the sizes of the transcripts.

5. Model and Future Work

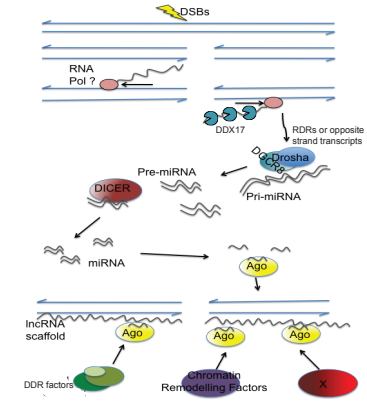

Key Questions:
1. **Which RNA polymerase is involved?**
2. **Do diRNA processing proteins localize to DSBs**
3. **Which Argonaute proteins are involved?**
4. **What factors are recruited by Argonaute proteins?**

6. References and Acknowledgments

1. **Suzuki *et al.* , Modulation of miRNA processing by P53 (2009), Nature, Vol.460, p529**
2. **Wei *et al.* , A role for Small RNAs in DNA Double-Strand Break Repair (2012), Cell, Vol. 149, p. 101-112**
3. **Francia *et al.* , Site-specific DICER and DROSHA RNA products control the DNA-damage response (2012), Nature, Vol. 488, p231-235**

We thank Gaelle Legube for kindly providing her AsiSI-U2OS cell line.
This work was supported by a Science Fundation Ireland Principal Investigator Award to NFL, a College of Science Scholarship and a Thomas Crawford-Hayes Fund awarded to JL.

The roles of RNA metabolism proteins and ncRNA in the DNA damage response

J. Luessing, N. Tsanov, N. F. Lowndes

Genome Stability Laboratory - Centre for Chromosome Biology,
School of Natural Sciences, National University of Ireland, Galway

NUI Galway OÉ Gaillimh

Centre for Chromosome Biology

NDP NATIONAL DEVELOPMENT PLAN

EUROPEAN UNION STRUCTURAL FUNDS

sfi science foundation ireland fondúireacht eolaíochta éireann

Key points:

Emerging roles for RNA in the DNA damage response
High number of RNA metabolism proteins in the recently carried out SILAC screen
DGCR8 and DDX3X are involved in DNA double-strand break repair
DGCR8 interacts with the C-terminal of ATM and has a Drosha independent role in the DDR
DDX3X, a novel ATM interactor is involved in homologous recombination

Involvement of DGCR8 in the DNA damage response

IR sensitivity | PARP inhibitor sensitivity | proficient G2/M checkpoint

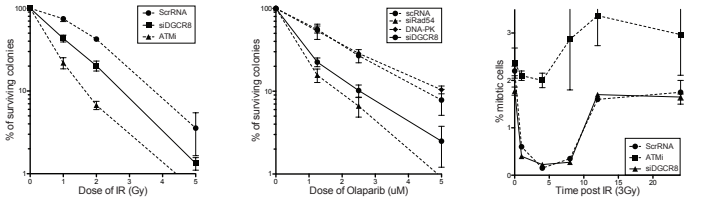

DGCR8 depletion results in sensitivity to IR and Olaparib, however cells exibit proficient G2/M checkpoint entry and recovery, suggesting efficient signalling and repair.

small RNA-seq

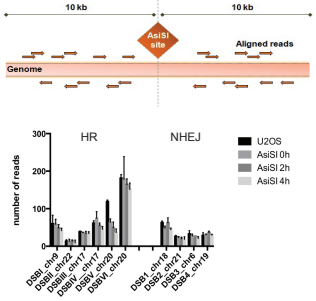

Future Directions:
- Filter out miRNAs and tRNAs using databases
- Analyse reads based on length distribution (diRNA vs miRNA)
- Perform an alignment to an artificial genome comprising 100 AsiSI sites
- Avoid aligning to repetitive elements in the genome

DGCR8 is required for accurate focal recruitment and HR repair

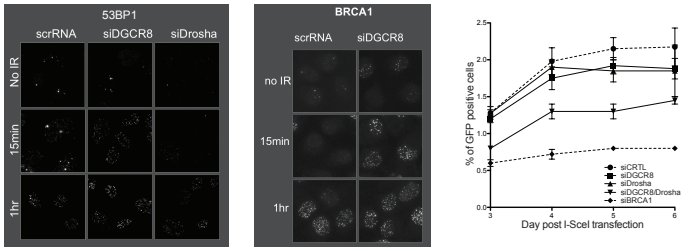

DGCR8 depleted cells show more rapid recruitment of DDR factors to IRIFs. They exhibit minor defects in HR, however when depleted in both DGCR8 and Drosha, cells have defective GC.

Future Directions

- Analyse the role of DGCR8 in other DSB repair pathways (NHEJ, SSA)
- Map ATM-interacting region of DGCR8 and characterise the function of non-interacting mutants of DGCR8
- Drosha-independent roles of DGCR8:
  - Characterise the function of DGCR8 mutant not interacting with Drosha
  - Is DGCR8 found in complexes without Drosha after DNA damage?

DDX3X is a new player in the DDR

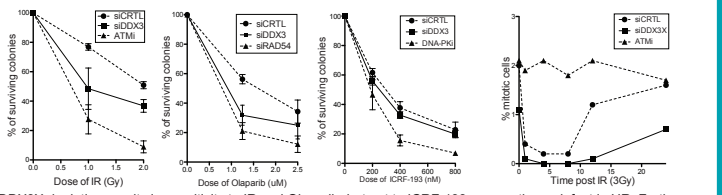

DDX3X depletion results in sensitivity to IR and Olaparib, but not to ICRF-193, suggesting a defect in HR. Furthermore, cells show a defect in checkpoint recovery, suggesting a defect in repair.

DDX3X is required for efficient recruitment of BRCA1 and RAD51

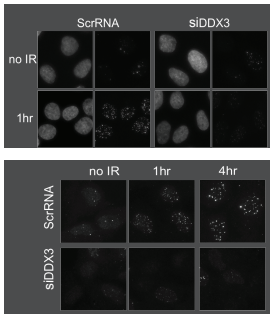

DDX3X depletion results in a defect in BRCA1 and RAD51 focal recruitment to IRIF.

DDX3X is involved in HR repair

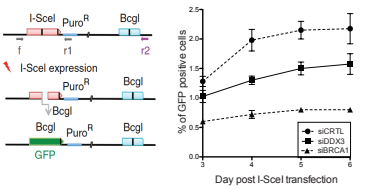

Depletion of DDX3X results in defective HR.

Future Directions

- Analyse the role of DDX3X in other DSB repair pathways (NHEJ, SSA)
- Functional characterisation of helicase-dead DDX3X mutant
- Map DDX3X interacting region of ATM
- Is DDX3X an ATM substrate?

References:

Ohle et al. (2016) *Cell*
Francia et al. (2012/2016) *Nature / J.Cell Sci.*
Iacovoni et a. (2010) *EMBO*

A role for the p53 tumour suppressor in regulating the balance between homologous recombination and non-homologous end joining

S. Moureau†, J. Luessing†, E. C. Harte, M. Voisin and N.F. Lowndes

Centre for Chromosome Biology
NUI Galway OÉ Gaillimh
NDP NATIONAL DEVELOPMENT PLAN
EUROPEAN UNION STRUCTURAL FUNDS
sfi science foundation ireland fondúireacht eolaíochta éireann

Abstract

Loss of p53, a transcription factor activated by cellular stress, is a frequent event in cancer. The role of p53 in tumour suppression is largely attributed to cell fate decisions. Here, we provide evidence supporting a novel role for p53 in the regulation of DNA double-strand break (DSB) repair pathway choice. 53BP1, another tumour suppressor, was initially identified as p53 Binding Protein 1, and has been shown to inhibit DNA end resection, thereby stimulating non-homologous end joining (NHEJ). Yet another tumour suppressor, BRCA1, reciprocally promotes end resection and homologous recombination (HR). Here, we show that in both human and mouse cells, the absence of p53 results in impaired 53BP1 focal recruitment to sites of DNA damage induced by ionizing radiation. This effect is largely independent of cell cycle phase and the extent of DNA damage. In p53-deficient cells, diminished localization of 53BP1 is accompanied by a reciprocal increase in BRCA1 recruitment to DSBs. Consistent with these findings, we demonstrate that DSB repair via NHEJ is abrogated, while repair via homology-directed repair (HDR) is stimulated. Overall, we propose that in addition to its role as an 'effector' protein in the DNA damage response, p53 plays a role in the regulation of DSB repair pathway choice.

Efficient recruitment of 53BP1 into ionizing radiation-induced foci requires p53

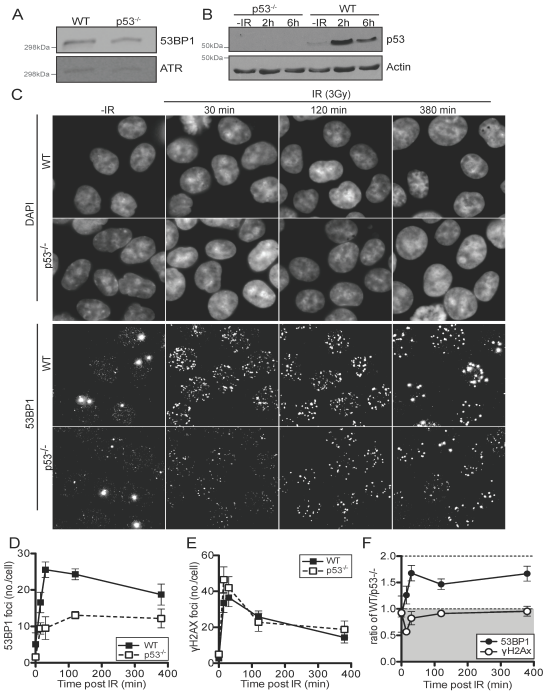

Figure 1. p53 promotes 53BP1 recruitment to DNA damage sites in human HCT116 cells. (a) 53BP1 protein levels in whole cell extracts prepared from either WT or p53-null HCT116 cells were analysed by western blotting. (b) p53 protein level in whole cell extracts from WT and p53-null HCT116 cells either before or after IR exposure (3 Gy) were analysed by western blotting. (c) Detection of endogenous 53BP1 by immunofluorescence in WT and p53-null HCT116 cells. Cells were either mock treated or irradiated with 3 Gy and allowed to recover for the indicated times before being fixed, stained with 53BP1 antibody and visualized on a Deltavision microscope. Note that large bright foci in unirradiated cells are 53BP1 nuclear bodies. (d) Quantification of the number of 53BP1 foci. (e) Quantification of the number of gH2AX foci. (f) Ratio of 53BP1 and gH2AX focal intensity in WT cells relative to p53-null HCT116 cells.

p53 regulates 53BP1 IRIF formation in a cell cycle-dependent manner

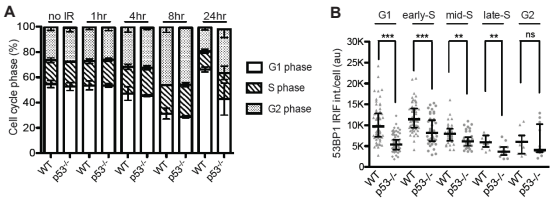

Figure 3. Quantification of the proportion of HCT116 WT and p53-null cells in each phase of the cell cycle before and after IR at the indicated times. (b) Quantification of endogenous 53BP1 and classification with respect to cell cycle phase for each cell type analysed. S phase cells are PCNA positive, G2 phase cells are ZWINT positive, while G1 phase cells are negative for both PCNA and ZWINT.

†These authors contributed equally to this study.
Full article is available online at http://dx.doi.org/10.1098/rsob.160225
Author for correspondence: N. F. Lowndes e-mail: noel.lowndes@nuigalway.ie

BRCA1 and RAD51 recruitment to DSBs is restrained by p53

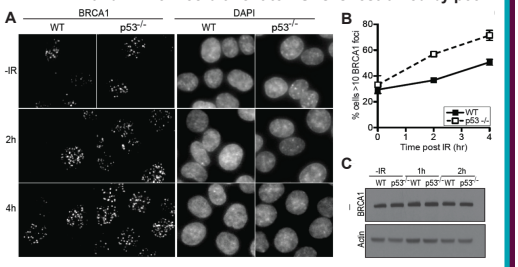

Figure 2. (a) Localization of endogenous BRCA1 by immunofluorescence in HCT116 WT and p53-null cells before and after IR (3 Gy). (b) Quantification of the proportion of cells with more than 10 BRCA1 foci per cell. (c) Western blot analysis of BRCA1 protein levels in WT and p53-null HCT116 cells at the indicated time points after IR (3 Gy).

p53 restrains DNA double-strand break repair via homologous recombination while promoting non-homologous end joining

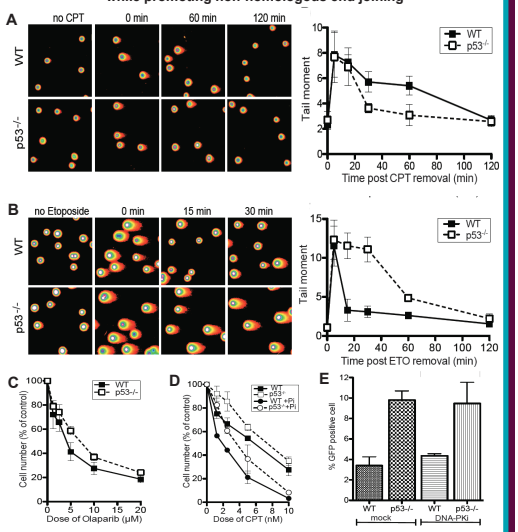

Figure 4. (a) neutral comet assay for WT and p53-null HCT116 cells after release from a 1hr camptothecin (CPT) treatment for the indicated times. (b) neutral comet assay for WT and p53-null HCT116 cells after release from a 1hr etoposide (ETO) treatment for the indicated times. (c) Proliferation of WT and p53-null HCT116 cells in the presence of Olaparib, an inhibitor of PARP. (d) Proliferation of WT and p53-null HCT116 cells in the presence of CPT. Cells were grown in the presence of absence of 1 uM Olaparib, as indicated. (e) Modified GFP reporter assay for HR of HCT116 WT and p53-null cells.

Conclusion and Future Directions:

Discovered over 35 years ago and regarded as a 'guardian of the genome', p53 is one of the most studied yet functionally complex proteins in biochemistry. With respect to its roles in the DDR, these are largely as 'effectors' of transient cell cycle delays and cellular fate. Our results highlight a new role for p53 in 'mediating' early events of the DDR important for regulating the balance between DSB repair pathways. The mechanism remains to be uncovered and more in depth questions will need to be answered in the future. How does p53 affect the recruitment of 53BP1 to DSBs? Is p53 involved in C-NHEJ or SSA, and do mutations in the TP53 gene lead to error-prone repair and thus genomic instability? Is p53 specifically interacting with a subset of 53BP1 in response to DNA damage? Does a subset of p53 relocate to DSBs in response to DSBs?

Appendix III: Antibody conditions

Table III.3: List of primary antibodies used for Western Blotting

Antibody	Dilution	Blocking	Species	Manufacturer	Cat.No.
Actin	1:5000	5%milk	rabbit	Sigma	A2066
ATM	1:2500	5%milk	goat	Bethyl	A300136A
ATM	1:1000	5%milk	rabbit	Abcam	ab17995
pATM(S1981)	1:1000	5%BSA	rabbit	R&D	AF1655
53BP1	1:5000	5%milk	rabbit	Bethyl	A300-272A
BRCA1(D9)	1:500	5%BSA	mouse	Santa Cruz	sc-6954
pBRCA1(S1423)	1:1000	5%BSA	rabbit	Bethyl	A300-008A
Chk1(G-4)	1:1000	5%milk	mouse	Santa Cruz	sc-8408
pChk1(S145)	1:1000	5%BSA	rabbit	Cell Signalling	2344
Chk2 (H300)	1:1000	5%milk	mouse	Santa Cruz	sc-9064
pChk2(T68)	1:1000	5%BSA	rabbit	Cell Signalling	2661
CSB	1:1000	5%milk	rabbit	Genetex	GTX104589
DDX3	1:5000	5%milk	rabbit	Bethyl	A300-474A
DDX5	1:5000	5%milk	rabbit	Bethyl	A300-523A
DDX17	1:1000	5%milk	rabbit	abcam	ab180190
DDX17	1:2500	5%milk	rabbit	Bethyl	A300-509A
DGCR8	1:5000	5%milk	rabbit	Bethyl	A203-468A
Drosha	1:1000	5%milk	rabbit	Abcam	ab12286
Dicer	1:1000	5%milk	mouse	Abcam	ab14601
γH2AX	1:5000	5%BSA	mouse	Millipore	05-636
H3	1:40000	5%milk	rabbit	abcam	ab1791

p21	1:1000	5%milk	rabbit	abcam	ab7960
p53	1:5000	5%milk	mouse	Santa Cruz	sc126
RAD51	1:2000	5%milk	rabbit	Calbiochem	PC130
RAD54	1:1000	5%milk	rabbit	abcam	10705
XPB	1:1000	5%milk	rabbit	Genetex	GTX105357
XPD	1:1000	5%milk	rabbit	Genetex	GTX112923
XRCC4	1:1000	5%milk	rabbit	abcam	ab145
V5 epitope	1:5000	5%milk	mouse	BioRad	MCA1360

Table III.4: List of primary antibodies used for Immunofluorescence

Antibody	Dilution	Species	Manufacturer	Cat.No.
53BP1	1:500	rb	Novus	NB100-304
pATM	1:500	ms	Millipore	MAB3806
BRCA1	1:400	ms	Santa Cruz	sc-6954
γH2AX	1:200	ms	Millipore	05-636
RAD51	1:500	rb	Calbiochem	PC130

Table III.5: List of antibodies used for Flow Cytometry

Antibody	Dilution	Species	Manufacturer	Cat.No.
pH3(S10)	1:50	rabbit	Millipore	06-570
BRDU	1:50	mouse	BD	347580

Table III.6: List of secondary antibodies

Antibody	Dilution	Conjugate	Manufacturer	Cat.No.
ProteinA-HRP	1:1000	HRP	Upstate	18-160
Mouse IgG H+L	1:500	DyLight®550	Bethyl	A90-516D3
Rabbit IgG H+L	1:500	DyLight®650	Bethyl	A120-201D5
Rabbit IgG	1:200	FITC	Bethyl	A120-201F
Goat-anti rabbit IgG	1:5000	HRP	Thermo Scientific	31460
Mouse IgG	1:5000	HRP	Thermo Scientific	31450

Appendix IV: Protocols

siRNA transfection

1. Plate 1-1.5x10^5cells/35mm dish depending on cell type. (Double for 60mm dish)
2. Grow for 24hrs at 37C and 5%CO2.
3. Transfect cells with control and target siRNA as follows:
   - Tube 1: 6μl Oligofectamine
     14μl Optimem
   - Tube 2: 2ul (40nmol) siRNA
     178μl Optimem
4. Combine siRNA mix with Oligofectamine mix and incubate for 20min at RT
5. Wash cells with 1xPBS and add 800μl Optimem.
6. Add siRNA mix to the cells and incubate for 3hrs at 37C and 5%CO2.
7. Add 500μl 3xDMEM (3xDMEM-F12 for RPE-1 cells)
8. Grow for 24hrs and then add 1ml DMEM to cell transfected cells.
9. Incubate a further 24hrs before treatment and/or harvesting.

Reagents:

- Optimem (Gibco)
- Oligofectamine (Invitrogen)
- Target and control siRNA
- 3XDMEM
  - 8ml DMEM (DMEM-F12 for RPE-1 cells)
  - 2ml FBS
  - 0.2ml L-Glutamine
- Cell culture media
- 1xPBS (sterile)

Calcium Phosphate transfection

Note: this method of transfection is very efficient for HEK293 and HEK293T cells, however less efficient than Lipofectamine for other cell type, i.e. U2OS or RPE-1.

1. Plate $2x10^6$ cells on a 10cm dish 24 hours prior to transfection.
2. Grow for 24hrs at 37ºC and 5%CO_2.
3. Prepare the transfection mix as follows:
   - Thaw the 2xHBS at room temperature (do not thaw and refreeze)
   - Add 500µl 2xHBS into a 1.5ml tube (per 10cm dish).
   - Dilute 10ug pDNA (that depends on your plasmid) in 61µl 2M $CaCl_2$.
   - Then fill up to 500µl final volume with TE buffer (pH8) or sterile milliQ H_2O.
4. Slowly add the pDNA mix to the 2xHBS. (Mix by pipetting gently up and down, you should see the solution is getting cloudy.)
5. Add the mix directly to the cells dropwise and evenly into the media. Try to cover all cells in the dish. (Do not swirl the dish, as this might disrupt the complexes.)
6. Incubate with the transfection mix for 16-18hrs in the incubator. (A precipitation will form a layer on top of the cells, which looks a bit like contamination.)
7. Then remove the media and wash the cells very gently twice with PBS. (Make sure to add the PBS to the side of the dish, as HEK293 cells are very loosely attached to the dish and might wash off easily.)
8. Then add 10ml new media to the cells and grow for 48hrs at 37ºC and 5% CO_2.
9. Harvest cells by scraping.

Buffers and Solutions:

2xHBS:
- 0.27M NaCl
- 1.5mM $NaHPO_4*7H_2O$
- 55mM HEPES

Bring up to pH7, and store in 500µl aliquots at -20ºC for up to 6 months.

Stable cell lines

1. Plate cells in medium w/o PenStrep on 10cm dish to be 80-90% confluent the next day.
2. Linearise the plasmid of interest (digest for 3-5hrs and check on an agarose gel, if necessary, gel purify the band, upon complete digest PCR purify)
3. Transfect the cell using Lipofectamine 2000 (Invitrogen) as follows (ratios of Lipofectamine to pDNA might need to be optimised for different plasmids and cell lines, but this is a good starting point):
   - Prepare two tubes:
     - Tube 1: 6µl Lipofectamine
       50µl Optimem
     - Tube 2: 3ug pDNA
       50µl Optimem
     - Incubate tube 1 for 5min at RT
     - Mix content of the tubes together
     - Incubate for 20min at RT
     - Add DNA:lipid mix to the 10cm dish
4. Incubate for 24hr at 37°C and 5% CO2
5. Trypsinise cells using 2ml Trypsin
6. Resuspend cells in 8ml media
7. Transfer 2ml of the cells into a new 10cm dish containing 6ml media
8. Repeat dilution 3 times more (4 dilutions)
9. Grow cells for 24hrs at 37ºC and 5%CO2
10. Remove media and add fresh media containing the selection marker (e.g. puromycin or G418) at the appropriate concentration
11. Grow cells until colonies are visible (colonies should cover a microscope field at 10x magnification)
12. Change media every 3 to 4 days (to keep the cells under selection)
13. After 10-14 days (depending on the size of the colonies), pick colonies using cloning disks.
    - Remove media from cells and wash with PBS

- Soak cloning disks in Trypsin (handle disks with IMS sterilized tweezers)
- Carefully place the disk onto a marked colony (make sure colonies are clearly separated to avoid mixed clones)
- Incubate with cloning disks for 3-5min in the incubator
- Carefully transfer the cloning disk with the cells into a 24-well plate containing 1ml media/well.

14. Grow cells under selection until confluent then transfer into a 6-well dish.
15. Once confluent, trypsinise cells with 0.5ml Trypsin and resuspend in 4.5ml media.
16. Add 1ml cells into two wells of a 6-well plate and pellet the rest at 1200rpm for 5min (the pellet can be used for primary screening by Western or PCR, positive clones can then be cultured and/or frozen down, while negative clones can be discarded straight away).
17. For positive clones, freeze the cells of one well down (300µl Freezing media), and harvest the corresponding well for Western Blotting (*see Protein extraction and Western Blotting Protocol*) and/or PCR and sequencing (*see genomic DNA extraction protocol* or alternatively use gDNA extraction kit from Eurogenentec).

Buffers:

Freezing media:

90% FBS
10% DMSO

CRISPR/Cas9 gene editing

Oligo annealing and cloning:

1. Digest 4ug of pX330 with *Bbs* I.
2. Incubate for 3hrs at 37C. Run 2µl of the digest on a 1% Agarose gel (TAE) and check the digest. If the digest is complete, use a PCR clean-up kit, otherwise run a 0.7% Agarose gel and extract the band from the gel using a gel extraction kit. Elute in 30µl Elution buffer.
3. To anneal the oligos use 25µl of the forward primer and 25µl of the reverse primer. (Both primers are at 100uM concentration).
4. Incubate for 5min at 95ºC and turn off the heatblock to let the samples cool down slowly and anneal in the heatblock. (This step could take a couple of hours, but the next step can be started once the heatblock is cooled down to around 28ºC.
5. Prepare the following mix to phosphorylate the oligos:
    - 5µl 10X Ligation buffer
    - 2µl T4 PNK
    - 5µl annealed oligos
    - 38µl ddH20

Note: It is important to use the T4 ligation buffer and not the PNK buffer for this step, as the PNK buffer will interfere with subsequent steps.

6. Incubate the annealed oligos for 30min at 37ºC, then boil for 5min at 95ºC to inactivate the PNK.
7. Re-anneal the oligos by allowing the mixture to cool down slowly in the heatblock.
8. Set up a ligation mix as follows:
    1. 50ng purified vector (pX330)
    2. 1µl 1/200 diluted annealed oligos
    3. 2µl 10x T4 DNA Ligase Buffer
    4. 1µl T4 DNA Ligase
    5. ddH2O up to 20µl
9. Incubate at RT for at least 45min. (Longer incubation up to 3hrs or overnight at 4ºC works too, but are not necessary.)

Transformation and sequencing:

10. Add 5µl of ligation mix to 50µl competent TOP10 *E.coli* and incubate for 30min on ice.
11. Heat-shock the bacteria for 1min at 42ºC and add 250µl LB broth.
12. Incubate the transformed bacteria for 1hr at 37ºC.
13. Plate transformed bacteria on LB agar containing 50ug/ml Ampicillin.
14. Incubate overnight at 37ºC.
15. Pick a single colony and inoculate into 3ml of LB broth containing 50ug/ml Ampicillin. Grow the bacteria on the shaker at 37ºC for 6-8hrs or overnight.
16. Miniprep the plasmids according to the manufacturers protocol and elute in 40µl Elution Buffer.
17. Digest 0.5-1ug of the plasmid with *Bbs*I to check if the guideRNA is successfully cloned in. (If the plasmid is not digested, the guide RNA is cloned in, as insertion of the oligo removes the two restriction sites.
18. Send 15µl pDNA of the positive clones together with 2µl 10uM sequencing primer for sequencing. The sequencing primer has the following sequence: GGCCTATTTCCCATGATTCC.

Transfection and Stable cell lines:

19. Transfect a 70-80% confluent dish as follows:
    1. prepare two tubes:
        i. tube 1:
            1. 10µl Lipofectamine
            2. 40µl Optimem
        ii. tube 2:
            1. 10ug pX330 pDNA (one or more guideRNAs)
            2. 1ug pLOX-puro
            3. up to 50µl Optimem

Note: You can transfect multiple guideRNAs at the same time, as well as a homology template (for insertions) as long as the ratio of guideRNA to the resistance plasmid is at least 5:1.

20. Incubate tube 1 for 5min at RT then add to the second tube and incubate for 20min at RT.
21. Add the DNA:lipid mix to the 10cm dish and incubate for 24hrs at 37ºC and 5% CO_2.
22. Trypsinize the cells in 1ml Trypsin and resuspend in 7ml medium supplemented with puromycin to obtain a final volume of 8ml.
23. Add 2ml of the cells to 6ml media supplemented with puromycin on a 10cm dish (1^{st} dilution) and freeze down the rest of the cells.
24. Add 2ml of the 1^{st} dilution to 6ml media supplemented with puromycin on a 10cm dish (2^{nd} dilution).
25. Add 2ml of the 2^{nd} dilution to 6ml media supplemented with puromycin on a 10cm dish (3^{rd} dilution).
26. Add 2ml of the 3^{rd} dilution to 6ml media supplemented with puromycin on a 10cm dish (4^{th} dilution).
27. Add 2ml of the 4^{th} dilution to 6ml media supplemented with puromycin on a 10cm dish (5^{th} dilution).

Note: The concentration of the puromycin depends on the cell line, i.e. for U2OS and HCT116 cells use 1ug/ml puromycin, for RPE1 cells use 4ug/ml puromycin. If you are unsure of what concentration you need for your cell line, do a kill curve (see *Kill curve* protocol).

28. Grow the cells under puromycin selection for 48hrs, then remove the media, wash the cell with PBS and add 10ml fresh drug-free media.
29. Grow cells until single colonies appear. This usually takes 10 to 14 days, depending on your cell line. The colonies are grown enough to be selected once they cover the area of the 10x lens of the microscope.
30. Transfer single colonies into a 48-well plate with 1ml medium using cloning discs. (Remove the media, rinse cells in PBS and place the cloning disc, soaked in trypsin, directly onto the colony. After 5min at 37ºC, transfer the cloning disk containing the cells to the 24-well plate.)
31. Expand the cells until they are confluent in two wells of a 6-well dish.

Screening and verification of clones:

32. Freeze down one well of cells and harvest the other well for Western Blotting and gDNA extraction as follows:
33. Trypsinize cells in 0.5ml Trypsin and resuspend in 1.5ml media. Then split the cells into 2 microfuge tubes. Spin the cells down, wash once with PBS and store the pellets at -80ºC until further use. (See *Protein extraction* and *gDNA extraction* protocols.)
34. Pre-screen the clones by Western Blotting.
35. Extract DNA from all positive clones and amplify a region around 600kb around your guide RNAs (300bp either side).
36. Clone the PCR fragment into pGEMT easy (to be able to sequence each allele individually) and send for sequencing. (As a sequencing primer, use the forward or reverse primer, which you amplified the DNA fragment with.)
37. Wake up all positive clones and grow up into 2 wells of a 6-well plate. Freeze one plate down and add puromycin to the other dish. Cells should die, when growing in puromycin, otherwise the plasmid as integrated and could have off-target effects.

Protein Extraction and Western Blotting

Cell lysis

1. Wash cells with 1ml 1xPBS and pellet at 1200rpm for 2min
2. Remove PBS
3. Resuspend cells in 500µl (10cm dish) or 50µl (35mm dish) Lysis Buffer containing 0.25 units/µl (1/1000 dilution) and 1mM $MgCl_2$.
4. Incubate lysate on ice for 45min (flick the tube gently every 10min to ensure even lysis).
5. Centrifuge lysate for 15min at 14,000rpm at 4ºC.
6. Transfer supernatant into a new 1.5ml Eppendorf tube.
7. Add 1µl lysate to 1ml milliQ H2O and then add 500µl Bradford Reagent.
8. Invert tube and incubate for 5min at RT.
9. Measure absorbance at 595nm to determine protein concentration.
10. Load 20-50ug TCE onto a polyacrylamide gel.

Western Blotting

1. Prepare denaturing gel:
    - Wash glass plates with 100%EtOH and wipe dry.
    - Pour the polyacrylamide mix (5ml for small and 20ml for big gels).
    - Add 1ml 100% Isopropanol on top of the running gel to prevent it drying out.
    - Leave the gel to set for 15-20min (until the remaining mix sets in the falcon tube).
    - Remove the Isopropanol, add the stacking gel and insert the comb (be careful when inserting the comb, as some of the stacking gel can squirt out).
    - Leave to set for 15-20min (until the remaining gel is set in the Falcon tube).
    - Assemble the gel in the running apparatus and fill with 1xRunning Buffer before removing the comb.
    - Flush the wells to ensure that no stacking gel is left in them.

2. Mix samples with 4xLaemmli Buffer containing 10%β-mercapto-ethanol (make sure to have a minimum volume of 20µl in the tube).
3. Boil samples for 5min at 95ºC.
4. Then load appropriate volume corresponding to 20-50ng TCE onto the polyacryamide gel.
5. Run the gel at 100V until samples have migrated into the running gel, then turn up to 120-150V (this depends on the acrylamide concentration, i.e. 6% gels should not be run higher than 120V, while 10% or higher can be run at 150V).
6. Run the gel until the blue loading dye has run out of the gel (further running will not increase separation!).
7. Submerge 3 sheets of whatman paper (cut to size) in cold transfer buffer and lay a sheet of Nitrocellulose membrane on top (cut to size).
8. Than add the polyacrylamide gel followed by another three sheets of Whatman paper.
9. Remove all bubbles and remove from the transfer buffer.
10. Add one sponge either side of the Whatman paper and insert into the transfer apparatus (make sure the membrane is on the positive and the gel on the negative side!).
11. Run the gel in ice-cold transfer buffer on ice (or in the coldroom) for 1hr at 100V.
12. Add ponceau onto the membrane to see whether the transfer was ok and the proteins are evenly loaded.
13. Remove the excess ponceau with ddH2O to visualize the protein bands (scan the membrane for your records).
14. Submerge the membrane in 1xTBST (TBS+0.1%Tween) and rock until the ponceau is washed off.
15. Block the membrane with 5%milk in TBST (unless otherwise stated) for 10min at RT on the rotator.
16. Transfer membrane into a 50ml Falcon containing the 1º antibody at the appropriate concentration and condition.
17. Incubate with 1ºantibody overnight at 4ºC.

18. Wash the membrane briefly in TBST before adding the corresponding 2ºantibody (1/5000 dilution in 5%milk in TBST) for 1hr at RT on the rotator.
19. Rinse the membrane in TBST to remove the excess 2º antibody, then wash for 10-15min in TBST on the rotator.
20. Remove excess TBST and add 1-3ml ECL onto the membrane (make sure the entire membrane is covered).
21. Incubate for 2min at RT then remove the excess ECL.
22. Insert the membrane into a polypocket and seal the edges with tape in a development cassette.
23. Expose to X-ray film (the length of exposure depends on the abundance of you protein and the strength of your antibody) in the darkroom from 10s to 20min (ECL wears off after 20min).
24. Visualise the bands using the developer.

Buffers:

Lysis Buffer:

150mM NaCl
0.5% NP-40
50mM Tris-HCl pH7.5
10% Glycerol
Protease & Phosphatase Inhibitors

Laemmli Buffer (4x):

250mM Tris-HCl pH6.8
8% SDS
30% Glycerol
0.02% Bromophenol Blue

Running Buffer:

1xTG
1% SDS

Transfer Buffer:

1xTG
20% MeOH
0.2% SDS

Ponceau:

5% Acetic Acid
0.5% Ponceau

TBST:

100mM Trizma Base
150mM NaCl
0.1% Tween-20

gDNA extraction

1. Pellet cells at 1200rpm for 5min at 4ºC. (1/10th of a 10cm dish or half of 60mm dish are enough cells to extract sufficient DNA. Using more cells results in less efficient DNA recovery and effects DNA quality.)
2. Wash cells in 1ml PBS.
3. Resuspend cells in 500µl TAIL buffer containing 60ug/ml Proteinase K. (The Proteinase K should be added in fresh, but the TAIL buffer is stable at room temperature.)
4. Incubate the resuspended cells at 37ºC overnight. (Alternatively, cells can be lysed for 3hrs at 55ºC, but overnight incubation improves DNA quality.)
5. Shake lysates vigorously for 2min.
6. Add 240µl 5M NaCl and shake vigorously for a further 2min.
7. Centrifuge lysates for 30min at 10ºC at 14,000rpm. (Lysates can also be spun down at RT temperature, however lower temperature facilitate precipitation of debris and thus result in higher quality DNA.)
8. Transfer the supernatant (containing the genomic DNA) into a new microfuge tube.
9. Add 700µl 100% Isopropanol (An upper cloudy layer will form after Isopropanol addition.) and invert the tubes 4-6 times. (You shoµld now be able to see the DNA in the tube.)
10. Pellet the DNA for 10min at 4ºC at 14,000rpm. (If possible, avoid a swing-out rotor centrifuge, as this will make it harder to see the DNA pellet at the bottom of the tube.)
11. Remove the supernatant and wash the pellet twice with 500µl 70% EtOH. (spin down the pellet at 14,000rpm for 2min at RT after each wash.)
12. Remove as much EtOH as possible and air-dry the DNA pellet.
13. Resuspend the purified DNA in 50µl TE buffer/milliQ H_2O containing 0.16mg/ml RNase A. (RNase A should be added in fresh.)
14. To facilitate resuspension of DNA, incubate the tubes for 15min at 37ºC with shaking.

15. Store the genomic DNA at -20ºC until further use. (Purified DNA can be stored long-term at -20ºC.)

Buffers

TAIL Buffer:

50mM Tris-HCl, pH8.8

100mM EDTA, pH8.0

100mM NaCl

1% SDS

Cell cycle analysis

1. Plate cells at $2x10^5$ cells/35mm dish 24hrs before harvesting (for siRNA transfection prior to the G2/M checkpoint assay, follow the siRNA transfection protocol).
   - Plate one dish per timepoint, (usually 0hr, 1hr, 4hr, 8hr, 12hr, 24hr) for each of your conditions.
2. Add 25uM BrdU to each dish (this is dependent on the cell line, but in general 25uM works well for most human and mouse adherent cell lines).
3. Incubate the cells in the incubator for 45min to incorporate the BrdU.
4. Remove the BrdU, wash cells three times with PBS and add fresh media (2ml media/35mm dish).
5. Immediately irradiate all samples (except the 0hr, i.e. untreated, this should be harvested directly, without prior removal of BrdU) at 3Gy then grow the cells for the indicated time.

Harvesting:

6. At the indicated times, remove the media, wash with PBS, add 0.5ml Trypsin to the cells and leave in the incubator for 2-4min.
7. Resuspend the cells with 4.5ml media and transfer to the 15ml Falcon.
8. Pellet the cells at 1200rpm for 5min.
9. Remove the supernatant and wash the cells in 1ml PBS.
10. Split the cells into two 500µl aliquots.
11. Pellet and remove the PBS.
12. Freeze one half of the sample at -80ºC for Western Blot analysis (*see Protein extraction and Western Blotting Protocol*, this is particularly important when using siRNA!*)*.
13. Resuspend the other half of the cells in 1ml cold PBS and transfer into a 15ml Falcon containing 3ml ice-cold 100%EtOH while vortexing. This gives a final concentration of 75%EtOH (prepare the Falcon tube with EtOH in advance and cool in the -20ºC freezer for at least 20min.

The vortexing ensures that the cells do not clump when being fixed, which could block the FACS.)

14. Store the fixed cells at -20ºC. (You can store them for up to two months once they are fixed.)

Antibody staining:

15. Add 3ml PBS to the samples and pellet the cells at 1200rpm for 5min.
16. Remove supernatant and transfer cells in 1ml PBS into a new 1.5ml mircofuge tube (do not you low adherent tube, as the cell will stick to the side of the tube.) Alternatively, resuspend the cells in 200µl PBS and transfer to a round-bottom 96-well plate, and then use 200µl volume for all washes and an extra wash step each time and pellet cells at 1200rpm.
17. Pellet the cells at 2000rpm for 2min at 4ºC (It is best to use a swing-out rotor for this to ensure that all the cells are at the bottom.
18. Remove the PBS.
19. Resuspend the cells in 250µl PBS.
20. Add 250µl 12.5% HCl and briefly vortex.
21. Incubate the cells for 15min at RT to denature the DNA. (This step is very important to enable the anti-BrdU antibody to access the incorporated BrdU.)
22. Pellet the cells at 1200rpm for 5min and remove the supernatant.
23. Wash the cells once in PBS and once in PBT.
24. Resuspend the cells in 50µl PBT containing 1µl anti-BrdU antibody (BD Biosciences).
25. Incubate with the 1º antibody for 1hr at RT.
26. Wash the cells three times in 1ml PBS.
27. Resuspend the cells in 50µl PBT containing 1µl anti-mouse FITC 2º antibody.
28. Incubate in the dark at RT for 1hr.
29. Wash cells twice with PBS.
30. Resuspend the cells in 300µl PBS containing 40ug/ml Propidium Iodide and 250ug/ml RNase A and filter them through a 0.3micron

filter into a FACS tube. (This is important to prevent blockage on the FACS)

31. Incubate the cells for 30-60 min in the dark on ice (This incubation can be used to set up the FACS).

FACS analysis:

32. For the FACS analysis you will also need a no stain control (just fixed cells), a no PI control (just fixed cells stained with BrdU antibody and the FITC 2ºantibody) and a no FITC control (just fixed cells with PI). This is required for compensate for overlapping of the PI with FITC and vice versa.
33. Draw the following plots on the BD-FACS Diva Software:
    - Scatter plot FSC vs. SSC (to see all events)
    - Scatter plot FSC-A vs. FSC-H (to exclude doublets)
    - Scatter plot PE-Cy7 (x-axis) vs. FITC (y-axis) (this show the different cell cycle stages)
    - Histogram of PE-Cy7 (to see cell cycle distribution)
    - Also create a statistics view to read of the percentage of cells in each cell cycle phase.

Note: FSC, SSC and PE-Cy7 channel should all be on a normal scale, while FITC should be on a log scale.

34. Run no stain control first, gate for single cell population (P1) on the FSC vs. SSC scatter plot (Note, voltage for both FSC and SSC will need to be adjusted depending on the cell type used).
35. Then gate out the doublets (FSC-A vs. FSC-H).
36. Next run the PI only control. Adjust the voltage for PE-Cy7, so that the G1 peak (1st peak) is at 100 and the G2 peak (2nd peak) is at 200. This ensures that you cells are single cells with a normal DNA content. Then adjust the FITC channel, so that all FITC negative cells fall just below 10^3.
37. The FITC only control should give a distinct population above $10^{3.}$

38. Use a quadrant gate with the horizontal axis just above 10^3 and the vertical axis at 150.
39. Run all sample through the FACS on low(!) throughput (this should be around 200-400 events per second) and collect a minimum of 20,000 to 30,000 cells per sample. Use SIT flush after each sample.
40. On the PE-Cy7 vs. FITC scatter plot, draw the following gates (use the untreated control for the gating):
    - G1 phase (lower left population)
    - G2 phase (lower right population)
    - S-phase (FITC positive population)
41. Mark these populations on the PE-Cy7 histogram. (This will show the cell cycle distribution.)
42. For the G1/S checkpoint assay, gate the FITC negative area between the G1 and G2 population (PE-Cy7 vs. FITC scatter plot). Cells entering S-phase after irradiation will be negative for BrdU.

Buffers and Solutions:

PBT (fresh):

1xPBS
0.5% BSA
0.1% Tween-20

G2/M checkpoint assay

1. Plate cells at $2x10^5$ cells/35mm dish 24hrs before harvesting (for siRNA transfection prior to the G2/M checkpoint assay, follow the siRNA transfection protocol).
   - Plate one dish per timepoint, (usually 0hr, 1hr, 4hr, 8hr, 12hr, 24hr) for each of your conditions.
2. Irradiate all samples at 3Gy (except the 0hr, i.e. untreated) then grow the cells for the indicated time.

Harvesting:

3. At the indicated times, transfer the media into a 15ml Falcon. (This ensures, that all mitotic cells will be in the pellet, as they are loosely attached and might come off when removing the media or washing the cells.)
4. Wash the cells with 1ml PBS (add the wash to the 15ml Falcon).
5. Add 0.5ml Trypsin to the cell and leave in the incubator for 2-4min.
6. Resuspend the cells with 4.5ml media and transfer to the 15ml Falcon.
7. Pellet the cells at 1200rpm for 5min.
8. Remove the supernatant and wash the cells in 1ml PBS.
9. Split the cells into two 500µl aliquots.
10. Pellet and remove the PBS.
11. Freeze one half of the sample at -80ºC for Western Blot analysis (*see Protein extraction and Western Blotting Protocol*, this is particularly important when using siRNA!*)*.
12. Resuspend the other half of cells in 1ml cold PBS and transfer into a 15ml Falcon containing 3ml ice-cold 100%EtOH while vortexing, this give a final concentration of 75%EtOH (prepare the Falcon tube with EtOH in advance and cool in the -20ºC freezer for at least 20min. The vortexing ensures that the cells do not clump when being fixed, which could block the FACS.)

13. Store the fixed cells at -20ºC. (You can store them for up to two months once they are fixed.)

Antibody staining:

14. Add 3ml PBS to the samples and pellet the cells at 1200rpm for 5min.
15. Remove supernatant and transfer cells in 1ml PBS into a new 1.5ml mircofuge tube (do not you low adherent tube, as the cell will stick to the side of the tube.) Alternatively, resuspend the cells in 200µl PBS and transfer to a round-bottom 96-well plate, and then use 200µl volume for all washes and an extra wash step each time and pellet cells at 1200rpm.
16. Pellet the cells at 2000rpm for 2min at 4ºC (It is best to use a swing-out rotor for this to ensure that all the cells are at the bottom.
17. Remove the PBS.
18. Resuspend the cells in 50µl PBS containing 1%BSA, 0.5% Triton-X and 1µl H3pS10 antibody (millipore).
19. Incubate with the 1º antibody for 2hrs at RT.
20. Wash the cells three times in 1ml PBS containing 1%BSA.
21. Resuspend the cells in 50µl PBS containing 1%BSA, 0.5% Triton-X and 1µl anti-rabbit FITC 2º antibody.
22. Incubate in the dark at RT for 1hr.
23. Wash cells three times in PBS containing 1%BSA.
24. Resuspend the cells in 300µl PBS containing 40ug/ml Propidium Iodide and 250ug/ml RNase A and filter them through a 0.3micron filter into a FACS tube. (This is important to prevent blockage on the FACS)
25. Incubate the cells for 30-60 min in the dark on ice.

FACS analysis:

26. For the FACS analysis you will also need a no stain control (just fixed cells), a no PI control (just fixed cells stained with H3pS10 antibody

and the FITC 2ºantibody) and a no FITC control (just fixed cells with PI). This is required for compensate for overlapping of the PI with FITC and vice versa.

27. Draw the following plots on the BD-FACS Diva Software:
    - Scatter plot FSC vs. SSC (to see all events)
    - Scatter plot FSC-A vs. FSC-H (to exclude doublets)
    - Scatter plot PE-Cy7 (x-axis) vs. FITC (y-axis) (to see mitotic staining)
    - Histogram of PE-Cy7 (to see cell cycle distribution)
    - Also create a statistics view to read of the percentage of mitotic cells.

Note: FSC, SSC and PE-Cy7 channel should all be on a normal scale, while FITC should be on a log scale.

28. Run no stain control first, gate for single cell population (P1) on the FSC vs. SSC scatter plot (Note, voltage for both FSC and SSC will need to be adjusted depending on the cell type used).
29. Then gate out the doublets (FSC-A vs. FSC-H).
30. Next run the PI only control. Adjust the voltage for PE-Cy7, so that the G1 peak (1^{st} peak) is at 100 and the G2 peak (2^{nd} peak) is at 200. This ensures that you cells are single cells with a normal DNA content. Then adjust the FITC channel, so that all FITC negative cells fall just below 10^3.
31. The FITC only control should give a distinct population above $10^{3.}$
32. Use a quadrant gate with the horizontal axis just above 10^3 and the vertical axis at 150. The top right quadrant is the number of mitotic cells for each sample.
33. Run all sample through the FACS on low(!) throughput (this should be around 200-400 events per second) and collect a minimum of 20,000 to 30,000 cells per sample. Use SIT flush after each sample.
34. Plot the percentage of mitotic cells v. time.

Clonogenic Survival Assay (IR)

Note: If using siRNA transfected cells, please see *siRNA transfection protocol.*

1. Add 4.5ml pre-warmed media to 6cm dishes, prepare dishes in duplicate for the following conditions:
   - Undamaged
   - 1Gy
   - 2Gy
   - 3Gy
   - 5Gy

   (The extent of damage depends on the cell line you are using, but these work well for U2OS cells. For RPE-1 cells, use conditioned media and plate twice as many cells.)
2. Trypsinize and count cells.
3. Resuspend cell to a final concentration of 1cell/µl (2cells/µl for RPE-1 cells).
4. Add 500µl (equivalent to 500/1000 cells) to the previously prepared dishes. (Make sure you also use a positive control, i.e. ATMi or siATM.)
5. Grow the cells for 10-14 days at 37ºC, 5%CO2. (No media change is needed.)
6. Once distinct colonies are forming, wash the dishes twice in 2-3ml PBS. (Make sure colonies are clearly visible, but not overgrown before staining.)
7. Add 1ml DMMB Stain to the cells and incubate at RT on the rocker (not faster than 25rpm) for 30min.
8. Remove the DMMB stain (the stain can be reused multiple times.)
9. Wash the cells three times with 2-3ml milliQ H2O (until the water runs clear).
10. Dry the dishes overnight on the bench before counting the colonies. This can be done be hand or using ImageJ software. (Dishes should also be scanned.)

Buffers and Solutions:

DMMB stain:

50% Methanol
25% Glacial Acetic Acid
0.5g Dimethylmethylene Blue

Clonogenic Survival Assay (Olaparib)

Note: If using siRNA transfected cells, please see *siRNA transfection protocol.*

1. Prepare media containing Olaparib at the following concentrations:
   - Untreated
   - 1.25μM
   - 2.5μM
   - 5μM

   The stock concentration of Olaparib is 50mM, there add 1.25μl of the stock solution into 45ml pre-warmed media to make a 1.25μM final solution (as 500μl of media containing the cells is added to 4.5ml of the media containing the drug to make it a final volume of 5ml per dish.)

   (The extent of damage depends on the cell line you are using, but these work well for U2OS cells.)
2. Add 4.5ml media containing the drug at the corresponding concentration into 6cm dishes (in duplicate per condition.)
3. Trypsinise and count cells.
4. Resuspend cells to a final concentration of 1cell/μl (2cells/μl for RPE-1 cells).
5. Add 500μl (equivalent to 500/1000 cells) to the previously prepared dishes. (Make sure you also use a positive control, i.e. RAD51i (at a concentration of 50μM or siRAD54L.)
6. Grow the cells for 10-14 days at 37ºC, 5%CO_2. (No media change is needed.)
7. Once distinct colonies are forming, wash the dishes twice in 2-3ml PBS. (Make sure colonies are clearly visible, but not overgrown before staining.)
8. Add 1ml DMMB Stain to the cells and incubate at RT on the rocker (not faster than 25rpm) for 30min.
9. Remove the DMMB stain (the stain can be reused mμltiple times.)

10. Wash the cells three times with 2-3ml milliQ H2O (until the water runs clear).
11. Dry the dishes overnight on the bench before counting the colonies. This can be done be hand or using ImageJ software. (Dishes should also be scanned.)

Buffers and Solutions:

DMMB stain:

50% Methanol
25% Glacial Acetic Acid
0.5g Dimethylmethylene Blue

Clonogenic Survival Assay (ICRF193)

Note: If using siRNA transfected cells, please see *siRNA transfection protocol.*

1. Prepare media containing ICRF-193 at the following concentrations:
   - Untreated
   - 200nM
   - 400nM
   - 800nM

   The stock concentration of ICRF-193 is 14mM (this corresponds to 4mg/ml), To make the final solution, first prepare a working dilution (1/100; 140μM). Then add 71.4μl of the working diltution into 45ml pre-warmed media to make a 200nM final solution (as 500μl of media containing the cells is added to 4.5ml of the media containing the drug to make it a final volume of 5ml per dish.) Add 148.8μl or 297.6μl of the working dilution to 45ml media to make 400nM or 800nM solution, respectively.

   (The extent of damage depends on the cell line you are using, but these work well for U2OS cells.)
2. Add 4.5ml media containing the drug at the corresponding concentration into 6cm dishes (in duplicate per condition.)
3. Trypsinise and count cells.
4. Resuspend cells to a final concentration of 1cell/μl (2cells/μl for RPE-1 cells).
5. Add 500μl (equivalent to 500/1000 cells) to the previously prepared dishes. (Make sure you also use a positive control, i.e. DNA-PKi (at a concentration of 10μM or siDNA-PK.)
6. Grow the cells for 10-14 days at 37ºC, 5%CO_2. (No media change is needed.)
7. Once distinct colonies are forming, wash the dishes twice in 2-3ml PBS. (Make sure colonies are clearly visible, but not overgrown before staining.)

8. Add 1ml DMMB Stain to the cells and incubate at RT on the rocker (not faster than 25rpm) for 30min.
9. Remove the DMMB stain (the stain can be reused multiple times.)
10. Wash the cells three times with 2-3ml milliQ H2O (until the water runs clear).
11. Dry the dishes overnight on the bench before counting the colonies. This can be done be hand or using ImageJ software. (Dishes should also be scanned.)

Buffers and Solutions:

DMMB stain:

50% Methanol
25% Glacial Acetic Acid
0.5g Dimethylmethylene Blue

Cell proliferation assays

1. Plate 2x10^5 cells per 35mm dish. Use one 35mm dish per condition. (if you use siRNA to knock down your protein, see *siRNA transfection* protocol)
2. After 24hrs, remove the media and add fresh media containing the drug to the cells. Use the following concentrations for the drugs below:
   - Campthotecin: 1nM, 2nM, 5nM, 10nM
   - Olaparib: 1μM, 2μM, 5μM, 10μM

   Note: the concentration of the drugs depends on the cell line in use, these concentrations are optimized for HCT116 cells.
3. Grow cells with the drugs for 48hrs, then remove the media and split the cells into two equal dishes. This ensures optimal growth conditions.
4. Grow the cells in drug-free media for a further 48hrs.
5. Harvest cells by trypsinisation, resuspend in 5ml to volume and count in triplicate using either the Coulter counter or a hemocytometer. (If you are using the Coulter counter, cells need to be washed and resuspended in 10ml PBS.

GFP Reporter assays (stable)

Note: This protocol is optimised for the original cell line for both HR (DR-GFP HeLA, M. Jasin) and NHEJ (pIRES-Tk-eGFP H1299, Ogiwara) assays.

1. Trypsinize cells, resuspend in 10ml total volume and count cells.
2. Pellet cells, wash once with PBS and resuspend to a total concentration of $2x10^6$ cells/ml in Optimem.
3. Add 500µl cells, 5ug pDNA (I-SceI), 1ug Cerulean and 2µl siRNA into a cuvette. (Make sure you also plate cells for the controls, i.e. GFP single stain, Cerulean single stain, ToPro3 single stain and unstained)
4. Incubate for 10min at RT, then electroporate at 280V, 1000uF and incubate for a further 10min at RT.
5. Plate the cells onto a 6-well plate with 2.5ml media. (If you are using inhibitors as control, supplement the media with the appropriate concentration of inhibitor. E.g. 10µM DNA-PKi; 50µM RAD51i).
6. Grow cells for 48hrs at 37ºC, 5%CO_2.
7. Trypsinise the cells, resuspend in 5ml media, pellet and wash with PBS.
8. Resuspend the cells in 1ml PBS. Split cell into two aliquots. Keep one for Western Blotting and add 1µl ToPro3 stain to the other cells just before analysis using the FACS CantoII. (It is important to keep cells for Western Blotting when using siRNA, as you will need to verify the knock-down for every single experiment.)

FACS analysis:

35. For the FACS analysis you will also need an untransfected control, a cerulean single stain control (transfection efficiency) and a GFP single stain (for compensation). This is required for compensate for overlapping of the Cyan with FITC and vice versa.
36. Draw the following plots on the BD-FACS Diva Software:
    - Scatter plot FSC vs. SSC (to see all events)
    - Scatter plot FSC-A vs. FSC-H (to exclude doublets)

- Scatter plot PE-Cy7 (x-axis) vs. FSC (y-axis) (to exclude dead cells)
- Scatter Plot Cyan (x-axis) vs. FITC (y-axis) (to count the percentage of GFP positive cells.)
- Also create a statistics view to read of the percentage of GFP-positive cells.

Note: FSC and SSC channels should be on a normal scale, while FITC PE-Cy7 and Cyan should be on a log scale.

37. Run no stain control first, gate for single cell population (P1) on the FSC vs. SSC scatter plot (Note, voltage for both FSC and SSC will need to be adjusted depending on the cell type used).
38. Then gate out the doublets (FSC-A vs. FSC-H).
39. Next run the ToPro3 single stain control. Exclude the ToPro3 positive cells (dead cells). Then adjust the voltage on the FITC and Cyan channels, so that all FITC and Cyan negative cells fall just below 10^3.
40. The FITC and Cyan single stain controls should give a distinct population above 10^3.
41. Draw a gate above the Cyan positive cells (FITC-Cyan double positive population). These are your transfected, GFP positive cells.
42. Run all samples through the FACS on low(!) throughput (this should be around 200-400 events per second) and collect a minimum of 20,000 to 30,000 cells per sample. Use SIT flush after each sample.
43. Plot the percentage of GFP positive cells on a bar-graph for each condition.

GFP reporter assays (transient)

Note: This protocol is optimised for the transfection of the DR-GFP plasmid (M. Jasin) in HCT116 cells. Other cell lines may need optimisation.

1. Plate cells at $5x10^5$ cells/well into a 6-well dish (3ml total volume) and grow for 24hrs.
2. Prepare a transfection mix as follows:
   - Tube 1: 5ug DR-GFP, 5ug pCBA-I-SceI, 1ug Cerulean in 250µl Optimem
   - Tube 2: 10µl Lipofectamine in 250µl Optimem

   Incubate Tube 2 for 5min at RT before adding to tube 1. Then incubate the DNA:lipid mix for 20min at RT. (if using siRNA, add 2µl siRNA to Tube 1).
3. Add the DNA:lipid mix to the cells and grow for 48hrs at 37ºC, 5%CO_2. (If you are using inhibitors as control, supplement the media with the appropriate concentration of inhibitor. E.g. 10µM DNA-PKi; 50µM RAD51i).
4. Trypsinise the cells, resuspend in 5ml media, pellet and wash with PBS.
5. Resuspend the cells in 1ml PBS. Split cell into two aliquots. Keep one for Western Blotting and add 1µl ToPro3 stain to the other aliquots just before analysis using the FACS CantoII. (It is important to keep cells for Western Blotting when using siRNA, as you will need to verify the knock-down for every single experiment.)

FACS analysis:

44. For the FACS analysis you will also need an untransfected control, a cerµlean single stain control (transfection efficiency) and a GFP single stain (for compensation). This is required for compensate for overlapping of the Cyan with FITC and vice versa.
45. Draw the following plots on the BD-FACS Diva Software:
    - Scatter plot FSC vs. SSC (to see all events)

- Scatter plot FSC-A vs. FSC-H (to exclude doublets)
- Scatter plot PE-Cy7 (x-axis) vs. FSC (y-axis) (to exclude dead cells)
- Scatter Plot Cyan (x-axis) vs. FITC (y-axis) (to count the percentage of GFP positive cells.)
- Also create a statistics view to read of the percentage of GFP-positive cells.

Note: FSC and SSC channels should be on a normal scale, while FITC PE-Cy7 and Cyan should be on a log scale.

46. Run no stain control first, gate for single cell population (P1) on the FSC vs. SSC scatter plot (Note, voltage for both FSC and SSC will need to be adjusted depending on the cell type used).
47. Then gate out the doublets (FSC-A vs. FSC-H).
48. Next run the ToPro3 single stain control. Exclude the ToPro3 positive cells (dead cells). Then adjust the voltage on the FITC and Cyan channels, so that all FITC and Cyan negative cells fall just below 10^3.
49. The FITC and Cyan single stain controls should give a distinct population above 10^3.
50. Draw a gate above the Cyan positive cells (FITC-Cyan double positive population). These are your transfected, GFP positive cells.
51. Run all samples through the FACS on low(!) throughput (this should be around 200-400 events per second) and collect a minimum of 20,000 to 30,000 cells per sample. Use SIT flush after each sample.
52. Plot the percentage of GFP positive cells on a bar-graph for each condition.

Immunofluorescence

In general cells are fixed with one of three fixing agents, depending on the 1ºantibody.

- PFA fixiation (with or without pre-extraction of soluble proteins)
- Methanol fixiation
- Acetone fixiation

This protocol will focus on the most common fixiation methods, i.e. Methanol and PFA fixiation.

1. Sterilize coverslips in a tissue culture dish for at least 15-20min under UV light.
2. Plate cells onto the coverslip.
   - For siRNA transfections see *siRNA transfection protocol*
   - For cells to be confluent the next day, plate 3-4x10^5cells/35mm dish (depending on the cell type)
3. Transfer coverslip directly from the media into a 6-well plate containing 1-2ml PBS.

Methanol Fixiation:

4. Remove the coverslip from the PBS, drain excess liquid and place into a 6-well dish containing 2ml ice-cold 100% Methanol (cooled down for at least 30min at -20ºC).
5. Incubate coverslip in MeOH at -20ºC for 15min. (Methanol also permeabilises the cells, so not second permeabilisation step is required.)
6. Wash the coverslip twice in at least 1ml PBS before staining with 1ºantibody.

Pre-extraction:

Using CSK buffer to pre-extract cells before fixiation will remove all soluble proteins from the cells, which can be useful to visualise foci).

3. Remove PBS from the cells and carefully add 1ml CSK-buffer to the wall of the 6-well dish (very slowly to prevent the cells from washing of the coverslip).
4. Incubate the cells for 5-10min at RT in CSK buffer. (Cell can also be pre-extracted for longer at 4C or shorter times at 37ºC, this needs to be optimised the every antibody and condition).
5. Remove the CSK buffer and carefully wash twice with 2ml PBS (make sure not to flush the cells of the coverslip).
6. Add 500µl 4%PFA to the edge of the coverslip to fix the cells.
7. Incubate in PFA for 10min at RT, then remove the PFA and wash twice with 1-2ml PBS.
8. Leave the cells in PBS until 1ºantibody staining.

PFA fixiation:

3. Remove excess PBS from the cells.
4. Carefully add 500µl 4% PFA to the edge of the coverslip and fix cells for 10min at RT.
5. Remove PFA and wash twice with 1-2ml PBS.
6. Add 1ml 0.25% Triton-X to the edge of the 6-well plate (to prevent washing the cells of the coverslip) and permeabilise for 2-10min at RT.
7. Remove Triton-X and wash twice in 1-2ml PBS.
8. Leave the cell in PBS until 1ºantibody staining.

Antibody Staining:

(All antibodies are diluted in 1-3% BSA in PBS)

9. Remove PBS and block cells with 1-3% BSA for 1hr at RT or at 4ºC overnight.
10. Prepare 1ºantibody mix (use appropriate concentration of the antibody).
11. Place 90µl 1ºantibody mix onto Parafilm in an IF box (protected from light).
12. Then carefully place the coverslip onto the antibody drop with the cells facing down.

13. To prevent the coverslips from drying out, place two moist tissues (soaked with ddH2O) inside the IF box.
14. Incubate cells with the antibody for 1hr at 37ºC.
15. Transfer the coverslips (cells facing up) back into the 6-well plate and wash three times with 1-2ml PBS.
16. Prepare 2ºantibody mix (use appropriate concentrations).
17. Pipette 90µl of the 2ºantibody mix onto parafilm in the IF box.
18. Carefully place the coverslip (cells facing down) onto the antibody.
19. Put moist tissue into the box and incubate cells with the 2ºantibody for 1hr at 37ºC.
20. Transfer coverslips (cells facing up) back into the 6-well dish and wash three times with PBS.

DAPI staining and sealing:

21. Place 8-10µl Vectrashield mounting media (containing DAPI) onto a microscope slide.
22. Remove excess liquid from the coverslip (this is best achieved by putting it vertically onto a dry piece of tissue and wait a few seconds until the tissue has absorbed the PBS).
23. Put the coverslip (cells facing down) onto the mounting media.
24. Seal the coverslip with common nail varnish and leave to dry in the dark at RT.
25. Store the IF slide either at 4ºC (short term, up to 3months) or -20ºC (long term).

The best DAPI staining can be seen from 12-24hrs after mounting the slides.

Buffers and Reagents:

PFA: 4% PFA in PBS
Triton-X: 0.25% in PBS
BSA: 1-3% in PBS
100% Methanol
Vectrashield with DAPI
CSK buffer:
100mM NaCl
300mM Sucrose
3mM $MgCl_2$
10mM PIPES pH6.8
0.5% Triton-X
Protease and Phophatase inhibitors

Cell fractionation (2-step)

Note: This protocol is adjusted to one confluent 10cm dish of adherent cells.

Soluble protein fraction:

1. Pellet cells at 1200rpm for 5min at 4ºC.
2. Wash cells with 1ml PBS.
3. Resuspend cell pellet in 750µl ice-cold Lysis Buffer.
4. Incubate cells on ice for 15min.
5. Centrifuge lysate at 1200rpm for 10min at 4ºC.
6. Transfer supernatant into a fresh microfuge tube (**soluble fraction)**.

Chromatin-bound fraction:

7. Add 200µl Lysis Buffer supplemented with 1/1000 (1µl/ml) Benzonase (Sigma) and 1mM $MgCl_2$ to the chromatin pellet.
8. Incubate the lysate on ice for 45min.
9. Centrifuge lysate for 15min at 4ºC at 14,000rpm.
10. Transfer Supernatant to a new microfuge tube (**chromatin fraction**)
11. Quantify protein concentration using the Bradford assay.

Analyse samples by Western Blotting (see *Western Blotting Protocol*). Load between 20-50ug of protein per fraction on a denaturing poly-acrylamide gel.

Note: The salt concentration of the Lysis Buffer is very important to see loosely chromatin-bound proteins. For proteins like BRCA1, to keep them on the chromatin, use a salt concentration of 140mM salt, to see even distribution between chromatin and soluble fraction use 145mM salt.

Buffers:
Lysis Buffer:
150mM NaCl
0.5% NP-40
50mM Tris-HCl pH7.5
10% Glycerol
Protease & Phosphatase Inhibitors

Cell fractionation (adapted form the Lamond Lab)

Note: This protocol is adjusted to four confluent 10cm dishes of adherent cells.

Lysis:

1. Trypsinize and pellet cells at 1200rpm for 5min at 4ºC.
2. Wash cells twice with 1ml cold PBS.
3. Resuspend cell pellet in 750µl ice-cold Buffer A.
4. Incubate cells on ice for 5min to allow cells to smell.
5. Break open cells with a pre-chilled 1ml dounce homogenizer (20 strokes with the tight pestle).
6. Centrifuge lysate at 1500rpm (228g) for 5min at 4ºC to pellet nuclei.

Cytoplasmic fraction:

7. Transfer the Supernatant into a new microfuge tube and keep the pelleted nuclei on ice.
8. Add 150µl 5xLysis Buffer to the supernatant and incubate on ice for 10min.
9. Centrifuge at 14,000rpm for 10min at 4ºC.
10. Transfer supernatant into a new microfuge tube (**cytoplasmic fraction).**

Nuclear fraction:

11. Resuspend nuclear pellet in 600µl of S1 buffer.
12. Layer over a 600µl Cushion of S3 buffer. (This removes most cytoplasmic remains from the nuclei.)
13. Centrifuge at 6000rpm (2800g) for 10min at 4ºC and discard the supernatant.
14. Wash once with 500µl 1x Lysis Buffer. (Do do leave in the lysis buffer and avoid pipetting the cells up and down, as this step is only to remove excess sucrose from the nuclei.)

15. Resuspend nuclear pellet in 300µl 1x Lysis buffer and incubate on ice for 10min. (Resuspend nuclei well in the lysis buffer to ensure even lysis.)
16. Pellet the chromatin for 10min at 4ºC at 10,000rpm.
17. Transfer supernatant to a new 1.5ml tube (**nuclear fraction**).

Chromatin fraction:

18. Resuspend the chromatin pellet in 200µl 1x Lysis Buffer supplemented with 1µl/ml Benzonase and 1mM MgCl2.
19. Incubate on ice for 45min on ice and centrifuge for 15min at 4ºC at 14,000rpm.
20. Transfer Supernatant to a new microfuge tube (**chromatin fraction**).

Cytoskeletal fraction:

21. Briefly wash the pellet once in Triton X-100 Buffer.
22. Boil the pellet in 75µl Triton X-100 buffer for 5min.
23. Centrifuge for 15min at 14,000rpm at 4ºC and transfer to a new tube (**Pellet Fraction**).

Analyse samples by Western Blotting (see *Western Blotting Protocol*). Load between 20-50ug of protein per fraction on a denaturing poly-acrylamide gel.

Note: The salt concentration of the Lysis Buffer is very important to see loosely chromatin-bound proteins. For proteins like BRCA1, to keep them on the chromatin, use a salt concentration of 140mM salt, to see even distribution between chromatin and soluble fraction use 145mM salt.

Buffers:

1x Lysis Buffer:

150mM NaCl
0.5% NP-40
50mM Tris-HCl pH7.5
10% Glycerol
Protease & Phosphatase Inhibitors

Buffer A (Hypotonic Buffer)

10mM HEPES, ph7.5
1.5mM $MgCl_2$
10mM KCl
0.5mM DTT
Protease & Phosphatase Inhibitors

S1 Buffer:

0.25mM Sucrose
10mM $MgCl_2$
Protease & Phosphatase Inhibitors

S3 Buffer:

0.88M Sucrose
0.5mM $MgCl_2$
Protease & Phosphatase Inhibitors

5xLysis Buffer:

250mM Tris, pH7.5
750mM NaCl
2.5% NP-40
50% Glycerol

Triton X-100 Buffer

50mM Tris, pH7.5
137mM NaCl
10% Glycerol
0.5% Triton X-100
Protease & Phosphatase Inhibitors

Immunoprecipitation

Treatment & harvesting:

1. Irradiate cells with 10Gy and incubate for 1hr at 37ºC, 5%CO_2.
2. Remove the media and wash the cells with ice-cold PBS.
3. Remove all excess PBS and scrape cells of the dish in 750µl ice-cold PBS. (Use pre-chilled low adhesion tubes, if possible.)
4. Pellet the cells for 5min at 1200rpm at 4ºC and remove excess PBS. (Cell pellets can be stored at -80ºC, if needed.)

Note: Depending on the cell line, more than one dish may be needed to obtain enough TCE for the IPs, e.g. One 10cm dish of HEK293 cells is sufficient, but you might need 2-3 10cm dishes of U2OS or RPE-1 cells to get the same amount of protein.

Cell lysis & Nuclease treatment:

5. Resuspend the cells in 750µl Lysis Buffer supplemented with 1mM $MgCl_2$ and 1µl/ml Benzonase.
6. Lyse the cells on ice for 45min, occasionally flicking the tubes to get even lysis.
7. Spin down the lysates for 15min at 4ºC at 14,000rpm.
8. Transfer the supernatant into a new 1.5ml tube and measure the concentration using Bradford reagent. (see *Protein Extraction Protocol.*)

Bead preparation & Immunoprecipitation:

9. To prepare the beads, add the total amount of beads (20µl G-beads/IP or 33µl Dynabeads (slurry)/IP) into a 1.5ml tube and wash three times with 1ml Lysis Buffer. (To pellet G-beads between every wash, spin the beads at max 2000rpm, higher speeds will damage the beads.)
10. Resuspend the beads in an equal volume of Lysis buffer. (i.e. make a 50% slurry)

11. *Optional*: Preclear the lysate with 20µl empty G-beads for 30min on the wheel at 4ºC. (This is not necessary unless you have unspecific binding in your IP.)

Note: Depending on your antibody, there are two possible ways to IP your protein. (If using a new antibody, you will need to optimise the IP.)

Option 1: Bind the antibody to the beads prior to IP

12. Add 1ug of antibody per mg of TCE to 20µl G-beads/33µl Dynabeads into each sample tube (for IgG sample, add 1ug IgG) in 200µl PBS-Tween (0.1%) and couple the antibody to the beads for 30min on the wheel at 4ºC.
13. Wash the beads twice with Lysis buffer.
14. Then add 20µl of the antibody coupled G-beads/33µl Dynabeads to 2ug TCE (10ug TCE for an ATM IP with 5ug antibody).
15. Incubate on the wheel at 4ºC for 2hrs.
16. Wash the beads five times in 1ml Lysis buffer. (Always spin the beads at 4ºC and keep the lyates on ice at all times.)
17. Then resuspend in 40µl 2xLaemmli Buffer supplemented with 10% β-mercapto ethanol.
18. Analyse samples by Western Blotting (see *Western Blotting Protocol*.) loading 10-20µl of the IP on a denaturing polyacrylamide gel.

Option 2: Binding the antibody to the protein prior to bead incubation.

19. Add 2ug antibody to 2mg TCE (Don't forget the negative control, IgG) and incubate for 2hrs at 4ºC on the wheel.
20. Then add 20µl G-beads/33µl Dynabeads into each sample and incubate for 1hr on the wheel at 4ºC.
21. Wash the beads five times in 1ml Lysis buffer. (Always spin the beads at 4ºC and keep the lyates on ice at all times.)
22. Then resuspend in 40µl 2xLaemmli Buffer supplemented with 10% b-mercapto ethanol.
23. Analyse samples by Western Blotting (see *Western Blotting Protocol*.) loading 10-20µl of the IP on a denaturing polyacrylamide gel.

Buffers:

1x Lysis Buffer:

150mM NaCl
0.5% NP-40
50mM Tris-HCl pH7.5
10% Glycerol
Protease & Phosphatase Inhibitors

Laemmli Buffer (2x):

125mM Tris-HCl pH6.8
4% SDS
15% Glycerol
0.01% Bromophenol Blue

Kinase assay

Lysate preparation

1. Plate 2x10^6 cells (HEK293) on a 10cm dish (Cell+).
2. Leave to settle for at least 4hrs (overnight is better).
3. Transfect cells with 10ug Flag-ATM plasmid (see *Calcium Phosphate transfection protocol*).
4. Harvest cells by scraping as follows:
   - Remove media.
   - Wash carefully with ice-cold PBS twice.
   - Remove all excess PBS.
   - Add 750µl ice-cold PBS onto the cells and scrape off.
   - Transfer cells into a 1.5ml microfuge tube on ice.
   - Pellet cells at 2000rpm for 1min at 4ºC.
   - Remove supernatant.

(At this point the cell pellets can be stored at -80ºC for up to a months.)

5. Resuspend pellet in 1ml TGN buffer containing 1/1000 Benzonase and 1mM $MgCl_2$.
6. Incubate for 45min on ice and gently flick the tubes every 10min to ensure even lysis.
7. Centrifuge for 10min at 14,000rpm at 4ºC to remove all the debris.
8. Measure the concentration by Bradford and aliquot into 2mg aliquots.

(At this point lysates can be stored for up to a month at -80ºC.)

Kinase Assay

10. Thaw lysate on ice.
11. Prepare 100µl Anti-FLAG M2 beads (Sigma)
    - Wash beads 3x in 1ml TGN buffer.
    - Resuspend in 50µl TGN buffer (final vol. 100µl, 50% slurry).
12. Add 2mg lysate to 50µl slurry (25µl beads).
13. Rotate for 3h at 4C on the wheel.
14. Wash beads twice in 1ml TGN buffer.

15. Wash beads once in 1ml TL buffer.
16. Wash 3x in 250µl Kinase buffer.
17. Resuspend beads in 400µl kinase buffer.
18. Mix well and divide into for 100µl aliquots.
19. Spin down beads at 200rpm, 1min, 4ºC.
20. Remove supernatant.
21. Resuspend in 30µl Kinase Buffer with ATP (10uC γATP P^{32} labelled).
    - If using a protein to inhibit ATM kinase activity add into the kinase buffer (also ATMi as a negative control).
22. Add 500-100ng H2Ax to the kinase mix and incubate at 30ºC.
    - 3-10min to see ATM kinase activity.
    - 15-20min to map ATM sites.
23. Add 35µl 2xSB (with 10%BME) to stop the reaction.
24. Boil samples for 15min at 95ºC.
25. Run half the sample on a SDS page gel (a 15% gel for γH2Ax to check kinase activity, and a 6% gel to check ATM autophosphorylation).
26. Freeze the gel and expose to a phospho-screen at -20ºC.
27. Visualize on phospho-imager.

Buffers and solutions:

TGN buffer:

50mM Tris pH7.5
50mM β-glycerophosphate
150µl 5M NaCl
10% Glycerol
1% Tween
1mM DTT
100x Pi
50x PPi

TL buffer:

50mM Tris pH7.5
0.5M LiCl

Kinase buffer:

10mM HEPES pH7.5
50mM β-glycerophosphate
10mM $MgCl_2$
10mM $MnCl_2$
1mM DT

Chromatin Immunoprecipitation (ChIP)

Note: It is very important that all buffers are filtered with 0.2µl filters. Use filter tips at all times to prevent contamination and prepare all buffers fresh on the day.

Crosslinking and harvesting:

1. Plate cells $5x10^6$cells the day before harvesting on 150mm dishes (20ml total medium).
2. Add 0.6µl 10mM 4OHT (300nM final conc.) to each dish (not the controls).
3. Incubate for 4h at 37°C, 5% CO_2.
4. To crosslink the proteins and DNA, add 556µl 36% Formaldehyde (1% final conc.) directly into the medium and incubate on the rocker for 15min at RT. (The media will turn yellow and slowly turn back to red, when the Formaldehyde is being used up. It is important to keep the time exactly, as more time will results in more crosslinking.)
5. To quench the crosslinking, add 1ml 2.5M Glycine (0.125M final conc.) to the medium and incubate on the rocker for 5min at RT. (The media will turn yellow permanently).
6. Remove medium and wash twice with cold PBS (keep plates on ice).
7. Add 750µl cold PBS to the cells, harvest cells by scaping and collect in a 1.5ml tube.
8. Pellet the cells at 4°C for 5min at 2000rpm, remove the supernatant and freeze cell pellets after harvesting at -80ºC. (Freezing for at least overnight to 24hrs will give better IP results.)

Note: Cross-linked cell pellets can be stored at -80ºC for up to six months.

Bead preparation:

Note: All quantities below are for the preparation of 10 ChIPs (mock ctrl, pos. ctrl, 3 samples, +/- treatment)

9. Use 100µl 50% slurry for each sample (50µl A/G beads) and 1ml 50% slurry (500µl A/G beads) for preclearing of the chromatin.
10. Add 1ml 50% A beads (500µl beads) and 625µl 80% G beads (500µl beads) into a 2ml tube on ice.
11. Wash the beads three times in 1ml IP buffer and resuspend in 750µl IP buffer.
12. Add 200µl 2mg/ml salmon sperm and 50µl 20mg/ml BSA to the beads for pre-clearing.
13. Incubate the beads for 4h at 4°C on the wheel then pellet the beads at 4°C for 2min at 2000rpm.
14. Wash the cells three times in 1ml IP buffer and resuspend in 1ml IP buffer. (You can store the beads short-term (up to 5 days) at 4ºC.)

Cellular and Nuclear Lysis:

15. Use 5 pellets per condition (i.e for untreated and 4OHT treated samples (10 pellets total)).
16. Resuspend the pellets in 1ml Cellular Lysis Buffer each and incubate for 10min on ice. (The hypotonic buffer will cause the cells to swell up and make it easier to separate the cytoplasm from the nuclei.)
17. Add all pellets (of one condition) into a 15ml Dounce homogenizer (Alternatively, homogenize them one by one in a 1ml Dounce homogenizer.)
18. Homogenize with the loose tip 20 times on ice, let the cells rest for two minutes on ice, then homogenize with the tight tip 20 times on ice.
19. Collect the cells in a 15ml Falcon tube and keep on ice at all times.
20. Pellet the nuclei at 4000rpm for 5min at 4°C and remove the supernatant.
21. Resuspend the nuclear pellet in 1.5ml Nuclear Lysis Buffer and incubate the lysate on ice for 10min.

Sonication:

Note: Use a Branson sonifier 450 with a microtip to obtain fragments around 500bp average. (If you are using the waterbath sonicator or

another microtip sonicator, you will need to optimise sonication conditions first.)

22. Keep nuclear extract on ice throughout sonication. (This is very important as lysates need to be kept cool to prevent degradation of proteins.)
23. Sonicate 10 times 10sec at 50% amplitude. (Make sure it does not foam, if it does, leave the samples on ice until the foam disappears. Foaming can disrupt the sonication of the sample.)
24. Measure the concentration of the DNA with the Nanodrop. (The A260/230 ratio will be around 1.3-1.5 as there is a lot of protein in the sample.)
25. Dilute the lysate with 13.5ml Dilution Buffer.

Preclearing:

26. Add 500µl of 50% A/G beads to 15ml of extract and pre-clear the chromatin for 1-2h at 4°C on the wheel.
27. Pellet the beads for 10min at 4000rpm at 4°C and transfer the supernatant (pre-cleared chromatin) into 150-300ug aliquots. (Pre-cleared chromatin can be stored at -80°C short-term.)
28. Remove 100µl of the extract for inputs and freeze at -20°C.

ChIP:

Note: Use 150-300ug of chromatin per IP.

29. Add 1-2ug of the antibody to the chromatin and incubate overnight at 4°C on the wheel. (Use a mock ctrl (with IgG) as a negative ctrl and gH2Ax (2µl of the abcam antibody/ per IP) as a positive ctrl. If looking at HR/NHEJ specific breaks also use Rad51 (15µl from Santa Cruz/ per IP) as a pos./neg. control.)
30. Add 100µl 50% A/G bead slurry to the IP and incubate for 2h at 4°C on the wheel.

31. Pellet the beads for 1min at 2000rpm at 4°C and transfer the beads in 1ml Dialysis Buffer to 1.5ml screwcap tubes. (Screw-cap tubes are very important, for the de-crosslinking step.)
32. Pellet the beads and remove the supernatant.
33. Wash the beads five times 5min with 1ml Wash Buffer at 4°C.
34. Wash the beads twice with 1ml TE buffer.
35. On the second wash, transfer 200µl into a 1.5ml tube, pellet the beads, remove the supernatant and resuspend in 20µl 2X Laemmli Buffer. (It is important to check to IP efficiency by Western Blotting to show that the protein was successfully precipitated.)
36. Store at -80ºC until Western Blotting analysis. (see *Western Blotting* protocol.)
37. Remove the supernatant of the remaining 80% of the beads and resuspend beads in 200µl TE Buffer.
38. Add 100µl TE Buffer to the input samples.
39. Add 2µl 5mg/ml RNase A to all samples and incubate for 30min at 37°C to remove all RNA.
40. Add 2µl 20% SDS to the samples and incubate overnight at 70°C at 1200rpm on the shaker to reverse crosslink. (Make sure the screw caps are tightly closed to prevent drying out of the samples.)

DNA purification:

41. Briefly spin down samples to remove condensated liquid from the lid.
42. Add 2µl 20mg/ml Proteinase K to each sample and incubate for 90min at 45°C on the heatblock with gentle shaking (400rpm).
43. Add 200µl Phenol, vortex and centrifuge for 5min at 14000rpm (make sure not to take the top layer of the phenol, when pipetting.)
44. Transfer supernatant (top layer) into new tube and add 200µl TE buffer to the Phenol fraction to back-extract the phenol.
45. Vortex and centrifuge for 5min at 14000rpm.
46. Transfer the top layer to the previously obtained samples to have 400µl final volume.

47. Add 400µl Chloroform, vortex and centrifuge at 14000rpm for 5min, then transfer supernatant into a new tube.
48. Add 375µl Chloroform to the supernatant, vortex and centrifuge for 5min at 14000rpm.
49. Transfer supernatant into a low adhesion tube and add 875µl 100% Ethanol (2.5V), 35µl 3M NaAc (0.1V) and 1µl Glycogen.
50. Incubate overnight at -20°C to precipitate the DNA.
51. Centrifuge for 30min at 4°C at 14000rpm to pellet DNA and remove the supernatant. (Small pellet should be visible at the bottom of the tube.)
52. Add 750µl 70% Ethanol to wash the pellet and centrifuge for 5min at 4°C at 14000rpm.
53. Remove as much Ethanol as possible (make sure you do not touch the pellet) and air-dry the pellet.
54. Add 50µl Nuclease-free H_2O and freeze for 1hr at -20°C to resuspend the pellet easier. Alternatively, leave the DNA shaking at 400rpm for 30min at 37ºC.)
55. Vortex the sample, spin down and store at -20°C until qPCR analysis.

quantitative PCR:

56. Heat samples for 5min at 65°C and pipette 2µl of DNA into the wells. (each point should be in duplicate or triplicate.)
57. Add 18µl of qPCR mastermix to each sample

- Mastermix:
  - 10µl 2x SyBr Green qPCR Mastermix (Invitrogen)
  - 0.1µl forward Primer
  - 0.1µl reverse Primer
  - 7.8µl PCR-grade H_2O

58. Run qPCR with SyBr Green settings on a fast cycle (include melting curves) for comparative C_t values.

Analysis:

59. Adjust the input C_t:

- log_2(Vol. of IP (µl)/Vol. (input (100µl))
- substact value obtained from the input C_t value

60. Calculate the %input of each of your samples.

- 100*2^(ct input – ct sample)

61. Normalize samples to the mock ctrl.

- sample/mock

62. Normalize 4OHT treated samples to control samples.

- 4OHT/ctrl

Reagents, stock solutions, Buffers:

Cellular Lysis Buffer (10ml)**:**

100µl 0.5M Pipes pH8.0
425µl 2M KCl
500µl 10% NP-40
100µl Protease Inhibitor Mix
8.875ml H_2O

Nuclear Lysis Buffer (10ml)**:**

500µl 1M Tris pH8.1
200µl 0.5M EDTA pH8.0
500µl 20% SDS
100µl Protease Inhibitor Mix
8.7ml H_2O

IP Buffer:

1ml Nuclear Lysis Buffer
9ml Dilution Buffer

Dilution Buffer (40ml)**:**

20µl 20% SDS
4.4ml 10% Triton X-100
96µl 0.5M EDTA pH8.0
668µl 1M Tris pH8.1
1336µl 5M NaCl
33.48ml H_2O

Dialysis Buffer (10ml)**:**

40µl 0.5M EDTA pH8.0

500µl 1M Tris pH8.1
100µl 10% Sarkosyl
100µl Protease Inhibitor Mix
9.26ml H_2O

Wash Buffer (50ml)**:**

1.66ml 3M Tris pH8.8
5ml 5M LiCl
5ml 10% NP-40
5ml 10% NaDoc
100µl Protease Inhibitor Mix
32.84ml H_2O

Neutral comet assay

Note: If using siRNA transfections, see *siRNA transfection* protocol.

1. Make a 1xLysis Solution and cool down to 4ºC for at least 20min.
2. Melt the LMA agarose and pipette 50µl into a pre-warmed 1.5ml tube and keep the tubes at 38ºC while harvesting the cells.
3. Harvest and count the cells. Resuspend the cells to a final concentration of $1x10^6$ cells/ml in cold PBS.
4. Add 5µl of the cells (5000cells) to 50µl of 38ºC LMA agarose. Vortex and spread onto a polylysine slide. (Pellet the rest of the cells for knock-down check, see *Protein extraction and Western Blotting* protocol.)
5. Incubate the slides for 30min at 4ºC to allow the agarose to set.
6. Carefully immerse slides in 1x Lysis solution and lyse the cells for at least 1hr (or overnight) at 4ºC.
7. Remove slides from the Lysis Buffer and drain of excess liquid.
8. Immerse slides in cold 1x Electrophoresis Buffer for 30min at 4ºC. (It is very important to keep everything at 4ºC, as higher temperatures will result in the agarose releasing from the coverslide.)
9. Align the slides equidistant from the electrodes, carefully add cold 1x Electrophoresis Buffer to the chamber until the buffer is no ore than 0.5cm above the slides.
10. Run for 1hr at 24V at 4ºC. (1 volt per cm electrode to electrode.)
11. Drain excess Buffer from the slides and immerse into DNA precipitation solution for 30min at RT in the dark.
12. Drain of excess DNA precipitation solution and immerse slides in 70%EtOH for 30min at RT.
13. Remove excess EtOH and dry the slides at 37ºC until the agarose is flat on the slide. (This ensures that the cells are all in a single plane, which facilitates imaging.)
14. Add 100µl SyBR green staining solution on top of the dried agarose and incubate for 30min in the dark. (Alternatively, use mounting

medium with DAPI and seal the slides with coverslips and nail varnish.)

15. View comets on the microscope using the 20x air lens (Alternatively, use 10x air lens) on a single plane. No Z-stacks or projections are needed.
16. Analyse comets using Comet Score Software.

Buffers:

Lysis Solution:
2.5M NaCl
0.1M EDTA
10mM Trizma Base
1% n-lauryl sarcosine
0.5% Triton X-100
10% DMSO
up to ph10.0

10x Electrophoresis Buffer:
500mM Trizma Base
2.5M sodium acetate
up to pH 9.0

DNA precipitation solution:
50mM NH_4Ac
85% EtOH

Proximity Ligation assay

1. Sterilize coverslips in a tissue culture dish for at least 15-20min under UV light.
2. Plate cells onto the coverslip.
   - For siRNA transfections see *siRNA transfection protocol*
   - For cells to be confluent the next day, plate 3-4x10^5cells/35mm dish (depending on the cell type)
3. Transfer coverslip directly from the media into a 6-well plate containing 1-2ml PBS.

PFA fixiation:

4. Remove excess PBS from the cells.
5. Carefully add 500µl 4% PFA to the edge of the coverslip and fix cells for 10min at RT.
6. Remove PFA and wash twice with 1-2ml PBS.
7. Add 1ml 0.25% Triton-X to the edge of the 6-well plate (to prevent washing the cells of the coverslip) and permeabilise for 2-10min at RT.
8. Remove Triton-X and wash twice in 1-2ml PBS.
9. Remove PBS and block cells with 1ml 1-3% BSA for 1hr at RT or at 4ºC overnight.

Primary antibody staining:

10. Prepare 1ºantibody mix (use appropriate concentration of the antibody).
11. Place 90µl 1ºantibody mix onto Parafilm in an IF box (protected from light).
12. Then carefully place the coverslip onto the antibody drop with the cells facing down. (To prevent the coverslips from drying out, place two moist tissues (soaked with ddH2O) inside the IF box.)
13. Incubate cells with the 1º antibody for 1hr at 37ºC.

14. Transfer the coverslips (cells facing up) back into the 6-well plate and wash three times with 1-2ml PBS.

Secondary Antibody staining:

15. Mix 20% PLA probe minus and 20% PLA probe plus with 1%BSA in a total reaction volume of 40µl. (I.e. 8µl PLA plus, 8µl PLA minus and 24µl 1%BSA per coverslip.) and incubate the mixture for 20min at RT.
16. Place 40µl PLA probe mix onto Parafilm in an IF box (protected from light).
17. Then carefully place the coverslip onto the antibody drop with the cells facing down. (To prevent the coverslips from drying out, place two moist tissues (soaked with ddH2O) inside the IF box.)
18. Incubate the coverslips for 1hr at 37ºC.
19. Transfer the coverslips (cells facing up) back into the 6-well plate and wash three times with 1-2ml Wash Buffer A.

Ligation and Amplification:

20. Dilute the Ligation stock 1:5 in water, then add the Ligase to the mix at a dilution of 1:40. (I.e. add 8µl Ligation mix to 31µl H_2O and then add 1µl Ligase per coverslip.)
21. Place 40µl of the Ligase mix onto Parafilm in an IF box (protected from light).
22. Then carefully place the coverslip onto the antibody drop with the cells facing down. (To prevent the coverslips from drying out, place two moist tissues (soaked with ddH2O) inside the IF box.)
23. Incubate the coverslips for 30min at 37ºC.
24. Transfer the coverslips (cells facing up) back into the 6-well plate and wash three times with 1-2ml Wash Buffer A.
25. Dilute the Amplification stock 1:5 in water, then add the Polymerase to the mix at a dilution of 1:80. (I.e. add 8µl Amplification mix to 31.5µl H_2O and then add 1µl Ligase per coverslip.)

26. Place 40µl of the Amplification mix onto Parafilm in an IF box (protected from light).
27. Then carefully place the coverslip onto the antibody drop with the cells facing down. (To prevent the coverslips from drying out, place two moist tissues (soaked with ddH2O) inside the IF box.)
28. Incubate the coverslips for 100min at 37ºC.
29. Transfer the coverslips (cells facing up) back into the 6-well plate, wash once with 1-2ml Wash Buffer B and twice with 0.01x Wash Buffer B.
30. Dry the coverslips at RT in the dark for 5-10min.
31. Mount the coverslips with mounting media containing DAPI and seal with nail varnish.
32. Analyse cells under the microscope using a 60x oil lens.

Buffers:

Wash Buffer A:
10mM Trizma Base
150mM NaCl
0.05% Tween-20
adjust to pH7.4

Wash Buffer B:
200mM Trizma Base
100mM NaCl
adjust to pH7.5

Appendix V: Publications

Contributions:

Figure 4a: Cell cycle analysis

Figure 6g: Cell proliferation assay

Figure 6h: Cell proliferation assay

Figure 6i: DR-GFP reporter assay

Rewriting and editing the manuscript

Editing of Figures

OPEN BIOLOGY

rsob.royalsocietypublishing.org

Research

Cite this article: Moureau S, Luessing J, Harte EC, Voisin M, Lowndes NF. 2016 A role for the p53 tumour suppressor in regulating the balance between homologous recombination and non-homologous end joining. *Open Biol.* **6**: 160225. http://dx.doi.org/10.1098/rsob.160225

Received: 28 July 2016
Accepted: 25 August 2016

Subject Area:
cellular biology/genetics/molecular biology/biochemistry

Keywords:
p53, 53BP1, BRCA1, non-homologous end joining, homologous recombination r, DNA double-strand break repair

Author for correspondence:
Noel Francis Lowndes
e-mail: noel.lowndes@nuigalway.ie

†These authors contributed equally to this study.

Electronic supplementary material is available online at https://dx.doi.org/10.6084/m9.figshare.c.3464592.

THE ROYAL SOCIETY PUBLISHING

A role for the p53 tumour suppressor in regulating the balance between homologous recombination and non-homologous end joining

Sylvie Moureau†, Janna Luessing†, Emma Christina Harte, Muriel Voisin and Noel Francis Lowndes

Genome Stability Laboratory, Centre for Chromosome Biology and School of Natural Science, Biomedical Science Building, National University of Ireland Galway, Dangan, Ireland

NFL, 0000-0002-3216-4427

Loss of p53, a transcription factor activated by cellular stress, is a frequent event in cancer. The role of p53 in tumour suppression is largely attributed to cell fate decisions. Here, we provide evidence supporting a novel role for p53 in the regulation of DNA double-strand break (DSB) repair pathway choice. 53BP1, another tumour suppressor, was initially identified as p53 Binding Protein 1, and has been shown to inhibit DNA end resection, thereby stimulating non-homologous end joining (NHEJ). Yet another tumour suppressor, BRCA1, reciprocally promotes end resection and homologous recombination (HR). Here, we show that in both human and mouse cells, the absence of p53 results in impaired 53BP1 focal recruitment to sites of DNA damage induced by ionizing radiation. This effect is largely independent of cell cycle phase and the extent of DNA damage. In p53-deficient cells, diminished localization of 53BP1 is accompanied by a reciprocal increase in BRCA1 recruitment to DSBs. Consistent with these findings, we demonstrate that DSB repair via NHEJ is abrogated, while repair via homology-directed repair (HDR) is stimulated. Overall, we propose that in addition to its role as an 'effector' protein in the DNA damage response, p53 plays a role in the regulation of DSB repair pathway choice.

1. Introduction

The p53 transcription factor is crucial for the maintenance of genome integrity [1,2]. Its role in tumour suppression has been largely associated with cell fate decisions upon damage with the potential to eliminate cancerous cells without affecting organismal integrity. Immediately after DNA damage, p53 regulates transient delays to cell cycle progression believed to allow cells greater time to repair genome damage prior to key cell cycle transitions, especially the transit from G1 into S phase. In the case of substantial DNA damage, p53 can regulate permanent exit from cell proliferation via either senescent or apoptotic mechanisms [2]. Interestingly, in the absence of crucial p53 target genes required for regulating the G1/S checkpoint, apoptosis and senescence, p53 retains some tumour suppressive functions, including genome stability [3], suggesting at least one further role for p53 in regulating tumour suppression. A candidate role could be direct regulation of DNA repair.

Cells have developed various strategies to respond to the many types of DNA damage [4]. Base excision repair (BER), nucleotide excision repair (NER), mismatch repair (MMR) and trans-lesion synthesis (TLS) are the four major pathways processing lesions affecting only one strand of the DNA [4,5]. The p53 protein has been implicated in all four of these pathways either through its role as a transcription factor of genes required for efficient single-strand break

repair or through direct protein–protein interaction with repair factors. It is worth noting that the role of p53 in BER could be cell-cycle-specific as it has been reported to enhance BER in G0 and G1, while being inhibitory in G2 and M phase [6]. With respect to DNA double-strand breaks (DSBs), p53 was shown in 1994 to interact with 53BP1, a DSB repair factor (discussed below), which interacts with the DNA binding domain of p53 through its BRCT domain and is reported to enhance p53 transcriptional activity [7–10].

DSBs are the most challenging and potentially harmful DNA lesions that a cell can encounter as genetic information can be altered through deletion, mutation or rearrangement. To repair these breaks cells have developed two principal repair mechanisms, one of which requires a homologous template and is termed homology-directed repair (HDR), also known as homologous recombination (HR) [11], while the other is homology independent and termed non-homologous end joining (NHEJ), or illegitimate recombination [12]. NHEJ-dependent repair catalyses the re-ligation of the broken DNA ends, sometimes with loss of one or more nucleotides resulting in error-prone repair. HDR occurs mainly during S and G2 when an intact sister chromatid is easily available as the preferred homologous template. In HDR, break detection is followed by one strand at each end being resected in the 5′ to 3′ direction resulting in a 3′ single-stranded DNA overhang that is initially coated by RPA and subsequently by RAD51. RAD51 is a recombinase that catalyses the search for intact homologous DNA sequences and subsequent strand exchange.

Conflicting results have been obtained when assessing the role of p53 in either HR or NHEJ. Using an episomal plasmid-based re-joining assay in mouse embryonic fibroblasts (MEFs), enhanced DNA end joining of short complementary ends in the presence of p53 has been reported [13], suggesting a role for p53 in the promotion of NHEJ. This *in vivo* role was supported by enhanced *in vitro* re-ligation of linearized plasmids in cellular extracts from p53 defective cells [14]. However, p53 has also been reported to downregulate NHEJ. For example, reduced NHEJ-dependent repair of I-*Sce1*-induced DSBs has been reported in the presence of p53 [15].

Involvement of p53 in HR is also subject to controversy. It has been suggested that p53 could suppress HR-dependent repair either through transcriptional repression of the HR factors RAD51 and BRCA1 or through direct protein–protein interactions with RPA, RAD51 and the RecQ helicases [6,16,17]. However, other studies did not observe any defect in the HR pathway in absence of p53 [18,19]. Recently, a model has been proposed suggesting crosstalk between the HR and NHEJ pathways regulated via phosphorylation of a p53-RPA complex by the PIKK kinases: ATR, ATM and DNA-PK [20]. These authors suggested that a low level of p53 is associated with RPA under non-stressed conditions, while upon DNA damage RPA is phosphorylated by DNA-PK and p53 is phosphorylated in an ATR-ATM-dependent manner. This resulting dissociation of the RPA-p53 complex was speculated to allow each protein to perform their respective functions in both DNA repair and cell cycle regulation.

The balance between DSB repair via either the HDR or NHEJ pathways has also been reported to be regulated via the DDR mediator proteins 53BP1 and BRCA1 [21–25]. While 53BP1 at DSBs inhibits DNA resection, thereby preventing HDR-dependent repair, BRCA1 recruitment to DSBs enhances the resection required for HDR [26,27]. The significance of reduced resection and consequently reduced HDR is that the increased genomic instability and cancer predisposition observed in *Brca1* knockout mice can be suppressed by co-deletion of *53Bp1* [21,28].

The rapid relocation of 53BP1 and BRCA1 to DSBs is easily monitored after ionizing radiation by the appearance of so-called ionizing radiation-induced foci (IRIF) within the nuclei of cells. Upon DNA damage, the histone variant H2AX is phosphorylated at serine 139. MDC1 binds directly to γH2AX and facilitates the recruitment of numerous components of the DNA damage response (DDR) including the E3-ubiquitin ligases, RNF8 and RNF168. Mono- and poly-ubiquitination of H2A-type histones in the vicinity of the DSB facilitate the recruitment and/or retention of 53BP1 and BRCA1-containing complexes [29–32]. Interestingly, 53BP1 recruitment requires the dynamic binding of its tandem Tudor domain with dimethylated histone H4 (H4K20me2), while its stable retention at chromatin surrounding DSBs requires a newly described ubiquitin-binding domain and RNF8/RNF168-dependent ubiquitination [33]. Lack of H4K20me2 has been reported to result in nearly complete abrogation of 53BP1 foci formation in HeLa cells for at least an hour after DNA damage induction [34–36]. In contrast, another study in MEFs has shown that lack of H4K20me2 results in a partial defect of 53BP1 IRIF exclusively during the first 5 min after DNA damage [37]. However, the different p53 status of the cell lines under investigation was not considered. In this respect, it is intriguing that other studies provide evidence for accumulation of p53 at sites of DNA damage—specifically, a form of p53 that is dimethylated on lysine 382 (p53K382me2) after DNA damage [38,39]. Furthermore, p53K382me2 was reported to have increased affinity for the tandem Tudor domain of 53BP1 [38,40].

Here, using human and primary mouse cell lines, we demonstrate that p53 regulates the recruitment of 53BP1 to sites of DSBs. In the absence of p53, recruitment of 53BP1 is less efficient, especially in G1 and early S phase, while recruitment of BRCA1 to DSBs is reciprocally promoted by lack of p53. Consistent with these results, recruitment of the RAD51 recombinase to sites of DSBs is also increased while recruitment of MDC1, which functions upstream of both BRCA1 and 53BP1, is not affected. We provide further support for the enhanced HDR implied by increased RAD51 recruitment to DSBs in p53-defective cells and through monitoring DSB repair in cells treated with specific topoisomerase inhibitors. Furthermore, we show decreased sensitivity to PARP inhibitors and increased rates of HDR in p53-depleted cells. Our study highlights a regulatory role for p53 early in the DDR in the regulation of the appropriate balance between competing DSB repair pathways. Specifically, we suggest that p53 is required for fine-tuning the balance between the recruitment of competing tumour suppressors, 53BP1 and BRCA1, to DSBs.

2. Results

2.1. Efficient recruitment of 53BP1 into ionizing radiation-induced foci requires p53

The Tudor domain of 53BP1, required for 53BP1 recruitment to DSBs, has also been reported to bind to a dimethylated lysine on the C-terminal of p53 (p53K382me2), suggesting a role for p53 at DSBs [38,40]. To assess whether p53 could

regulate the recruitment of 53BP1 to DSBs, we assayed 53BP1 ionizing radiation-induced foci (IRIF) formation in human HCT116 WT and isogenic p53-null cells [1]. While expression of 53BP1 is normal in these p53-null cells, p53 cannot be detected either before or after IR (figure 1*a*,*b*). We detected significantly fewer and less intense 53BP1 IRIF in p53-null cells compared with the WT, whereas γH2AX foci were not affected by loss of p53 (figure 1*c*; electronic supplementary material, figure S1). Quantification of the number of foci per cell revealed fewer detectable 53BP1 IRIF in *TP53*$^{-/-}$ HCT116 cells (figure 1*d*), whereas the number of γH2AX IRIF was not significantly different between either cell line (figure 1*e*). This defect in 53BP1 IRIF could also be detected by quantifying focal intensity (figure 1*f*). The ratio of average focal intensity per cell between the two cell types revealed that 53BP1 IRIF were significantly brighter relative to p53-null cells across the time course used, whereas γH2AX IRIF were not more intense in WT relative to p53-null cells.

We also examined the recruitment of mouse 53Bp1 into IRIF using early passage MEFs (either WT or null) for p53 (figure 2). Mouse 53Bp1 is expressed normally in these *TRP53*$^{-/-}$ MEFs both before and after irradiation (figure 2*a*), whereas p53 could not be detected in p53-null cells, as expected (figure 2*b*). Similarly, to our results in human HCT116 cells, early passage MEFs also displayed deficient IRIF formation of mouse 53Bp1 in p53-null relative to WT cells (figure 2*c*). In MEFs, the number of detectable 53Bp1 IRIF is significantly reduced in p53-deficient MEFs relative to WT within the first 2 h after IR (figure 2*c*,*d*), whereas γH2AX foci remained unaffected by p53 status (figure 2*e*; electronic supplementary material, figure S2). In addition to reduced 53Bp1 focal number, 53Bp1 focal intensity was weaker in MEFs deficient for p53 compared with WT cells in the first 2 h after IR (figure 2*f*). As 53BP1 expression is unaffected by the status of the p53 transcription factor (figures 1*a* and 2*a*) our data are consistent with a role for p53 in the efficient recruitment of 53BP1/53Bp1 to sites of DNA damage in both human and mouse cell types.

2.2. p53 is required for efficient 53BP1 IRIF formation irrespective of the extent of DNA damage

The function of both p53 and 53BP1 can vary depending upon the degree of DNA damage inflicted on cells. Reparable levels of DNA damage result in p53-dependent transient arrests to cell proliferation, whereas p53 also regulates cellular senescence or apoptosis presumably after higher levels of DNA damage [42]. Similarly, 53BP1 depletion has been reported to result in a defective G2/M checkpoint at low (3 Gy) but not high (10 Gy) IR doses [43]. In addition, 53BP1 has been shown to facilitate the phosphorylation of CHK2 specifically at IR doses below 5 Gy [44]. In chicken DT40 cell lines clonogenic survival of *53Bp1* null cells displayed IR sensitivity only below 4 Gy IR [45,46]. Therefore, we followed the IR dose response of 53BP1 recruitment into foci with respect to p53 status (figure 3). Across all doses used, from low- (1 Gy) to high-dose (10 Gy) irradiation, p53-null HCT116 cells presented with both reduced numbers of detectable 53BP1 foci and weaker 53BP1 focal intensity compared with WT cells at 30 min after irradiation (figure 3*a*–*c*). Thus, the role of p53 in the efficient recruitment of 53BP1 into foci after ionizing radiation is dose independent.

2.3. p53-dependent regulation of 53BP1 IRIF is independent of the upstream mediator, MDC1

The recruitment of 53BP1 to chromatin in the proximity of DSBs results from a complex cascade of events involving the MDC1 mediator protein [47]. Specifically, in the absence of MDC1, 53BP1 IRIF formation is strongly decreased [48,49]. To determine whether p53-dependent regulation of 53BP1 IRIF occurs upstream of MDC1, we examined focal recruitment of MDC1 after IR. Depletion of p53 in HCT116 cells did not alter the recruitment of MDC1 to DNA lesions (electronic supplementary material, figure S3*a*). Neither the number nor the intensity of MDC1 IRIF was affected by the absence of p53 (electronic supplementary material, figure S3*b*,*c*). These data are consistent with p53-dependent regulation of 53BP1 IRIF formation and/or retention being downstream of the role of MDC1.

2.4. p53 regulates 53BP1 IRIF formation in a cell-cycle-dependent manner

It has been shown previously that upon DNA damage, 53BP1 IRIFs were larger and more intense in G0 and G1 cells, and their intensity progressively decreases during the subsequent phases of the cell cycle [24]. Less numerous and reduced intensity 53BP1 IRIF in p53-null cells are not likely to reflect a faster transit through the early phases of the cell cycle as cell cycle profiles of exponentially growing WT and p53-null HCT116 cells are very similar for at least 8 h after IR (figure 4*a*). Twenty-four hours after IR p53-null cells display a reduced proportion of cells in G1. However, as the p53-dependent defect in human 53BP1, as well as mouse 53Bp1, we observed are both well within 8 h, this defect cannot be explained by a lower proportion of G1 cells in p53-null cells.

To further assess whether cell cycle phase impacts on the role of p53 in the efficient recruitment of 53BP1 into IRIF, asynchronous WT and p53-null HCT116 cells were irradiated and 53BP1 foci formation monitored alongside PCNA and ZWINT, two cell-cycle-phase-specific markers. ZWINT is required for kinetochore assembly and can be observed as foci primarily in G2 [50]. PCNA is required for DNA replication and can be observed during the S phase in distinct focal staining patterns specific for early, mid and late stages of DNA replication. Exponentially growing cells negative for ZWINT or PCNA staining are in G1 phase. Consistent with the observations of Chapman *et al.* [24] in WT cells, we observed more efficient recruitment of 53BP1 into IRIF at early stages of the cell cycle, specifically in G1 and early S phase (figure 4*b*,*c*). The average intensity of 53BP1 foci decreased steadily, reaching a minimum in G2 phase (figure 4*c*). In the absence of p53, 53BP1 focal intensity was also observed to be at its maximum early in the cell cycle, decreasing steadily as cells progressed through S phase and into G2 as observed in WT cells. However, although the effect is most notable early in the cell cycle when 53BP1 foci are most prominent, the intensity of 53BP1 foci in *TP53*$^{-/-}$ cells is reduced relative to WT cells at all cell cycle stages (figure 4*c*). Thus, p53-dependent regulation of 53BP1 IRIF formation is largely independent of the cell cycle stage.

2.5. BRCA1 recruitment to DSBs is restrained by p53

There is a reciprocal relationship between 53BP1 and BRCA1 localization to DSBs [24]. 53BP1 is also known to negatively regulate HR by inhibiting DNA end resection, while

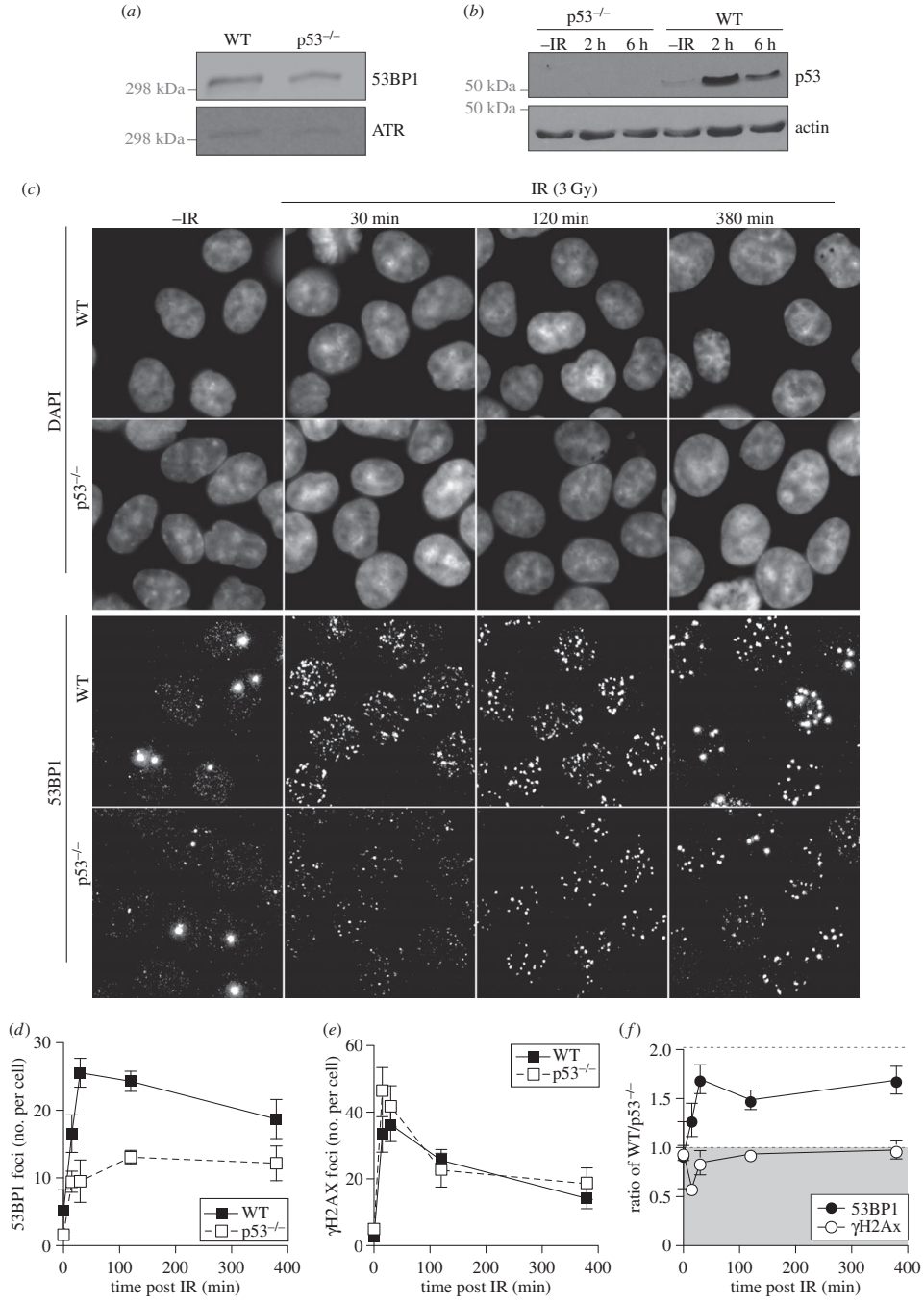

Figure 1. p53 promotes 53BP1 recruitment to DNA damage sites in human HCT116 cells. (*a*) 53BP1 protein levels in whole cell extracts prepared from either WT or p53-null HCT116 cells were analysed by western blotting. (*b*) p53 protein level in whole cell extracts from WT and p53-null HCT116 cells either before or after IR exposure (3 Gy) were analysed by western blotting. (*c*) Detection of endogenous 53BP1 by immunofluorescence in WT and p53-null HCT116 cells. Cells were either mock treated or irradiated with 3 Gy and allowed to recover for the indicated times before being fixed, stained with 53BP1 antibody and visualized on a Deltavision microscope. Note that large bright foci in unirradiated cells are 53BP1 nuclear bodies. (*d*) Quantification of the number of 53BP1 foci. (*e*) Quantification of the number of γH2AX foci. (*f*) Ratio of 53BP1 and γH2AX focal intensity in WT cells relative to p53-null HCT116 cells.

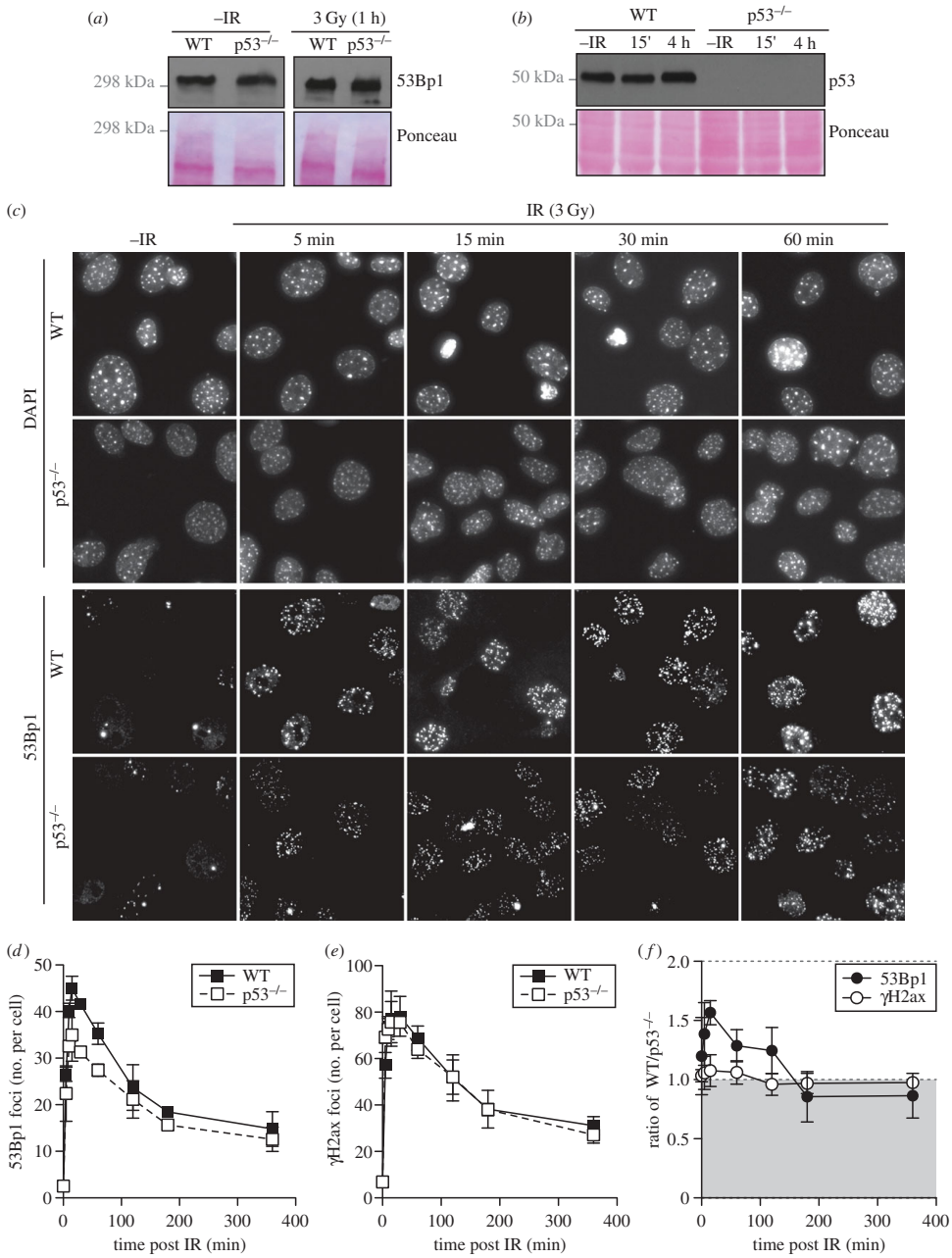

Figure 2. p53 promotes 53Bp1 recruitment to DNA damage sites in MEFs. (*a*) Mouse 53Bp1 protein levels in whole cell extracts prepared from WT or p53-null MEF cells either before or after IR exposure (3 Gy) were analysed by western blotting. (*b*) p53 protein levels in whole cell extracts from WT and p53-null MEF cells either before or after IR exposure (3 Gy) were analysed by western blotting. Note that in early passage MEFs, but not later passage nor transformed MEFs, high levels of p53 are detected irrespective of damage [41]. (*c*) Detection of endogenous mouse 53Bp1 by immunofluorescence in WT and p53-null MEFs. Cells were irradiated with 3 Gy, fixed at the indicated time and stained with 53Bp1 antibody. Note that the focal structures detected in MEFs by DAPI staining are heterochromatic foci. (*d*) Quantification of the number of 53BP1 foci. (*e*) Quantification of the number of γH2AX foci. (*f*) Ratio of γH2AX and 53Bp1 focal intensity in WT cells relative to p53-null MEFs.

BRCA1 promotes end resection [21,23,25,51]. Furthermore, the recruitment of 53BP1 to DSBs is associated with an exclusion of BRCA1 from sites of DNA damage [24,52].

To investigate the effect of p53 status on BRCA1 recruitment to DSBs, we evaluated BRCA1 IRIF in WT and isogenic p53-null HCT116 cells (figure 5*a*). BRCA1 also

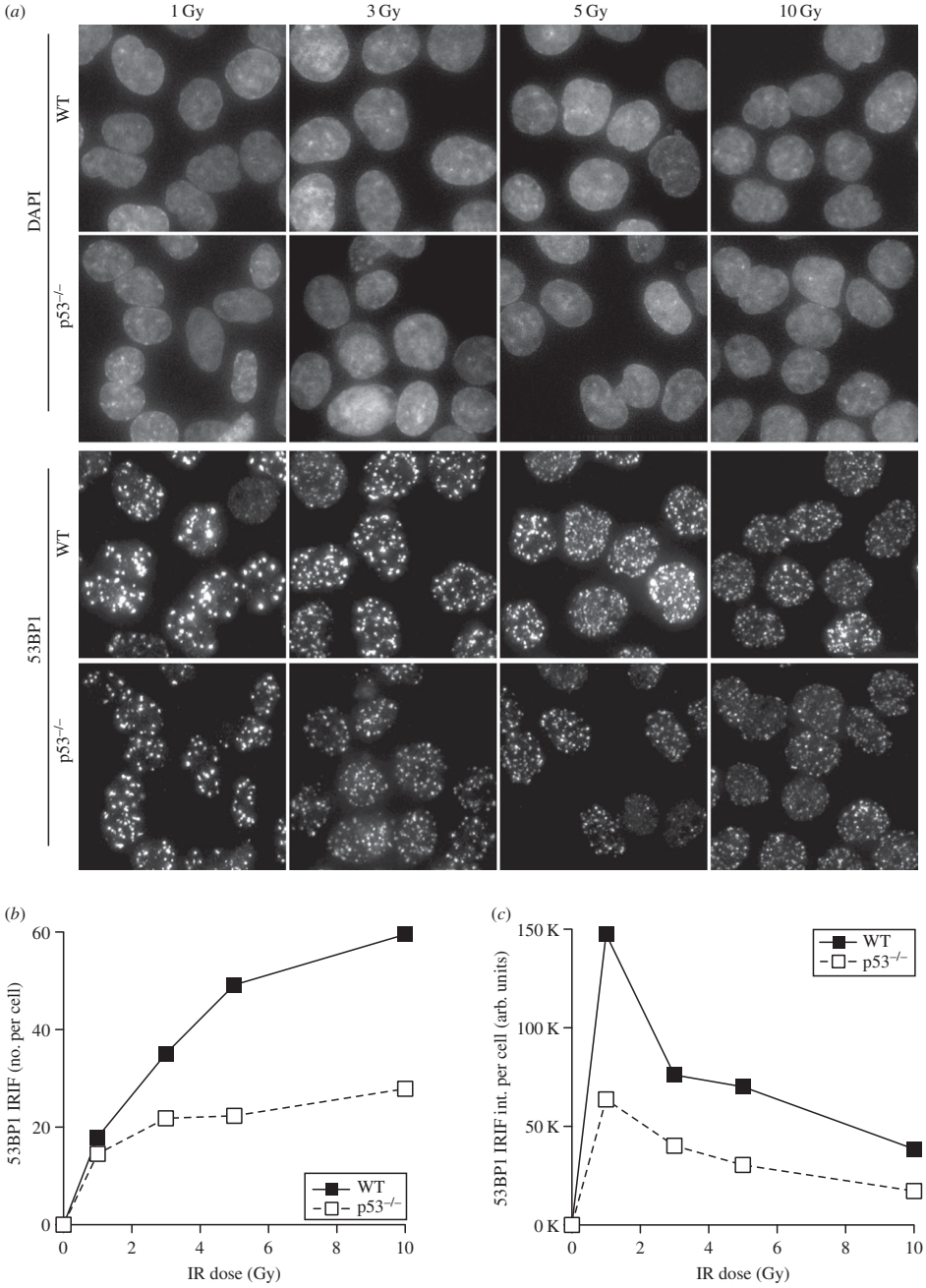

Figure 3. p53 promotes 53BP1 recruitment to DNA damage sites independent of IR dose. (*a*) Detection of endogenous 53BP1 by immunofluorescence in WT and p53-null HCT116 cells. Cells were irradiated, fixed after 30 min of recovery and then stained with 53Bp1 antibody. (*b*) Quantification of 53BP1 IRIF number. (*c*) Quantification of 53BP1 IRIF intensity.

form focal structures in S phase cells [53] and, consistent with the similar cell cycle profiles of WT and p53-null cells (figure 4*a*,*b*), in both cell types about one-third of the exponentially growing unirradiated cells display BRCA1 foci (figure 5*b*). After irradiation, and as before (figure 1), while p53-null cells display reduced 53BP1 foci intensity (figure 5*a*,*c*), the proportion of cells displaying BRCA1 foci is greater in p53-null cells at both 2 and 4 h after IR

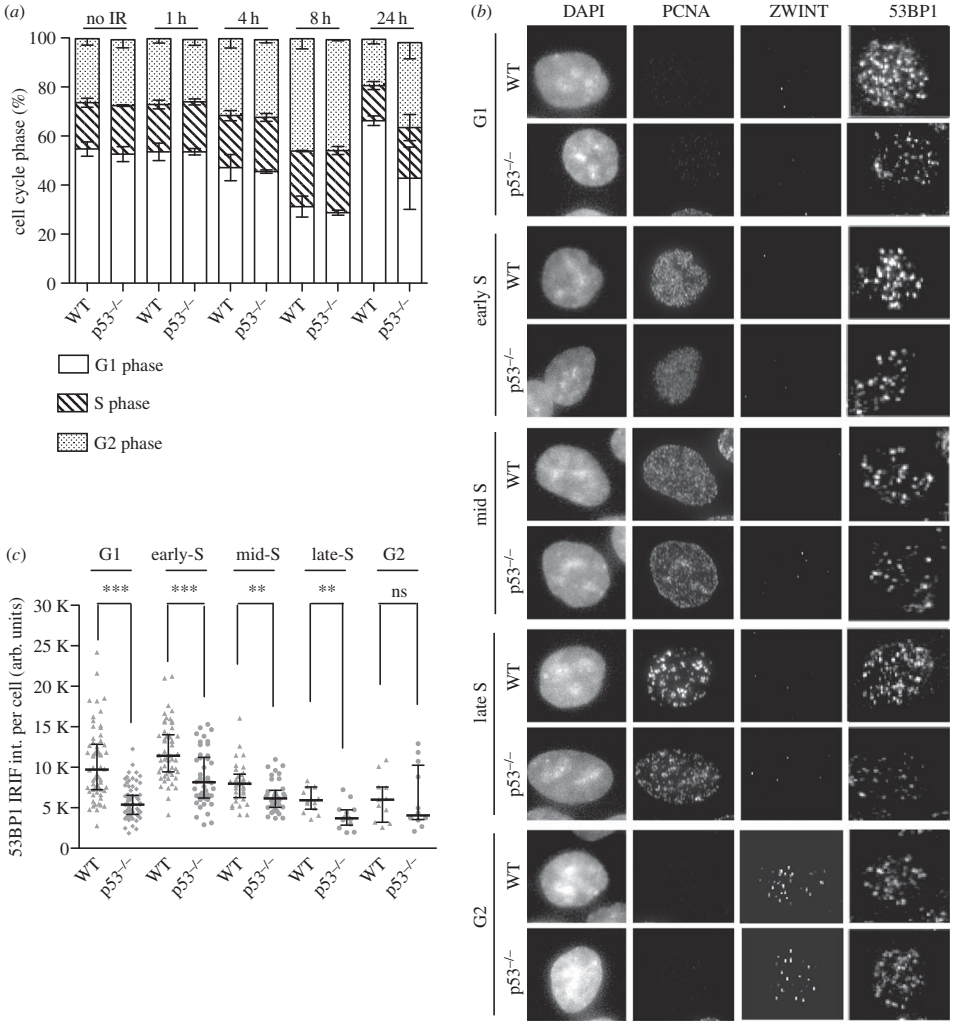

Figure 4. p53 regulation of 53BP1 IRIF is independent of cell cycle stage. (*a*) Quantification of the proportion of cells in each phase of the cell cycle before and after IR at the indicted times. (*b*) Detection of endogenous 53BP1 and classification with respect to cell cycle phase for each cell type analysed. S phase cells are PCNA positive, G2 phase cells are ZWINT positive, while G1 phase cells are negative for both PCNA and ZWINT. (*c*) Quantification of 53BP1 focal intensity for each cell analysed in its respective phase of the cell cycle. In total, 175 cells were scored for each cell type. Each dot represents a single cell. ***$p < 0.0001$, **$p < 0.001$, Mann–Whitney test.

(figure 5*a*,*b*). These data are consistent with p53 being a positive regulator of 53BP1 recruitment into IRIF, with 53BP1 in turn being a negative regulator of BRCA1 IRIF.

BRCA1 protein levels at late times (12–24 h) after irradiation have been reported to be p53-dependent [54]. Even though the time points after irradiation used in our study are much earlier, we nevertheless compared BRCA1 protein levels in response to IR at these early time points. We could not detect a change in BRCA1 protein levels 1 or 2 h after irradiation (figure 5*d*). Therefore, the enhanced recruitment of BRCA1 in p53-null cells is unlikely to result from altered expression of BRCA1 at early time points. Rather, it is consistent with the reduced recruitment of 53BP1, a known negative regulator of BRCA1, to DSBs at early time points.

2.6. p53 restrains DNA double-strand break repair via homologous recombination while promoting non-homologous end joining

Our data are consistent with a role for p53 in the promotion of 53BP1 recruitment to DSBs, which in turn restricts the accumulation of BRCA1. As BRCA1 facilitates repair of DSBs by HR, increased BRCA1 at sites of DNA damage in p53-null cells would be expected to result in increased HDR. Consistent with this reasoning, analysis of the formation of RAD51 foci revealed that the percentage of cells positive for RAD51 foci, as well as the number of RAD51 foci per cell, is increased in the absence of p53 (figure 6*a*,*b*).

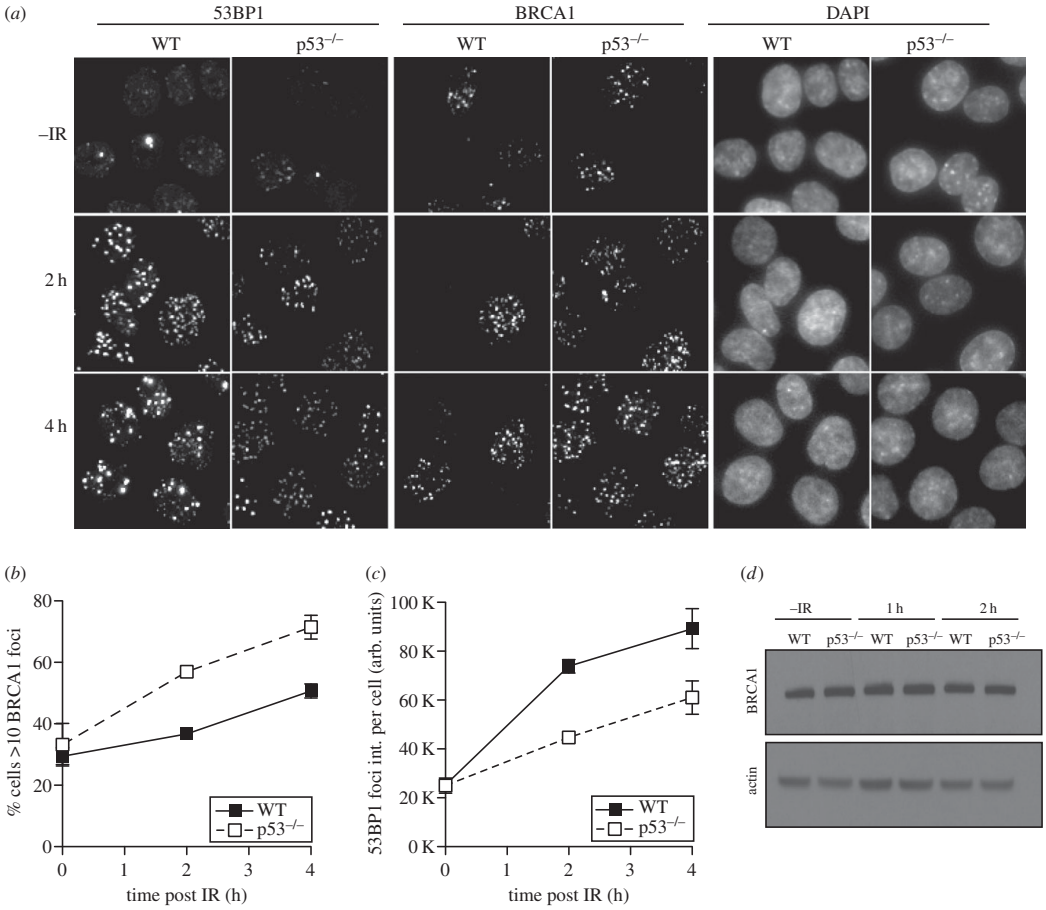

Figure 5. Loss of p53 results in increased recruitment of BRCA1 to DSBs. (*a*) Localization of endogenous 53BP1 and BRCA1 by immunofluorescence in HCT116 WT and p53-null cells before and after irradiation (3 Gy). (*b*) Quantification of the proportion of cells with more than 10 BRCA1 foci per cell. (*c*) Quantification of the intensity of 53BP1 foci per cell. (*d*) Western blot analysis of BRCA1 protein levels in WT and p53-null HCT116 cells at the indicated time points after IR (3 Gy).

To further investigate DNA repair in WT versus p53-null cells, we performed neutral comet assays to measure the resolution of DSBs induced by treatment of cells with camptothecin (CPT), an inhibitor of topoisomerase I. The collision of replication forks with CPT-induced lesions generates one-ended DSBs that are a preferential substrate for HDR [11,56]. Therefore, in asynchronously growing cell populations, it is mostly cells in S phase that present with γH2AX foci after CPT treatment. While 1 h of CPT treatment induces similar extents of DNA damage in both WT and p53-null cells, after removal of CPT, DSBs induced by this drug were progressively repaired (figure 6*c*,*d*). However, consistent with enhanced homology direct repair in the absence of p53, repair of CPT-induced lesions was completed more efficiently in p53-null cells relative to WT cells.

To investigate the role of p53 in DSB repair via the NHEJ pathway we used etoposide (ETO), an inhibitor of topoisomerase 2, reported to induce DSBs that are primarily repaired by NHEJ [12]. After 1 h of ETO treatment DSBs were assayed by neutral comet assay (figure 6*e*,*f*). The treatment resulted in similar levels of damage in both WT and p53-null cells; while repair of these ETO-induced DSBs was achieved rapidly in WT cells (within 15 min of ETO removal), in p53-null cells DSB repair was much less efficient, being still incomplete 1 h after treatment. Thus, while HDR-dependent repair of CPT-induced DSBs is more efficiently repaired in p53 defective cells, the opposite is true of NHEJ-dependent repair of ETO-induced DSBs as these lesions are less efficiently repaired in p53 defective cells.

To further assess HDR in WT and p53-null cells, we examined cell proliferation in the presence of Olaparib, an inhibitor of PARP inhibitor (figure 6*g*). PARP is required for efficient repair of single-stranded breaks (SSBs) and its inhibition results in conversion of SSBs into DSBs that are primarily repaired via HDR [57,58]. Thus, sensitivity to PARP inhibition can be used as a read-out for defective HDR. *TP53*$^{-/-}$ cells proliferated more rapidly in the presence of a range of Olaparib concentrations than did WT cells, as would be expected for cells with greater capacity for HDR. We also combined low-level PARP inhibition with increasing concentration of CPT (figure 6*h*). Consistent with previous reports using a different PARP inhibitor, KU58948 [59], p53-null cells displayed enhanced proliferation relative to WT cells both in the absence or presence of Olaparib.

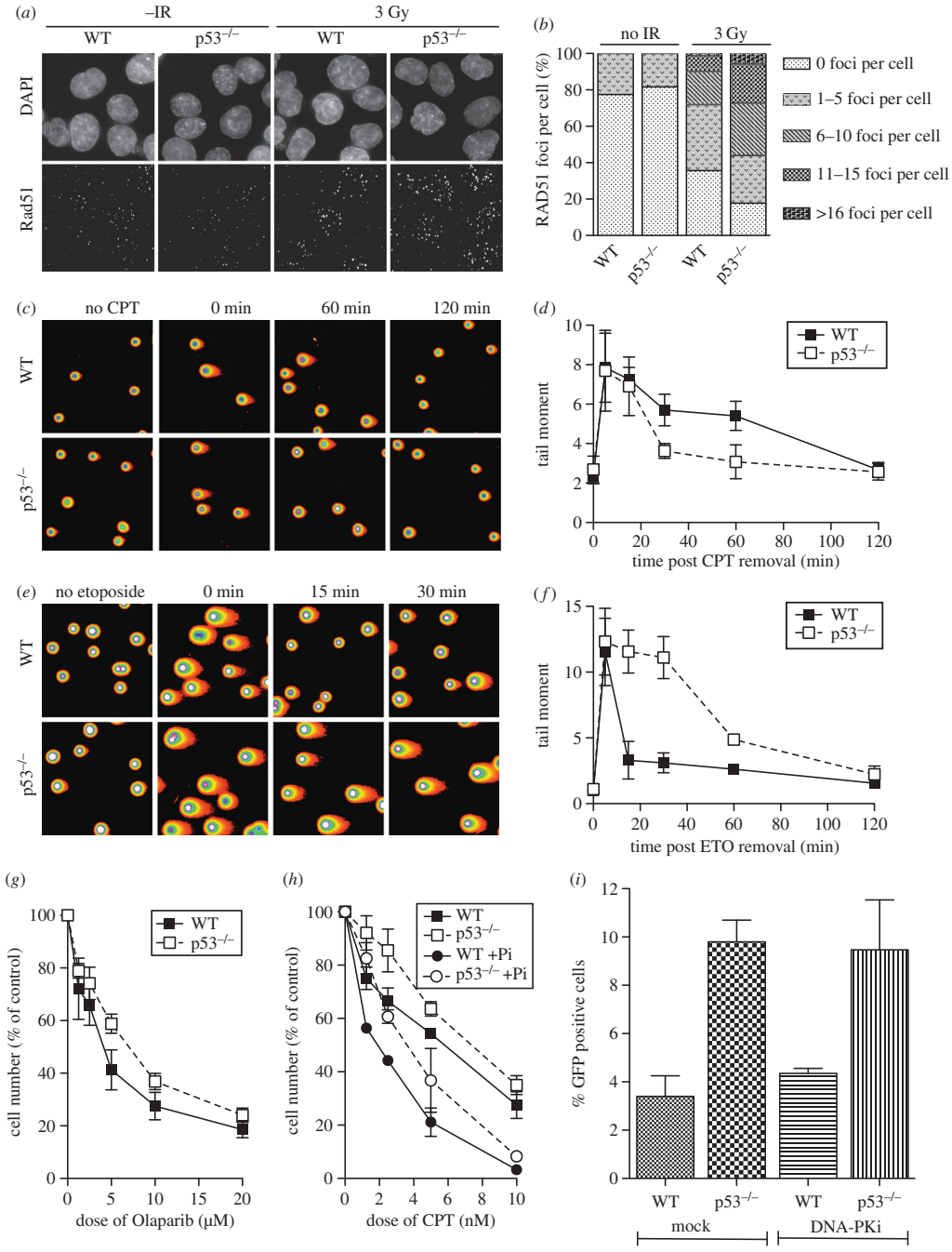

Figure 6. p53 inhibits HR and promotes NHEJ. (*a*) Detection of endogenous RAD51 in HCT116 WT and p53-null cells by immunofluorescence 5 h after irradiation (3 Gy). (*b*) Quantification of the numbers of RAD51 foci per cell for the indicated categories. (*c*) Representative images of a neutral comet assay (spectrum view) for WT and p53-null HCT116 cells after release from a 1 h camptothecin (CPT) treatment for the indicated times. (*d*) Quantification of CPT-induced DSBs analysed by comet assay. (*e*) Representative images of a neutral comet assay (spectrum view) for WT and p53-null HCT116 cells after release from a 1 h etoposide (ETO) treatment for the indicated times. (*f*) Quantification of ETO-induced DSBs analysed by comet assay. (*g*) Proliferation of WT and p53-null HCT116 cells in the presence of the indicated doses of Olaparib, an inhibitor of PARP. (*h*) Proliferation of WT and p53-null HCT116 cells in the presence of the indicated doses of CPT. Cells were grown in the presence of absence of 1 μM Olaparib, as indicated. (*i*) Modified GFP reporter assay for HR [55]. The percentage of live, transfected, GFP-positive cells in HCT116 WT and p53-null cells is shown. Cells were also subjected to inhibition of DNA-PK, as indicated.

Finally, in order to directly investigate the efficiency of HDR, we transiently transfected pDR-GFP, a GFP reporter construct specific for HDR [55], into WT and p53-null cell lines (figure 6*i*). Relative to WT, an increased efficiency of HDR in p53-null cells was measured. Interestingly, the efficiency of HDR in WT cells could be stimulated, as expected, by inhibition of the competing NHEJ pathway (using NU7026, an inhibitor of DNA-PK). However, a further increase in HDR efficiency was not observed when p53-null cells were treated with NU7026, suggesting that HDR has reached its full capacity under these conditions.

Our data are consistent with p53 reciprocally regulating the two major pathways of DSB repair. Specifically, p53 is a positive regulator of NHEJ but a negative regulator of HDR, suggesting that p53 is required for fine-tuning the balance between these two competing pathways of DSB repair.

3. Discussion

The mechanism behind 53BP1 recruitment to DSBs is still not fully characterized. Earlier studies established roles for both the 53BP1 oligomerization and Tudor domains for its recruitment into foci after ionizing radiation [60]. A more recent study has established that stable retention of 53BP1 at chromatin surrounding DSBs requires a newly described ubiquitin-binding domain and RNF8/RNF168-dependent ubiquitination [31]. With respect to the 53BP1 Tudor domain, two distinct histone modifications, H3K79me2 and H4K20me2, have been reported to be required for 53BP1 recruitment to sites of DNA damage [34,61]. While the relationship between H3K79me2 and 53BP1 recruitment to chromatin in the proximity of DSBs remains unclear, lack of H4K20me2 is consistently associated with a defect in 53BP1 recruitment to DSBs. However, the extent of the 53BP1 recruitment defect reported in H4K20me2-deficient cells varies between studies. In HeLa cells, it has been shown that lack of H4K20me2 abrogates 53BP1 foci formation for at least an hour following IR treatment [34–36], while in MEFs depleted for H4K20me2, 53BP1 foci formation was merely delayed for the first 5 min post-IR treatment [37]. Interestingly, one noteworthy difference between the two cell lines used in these studies is their p53 status, with MEFs being WT for p53 while HeLa cells are defective for p53 function.

A complex between 53BP1 and p53 was originally shown to be associated with upregulation of p53 transcriptional activity [9]. More recently, a newly identified post-transcriptional modification of p53, p53K382me2, has been shown to have affinity for the 53BP1 tandem Tudor domain and is induced upon DNA damage [38,40]. These authors suggested that the presence of 53BP1 at DSBs might help to recruit and stabilize p53 at DSBs in order to regulate p53 functions that are independent of its known transcriptional transactivation activity.

In this study, we observed that the formation of 53BP1 foci at DSBs is abrogated in the absence of p53 in both human and mouse cells. This p53-dependent defect in 53BP1 ionizing radiation-induced foci (IRIF) was IR dose-independent, while 53BP1 protein levels were unaffected by the absence of p53, suggesting a regulatory role for p53 in recruitment of 53BP1 into IRIF. We found that loss of p53 resulted in defective accumulation of 53BP1 into IR-induced foci that was both immediate and persistent in both human and mouse cells. This contrasts with a report showing that MEFs defective for the histone H4K20me2 modification but WT for p53 displayed only a modest defect, restricted to just the first 5 min after irradiation, in 53BP1 recruitment into IRIF [37].

Although many details remain to be deciphered, our data are consistent with a model in which the recruitment of 53BP1 to DSBs involves complex steps that require both direct interactions with histones, as well as interactions with non-histone proteins. The initial histone-dependent process involves dynamic interactions between the Tudor domain of 53BP1 and a constitutive chromatin mark, H4K20me2, that may be more easily accessed around DSBs [62]. This initial histone-dependent interaction is then stabilized via another histone-dependent interaction between the recently described 53BP1 ubiquitin-binding domain and RNF168-dependent ubiquitination of H2A-type histones, an interaction that also requires 53BP1 oligomerization [31]. Finally, 53BP1 retention at DSBs also requires the damage-inducible γH2AX modification [49]. Our data suggest that in addition to these directly histone-dependent processes, p53 also plays a role in the accumulation and stabilization of 53BP1 at DSBs.

The defect in p53-dependent 53BP1 accumulation at DSBs is prevalent in G1 and early S phase, and then progressively diminishes in mid and late S phase, becoming minimal in G2. The G1 and early S phases correspond to the predominant phase of the cell cycle for the NHEJ repair. Although only relevant to DSBs that do not remain in close proximity, one reported mechanism by which 53BP1 promotes NHEJ is enhancing the mobility of broken chromatids [22]. Of more relevance to all DSBs, 53BP1 is also known to decrease HDR by downregulating DNA end resection [21–23]. Indeed, this initial step in the HDR pathway is dependent upon the balance between 53BP1 and the BRCA1 protein that promotes the resection of DNA ends [21]. It has been shown using super-resolution microscopy that recruitment of BRCA1 into IRIFs correlates with exclusion of 53BP1 away from the focal core and towards its periphery [24]. Consistent with this observation, we observed that the abrogation of 53BP1 IRIF in the absence of p53 is accompanied by enhanced BRCA1 foci formation, which in turn resulted in increased formation of RAD51 IRIF.

We confirmed a role for p53 in regulating DSB repair by demonstrating that DSB repair of CPT-induced lesions, which are preferentially repaired by HR, were more efficiently repaired in the absence of p53. Correspondingly, p53-deficient cells are more efficient at repairing ETO-induced lesions that are preferentially repaired by NHEJ. Additionally, they are less sensitive to PARP inhibition and exhibit elevated levels of HDR. Altogether, our results suggest a new function for p53 as a regulator of the balance between HDR and NHEJ through its stimulation of efficient recruitment of 53BP1 to sites of DNA damage. The requirement for p53 in the efficient recruitment of 53BP1 into IRIF is most striking in G1 and early S phase of the cell cycle. As reduced 53BP1 recruitment is accompanied by a reciprocal increase in BRCA1 recruitment it is likely that inappropriate upregulation of HDR, despite being an error-free pathway, could be threatening for genome integrity. In G0 and G1 cells, the absence of a homologous sister chromatid could result in the loss or even rearrangement of genetic information.

Discovered over 35 years ago and regarded as a ‘guardian of the genome’, p53 is one of the most studied yet functionally complex proteins in biochemistry. With respect to its roles in the DDR, these are largely as ‘effectors’ of transient cell cycle delays and cellular fate. Our results highlight a new role for

p53 in 'mediating' early events of the DDR important for regulating the balance between DSB repair pathways.

4. Material and methods

4.1. Cell culture and transfection

HCT116 and p53-null (*TP53*$^{-/-}$) derivative cells were supplied by B. Vogelstein [63]. HCT116 cells were grown in DMEM media with 10% FBS (Lonza) and 1% PenStrep (Sigma). MEFs and *Trp53*-null (*Trp53*$^{-/-}$) derivative cells were a gift from S. Jones (University of Massachusetts). MEFs were grown in DMEM media supplemented with 15% FBS and 1% PenStrep.

4.2. Cell extracts and western blotting

Harvested cells were washed in cold PBS, resuspended in sample buffer (5 µl 5 × SB per 2 × 10^5 cells), lysed by heating at 95°C for 10 min, sonicated (40% amplitude, 10 s, Branson 250 Sonicator) and heated at 95°C for a further 10 min. Lysed extracts were subject to SDS-PAGE and transferred to nitrocellulose membranes by electroblotting. The membranes were blocked with 4% milk, incubated overnight with 1° antibody as indicated, washed and incubated with HRP-coupled secondary antibodies as relevant. Antibodies used for western blotting were anti-53BP1 (Novus #NB100-904, 1/1000), anti-γH2AX (Millipore #05-636, 1/2000), anti-BRCA1 (Santa Cruz, D-9 #sc6954, 1/500), anti-p53 (Cell Signalling, #9282, 1/1000), anti-p53 DO1 (Santa Cruz, #sc-126, 1/1000) and anti-ATR (Santa Cruz, #sc-1887, 1/2000).

4.3. Immunofluorescence and microscopy

Human HCT116 cells or mouse MEFs, either WT or null for p53, were fixed with 4% PFA and permeabilized with 0.125% of Triton-X100. After briefly blocking in 4% BSA, cells were incubated for 1 h at 37°C with 1° antibody, washed and incubated for 1 h at 37°C with 2° antibody. Slides were mounted using Vectashield mounting media with DAPI (Vector Laboratories). The following antibodies were used for Immunofluorescence staining: anti-53BP1 (Novus Biological, #NB100-904, 1/400), anti-γH2AX (Millipore, #05-636, 1/200), anti-BRCA1 (Santa Cruz, #sc6954, 1/500), anti-PCNA (Kevin Sullivan, CCB), anti-ZWINT (Kevin Sullivan, CCB) and anti-RAD51 (Abcam, #ab63801, 1/200). Microscopy imaging was performed on a Deltavision microscope using SoftWoRx software (Applied Precision, Issaquah). Z-stacks (0.5 µm) were collected, deconvolved and projected. Quantification of foci was performed using Image-Pro Analyser software (MediaCybernetics).

4.4. Cell cycle analysis

HCT116 WT or *TP53*$^{-/-}$ cells were plated at 2 × 10^5 cell per 35 mm dish and grown for 24 h prior to treatment. Cells were then treated with 25uM BRDU for 1 h, washed with PBS and fresh media was added. Cells were then γ-irradiated (3 Gy) with a caesium-137 source (Mainance, UK), harvested at the indicated times, fixed in 70% ice-cold ethanol, washed with PBS and the DNA was denatured using 2N HCl for 10 min before being stained with anti-BRDU antibody (B-D, Ca #347580) for 1 h and anti-mouse secondary for 1 h. Cells were then stained with propidium iodide solution (PI) (40 µg ml^{-1} of PI (Sigma) and 250 µl ml^{-1} of RNAse A (Qiagen) in PBS) for 30 min in the dark. The analysis was performed using BD FACSCantoII and BD FACSDiva software (BD Biosciences).

4.5. Comet assay

Cells were treated with 1.25 µM CPT or 50 µM ETO for 1 h, washed with PBS then collected at the indicated time of recovery. The neutral comet assay method was adapted from the manufacturer's instructions (Trevigen). Cells were harvested, combined with LMA agarose (Trevigen) at a concentration of 1 × 10^5 cells ml^{-1} and loaded on polylysine slides. The slides were incubated at 4°C in the dark for 30 min to allow the agarose to set. Cell lysis was performed by placing the slides in ice-cold lysis buffer overnight and neutralized in neutral electrophoresis buffer for 30 min. Slides were then place in an electrophoresis chamber and run for 1 h at 24 V corresponding to 1 V cm^{-1} between electrodes. Cells trapped in agarose were treated with DNA precipitation buffer and washed with 70% ethanol. Slides were allowed to dry at 37°C before staining with SyBR-green and visualized by microscopy. COMET analysis was performed using the software CometScore from Tritek Corporation.

4.6. Cell proliferation assays

HCT116 WT or *TP53*$^{-/-}$ cells were plated at 2 × 10^5 cell per 35 mm dish 24 h prior to treatment. For Olaparib treatment, new media containing the drug at the indicated concentrations was added to the cells and the cells were cultured for 48 h. After 48 h of drug treatment, cells were trypsinized and re-plated in drug-free media onto two 35 mm dishes to ensure optimal growth conditions. After culturing for a further 48 h in drug-free media, cells were harvested by trypsinization and counted. For campthotecin (CPT) treatment, fresh media containing the drug at the indicated concentrations was added to the cells. Addition of PARP inhibitor (1uM Olaparib) was as indicated and the cells were grown for a further 48 h. Cells were then trypsinized and re-plated in drug-free media onto two 35 mm dishes to ensure optimal growth conditions for a further 48 h after which cells were harvested by trypsinization and counted.

4.7. GFP reporter assays

HCT116 WT or *TP53*$^{-/-}$ cells were plated at 1 × 10^6 cells per 35 mm dish 24 h prior to transfection. Cells were co-transfected with 1 µg pCerulean-N1 (Addgene #54742), expressing Cerulean Fluorescent Protein to identify transfected cells, 5 µg pDR-GFP [55] and 5 µg pCBA-I-SceI [55] using Lipofectamine (Invitrogen) and cultured as normal. The DNA-PK inhibitor, NU7026 (Tocris Biosciences), was used as a control as the level of HR increases upon inhibition of the competing NHEJ pathway. 48 h after co-transfection, cells were trypsinized and resuspended in 500ul PBS containing 40 nM TO-PRO-3 iodide (Life Technologies, #T3605) to identify live cells. FACS analysis was carried out using BD FACSCantoII and BD FACSDiva software. Briefly, cells were gated as follows: live cells (ToPro3 negative), singlet cells (FSC-A verses FSC-H), transfected cells (Cerulean positive). The percentage of GFP-positive cells was derived from the live, transfected, single-cell population.

Author's contributions. N.F.L., S.M. and J.L. conceived and designed the research. S.M. performed microscopy and comet assays. J.L. performed cell cycle and repair assays. E.C.H. and M.V. assisted with microscopy and presentation of data. N.F.L., S.M., J.L. and E.C.H. analysed the data. N.F.L., S.M. and J.L. wrote the paper. All authors read and approved the final manuscript.

Competing interests. The authors declare no conflict of interests.

Funding. This work was supported by the Science Foundation Ireland (http://www.sfi.ie/) PI Award 07/IN1/B958 and SFI-IvP Award (13/IA/1954) to N.F.L. Additional support was also obtained from the European Union FP6 Integrated Project DNA repair contract no. 512113 to N.F.L., the Health Research Board (Ireland) Programme Grand No. PR001/2001 and the College of Science Scholarship awarded to J.L.

Acknowledgements. We thank Professor B. Vogelstein (John Hopkins University, USA) and Dr S. Jones (University of Massachusetts, USA) for kindly supplying us with the HCT116 and MEF cell lines. The authors acknowledge the facilities and technical assistance of the Flow Cytometry Facility at the National University of Ireland Galway, a facility that is funded by NUI Galway and the Irish Government's Programme for Research in Third Level Institutions, Cycle5, National Development Plan 2007–2013.

References

1. Asker C, Wiman KG, Selivanova G. 1999 p53-induced apoptosis as a safeguard against cancer. *Biochem. Biophys. Res. Commun.* **265**, 1–6. (doi:10.1006/bbrc.1999.1446)
2. Lane DP. 1992 p53, guardian of the genome. *Nature* **358**, 15–16. (doi:10.1038/358015a0)
3. Valente LJ, Gray DH, Michalak EM, Pinon-Hofbauer J, Egle A, Scott CL, Janic A, Strasser A. 2013 p53 efficiently suppresses tumor development in the complete absence of its cell-cycle inhibitory and proapoptotic effectors p21, Puma, and Noxa. *Cell Rep.* **3**, 1339–1345. (doi:10.1016/j.celrep.2013.04.012)
4. Lindahl T. 1993 Instability and decay of the primary structure of DNA. *Nature* **362**, 709–715. (doi:10.1038/362709a0)
5. Hoeijmakers JH. 2001 Genome maintenance mechanisms for preventing cancer. *Nature* **411**, 366–374. (doi:10.1038/35077232)
6. Helton ES, Chen X. 2007 p53 modulation of the DNA damage response. *J. Cell. Biochem.* **100**, 883–896. (doi:10.1002/jcb.21091)
7. Derbyshire DJ *et al.* 2002 Crystal structure of human 53BP1 BRCT domains bound to p53 tumour suppressor. *EMBO J.* **21**, 3863–3872. (doi:10.1093/emboj/cdf383)
8. Iwabuchi K, Bartel PL, Li B, Marraccino R, Fields S. 1994 Two cellular proteins that bind to wild-type but not mutant p53. *Proc. Natl Acad. Sci. USA* **91**, 6098–6102. (doi:10.1073/pnas.91.13.6098)
9. Iwabuchi K, Li B, Massa HF, Trask BJ, Date T, Fields S. 1998 Stimulation of p53-mediated transcriptional activation by the p53-binding proteins, 53BP1 and 53BP2. *J. Biol. Chem.* **273**, 26 061–26 068. (doi:10.1074/jbc.273.40.26061)
10. Joo WS, Jeffrey PD, Cantor SB, Finnin MS, Livingston DM, Pavletich NP. 2002 Structure of the 53BP1 BRCT region bound to p53 and its comparison to the Brca1 BRCT structure. *Genes Dev.* **16**, 583–593. (doi:10.1101/gad.959202)
11. Reid RJ, Fiorani P, Sugawara M, Bjornsti MA. 1999 CDC45 and DPB11 are required for processive DNA replication and resistance to DNA topoisomerase I-mediated DNA damage. *Proc. Natl Acad. Sci. USA* **96**, 11 440–11 445. (doi:10.1073/pnas.96.20.11440)
12. Kantidze OL, Iarovaia OV, Razin SV. 2006 Assembly of nuclear matrix-bound protein complexes involved in non-homologous end joining is induced by inhibition of DNA topoisomerase II. *J. Cell. Physiol.* **207**, 660–667. (doi:10.1002/jcp.20597)
13. Tang W, Willers H, Powell SN. 1999 p53 directly enhances rejoining of DNA double-strand breaks with cohesive ends in gamma-irradiated mouse fibroblasts. *Cancer Res.* **59**, 2562–2565.
14. Bill CA, Yu Y, Miselis NR, Little JB, Nickoloff JA. 1997 A role for p53 in DNA end rejoining by human cell extracts. *Mutation Res.* **385**, 21–29. (doi:10.1016/S0921-8777(97)00040-2)
15. Akyuz N, Boehden GS, Susse S, Rimek A, Preuss U, Scheidtmann KH, Wiesmuller L. 2002 DNA substrate dependence of p53-mediated regulation of double-strand break repair. *Mol. Cell. Biol.* **22**, 6306–6317. (doi:10.1128/MCB.22.17.6306-6317.2002)
16. Yang Q *et al.* 2002 The processing of Holliday junctions by BLM and WRN helicases is regulated by p53. *J. Biol. Chem.* **277**, 31 980–31 987. (doi:10.1074/jbc.M204111200)
17. Romanova LY, Willers H, Blagosklonny MV, Powell SN. 2004 The interaction of p53 with replication protein A mediates suppression of homologous recombination. *Oncogene* **23**, 9025–9033. (doi:10.1038/sj.onc.1207982)
18. Wiktor-Brown DM, Sukup-Jackson MR, Fakhraldeen SA, Hendricks CA, Engelward BP. 2011 p53 null fluorescent yellow direct repeat (FYDR) mice have normal levels of homologous recombination. *DNA repair* **10**, 1294–1299. (doi:10.1016/j.dnarep.2011.09.009)
19. Willers H, McCarthy EE, Hubbe P, Dahm-Daphi J, Powell SN. 2001 Homologous recombination in extrachromosomal plasmid substrates is not suppressed by p53. *Carcinogenesis* **22**, 1757–1763. (doi:10.1093/carcin/22.11.1757)
20. Serrano MA, Li Z, Dangeti M, Musich PR, Patrick S, Roginskaya M, Cartwright B, Zou Y. 2013 DNA-PK, ATM and ATR collaboratively regulate p53-RPA interaction to facilitate homologous recombination DNA repair. *Oncogene* **32**, 2452–2462. (doi:10.1038/onc.2012.257)
21. Bunting SF *et al.* 2010 53BP1 inhibits homologous recombination in Brca1-deficient cells by blocking resection of DNA breaks. *Cell* **141**, 243–254. (doi:10.1016/j.cell.2010.03.012)
22. Dimitrova N, Chen YC, Spector DL, de Lange T. 2008 53BP1 promotes non-homologous end joining of telomeres by increasing chromatin mobility. *Nature* **456**, 524–528. (doi:10.1038/nature07433)
23. Zimmermann M, Lottersberger F, Buonomo SB, Sfeir A, de Lange T. 2013 53BP1 regulates DSB repair using Rif1 to control 5′ end resection. *Science* **339**, 700–704. (doi:10.1126/science.1231573)
24. Chapman JR, Sossick AJ, Boulton SJ, Jackson SP. 2012 BRCA1-associated exclusion of 53BP1 from DNA damage sites underlies temporal control of DNA repair. *J. Cell Sci.* **125**, 3529–3534. (doi:10.1242/jcs.105353)
25. Escribano-Diaz C *et al.* 2013 A cell cycle-dependent regulatory circuit composed of 53BP1-RIF1 and BRCA1-CtIP controls DNA repair pathway choice. *Mol. Cell* **49**, 872–883. (doi:10.1016/j.molcel.2013.01.001)
26. Schlegel BP, Jodelka FM, Nunez R. 2006 BRCA1 promotes induction of ssDNA by ionizing radiation. *Cancer Res.* **66**, 5181–5189. (doi:10.1158/0008-5472.CAN-05-3209)
27. Yun MH, Hiom K. 2009 CtIP-BRCA1 modulates the choice of DNA double-strand-break repair pathway throughout the cell cycle. *Nature* **459**, 460–463. (doi:10.1038/nature07955)
28. Ismail IH, Gagne JP, Genois MM, Strickfaden H, McDonald D, Xu Z, Poirier GG, Masson J-Y, Hendzel MJ. 2015 The RNF138 E3 ligase displaces Ku to promote DNA end resection and regulate DNA repair pathway choice. *Nat. Cell Biol.* **17**, 1446–1457. (doi:10.1038/ncb3259)
29. Bohgaki T *et al.* 2011 Genomic instability, defective spermatogenesis, immunodeficiency, and cancer in a mouse model of the RIDDLE syndrome. *PLoS Genet.* **7**, e1001381. (doi:10.1371/journal.pgen.1001381)
30. Pinato S, Scandiuzzi C, Arnaudo N, Citterio E, Gaudino G, Penengo L. 2009 RNF168, a new RING finger, MIU-containing protein that modifies chromatin by ubiquitination of histones H2A and H2AX. *BMC Mol. Biol.* **10**, 55. (doi:10.1186/1471-2199-10-55)
31. Nakada S *et al.* 2010 Non-canonical inhibition of DNA damage-dependent ubiquitination by OTUB1. *Nature* **466**, 941–946. (doi:10.1038/nature09297)
32. Huen MS, Grant R, Manke I, Minn K, Yu X, Yaffe MB, Chen J. 2007 RNF8 transduces the DNA-damage signal via histone ubiquitylation and checkpoint protein assembly. *Cell* **131**, 901–914. (doi:10.1016/j.cell.2007.09.041)

33. Fradet-Turcotte A *et al.* 2013 53BP1 is a reader of the DNA-damage-induced H2A Lys 15 ubiquitin mark. *Nature* **499**, 50–54. (doi:10.1038/nature12318)
34. Botuyan MV, Lee J, Ward IM, Kim JE, Thompson JR, Chen J, Mer G. 2006 Structural basis for the methylation state-specific recognition of histone H4-K20 by 53BP1 and Crb2 in DNA repair. *Cell* **127**, 1361–1373. (doi:10.1016/j.cell.2006.10.043)
35. Yan Q, Dutt S, Xu R, Graves K, Juszczynski P, Manis JP, Shipp MA. 2009 BBAP monoubiquitylates histone H4 at lysine 91 and selectively modulates the DNA damage response. *Mol. Cell* **36**, 110–120. (doi:10.1016/j.molcel.2009.08.019)
36. Yang H, Pesavento JJ, Starnes TW, Cryderman DE, Wallrath LL, Kelleher NL, Mizzen CA. 2008 Preferential dimethylation of histone H4 lysine 20 by Suv4-20. *J. Biol. Chem*. **283**, 12 085–12 092. (doi:10.1074/jbc.M707974200)
37. Schotta G *et al*. 2008 A chromatin-wide transition to H4K20 monomethylation impairs genome integrity and programmed DNA rearrangements in the mouse. *Genes Dev*. **22**, 2048–2061. (doi:10.1101/gad.476008)
38. Kachirskaia I, Shi X, Yamaguchi H, Tanoue K, Wen H, Wang EW, Appella E, Gozani O. 2008 Role for 53BP1 Tudor domain recognition of p53 dimethylated at lysine 382 in DNA damage signaling. *J. Biol. Chem*. **283**, 34 660–34 666. (doi:10.1074/jbc.M806020200)
39. Kodama M, Otsubo C, Hirota T, Yokota J, Enari M, Taya Y. 2010 Requirement of ATM for rapid p53 phosphorylation at Ser46 without Ser/Thr-Gln sequences. *Mol. Cell. Biol*. **30**, 1620–1633. (doi:10.1128/MCB.00810-09)
40. Roy S, Musselman CA, Kachirskaia I, Hayashi R, Glass KC, Nix JC, Gozani O, Appella E, Kutateladze TG. 2010 Structural insight into p53 recognition by the 53BP1 tandem Tudor domain. *J. Mol. Biol*. **398**, 489–496. (doi:10.1016/j.jmb.2010.03.024)
41. Krones-Herzig A, Adamson E, Mercola D. 2003 Early growth response 1 protein, an upstream gatekeeper of the p53 tumor suppressor, controls replicative senescence. *Proc. Natl Acad. Sci. USA* **100**, 3233–3238. (doi:10.1073/pnas.2628034100)
42. Wahl GM, Carr AM. 2001 The evolution of diverse biological responses to DNA damage: insights from yeast and p53. *Nat. Cell Biol*. **3**, E277–E286. (doi:10.1038/ncb1201-e277)
43. Fernandez-Capetillo O *et al*. 2002 DNA damage-induced G2-M checkpoint activation by histone H2AX and 53BP1. *Nat. Cell Biol*. **4**, 993–997. (doi:10.1038/ncb884)
44. Ward IM, Minn K, van Deursen J, Chen J. 2003 p53 Binding protein 53BP1 is required for DNA damage responses and tumor suppression in mice. *Mol. Cell. Biol*. **23**, 2556–2563. (doi:10.1128/MCB.23.7.2556-2563.2003)
45. FitzGerald J, Moureau S, Drogaris P, O'Connell E, Abshiru N, Verreault A, Thibault P, Grenon M, Lowndes NF. 2011 Regulation of the DNA damage response and gene expression by the Dot1 L histone methyltransferase and the 53Bp1 tumour suppressor. *PLoS ONE* **6**, e14714. (doi:10.1371/journal.pone.0014714)
46. Nakamura K, Sakai W, Kawamoto T, Bree RT, Lowndes NF, Takeda S, Taniguchi Y. 2006 Genetic dissection of vertebrate 53BP1: a major role in non-homologous end joining of DNA double strand breaks. *DNA Repair* **5**, 741–749. (doi:10.1016/j.dnarep.2006.03.008)
47. Stucki M, Jackson SP. 2004 MDC1/NFBD1: a key regulator of the DNA damage response in higher eukaryotes. *DNA Repair* **3**, 953–957. (doi:10.1016/j.dnarep.2004.03.007)
48. Stewart GS, Wang B, Bignell CR, Taylor AM, Elledge SJ. 2003 MDC1 is a mediator of the mammalian DNA damage checkpoint. *Nature* **421**, 961–966. (doi:10.1038/nature01446)
49. Bekker-Jensen S, Lukas C, Melander F, Bartek J, Lukas J. 2005 Dynamic assembly and sustained retention of 53BP1 at the sites of DNA damage are controlled by Mdc1/NFBD1. *J. Cell Biol*. **170**, 201–211. (doi:10.1083/jcb.200503043)
50. Kasuboski JM *et al.* 2011 Zwint-1 is a novel Aurora B substrate required for the assembly of a dynein-binding platform on kinetochores. *Mol. Biol. Cell* **22**, 3318–3330. (doi:10.1091/mbc.E11-03-0213)
51. Escribano-Diaz C, Durocher D. 2013 DNA repair pathway choice—a PTIP of the hat to 53BP1. *EMBO Rep*. **14**, 665–666. (doi:10.1038/embor.2013.99)
52. Cruz-Garcia A, Lopez-Saavedra A, Huertas P. 2014 BRCA1 accelerates CtIP-mediated DNA-end resection. *Cell Rep*. **9**, 451–459. (doi:10.1016/j.celrep.2014.08.076)
53. Scully R *et al.* 1997 Dynamic changes of BRCA1 subnuclear location and phosphorylation state are initiated by DNA damage. *Cell* **90**, 425–435. (doi:10.1016/S0092-8674(00) 80503-6)
54. Arizti P *et al.* 2000 Tumor suppressor p53 is required to modulate BRCA1 expression. *Mol. Cell. Biol*. **20**, 7450–7459. (doi:10.1128/mcb.20.20.7450-7459.2000)
55. Pierce AJ, Johnson RD, Thompson LH, Jasin M. 1999 XRCC3 promotes homology-directed repair of DNA damage in mammalian cells. *Genes Dev*. **13**, 2633–2638. (doi:10.1101/gad.13.20.2633)
56. Saleh-Gohari N, Bryant HE, Schultz N, Parker KM, Cassel TN, Helleday T. 2005 Spontaneous homologous recombination is induced by collapsed replication forks that are caused by endogenous DNA single-strand breaks. *Mol. Cell. Biol*. **25**, 7158–7169. (doi:10.1128/MCB.25.16.7158-7169.2005)
57. Bryant HE, Helleday T. 2006 Inhibition of poly (ADP-ribose) polymerase activates ATM which is required for subsequent homologous recombination repair. *Nucleic Acids Res*. **34**, 1685–1691. (doi:10.1093/nar/gkl108)
58. Farmer H *et al*. 2005 Targeting the DNA repair defect in BRCA mutant cells as a therapeutic strategy. *Nature* **434**, 917–921. (doi:10.1038/nature03445)
59. Oplustilova L *et al.* 2012 Evaluation of candidate biomarkers to predict cancer cell sensitivity or resistance to PARP-1 inhibitor treatment. *Cell Cycle* **11**, 3837–3850. (doi:10.4161/cc.22026)
60. Zgheib O, Pataky K, Brugger J, Halazonetis TD. 2009 An oligomerized 53BP1 tudor domain suffices for recognition of DNA double-strand breaks. *Mol. Cell. Biol*. **29**, 1050–1058. (doi:10.1128/MCB.01011-08)
61. Huyen Y *et al.* 2004 Methylated lysine 79 of histone H3 targets 53BP1 to DNA double-strand breaks. *Nature* **432**, 406–411. (doi:10.1038/nature03114)
62. Du Toit A. 2013 DNA damage: limiting 53BP1. *Nat. Rev. Mol. Cell Biol*. **14**, 132. (doi:10.1038/nrm3532)
63. Bunz F, Dutriaux A, Lengauer C, Waldman T, Zhou S, Brown JP, Sedivy JM, Kinzler KW, Vogelstein B. 1998 Requirement for 53 and p21 to sustain G2 arrest after DNA damage. *Science* **282**, 1497–1501. (doi:10.1126/science.282.5393.1497)